



**Protein kinase D1 deletion in adipocytes  
enhances energy dissipation and protects  
against adiposity**



**Deletion der Protein Kinase D1 in Adipocyten  
fördert den Energieumsatz und schützt  
dadurch vor Adipositas**

Doctoral thesis for a doctoral degree  
at the Graduate School of Life Sciences,  
Julius-Maximilians-Universität Würzburg,  
Section Biomedicine

Submitted by

**Mona Christina Löffler**

from Illertissen

Würzburg, 2019

Submitted on: \_\_\_\_\_

Office stamp

Members of the *Promotionskomitee*:

Chairperson: Prof. Dr. Manfred Gessler

Primary Supervisor: Dr. Grzegorz Sumara

Supervisor (Second): Prof. Dr. Antje Gohla

Supervisor (Third): Prof. Dr. Carsten Hoffmann

Supervisor (Fourth): Dr. Nabil Djouder

Date of Public Defense: \_\_\_\_\_

Date of Receipt of Certificates: \_\_\_\_\_



## ABSTRACT

Adaptation to alterations in nutrient availability ensures the survival of organisms. In vertebrates, adipocytes play a decisive role in this process due to their ability to store large amounts of excess nutrients and release them in times of food deprivation. In today's western world, a rather unlimited excess of nutrients leads to high-caloric food consumption in humans. Nutrient overload together with a decreased energy dissipation result in obesity as well as associated diseases such as insulin resistance, diabetes, and liver steatosis. Obesity causes a hormonal imbalance, which in combination with altered nutrient levels can aberrantly activate G-protein coupled receptors utilizing *diacylglycerol* (DAG) as secondary messenger. *Protein kinase D* (PKD) 1 is a DAG effector integrating multiple hormonal and nutritional inputs. Nevertheless, its physiological role in adipocytes has not been investigated so far. In this thesis, evidence is provided that the deletion of PKD1 in adipocytes suppresses lipogenesis as well as the accumulation of triglycerides. Furthermore, PKD1 depletion results in increased mitochondrial biogenesis as well as decoupling activity. Moreover, PKD1 deletion promotes the expression of the  $\beta$ 3-adrenergic receptor (ADRB3) in a CCAAT/enhancer-binding protein (C/EBP)- $\alpha$  and  $\delta$ -dependent manner. This results in elevated expression levels of beige markers in adipocytes in the presence of a  $\beta$ -agonist. Contrarily, adipocytes expressing a constitutive active form of PKD1 present a reversed phenotype. Additionally, PKD1 regulates adipocyte metabolism in an AMP-activated protein kinase (AMPK)-dependent manner by suppressing its activity through phosphorylation of AMPK  $\alpha$ 1/ $\alpha$ 2 subunits. Thus, PKD1 deletion results in an enhanced activity of the AMPK complex. Consistent with the *in vitro* findings, mice lacking PKD1 in adipocytes demonstrate a resistance to high-fat diet-induced obesity due to an elevated energy expenditure caused by trans-differentiation of white into beige adipocytes. Moreover, deletion of PKD1 in murine adipocytes improves systemic insulin sensitivity and ameliorates liver steatosis. Finally, PKD1 levels positively correlate with HOMA-IR as well as insulin levels in human subjects. Furthermore, inhibition of PKD1 in human adipocytes leads to metabolic alterations, which are comparable to the alterations seen in their murine counterparts. Taken together, these data demonstrate that PKD1 suppresses energy dissipation, drives lipogenesis, and adiposity. Therefore, increased energy dissipation induced by several complementary mechanisms upon PKD1 deletion might represent an attractive strategy to treat obesity and its related complications.

### ZUSAMMENFASSUNG

Die Anpassung an veränderte Nährstoffverfügbarkeiten sichert das Überleben eines jeden Organismus. Dabei spielen in Vertebraten vor allem Adipozyten eine entscheidende Rolle. Sie haben die Fähigkeit, große Mengen überschüssiger Nährstoffe zu speichern und diese in Zeiten des Mangels wieder freizusetzen. Heutzutage herrscht jedoch besonders in Industrieländern ein ausreichendes Angebot an Nahrungsmitteln, was zu einer übermäßigen Kalorienzufuhr einzelner Individuen führt. Durch überschüssige Energiezufuhr in Verbindung mit einem verringerten Energieverbrauch kommt es zu Fettleibigkeit und damit verbundenen Erkrankungen wie Insulinresistenz, Diabetes und nichtalkoholischer Fettleber. Übergewicht führt zu einem hormonellen Ungleichgewicht, das im Zusammenhang mit veränderten Nährstoffgehalten, unter Verwendung von *Diacylglycerol* (DAG) als sekundären Botenstoff, G-Protein-gekoppelte Rezeptoren unkontrolliert aktiviert. *Protein Kinase D* (PKD) 1 ist ein DAG Effektor, der an unterschiedlichsten hormonellen und ernährungsphysiologischen Vorgängen beteiligt ist. Die zugrunde liegende physiologische Rolle von PKD1 in Adipozyten ist jedoch weitgehend unverstanden. In dieser Doktorarbeit wird gezeigt, dass eine Adipozyten spezifische PKD1 Defizienz sowohl Lipogenese als auch die Akkumulation von Triglyceriden unterdrückt. Darüber hinaus wird durch die Deletion von PKD1 sowohl der Mitochondriengehalt als auch die Dynamik erhöht und die Entkopplungsaktivität gesteigert. Zudem wird die Expression des  $\beta$ 3-adrenergen Rezeptors (ADRB3) durch die PKD1 Defizienz in einer CCAAT/Enhancer-Bindungsprotein (C/EBP) - $\alpha$  und  $\delta$ -abhängigen Weise gefördert. In Gegenwart eines  $\beta$ -Agonisten kommt es dadurch zu einer erhöhten Expression von Genen, die auf beige Fettzellen hindeuten. Im Gegensatz dazu weisen Adipozyten, die eine konstitutiv aktive Form von PKD1 exprimieren, einen umgekehrten Phänotyp auf. Zusätzlich reguliert PKD1 den Adipozytenmetabolismus abhängig von *AMP-aktivierter Proteinkinase* (AMPK). PKD1 unterdrückt die AMPK-Aktivität durch Phosphorylierung von AMPK- $\alpha$ 1/ $\alpha$ 2-Untereinheiten. Daher steigert die PKD1-Deletion die Tätigkeit des AMPK-Komplexes. In Übereinstimmung mit den *In-vitro*-Daten zeigen Mäuse, denen PKD1 in Adipozyten fehlt, eine Resistenz gegen nahrungsinduzierte Fettleibigkeit. Dies lässt sich durch eine gesteigerte Transdifferenzierung von weißen zu beigen Fettzellen erklären, die einen erhöhten Energieumsatz aufweisen. Weiterhin verbessert die Deletion von PKD1 in Adipozyten der Maus die systemische Insulinsensitivität und schützt vor einer Lebersteatose. In humanen Fettzellen zeigen

## ZUSAMMENFASSUNG

---

sich ähnliche Veränderungen im Metabolismus, wie bereits in den Adipozyten der Maus beobachtet wurden. Des Weiteren korreliert die Expression von PKD1 in humanem Fettgewebe positiv mit HOMA-IR, einem Marker für Insulin-Resistenz sowie den Insulinwerten beim Menschen. Zusammengefasst weisen die Daten dieser Thesis auf, dass PKD1 den Energieverbrauch unterdrückt und sowohl Lipogenese als auch Adipositas fördert. Adipozyten, denen PKD1 fehlt, zeigen demnach einen erhöhten Energieumsatz, der durch unterschiedliche komplementäre Mechanismen verursacht wird. Dadurch könnte sich eine attraktive Strategie zur Behandlung von Fettleibigkeit und den damit verbundenen Komplikationen ergeben.

## TABLE OF CONTENTS

<b>1</b>	<b>INTRODUCTION.....</b>	<b>1</b>
1.1	<b>Adipose Tissue.....</b>	<b>1</b>
1.1.1	Types of Adipose Tissue .....	1
1.1.2	Physiological Function.....	3
1.1.3	Obesity .....	6
1.1.4	Insulin resistance and T2D .....	9
1.2	<b>Mitochondrial dynamics in adipocytes .....</b>	<b>11</b>
1.3	<b><i>Protein kinase D (PKD)</i>.....</b>	<b>13</b>
1.3.1	Structure and signaling.....	13
1.3.2	The role of PKD in health and disease .....	15
1.4	<b>AMPK .....</b>	<b>17</b>
1.4.1	AMPK regulation.....	17
1.4.2	The function of AMPK in adipose tissue metabolism.....	19
1.5	<b>The impact of the <math>\beta</math>3 adrenergic receptor on adipocyte metabolism and regulation of its abundance .....</b>	<b>20</b>
1.6	<b>Aim of the study .....</b>	<b>21</b>
<b>2</b>	<b>MATERIALS AND METHODS.....</b>	<b>23</b>
2.1	<b>Materials .....</b>	<b>23</b>
2.1.1	Equipment and reagents .....	23
2.1.2	Media and buffers.....	23
2.1.3	Mice.....	23
2.1.4	Cell lines.....	25
2.1.5	Explants derived from sWAT .....	26
2.1.6	Human samples.....	26
2.2	<b>Methods .....</b>	<b>27</b>
2.2.1	Mouse genotyping .....	27
2.2.1.1	Isolation of genomic DNA from mouse tissue.....	27
2.2.1.2	Mouse genotyping by PCR.....	27
2.2.1.3	Agarose gel electrophoresis.....	30
2.2.2	Generation of stable cell lines .....	30
2.2.2.1	Molecular cloning .....	30

## TABLE OF CONTENTS

---

2.2.2.2	Transformation .....	32
2.2.2.3	Mini and Midi preps .....	32
2.2.2.4	Transfection.....	32
2.2.2.5	Transduction and selection.....	33
2.2.3	<i>In vitro</i> analysis.....	33
2.2.3.1	Transient transfection with <i>small interfering RNA</i> (siRNA) .....	33
2.2.3.2	AMPK activity assay .....	34
2.2.3.3	Quantification of TG accumulation .....	34
2.2.3.4	Lipolysis assay .....	35
2.2.3.5	Lipogenesis Assay .....	35
2.2.3.6	Mitochondrial respiration .....	36
2.2.4	Biochemistry.....	36
2.2.4.1	Immunoblotting.....	36
2.2.4.2	<i>Immunoprecipitation</i> (IP) .....	37
2.2.4.3	Coomassie gel.....	37
2.2.4.4	<i>Mass Spectrometry</i> (MS) analysis.....	38
2.2.4.5	RT-qPCR analysis.....	38
2.2.4.6	RNA sequencing .....	40
2.2.4.7	DAG content.....	41
2.2.5	<i>Immunofluorescence</i> (IF) and histological analysis .....	43
2.2.5.1	Mitochondrial staining.....	43
2.2.5.2	IF staining of cells.....	43
2.2.5.3	Histology – <i>hematoxylin and eosin</i> (H&E) staining of paraffin sections 44	
2.2.5.4	Cell size quantification.....	44
2.2.5.5	Histology – <i>Immunohistochemistry</i> (IHC) on paraffin sections .....	44
2.2.5.6	Histology – Oil Red O staining of cryo sections.....	45
2.2.6	<i>In vivo</i> analysis .....	45
2.2.6.1	Glucose and insulin tolerance and test.....	45
2.2.6.2	Indirect calorimetry analysis .....	45
2.2.6.3	Body composition.....	46
2.2.6.4	Liver TG Extraction.....	46
2.2.6.5	Analysis of blood samples in mice.....	46



## TABLE OF CONTENTS

---

2.2.6.6	Analysis of blood samples in humans .....	47
2.2.7	Statistical analysis .....	47
<b>3</b>	<b>RESULTS .....</b>	<b>48</b>
<b>3.1</b>	<b>DAG-activated PKD1 promotes TG accumulation in adipocytes.....</b>	<b>48</b>
3.1.1	PKD1 is predominantly expressed in adipose tissue .....	48
3.1.2	ATP and DAG activate PKD1 in white adipocytes .....	48
3.1.3	PKD1 is not primarily activated by purines in differentiated brown adipocytes .....	50
3.1.4	Deletion of PKD1 suppresses lipid accumulation in adipocytes .....	51
<b>3.2</b>	<b>PKD1 decreases mitochondrial respiration and promotes lipogenesis in adipocytes.....</b>	<b>54</b>
3.2.1	Changes in TG accumulation are not correlating with the adipocyte differentiation or their lipolysis rate.....	54
3.2.2	PKD1 promotes lipogenesis in adipocytes .....	56
3.2.3	PKD1 suppresses OCR in adipocytes .....	57
3.2.4	PKD1 mainly affects white adipose tissue, without changing energy metabolism in brown adipocytes .....	60
3.2.5	PKD1 suppresses gene expression of the creatine metabolism and mitochondrial fragmentation .....	60
<b>3.3</b>	<b>PKD1 regulates adipocyte function by targeting AMPK- and possibly mTORC signaling.....</b>	<b>63</b>
3.3.1	Rictor is a possible interaction partner of PKD1 in adipocytes .....	63
3.3.2	PKD1 possibly regulates adipocyte function through the phosphorylation of Akt, a downstream target of mTOR.....	64
3.3.3	PKD1 regulates adipocyte function mainly by suppressing AMPK activity	66
3.3.4	AMPK deletion or activation can reverse the phenotype caused by altered PKD1 activity.....	70
<b>3.4</b>	<b>Mice lacking PKD1 in adipocytes are protected against the development of diet-induced obesity, diabetes, and liver steatosis .....</b>	<b>75</b>
3.4.1	DAG levels are independent of the diet.....	75
3.4.2	PKD1 is upregulated upon feeding .....	76
3.4.3	PKD1 deletion in adipocytes protects against diet-induced obesity.....	77

## TABLE OF CONTENTS

---

3.4.4	PKD1 suppresses activity of AMPK in murine adipose tissue .....	80
3.4.5	Deletion of PKD1 alters AMPK activity in response to refeeding.....	83
3.4.6	Deletion of PKD1 protects against diet-induced obesity by enhancing energy expenditure .....	84
3.4.7	PKD1 deletion reduces overall adipocyte size.....	86
3.4.8	Deletion of PKD1 induces beiging of white adipocytes in mice .....	88
3.4.9	Effects on energy expenditure are abolished under thermoneutral conditions.....	96
3.4.10	PKD1 suppresses ADRB3 expression in an AMPK-C/EBP- $\alpha$ /C/EBP- $\delta$ - dependent manner .....	97
3.4.11	PKD1 deletion in adipocytes protects against the development of type 2 diabetes and diet-induced fatty liver disease.....	100
3.4.12	PKD1 also regulates human adipose tissue function.....	104
3.4.13	Abrogation of PKD1-dependent signalling in adipose tissue can attenuate the course of the disease .....	106
<b>4</b>	<b>DISCUSSION .....</b>	<b>110</b>
4.1	PKD1 activation through DAG and extracellular purines .....	111
4.2	The impact of PKD1 on lipolysis, lipogenesis, OCR, and mitochondrial fragmentation.....	112
4.3	PKD1 regulates adipose tissue function in an AMPK-dependent manner.....	114
4.4	PKD1 deletion induces beiging of white adipocytes and increases energy expenditure.....	118
4.5	The role of PKD1 in adipocytes under physiological and pathophysiological conditions .....	121
<b>5</b>	<b>CLOSING REMARKS AND FUTURE PERSPECTIVES .....</b>	<b>126</b>
<b>6</b>	<b>REFERENCES.....</b>	<b>127</b>
<b>7</b>	<b>APPENDIX.....</b>	<b>144</b>
7.1	<b>Materials and Reagents .....</b>	<b>144</b>
7.1.1	Appliances and consumables .....	144
7.1.2	Reagents .....	150
7.1.3	Media.....	162

## TABLE OF CONTENTS

---

7.1.4	Buffers .....	166
7.1.5	Real time PCR primers.....	170
7.1.6	Plasmid sequences .....	174
<b>7.2</b>	<b>List of Figures .....</b>	<b>184</b>
<b>7.3</b>	<b>List of Tables.....</b>	<b>187</b>
<b>7.4</b>	<b>List of Abbreviations .....</b>	<b>188</b>
<b>7.5</b>	<b>Acknowledgements .....</b>	<b>197</b>
<b>7.6</b>	<b>Publications.....</b>	<b>199</b>
7.6.1	Original articles.....	199
7.6.2	Reviews.....	199
7.6.3	Oral presentations .....	199
7.6.4	Posters .....	200
<b>7.7</b>	<b>Curriculum vitae.....</b>	<b>201</b>
<b>7.8</b>	<b>Affidavit.....</b>	<b>203</b>
<b>7.9</b>	<b>Eidesstattliche Erklärung .....</b>	<b>203</b>

# 1 INTRODUCTION

## 1.1 Adipose Tissue

### 1.1.1 Types of Adipose Tissue

Adipose tissue is a highly active metabolic and endocrine organ. It consists of adipocytes, connective tissue matrix, *stromal vascular cells* (SVC), immune cells, and nerve tissue<sup>1</sup>. Originally, two main functionally different types of fat depots have been distinguished in mammals: *brown adipose tissue* (BAT) and *white adipose tissue* (WAT), both differing in their morphology and function.

BAT is important to maintain the core body temperature by dissipating energy generated from *fatty acid oxidation* (FAO) in the form of heat. Both thermogenic function and growth of BAT are regulated by the sympathetic nervous system. Upon cold exposure, these sympathetic nerves release *norepinephrine* (NE) in order to activate thermogenesis<sup>2</sup>. Brown adipocytes are highly specialized, multilocular cells, containing multiple small lipid droplets. They are characterized by densely packed and large mitochondria endowed with laminar cristae containing the *uncoupling protein* (UCP) 1<sup>3,4</sup>. Generally, an established proton gradient across the inner mitochondrial membrane is used to synthesize *adenosine triphosphate* (ATP), a process catalyzed by complex V, which is embedded into the respiratory chain<sup>5</sup>. UCP1 uncouples coherent substrate oxidation from ATP production in order to generate heat by catalyzing a regulated proton leak across the inner mitochondrial membrane<sup>6</sup>. There are large BAT depots in mice including the interscapular, axillary, and cervical BAT<sup>4</sup>. In humans, BAT was originally described to be exclusively found in newborns providing heat in cold environments, unless subjects were specifically challenged by chronic cold as seen in Scandinavian outdoor workers<sup>7</sup>. Recently however, metabolically active brown adipose tissue has been identified in adult humans using radiological observations of *2-fluoro-D-2-deoxy-D-glucose positron emission tomography* (FDG PET) combined with *computed tomography* (CT). Several studies confirmed the existence of several regions as UCP1-positive adipocytes using biopsies<sup>8-10</sup>.

In contrast to BAT, white adipocytes consist of a single, large lipid droplet with fewer and elongated mitochondria, structured by randomly oriented cristae<sup>4</sup>. It is distributed

## INTRODUCTION

---

within subcutaneous and gonadal regions, with the gonadal fat depot correlating to the development of metabolic diseases. Subcutaneous fat depots on the other hand do not show this correlation and are even discussed to be beneficial<sup>11</sup>. As it was shown in transplantation studies, the displacement of gonadal fat into subcutaneous fat depots only had minor effects, whereas the other way around, reduced adiposity and glucose homeostasis occurred<sup>12</sup>. WAT shows broad functions, such as mechanical protection of inner organs, thermal isolation, as well as sliding of muscle bundles. However, its most important function is the maintenance of energy balance. WAT has the capability to store large amounts of excess energy in form of *triglycerides* (TGs), which can be released again in terms of energy deprivation or high demand in form of *free fatty acids* (FFAs) for oxidation in other organs<sup>13</sup>. As an endocrine organ it is also responsible to maintain the overall lipid homeostasis<sup>14</sup>, which determines whole-body weight, insulin sensitivity, and peripheral energy handling in both humans and mice<sup>15</sup>.

Recent studies indicated the existence of a third form, so called beige or brite adipocytes. These adipocytes show a similar, but distinct gene expression pattern in comparison to classical brown adipocytes. On the molecular level, the transition of white to beige or brite adipocytes is characterized by the acquisition of new mitochondria and enhanced expression of thermogenic and mitochondrial genes, including UCP1, which decouple the proton gradient from ATP production<sup>16</sup>. However, another mechanism of heat dissipation utilized primarily by beige adipocytes has been proposed. A proteomic study revealed that beige adipocytes also possess a creatine enzyme signature. Creatine drives energy dissipation through mitochondria of beige adipocytes by accepting a phosphate group from ATP and its subsequent release mediated by the phosphatase *phosphoethanolamine/phosphocholine phosphatase 1* (PHOSPHO1). This process largely contributes to the total energy balance in rodents and possibly also in humans<sup>17</sup>. Beige adipocytes are formed within the white adipose tissue at a high prevalence in subcutaneous and retroperitoneal fat and to a lower extent in gonadal fat. Their appearance positively correlates with resistance to diet-induced obesity<sup>18</sup> and can be induced upon cold exposure or  $\beta$ -adrenergic stimulation<sup>19,20</sup>. This indicates that white adipocytes show a high degree of plasticity by acquiring a molecular machinery, which allows them to dissipate energy in the form of heat<sup>17,21</sup>. Recent studies have shown that a trans-differentiation occurs from white into beige adipocytes, which is impaired upon obesity causing acceleration of the

beige-to-white transition<sup>19,22</sup>. Thus, increasing energy dissipation in adipocytes is a new strategy of anti-obesity therapies<sup>17,23,24</sup> (Figure 1).

Another type of adipose tissue, termed pink adipocytes, has been discussed. These adipocytes have been discovered in female mouse subcutaneous fat depots during pregnancy and lactation. These parenchymal cells are clustered as adipocytes due to their ability to store large amounts of lipids<sup>25</sup>. Pink adipocytes are mammary gland alveolar epithelial cells that can reversibly transdifferentiate from white adipocytes during pregnancy<sup>26</sup>. Besides their major role in producing and secreting milk, pink adipocytes also secrete leptin<sup>27</sup>. This seems to have a crucial effect in preventing obesity later on in life<sup>28</sup>.

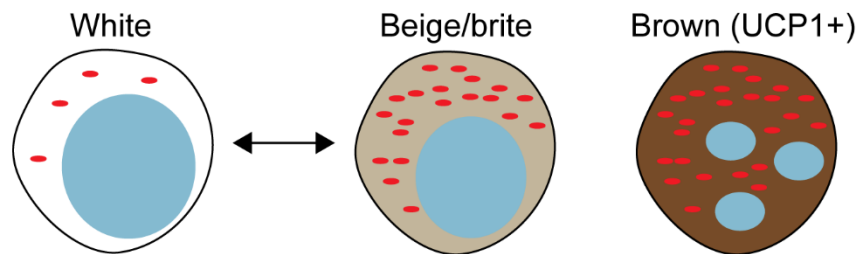


**Figure 1. Different types of adipose tissue.** Different types of adipose tissue, which originate from different precursors can be found in mammals. White and brown adipocytes show specific characteristics. The intermediate beige form has been shown to transdifferentiate from white adipocytes (modified from Gaggini *et al.*, 2015)<sup>29</sup>.

### 1.1.2 Physiological Function

Adipose tissue is an important storage organ, which can accumulate excess energy through the absorption of sugars and lipids. During the process of lipogenesis, glucose is converted into *fatty acids* (FAs) and subsequently to TGs, which are generated by esterification of FAs and glycerol-3-phosphate and are then stored in lipid droplets<sup>30</sup>. The first step in *de novo* lipogenesis is catalyzed by the *fatty acid synthase* (FAS). Mice lacking FAS in adult adipose tissue display an increase in beige adipocytes, as well as enhanced energy expenditure, and further show resistance towards diet-induced obesity<sup>31</sup>. Long chain FA synthesis is also regulated by the key enzyme *acetyl-coenzyme A (CoA) carboxylase* (ACC), which catalyzes the rate-limiting step in FA synthesis, namely the conversion of acetyl-CoA to malonyl-CoA<sup>32</sup>. Mice lacking ACC2 in adipocytes showed increased FA and glucose oxidation and a higher lipolysis rate. Both normal as well as fat- and cholesterol-enriched diet led to efficient

## INTRODUCTION

---

maintenance of insulin sensitivity and leanness in these mice<sup>33</sup>. In another study, elevated fat and carbohydrate oxidation resulted in an increase in total energy expenditure as well as a reduction in fat and lean body mass. This is linked to the prevention from diet-induced obesity and diet-induced peripheral and hepatic insulin resistance<sup>34</sup>. Nutrient deprivation or exercise induce lipolysis, leading to the mobilization and release of FFAs and glycerol through the hydrolyzation of stored TGs, which serve as substrates for  $\beta$ -oxidation and ATP generation in peripheral tissues or hepatic gluconeogenesis<sup>35</sup>. This requires the enzymatic activity of lipases. *Adipose triglyceride lipase* (ATGL) (the major TG lipase), the *hormone-sensitive lipase* (HSL) (the major *diacylglycerol* (DAG) lipase), and the *monoglyceride lipase* (MGL) consecutively hydrolyze all three ester bonds of TGs to release FFAs<sup>36</sup>. Furthermore, lipid droplet-associated proteins such as perilipin are necessary for efficient stimulation of lipolysis<sup>35</sup>. Remarkably, a genetic inactivation of ATGL led to an almost complete blockage of FFAs and glycerol release<sup>37</sup>, whereas HSL and MGL deletion in adipose tissue of mice only minorly affected lipolysis rate<sup>38-40</sup>. In line with this, humans and mice lacking ATGL are only moderately obese but suffer from cardiac defects<sup>37,41</sup>. Interestingly, mice with attenuated lipolysis rate due to the inhibition of lipolysis enzymes (ATGL, HSL) effectively improved *high-fat diet* (HFD)-induced obesity and insulin resistance<sup>42-44</sup>. The reduced amount of FFAs, which acts as an insulin desensitizing factor, caused improved glucose tolerance and insulin sensitivity, indicating that ATGL is an important enzyme in energy homeostasis<sup>37,43,44</sup>. Furthermore, *single nucleotide polymorphisms* (SNP) in the ATGL gene were highly associated with FFA concentrations<sup>45</sup>.

Rapid adaptation of an organism to both feeding and fasting is mediated by the nervous system and hormonal signals<sup>46</sup>. In general, lipogenesis as a highly dynamic process featuring various regulatory mechanisms. It is driven by insulin, which is produced in pancreatic  $\beta$  cells and released upon elevated glucose levels, thus promoting nutrient clearance from the blood as well as adiposity<sup>47,48</sup>. Glucocorticoids, produced by adrenal glands, represent the second potent inducers of gluconeogenesis in liver and lipolysis in adipose tissue. They suppress  $\beta$ -oxidation and promote lipogenesis in liver<sup>49,50</sup>. Catecholamines (epinephrine and NE) promote lipolysis through  $\beta$ -adrenergic signaling, which increases *cyclic adenosine monophosphate* (cAMP) and *protein kinase A* (PKA) activity<sup>51</sup>. Additionally, glucagon promotes lipolysis in adipose tissue<sup>52</sup>,

## INTRODUCTION

---

although recent studies suggested that it also decreases FFA and TG levels due to its potential to increase FFA utilization in the process of  $\beta$ -oxidation<sup>53</sup>. Furthermore, gut-derived serotonin promotes lipolysis through the *5-hydroxytryptamine receptor 2b* (HTR2B)<sup>54</sup>. Additionally, *fibroblast growth factor 21* (FGF21) is another hormone that has been identified to promote lipolysis in adipose tissue upon fasting<sup>55</sup>.

All of this reflects the remarkable ability of adipose tissue to not only act as a lipid storage organ but as a highly active endocrine organ. It secretes a variety of bioactive peptides, also known as adipokines, which regulate numerous biological processes such as energy homeostasis, neuroendocrine, or immune function (Figure 2)<sup>56</sup>.

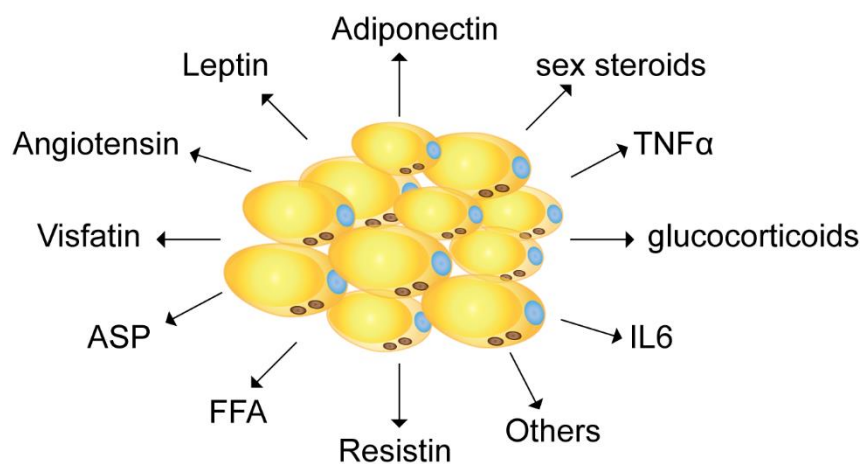


**Figure 2. Adipokines secreted from adipose tissue.** Some of the adipokines and other factors secreted by adipose tissue: adiponectin, leptin, angiotensin, resistin, visfatin, *acylation* stimulating protein (ASP), sex steroids, glucocorticoids, tumor necrosis factor  $\alpha$  (TNF $\alpha$ ), interleukin-6 (IL-6), and *free fatty acids* (FFAs) among others (modified from Coelho *et al.*, 2012)<sup>57</sup>.

Leptin, as one of the first identified adipokines, is secreted in direct proportion to the adipocyte mass. Released in response to food intake, it suppresses appetite by acting on surface receptors in the central nervous system. Individuals carrying mutations in either leptin or the leptin receptor present increased appetite and are prone to obesity and insulin resistance<sup>58</sup>. Another adipokine, the polypeptide adiponectin, has anti-obesity and anti-diabetic effects, since it helps to maintain insulin sensitivity. It is reduced in obese and insulin-resistant states and its level is increased upon weight loss<sup>59</sup>. Resistin is a key adipocyte signal in the induction of insulin resistance due to the activation of inflammatory processes. Resistin was shown to be elevated during



obesity and insulin resistance in mice<sup>60</sup> and its absence in mice caused a lower hepatic glucose production.<sup>61</sup>

Besides their energy-supportive purpose, especially brown and beige adipocytes have a thermogenic function. This function is highly controlled by the key regulator of adaptive thermogenesis, UCP1. Located in the inner mitochondrial membrane, it increases energy expenditure through uncoupling of oxidative metabolism from ATP production by dissipating the electrochemical gradient of the *electron transport chain* (ETC), which catalyzes a proton leak across the inner membrane<sup>2,62,63</sup>. This mechanism is triggered for example by cold exposure, sympathetic stimulation via  $\beta$ -adrenergic receptors or high levels of cAMP in brown and beige fat<sup>2,64</sup>. Several transcription factors, like *PR domain containing 16* (PRDM16) and *proliferator-activated receptor  $\gamma$  coactivator 1 $\alpha$*  (PGC-1 $\alpha$ ) are strong inducers of brown and beige adipocyte biogenesis<sup>65</sup>. Both regulators have been shown to induce thermogenesis by upregulating the expression of UCP1<sup>66</sup>. Additionally, catecholamine stimulation using NE increased uncoupled respiration and energy expenditure by mitochondrial fragmentation in brown adipocytes<sup>67</sup>. UCP1-deficient mice were able to tolerate coldness upon gradual reduction of ambient temperature<sup>68</sup>, suggesting the existence of alternative thermogenic pathways independent of the UCP1-based non-shivering thermogenesis. It was shown that Ca<sup>2+</sup>-ATPases in mitochondria of brown adipocytes generated heat independent of a proton gradient<sup>69</sup>. Increased *sarcoendoplasmic reticulum Ca<sup>2+</sup>-ATPase* (SERCA) activity was further found in subcutaneous adipocytes of mice lacking UCP1 upon long-term cold exposure. This led to elevated fat oxidation in this tissue and thus increased thermogenesis<sup>70</sup>. Moreover, glycerol-3-phosphate shuttle, activation, and lipid turnover have been proposed to act UCP1 independently<sup>71,72</sup>. Recently, another way to induce adaptive thermogenesis, independently of UCP1, has been proposed. Creatine kinase and genes associated with the creatine metabolism were shown to be induced upon cold in beige adipocytes increasing energy dissipation by accepting a phosphate group from ATP to drive *adenosine diphosphate* (ADP)-dependent respiration<sup>17</sup>.

### 1.1.3 Obesity

Obesity is a worldwide epidemic with increasing incidences over the years<sup>73</sup>. It is defined as an abnormal or excessive fat accumulation, leading to health impairments.

## INTRODUCTION

---

In general, weight gain and obesity premise a long-term positive energy balance in which the consumed energy in form of high caloric diets is greater than the energy expenditure via physical activity, basal metabolism, and adaptive thermogenesis. Genetic, environmental, and psychological factors also play a crucial role in this (Figure 3)<sup>74-76</sup>. In addition to the lifestyle, genome-wide association studies identified certain genes as being a risk factor for obesity. These genes are known to control insulin signaling, adipogenesis, lipid turnover, energy expenditure and adipokine secretion<sup>76</sup>. Hormonal dysregulation can promote development of obesity since various hormones regulate appetite and satiety<sup>77</sup>. Leptin as a signaling molecule binds to receptors in the hypothalamus and inhibits appetite depending on the adipose tissue energy reserves. It is known that chronically elevated leptin levels cause leptin resistance, further promoting obesity<sup>78</sup>.

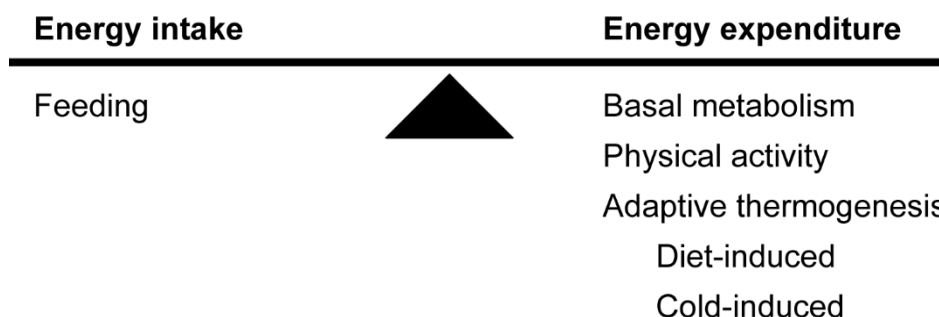


**Figure 3. Energy balance.** Obesity develops if energy intake, in the form of availability and composition of food exceeds energy expenditure, including basal metabolism, physical activity, and adaptive thermogenesis (modified from Spiegelman and Flier, 2001)<sup>74</sup>.

Obesity is defined as a *body mass index* (BMI) greater than 30 kg/m<sup>2</sup>, which is calculated by the quotient of body weight in kilograms divided by the height in meters squared. In 2016, the *world health organization* (WHO) estimated over 13 percent of the adult population (18 years and above) to be obese worldwide. In addition, 41 million children under 5 years old were found to be obese or overweight (BMI equal or greater than 25)<sup>75</sup>. Obesity is associated with the development of several diseases, such as *type 2 diabetes* (T2D), cardiovascular disease, *non-alcoholic fatty liver disease* (NAFLD), Alzheimer's disease, and cancer, increasing the mortality rate worldwide<sup>79</sup>. Under normal conditions, adipose tissue can balance the fat mass between storage and removal of TGs. During terms of food uptake, excess energy is stored in adipose tissue in form of TGs in lipid droplets. In the process of lipogenesis, FAs are

## INTRODUCTION

synthesized followed by TG synthesis. In situations of energy demand, these stored lipids are released in form of FFAs and glycerol during the process of lipolysis<sup>80</sup>. This important evolutionary function of the adipose tissue, fails in the obese population due to an excess of nutrients in the western world. Excess energy is stored in adipocytes to protect peripheral organs from lipotoxicity. During this process of increased lipogenesis in adipose tissue due to chronic overfeeding, adipocyte hypertrophy and hyperplasia occur, leading to adipocyte death, hypoxia, and fibrosis, as well as infiltration of immune cells, promoting a chronic low-grade inflammation<sup>81,82</sup>. The ability of dysfunctional adipocytes to store TGs becomes impaired. This leads to a storage of lipids in peripheral organs, such as liver and skeletal muscle. Further, circulating proinflammatory cytokines and FFAs derived from adipose tissue impair peripheral insulin sensitivity and lead to the development of T2D (Figure 4)<sup>3</sup>.

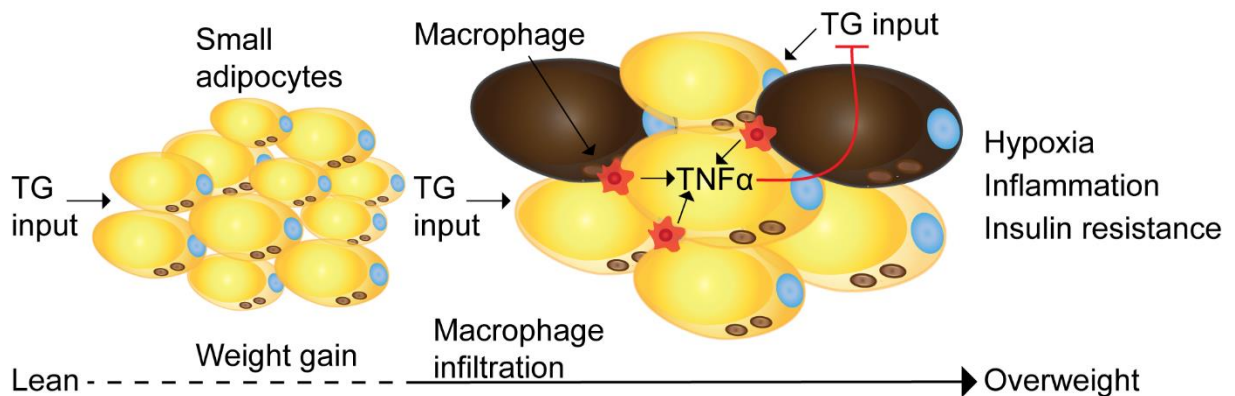


**Figure 4. High caloric food consumption leading to adiposity.** During excess food consumption, adipocytes increase in size and mass until they become maladaptive and undergo fibrotic changes. This leads to hypoxia and fibrosis, inducing inflammation and cell death, which in the long run causes insulin resistance (modified from Rosen and Spiegelmann, 2014)<sup>3</sup>. *Triglycerides* (TGs); *tumor necrosis factor  $\alpha$*  (TNF $\alpha$ ).

The infiltration of immune cells, especially macrophages, plays an important role in the adipose tissue biology. Adipose tissue is an important source of *tumor necrosis factor  $\alpha$*  (TNF $\alpha$ ) and cytokines, and their levels are highly elevated upon overnutrition<sup>83</sup>. These proinflammatory cytokines are mainly produced by macrophages, which infiltrate adipose tissue in the obese state and positively correlate with measures of insulin resistance in adipocytes as well as in liver and muscle in the periphery<sup>84,85</sup>. Furthermore, adipocytes produce *monocyte chemoattractant protein 1* (MCP1). Increased MCP1 levels in obese subjects stimulate macrophage infiltration of adipose tissue<sup>86</sup>. Both adipocytes and macrophages contribute to *interleukin 6* (IL-6)

concentrations in WAT with the abdominal fat presenting higher levels of IL-6 than subcutaneous fat<sup>87,88</sup>. In fact, the number of macrophages is higher in gonadal compared to subcutaneous fat depots<sup>89</sup>. This is consistent with the hypothesis that gonadal fat mass plays a more prominent role in obesity-associated pathology than overall adiposity<sup>90,91</sup>. Two different types of macrophages can be found in adipose tissue. M2 or “alternatively activated” macrophages mainly occur in adipose tissue of lean mice and are important for the tissue remodeling. The “classically activated” M1 macrophages have a proinflammatory phenotype and produce cytokines like TNF $\alpha$  and IL-6. They infiltrate the fat mass during progression of obesity<sup>92</sup>. It was demonstrated that macrophages in adipose tissue undergo a phenotypic switch from an anti-inflammatory M2-polarised state in lean mice to a M1 proinflammatory state during diet-induced obesity, thus contributing to insulin resistance<sup>93</sup>. In addition, HFD feeding in mice changes adipose tissue biology and its metabolism due to hypertrophic restructuring of the tissue. Changes in mitochondrial gene expression, loss of mitochondrial biogenetic capacity, as well as dysregulation of lipid, amino acid, and nucleotide metabolism can lead to increased adiposity, reduced energy expenditure, as well as glucose and insulin sensitivity compared to low-fat fed mice<sup>94</sup>.

### 1.1.4 Insulin resistance and T2D

Hyperglycemia, hyperinsulinemia, and hyperlipidemia are the major causes of T2D. Persistent obesity as one of the critical risk factors of insulin resistance leads to the development of T2D. Most obese individuals have elevated plasma levels of FFAs, glycerol, certain hormones, and cytokines, which are involved in the development of peripheral insulin resistance<sup>95,96</sup>. This results in impaired insulin-stimulated glucose uptake, since FFAs compete with glucose for substrate oxidation. In turn, inhibition of the pyruvate dehydrogenase, phosphofructokinase and hexokinase II activity leads to a reduced glucose uptake<sup>97</sup>. Moreover, this mechanism involves intracellular accumulation of fatty acyl-CoA, DAG, and activation of *protein kinase C* (PKC). This causes a phosphorylation of *insulin receptor substrate* (IRS) 1 and IRS2, which hinders the activation of *phosphoinositid-3-kinasen* (PI3K), thus diminishing the effects downstream of the *insulin receptor* (IR)<sup>98,99</sup>. Another lipid metabolite exacerbating insulin resistance is the sphingolipid ceramide. Saturated FAs, other than unsaturated FAs, induce the biosynthesis of ceramide, which impairs insulin action on glucose

uptake and glycogen synthesis by inhibiting the insulin stimulated *protein kinase B* (Akt/PKB) activation<sup>100</sup>. Hyperactive *mammalian target of rapamycin complex* (mTORC) 1, elicited through amino acids and insulin, also induces insulin resistance through *endoplasmic reticulum* (ER) stress, thereby causing the generation of *reactive oxygen species* (ROS) leading to chronic inflammation<sup>101,102</sup>. Additionally, high glucose and fat intake as well as hypertrophic adipocytes induce inflammation through increased oxidative stress and production of proinflammatory cytokines like TNF $\alpha$ , IL-6, resistin, and MCP1<sup>103,104</sup>. Infiltration of macrophages amplifies the inflammation signal by expression of additional proinflammatory genes<sup>85</sup>. Many of these proinflammatory factors like TNF $\alpha$  or IL-6 activate the *nuclear factor 'kappa-light-chain-enhancer' of activated B-cells* (NF- $\kappa$ B) pathway, through inhibition of the *inhibitor of kappa B (I $\kappa$ B)-kinase-complexes* (IKK), and the *c-Jun NH2-terminal kinase* (JNK) pathway<sup>104</sup>. Moreover, obesity-induced ROS, ER stress, and ceramides have also been shown to activate JNK as well as NF- $\kappa$ B<sup>105-107</sup>. JNK catalyzes an inhibitive phosphorylation on a serine residue of IRS1 diminishing its tyrosine phosphorylation activity, thus impairing signaling transduction<sup>108,109</sup>. The observed effects of obesity-induced activation of NF- $\kappa$ B are due to expression of NF- $\kappa$ B target genes<sup>96</sup>. TNF $\alpha$  for example, reduces insulin sensitivity by *mitogen-activated protein kinase* (MAPK) pathway-dependent phosphorylation of a serine within IRS1<sup>110</sup>. It activates the protein tyrosine phosphatase SH-PTPase, which dephosphorylates a tyrosine residue of IRS1 causing a disruption in the insulin signaling cascade<sup>111</sup>. Other target genes of NF- $\kappa$ B like resistin act within a positive feedback loop and increase the expression of inflammatory cytokines by activation of NF- $\kappa$ B<sup>112</sup>.

The effect of obesity on insulin sensitivity depends on the adipose tissue depot that is predominately expanded. *Gonadal WAT* (gWAT) that is located between organs in the abdominal cavity is known to be more lipolytic and more prone to inflammatory cytokine production than other fat depots. Therefore, it is more associated with insulin resistance and impairments in insulin signaling resulting in the development of T2D<sup>113</sup>. T2D is characterized by hyperglycemia and hyperlipidemia and often occurs together with other metabolic disorders such as NAFLD and atherosclerosis<sup>74</sup>. Two features are particularly relevant for the development of T2D. Primarily, it develops during prolonged peripheral insulin resistance in muscle and liver. However, obesity-induced insulin resistance is not constrained leading directly to T2D. Individuals with healthy  $\beta$ -

cells can initially compensate insulin resistance by an increased  $\beta$ -cell mass with consequential higher release of insulin to maintain blood glucose levels. Nevertheless, prolonged periods of increased insulin demand in the periphery in combination with a metabolic overload results in ER and oxidative stress in pancreatic islets. Consequently, a  $\beta$ -cell failure results in inadequate expansion of  $\beta$ -cell mass or failure of the existing  $\beta$ -cell mass to respond to glucose<sup>114,115</sup>. Recently, mitochondrial dysfunction was proposed to cause both insulin resistance in the periphery and impairment of glucose-induced insulin secretion in  $\beta$ -cells<sup>116</sup>. Different genes have been identified to be associated with this  $\beta$ -cell dysfunction<sup>117</sup>. Inefficient response of cells to secretagogues is another reason for  $\beta$ -cell failure. This stimulation is needed to trigger insulin release by  $\beta$ -cells<sup>47</sup>. Furthermore, insufficient insulin signaling leads to inadequate suppression of hepatic *de novo* glucose production (gluconeogenesis). It promotes release of glucose stores (glycogenolysis), and suppresses hepatic glucose uptake. Altogether, these factors greatly promote hyperglycemia. Similarly, lipogenesis in hepatocytes and adipocytes as well as elevation in lipolysis promotes hyperlipidaemia<sup>46,118</sup>. The resulting elevated glucose and FFA levels reduce secretion and production of insulin and impair  $\beta$ -cell health<sup>119-121</sup>. Overall, these effects can slowly lead to the development of T2D over several years.

### **1.2 Mitochondrial dynamics in adipocytes**

Mitochondria play a central role in the regulation of energy dissipation and thermoregulation in brown and beige/brite adipocytes. Mitochondria undergo constant changes in their morphology, including size and shape in order to respond to changes in the intracellular environment. Mitochondrial dynamics, fission and fusion, are necessary to maintain the cellular homeostasis<sup>122,123</sup>. Changes in the mitochondrial architecture represent an adaption to the cellular bioenergetic needs. Mitochondrial fusion is rather stimulated in response to energy demand or stress. It enables the spreading and exchange of proteins, substrates, and mitochondrial DNA through the network enhancing the stability of the mitochondria<sup>124</sup>. Mitochondrial fission is increased under conditions of excess energy supply. It allows an increase in mitochondrial number and capability during cell division. It further controls the mitochondrial quality by removing damaged mitochondria via mitophagy<sup>125,126</sup>. The mitochondrial fusion process is mainly conducted by *mitofusin* (MFN) 1, MFN2, and

## INTRODUCTION

*optic atrophy-1* (OPA1). MFN1 and MFN2 are anchored in the outer mitochondrial membrane with a cytosolic oriented *guanosine triphosphate hydrolase* (GTPase) domain, allowing the fusion of opposing mitochondria on their outer membrane. OPA1, located in the intermembrane space, coordinates the inner mitochondrial membrane fusion. *Dynamin related protein 1* (DRP1), *mitochondrial fission factor* (MFF), and *fission 1 homolog protein* (FIS1) are the key regulators of the mitochondrial fission. DRP1 is generally found in the cytosol, but during the fission process it is recruited to the outer mitochondrial membrane, where FIS1 and MFF function as adaptor proteins for DRP1 (Figure 5)<sup>127,128</sup>.

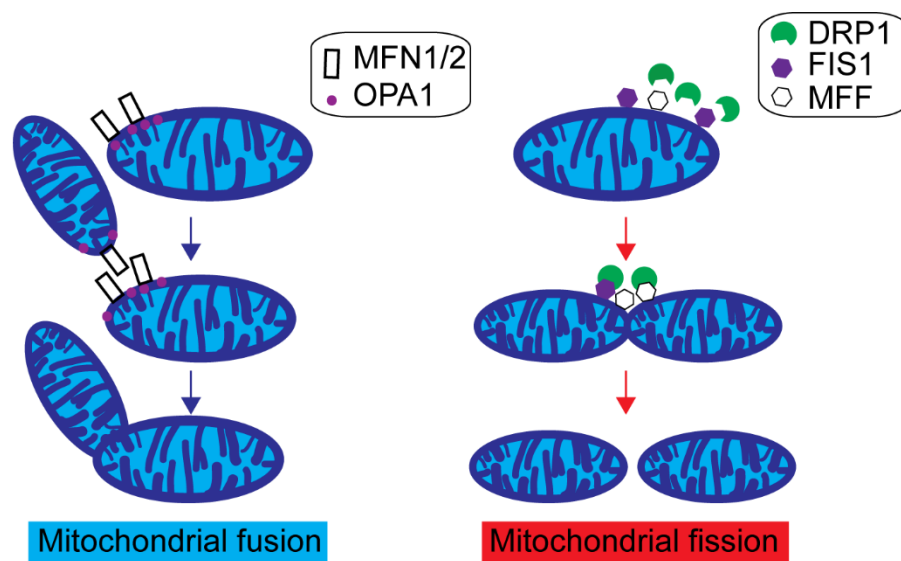


**Figure 5. Mitochondrial fission and fusion processes.** Under physiological conditions, the mitochondria continuously change their morphology through fusion (left) and fission (right) to maintain the cellular homeostasis. *Mitofusin 1* (Mfn1); *mitofusin 2* (Mfn2); *fission protein-1* (Fis1); *mitochondrial fission factor* (Mff); *dynamin-related protein-1* (DRP1); *optic atrophy-1* (OPA1) (modified from Saotome *et al.*, 2014)<sup>127</sup>.

Recently, it was proposed that the induction of mitochondrial fragmentation also promotes decoupling activity in adipocytes. The master regulator of adipocytes, *peroxisome proliferator-activated receptor* (PPAR)  $\gamma$ , transcriptionally induces *B-cell lymphoma 2 (BCL2) interacting protein 3* (Bnip3) to regulate the mitochondrial fusion-fission balance by increasing mitochondrial fragmentation, which protects mice from developing diabetes and fatty liver disease<sup>129</sup>. NE was also shown to induce mitochondrial fragmentation in brown adipocytes, thus promoting uncoupled respiration and increased energy expenditure. This leads to a shift of nutrient oxidation towards heat production, rather than mitochondrial ATP synthesis. Increased fission

was characterized by OPA1 cleavage as well as DRP1 phosphorylation<sup>67</sup>. *AMP-activated protein kinase* (AMPK) was suggested to promote mitochondrial fragmentation in the presence and absence of mitochondrial stress in various cell types (hepatocytes and MEFs, but mostly human U2OS osteosarcoma cells). This is one pathway inducing mitophagy after prolonged energy stress by initiating the replacement of damaged mitochondria through the biogenesis of new ones<sup>130</sup>.

### **1.3 *Protein kinase D* (PKD)**

#### **1.3.1 Structure and signaling**

The PKD family of serine/threonine protein kinases was first identified in 1994 and belongs to the *Ca<sup>2+</sup>/calmodulin-dependent protein kinase* (CAMK) superfamily<sup>131,132</sup>. It comprises three different isoforms in mammals encoded by three different genes, *PKD1*, *PKD2*, and *PKD3*, which are differentially expressed in cells and tissues. PKD is a DAG and PKC effector that integrates multiple hormonal and nutritional inputs. It has further been shown to be involved in the regulation of various fundamental biological processes<sup>133</sup>. All mammalian PKD isoforms share a similar domain architecture. Two highly conserved N-terminal *cysteine-rich domains* (C, C1a and C1b) bind to DAG and phorbol esters. The central autoinhibitory *pleckstrin homology* (PH) domain is mainly involved in regulatory mechanisms and flanked by the catalytically active C-terminal kinase domain (Figure 6)<sup>134,135</sup>.



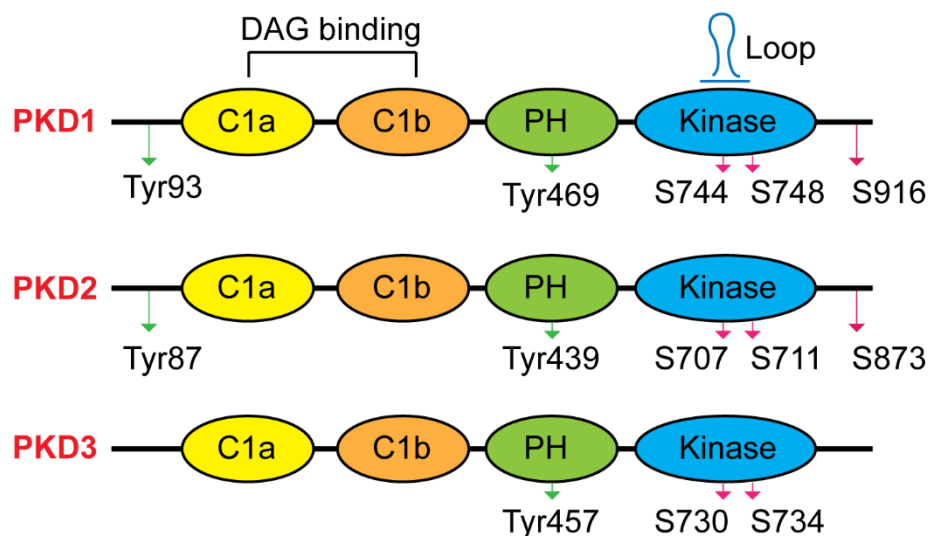


**Figure 6. PKD isoforms.** Domain organization of the three mammalian PKD isoforms (modified from Fu and Rubin, 2011)<sup>136</sup>. *Protein kinase D* (PKD); *diacylglycerol* (DAG); *cysteine-rich domains* (C); *pleckstrin homology* (PH); *tyrosine* (Tyr); *serine* (S).

Since stimulation of two major types of cell surface receptors, *G-protein coupled receptors* (GPCR) and receptor tyrosine kinases, can result in elevation of DAG, PKD isoforms are activated in response to a plethora of auto-, para-, and endocrine factors, neurotransmitters as well as nutrients. The vast number of PKD activators includes acetylcholine, extracellular ATP, vasoactive peptides, bioactive lipids, chemokines and hormones like gastrin, neurotensin and osteocalcin amongst others<sup>133,137,138</sup>. PKD in its inactive state is mainly located in the cytosol of resting cells. Activation of PKD occurs by ligand binding of GPCR or tyrosine kinase receptors. This leads to activation of *phospholipase C* (PLC)  $\beta$  or  $\gamma$ , which hydrolyze *phosphatidylinositol-4,5-bisphosphate* (PIP<sub>2</sub>) into its derivatives DAG and *inositol-1,4,5-trisphosphate* (IP<sub>3</sub>). Membrane-associated DAG in turn activates PKC and recruits cytosolic PKD to the plasma membrane through its C1a and C1b<sup>139</sup>. Active PKC phosphorylates two serine residues (S744, S748), which are located in the PKD activation loop. This posttranslational modification causes a conformational change in the protein structure, which enhances its kinase activity<sup>134</sup>. Additionally, PKD gets activated by Ca<sup>2+</sup> and the DAG activated *conventional PKC* (cPKC)  $\alpha$ ,  $\beta$ I and  $\beta$ II<sup>140</sup>. The phosphorylation of S744 in PKD1 is crucial for its catalytic activity during short-term and long-term stimulation and mediates further autophosphorylation of S748 and S916<sup>141,142</sup>. S916 is exclusive to PKD1 and PKD2 and is located within the carboxy terminal motif that binds to *postsynaptic density 95/Discs large/zona occludens 1* (PDZ) of substrates or scaffold

proteins<sup>143</sup>. Thereby it reverses the anchoring of PKD to PDZ domains and acts as a priming site needed for autophosphorylation of S748. Simultaneously phosphorylated S748 and S916 might lead to a faster deactivation of S744<sup>144</sup>. During long-term stimulation, S748 stays phosphorylated independently of PKC by autophosphorylation, which might mediate long-term effects of PKD on cellular processes<sup>141,142</sup>. The catalytic activity of all three PKD isoforms can be inhibited by the selective inhibitors 2,3,4,5-tetrahydro-7-hydroxy-1H-benzofuro[2,3-c] azepin-1-one (CID 755673)<sup>145</sup> and 2-[4-[[[(2R)-2-aminobutyl]amino]-2-pyrimidinyl]-4-(1-methyl-1H-pyrazol-4-yl)] phenol dihydrochloride (CRT 0066101)<sup>146</sup>.

### 1.3.2 The role of PKD in health and disease

Previous studies implicated different PKD isoforms in the regulation of many fundamental cellular processes depending on the cell type, substrate, and intracellular localization. As cellular linchpins, they are involved in muscle differentiation, pathophysiological heart remodeling, carcinogenesis, immune response, blood coagulation, insulin secretion, actin remodeling, *trans-Golgi network* (TGN) dynamics, cell proliferation, migration, oxidative stress, and apoptosis (Figure 7)<sup>133,147-162</sup>.

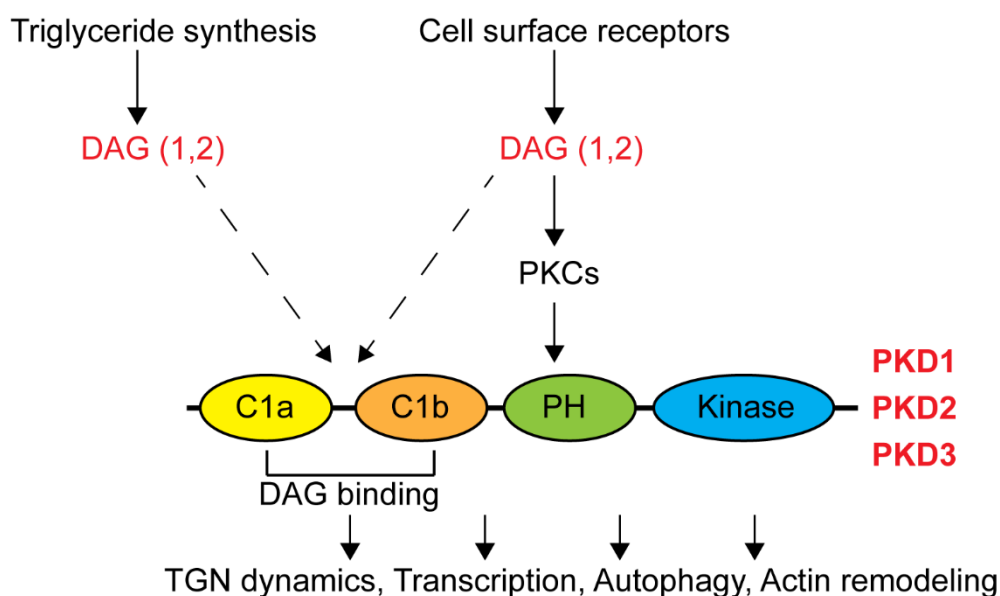


**Figure 7. Signaling pathway of the PKD isoforms.** PKD either gets activated through PKC after ligand binding to the receptor or through DAG directly during TG synthesis. PKD isoforms have been shown to be involved in many fundamental cellular processes. *Protein kinase C* (PKC); *diacylglycerol* (DAG); *protein kinase D* (PKD); *cysteine-rich domains* (C); *pleckstrin homology* (PH); *trans-Golgi network* (TNG).

## INTRODUCTION

---

On the cellular level, PKD activity depends on its localization. It is found in the cytosol of resting cells. Upon activation, PKD is recruited to different cellular compartments such as the plasma membrane, cytoplasm, mitochondria, TGN, or nucleus<sup>163</sup>. In lymphocytes, PKD is located at the plasma membrane during the initial activation phase, whereas during sustained responses to antigen receptor ligation, it functions within the cytosol<sup>164</sup>. Another study showed that upon T cell activation PKD rapidly, but transiently, associates with the immune synapse. In this setting, DAG binding to PKD is essential for its membrane translocation<sup>165</sup>. At the mitochondria, PKD1 was shown to be activated in response to ROS upon formation of mitochondrial DAG, which is binding to PKD1 and triggering its translocation to the mitochondria<sup>166</sup>. In general, ROS were also shown to activate PKD1 through the Src-Abl-pathway. Furthermore, oxidative stress activates PKC leading to an increased PKD phosphorylation and kinase activity. Fully activated PKD1 in turn results in an active NF- $\kappa$ B pathway and cell survival<sup>161</sup>. In neurodegenerative diseases PKD1 was identified as a key kinase to support cell survival and to protect neurons from oxidative stress, which can also be explained by a PKC-dependent phosphorylation of PKD1<sup>162</sup>.

PKD is translocated to the Golgi complex through DAG binding to C1a, where it is involved in vesicle formation and fission<sup>167,168</sup>. Generation of *phosphatidylinositol 4-phosphate* (PI4P) at the TGN through PKD phosphorylation of *phosphatidylinositol 4-kinase III $\beta$*  (PI4KB), a key protein required for fission of the TGN to plasma membrane carriers, recruits the machinery, which is crucial for vesicle formation<sup>169-171</sup>. PKD1 was shown to be involved in the regulation of insulin secretion from pancreatic  $\beta$ -cells and therefore in the regulation of glucose homeostasis. It was demonstrated that PKD1 is negatively modulated by p38 $\delta$  MAPK and active PKD1 promotes insulin secretion by acting at the TGN, where granules containing insulin are generated, thus leading to an insulin granule secretion. Activation of PKD1 also improves  $\beta$ -cell survival presumably by distinct mechanisms<sup>156,157</sup>. Another study demonstrated that p38 $\delta$  also counteracts the activity of PKD1 in neutrophils and that inactivation of PKD1 leads to increased lung inflammation. Importantly, *phosphatase and tensin homolog* (PTEN) activity is conversely regulated by p38 $\delta$  and PKD1 in neutrophils, thereby controlling their migration and chemotaxis<sup>154</sup>.

Activated PKD can also accumulate in the nucleus through DAG binding to C1b, where it functions as a transcriptional regulator for certain genes, thus interfering with different

signaling pathways. The influence of PKD on cell proliferation and differentiation is linked to the *extracellular regulated protein kinase* (ERK) cascade. PKD seems to increase the duration of this pathway leading to accumulation of immediate gene products that stimulate cell cycle progression<sup>142,172</sup>. Importantly, PKD1 can also promote transcription by regulating the activity of *class II histone deacetylases* (HDACs). In the phosphorylated state, these HDACs bind to 14-3-3 proteins leading to their release from *deoxyribonucleic acid* (DNA), thereby enabling the expression of different genes<sup>153,173</sup>. This mechanism is of high relevance in the regulation of heart remodeling after hypertrophic stimuli. Mice lacking PKD1 specifically in cardiomyocytes, are partially resistant to pathological heart remodeling due to enhanced nuclear location of class II HDACs that suppress transcription of key genes mediating pathological heart remodeling<sup>150</sup>. In skeletal muscle, PKD1 phosphorylates HDACs and thereby activates *myocyte enhancer factor-2* (MEF-2) leading to an increased expression of type I, slow-twitch fibers that mediate muscle endurance<sup>151</sup>. Furthermore, PKD1 was found to enhance transcriptional activity through phosphorylation of *cAMP-response element-binding protein* (CREB)<sup>174</sup>. In the context of heart remodeling CREB was identified as a substrate of PKD. The PKD-CREB phosphorylation pathway leads to the activation of a *cAMP response element* (CRE)-responsive promoter in the nucleus of cardiomyocytes, suggesting participation of PKD in cardiac remodeling<sup>175</sup>. Moreover, PKD interferes with other signaling cascades like MAPK signaling<sup>176</sup>. These regulators of transcription are central for regulation of glucose and lipid metabolism in liver and adipose tissue<sup>153,176-178</sup>. Furthermore, a genome-wide association study has identified PKD1 as one of the 97 body mass index-associated single nucleotide polymorphisms<sup>179</sup>. However, the impact of PKD on the regulation of metabolic homeostasis and its physiological role in adipose tissue remains yet unknown.

## 1.4 AMPK

### 1.4.1 AMPK regulation

AMPK is a serine/threonine kinase and has been identified as one of the key regulators of cellular energy homeostasis and whole-body energy balance. This heterotrimeric complex consists of a catalytic  $\alpha$ -subunit and two regulatory  $\beta$ - and  $\gamma$ -subunits, which

have at least two different isoforms ( $\alpha 1$ ,  $\alpha 2$ ,  $\beta 1$ ,  $\beta 2$ ,  $\gamma 1$ ,  $\gamma 2$ , and  $\gamma 3$ )<sup>180,181</sup>. Each isoform of the AMPK subunits shows differential tissue expression and acts in diverse molecular pathways depending on the physiological conditions. AMPK can be regulated allosterically as well as by post-translational modifications. The most prominent AMPK activation mechanism is through phosphorylation of threonine 172 (T172), which is located within the  $\alpha$ -subunit. This activation is tightly regulated by different phosphatases and kinases such as *liver kinase B 1* (LKB1). Furthermore, AMP and ADP bind to the  $\gamma$ -subunit, allosterically activating the kinase and inhibiting its dephosphorylation, whereas ATP antagonizes this activation. The AMPK activator, *5-aminoimidazole-4-carboxamide 1- $\beta$ -d-ribofuranoside* (AICAR), is phosphorylated to the nucleotide *5-amino-4-imidazolecarboxamide riboside 5'-monophosphate* (ZMP), thus mimicking AMP leading to AMPK activation without changing adenine nucleotide ratios (Figure 8)<sup>182</sup>.

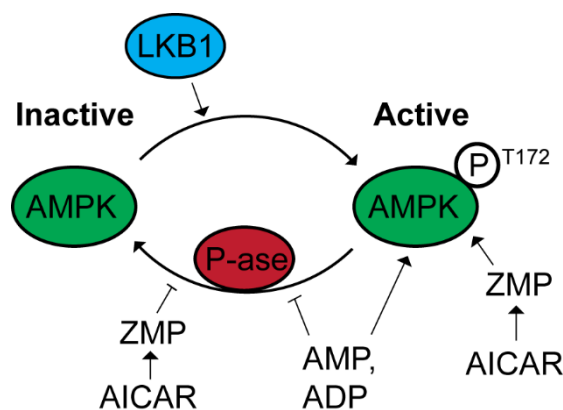


**Figure 8. Activation of AMPK.** AMPK is activated upon phosphorylation of T172 in the  $\alpha$ -subunit. AMP and ADP bind to the  $\gamma$ -subunit activating AMPK and inhibiting dephosphorylation at T172 by a still unknown protein phosphatase (P-ase). In response to AICAR treatment, the intracellular ZMP levels increase, leading to an activation of AMPK (modified from Bijland *et al.*, 2013)<sup>182</sup>. AMP-activated protein kinase (AMPK); *liver kinase B 1* (LKB1); adenosine monophosphate (AMP); adenosine diphosphate (ADP); *5-aminoimidazole-4-carboxamide 1- $\beta$ -d-ribofuranoside* (AICAR); protein phosphatase (P-ase); threonine 172 (T172).

During high AMP:ATP ratios, when cellular energy levels are low, AMPK is activated and increases catabolic processes, such as glucose uptake, mitochondrial biogenesis, and FAO, while anabolic processes such as protein and TG synthesis as well as mTOR-mediated protein translation are inhibited<sup>183</sup>. Thus, AMPK is highly regulated by the nutritional state. Insulin, for instance, was shown to inhibit AMPK through Akt phosphorylation at S485 in the  $\alpha 1$ -subunit, which blocks upstream kinases from phosphorylating T172<sup>184</sup>. DAG levels, which activate PKD1, are usually increased during hyperglycemia and hyperlipidemia. Indeed, a recent study indicated that in

muscle cells, PKD1 phosphorylates S485/491 of the AMPK  $\alpha$ -subunits and inactivates the kinase activity of the whole complex resulting in impaired insulin signaling in these cells<sup>185</sup>.

### 1.4.2 The function of AMPK in adipose tissue metabolism

In adipose tissue, AMPK is activated through exercise and fasting, when energy demand is high<sup>186</sup>. Therefore, AMPK is involved in regulating many processes of energy homeostasis in adipocytes (Figure 9)<sup>182</sup>. AMPK was shown to inhibit protein synthesis during energy stress by indirectly inhibiting mTORC1 through the phosphorylation of the mTOR binding partner raptor, leading to a cell cycle arrest induced by energy stress<sup>187</sup>. In addition, *de novo* lipogenesis is inhibited by AMPK, whereas FA uptake and  $\beta$ -oxidation are activated. ACC, which catalyzes the rate-limiting step of FA synthesis from acetyl-CoA, is inhibited by AMPK-mediated phosphorylation of S79 on ACC1 or S212 on ACC2<sup>188</sup>. Additionally, *sterol regulatory element-binding protein* (SREBP) 1c, a transcription factor promoting lipogenic enzyme expression, such as ACC1 and FAS, is inhibited by AMPK in the liver<sup>189</sup>. AMPK also enhances the energy metabolism of cells by increasing its FAO due to an increase in *carnitine palmitoyl-transferase 1* (CPT1), the rate-limiting enzyme of FA entry into the mitochondria necessary for  $\beta$ -oxidation. The inhibitory phosphorylation of ACC by AMPK leads to reduced concentrations of malonyl-CoA, a potent allosteric inhibitor of CPT1<sup>188</sup>. FAO is also indirectly regulated through AMPK by controlling the mitochondrial homeostasis. AMPK triggers the mitochondrial content and fission through Mff<sup>130</sup> and PGC-1 $\alpha$ , a cofactor promoting the transcription of nuclear-encoded mitochondrial genes<sup>190</sup>.

Another way to induce energy metabolism in adipocytes is the so-called browning of WAT. *Inositol hexakisphosphate kinase 1* (IP6K1) was previously identified to modulate AMPK-mediated adipose tissue browning and thermogenesis in order to regulate the global energy homeostasis. Thus, mice lacking IP6K1 in adipocytes showed enhanced AMPK activity leading to increased beiging of adipocytes and thermogenic energy expenditure, thereby protecting mice from HFD-induced weight gain<sup>191</sup>. On the other hand, mice lacking the  $\beta$ -subunits in adipocytes were cold intolerant and showed reduced thermogenesis, indicating a defect in BAT and beige fat. They also showed impairments in mitochondrial structure and function and upon

HFD, mice developed liver steatosis and insulin resistance<sup>192</sup>. Another study revealed that reduced AMPK activity led to an increased gonadal adipocyte inflammation, which further promotes whole-body insulin resistance in obese individuals<sup>193</sup>.

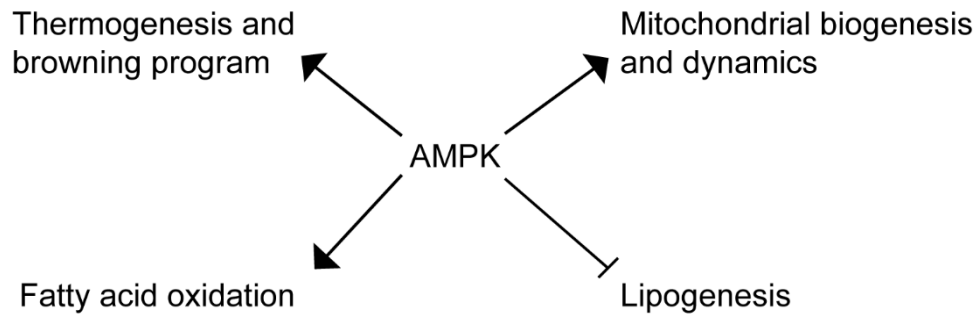


**Figure 9. The role of AMPK in the regulation of energy homeostasis in adipocytes.** AMPK has been shown in several studies to promote mitochondrial biogenesis, thermogenesis, and FAO, whilst suppressing lipogenesis. *AMP-activated protein kinase* (AMPK).

Several studies propose AMPK to be important for the treatment of obesity, insulin resistance and NAFLD, since global deletion of AMPK subunits results in a metabolic phenotype. *Ampka2*<sup>-/-</sup> mice, for example, demonstrated high glucose levels in the fed stage and during an oral glucose challenge, which was associated with low levels of insulin, indicating that AMPK $\alpha$ 2 regulates insulin signaling<sup>194</sup>. Upon HFD-feeding, mice lacking the  $\alpha$ 2-subunit exhibited increased body weight and fat mass, caused by enlargement of the pre-existing adipocytes and hypertrophy due to TG accumulation. Despite the increased adiposity, glucose tolerance and insulin sensitivity in *Ampka2*<sup>-/-</sup> mice on a HFD were similar to those of wild-type mice<sup>195</sup>. Furthermore, animals lacking the  $\beta$ 2-subunit of AMPK showed classical symptoms of a metabolic syndrome, including hyperglycemia, glucose intolerance, and insulin resistance when maintained on a HFD<sup>196</sup>.

### 1.5 The impact of the $\beta$ 3 adrenergic receptor on adipocyte metabolism and regulation of its abundance

The  $\beta$ 3 adrenergic receptor (ADRB3) belongs to a superfamily of integral membrane proteins and is associated with a rather diverse intracellular G-protein complex. This complex is able to recognize extracellular ligands, which in the first step bind to the protein. Ligand recognition leads to a conformational change of the receptor, which triggers an intracellular signaling cascade. In case of ADRB3, catecholamines act as

a ligand. The activated G-protein triggers a downstream cascade in order to produce the second messenger cAMP. ADRB3 is predominantly expressed in white and brown adipocytes<sup>197</sup> and involved in the regulation of lipolysis and non-shivering thermogenesis. Expression and functional activity of this receptor are impaired upon obesity<sup>17,198-200</sup>. Furthermore, *CCAAT/enhancer-binding protein (C/EBP)  $\alpha$*  was identified as a key transcriptional regulator of ADRB3 during adipocyte differentiation<sup>201</sup>. In general, the C/EBP family belongs to the *basic leucine zipper (bZip)* transcription factors, which consist of a C-terminal leucine zipper domain, important for dimerization, and a basic domain for DNA binding. Out of the C/EBP family, C/EBP $\alpha$ ,  $\beta$ , and  $\delta$  are expressed in WAT and BAT and are essential for terminal adipocyte differentiation<sup>202,203</sup>. Together with PPAR $\gamma$ , these four adipogenic regulators have been identified to play a key role in adipogenesis. While C/EBP $\beta$  and  $\delta$  expression is rapidly induced at the early stage of differentiation, PPAR $\gamma$  and C/EBP $\alpha$  are subsequently activated by them and regulate each other's expression. Furthermore, they are important regulators of the brown and beige adipocyte thermogenic programme<sup>204,205</sup>. Moreover, deletion of C/EBP- $\alpha$  and C/EBP- $\delta$  in mice results in reduction of UCP1 expression in adipose tissue<sup>202</sup>. These findings suggest an important role of C/EBPs in the regulation of adipocyte differentiation and non-shivering thermogenesis by regulating ADRB3 expression.

### **1.6 Aim of the study**

Excess of energy intake over energy dissipation results in obesity, insulin resistance, and can lead to the development of T2D<sup>46,74</sup>. Obesity-related metabolic overload results in the accumulation of different species of lipids, including DAG in multiple tissues<sup>118</sup>. Nevertheless, DAG-evoked signaling and its effects on adipocyte function are still poorly characterized. PKD1 is a DAG and PKC effector that integrates multiple hormonal and nutritional inputs. It is further involved in the regulation of numerous fundamental biological processes. However, the impact of PKD1 in the regulation of adipose tissue function remains unknown.

Whilst white adipocytes are known to store excess energy in form of TGs, which can be released in form of FFAs during high energy demand<sup>13</sup>, brown adipocytes dissipate energy in form of heat with the help of UCP1<sup>3</sup>. It is of high interest to also increase energy dissipation in white adipocytes in order to prevent the development of obesity.



## INTRODUCTION

---

One possibility is to increase beiging of the white adipose tissue. In this study, the role of PKD1 in the regulation of adipose tissue function under physiological and pathophysiological conditions was investigated. First, the role of PKD1 in the adipocyte regulation was assessed *in vitro* using different stable cell lines, which were either lacking PKD1 or overexpressing a constitutive active form of the kinase.

In order to generate efficient antidiabetic agents, it is of great interest to further understand the signaling cascades of new potential targets. Therefore, a knockout mouse strain was generated, specifically lacking PKD1 in adipocytes, to further study the role of PKD1 during the development of obesity, insulin resistance, and T2D. With this tool, the impact of PKD1 on energy metabolism of adipocytes and the development of obesity as well as associated diseases can be investigated (Figure 10).

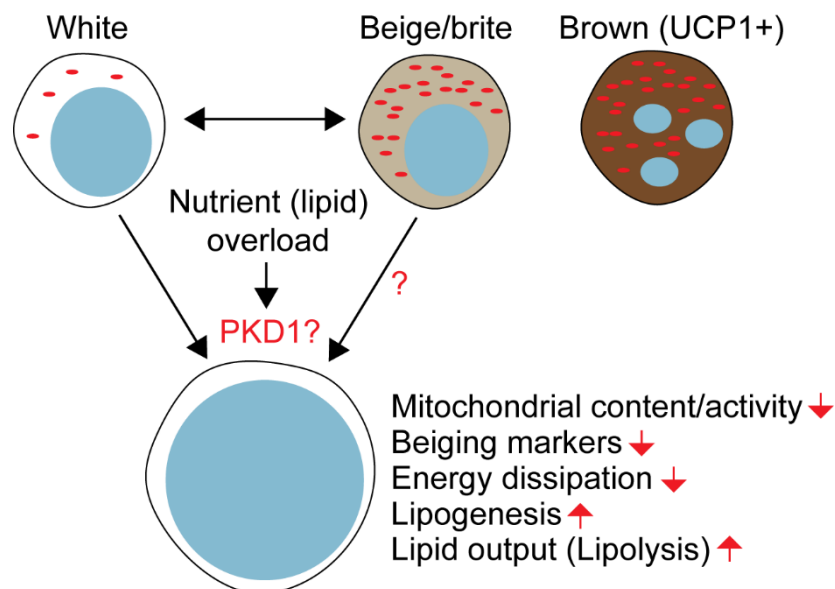


**Figure 10. The potential impact of PKD1 in the development of adipocyte dysfunction and obesity.** Beiging occurs in white adipose tissue increasing the energy metabolism of the cells. Upon obesity, a trans-differentiation of beige back to white adipocytes occurs, leading to a reduction of the cellular mitochondrial content, decreased expression of beiging markers, and reduced energy expenditure. On the other hand, lipogenesis and lipolysis are enhanced, further promoting adiposity of the cells, which will lead to the development of metabolic disorders. The aim of this study was to investigate the role of PKD1 in these complex processes. *Protein kinase D* (PKD); *uncoupling protein 1* (UCP1).

## 2 MATERIALS AND METHODS

### 2.1 Materials

#### 2.1.1 Equipment and reagents

Equipment and reagents used in this thesis are listed in the appendix under 7.1.1 and 7.1.2.

#### 2.1.2 Media and buffers

Media and buffers used in this thesis are listed in the appendix under 7.1.3 and 7.1.4.

#### 2.1.3 Mice

All the animal studies conducted in this thesis were approved by the local institutional animal care (Regierung von Unterfranken, Germany) and performed according to the guidelines and state regulations. Animal protocol number AK 55.2-2531.01-124/13, approved on 28.01.2014.

Conditional deletion of PKD1 was generated by cross-breeding *PKD1 flox/flox* (*PKD1f/f*) mice<sup>150</sup> (exons 12 and 14 flanked by loxP sites) with mice carrying the Cre-recombinase under the adiponectin promoter<sup>160</sup> or adiponectin promoter-driven Cre-ERT mice<sup>206</sup>. Due to this system, the PKD1 (also known as Prkcm) allele was specifically deleted in adipocytes. Eric Olson generated the *PKD1f/f* mice by inserting the loxP sites into the introns of the PKD1 locus to flank exons 12 through 14, as the N-terminal region of the catalytic domain of PKD1 is encoded by exon 13 and 14, including the ATP binding motif that is essential for kinase function. Expression of Cre recombinase leads to the deletion of exon 12, 13 and 14, the region between the loxP sites, eliminating the function of PKD1 as a kinase (Figure 11)<sup>150</sup>. Breeding *PKD1f/f* mice to either Adiponectin-Cre or Adiponectin-Cre-Ert transgenic mice resulted in mice with a targeted deletion of PKD1 specifically in adipocytes of white and brown adipose tissue from the beginning or after injection of 100 mg/kg Tamoxifen for 5 consecutive days to induce depletion.

## RESULTS

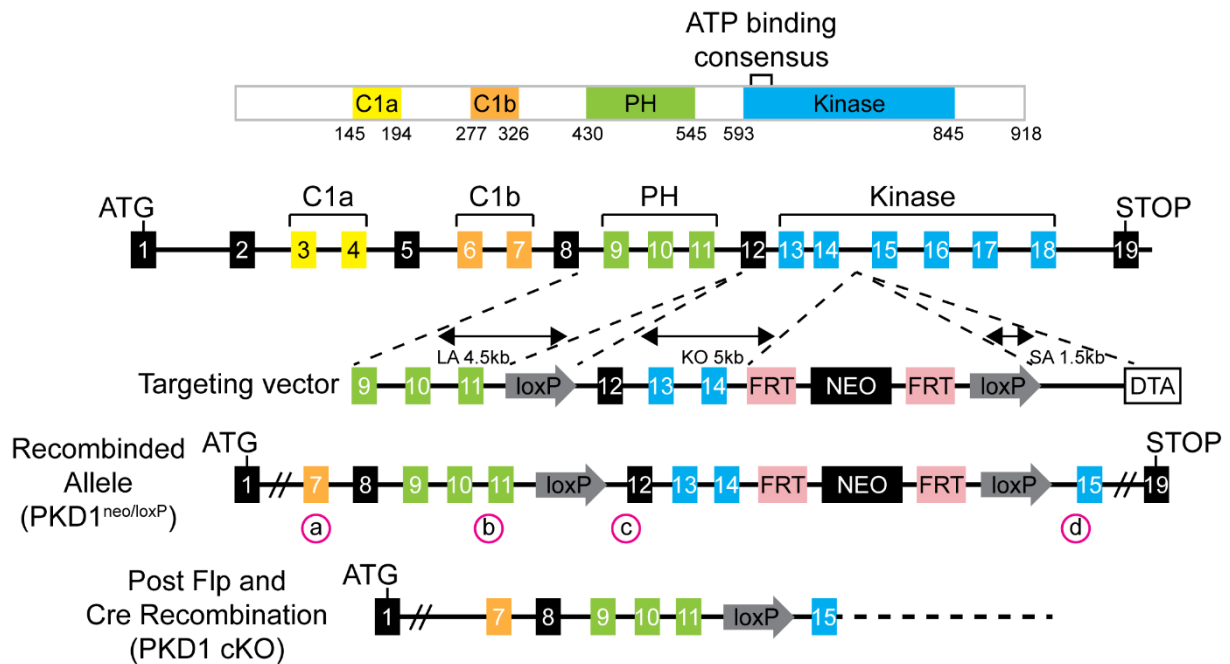


**Figure 11. Scheme of mutation in mice to generate conditional PKD1 deletion.** Targeting strategy and PKD1 mouse locus. Since exons 13 and 14 encode the N-terminal region of the kinase domain including the ATP-binding motif, the LoxP sites were inserted in the introns flanking exons 12 and 14. Breeding heterozygous mice to hACTB:FLPe transgenic mice resulted in the removal of the NEO in the mouse germ line (modified from Fielitz *et al.*, 2008<sup>150</sup>). Cysteine-rich domains (C); pleckstrin homology (PH); adenosine triphosphate (ATP); neomycin resistance cassette (NEO).

Genotyping protocols for the given mouse lines are available from Jackson Laboratory and will be explained in detail in chapter 2.2.1. All animals were kept in autoclaved cages from Tecniplast in a green Line IVC-rack system and handled in laminar flow workstations. Mice were housed in groups of maximal five animals with a 12-hours (h) light/dark cycle at a constant temperature of 23 °C and 55% humidity. Mice were provided with sterile water and irradiated rodent *normal diet* (ND) (sniff Spezialdiäten) at all times, which was only removed or exchanged if necessary for an experiment. Whenever indicated, HFD (ResearchDiets) was given to mice. Under thermoneutral conditions, mice were kept at 30 °C during the duration of the experiment. For tissue harvesting, animals were sacrificed by cervical dislocation or CO<sub>2</sub> overdose, blood was withdrawn from the heart, organs were immediately removed, weight, cut into pieces, and snap frozen or placed in 10% formalin for further analysis.

## RESULTS

---

### 2.1.4 Cell lines

3T3-L1 pre-adipocytes originate from Swiss 3T3 mouse embryos. Their culture medium contains *Dulbecco's modified eagle's medium* (DMEM), 10% *fetal calf serum* (FCS), and 40 µg/mL gentamicin. These cells show a fibroblast like morphology and can be differentiated into adipocytes as described before<sup>207</sup>. Briefly, 2 days after cells reached confluence, differentiation was started by adding 1 µM dexamethasone, 0.5 mM *3-isobutyl-1-methylxanthine* (IBMX), and 1.5 µg/mL insulin into DMEM supplemented with 10% *fetal bovine serum* (FBS) and 40 µg/mL gentamicin for 48 h, which was repeated for additional 48 h. Cells were further differentiated by adding insulin into the medium for another 6 days until more than 80% of the cells turned into mature adipocytes filled with multiple lipid droplets.

T37I cells, derived from inferior tumors in the interscapular region of founder 37, were cultured in DMEM-F12 containing 10% FCS, 1% *sodium pyruvate* (SP), and 1% *Penicillin-Streptomycin* (P/S). 2 days post-confluence, differentiation was induced by adding 100 nM T3-hormone and 1.5 µg/ml insulin for 7 days to achieve full differentiation as previously described<sup>208</sup>.

SVC were isolated from *subcutaneous WAT* (sWAT) and BAT of 5-9-weeks old mice. Concisely, sWAT was collected from mice and treatment with 2 mg/mL collagenase D in *phosphate-buffered saline* (PBS) containing 5 mM CaCl<sub>2</sub> and 1% BSA for 40 *minutes* (min), followed by filtration of adipose tissue through a 40 µm mesh. The sample was washed in PBS by centrifugation and cultured in DMEM/F-12 containing 10% FBS, 1% SP, 1% *non-essential amino acids* (NEAA) and 1% P/S. Differentiation of SVC was induced 2 d post-confluence by adding a cocktail including 0.2 µM indomethacin, 1 µM dexamethasone, 0.5 mM IBMX and 1.5 µg/mL insulin for the first 4 days, followed by insulin treatment for additional 4 days to achieve mature adipocyte differentiation. In case of SVC derived from BAT, 100 nM T3 and 1.5 µg/ml insulin were additionally added to the medium throughout differentiation.

Before any treatment, cells were serum starved for 2 h in DMEM supplemented with 0.5% BSA, followed by a stimulation as indicated in each experiment. Afterwards, cell lysates were used for *western blot* (WB) or *real time quantitative polymerase chain*

## RESULTS

---

*reaction* (RT-qPCR) analysis. In case of lipogenesis assay, cells were serum starved for 3 h before stimulation with Insulin.

Human subcutaneous preadipocytes were cultured and differentiated into adipocytes according to the manufacturer's protocol. Differentiated human preadipocytes were pretreated with 3  $\mu$ M CRT 0066101 for 3 days and used to measure lipogenesis rate or *oxygen consumption rate* (OCR).

Adherent *human embryonic kidney* (HEK) 293 cells were used for lentiviral transfection experiments. *Platinum* (Plat)-E cells are based on the HEK293T cell line and used for retroviral transfection of cells. Both cell lines were cultivated in DMEM supplemented with 10% FCS and 1% P/S.

### **2.1.5 Explants derived from sWAT**

Explants were harvested freshly from mouse sWAT. After removal of fibrotic tissue and obvious vasculature, the tissue was cut into pieces of around 15 mg, which were embedded into individual tubes containing DMEM and 0.5% BSA and incubated for 2 h at 37 °C to equilibrate. Explants were either stimulated as indicated in the experiment and further used for WB analysis or lipogenesis assay was performed in these explants by additional treatment with *compound C* (CC) (5  $\mu$ M) for 4 h.

### **2.1.6 Human samples**

The human studies were approved by the Ethics Committee of the University Hospital of Salamanca. All subjects provided written informed consent to undergo subcutaneous fat biopsy under direct vision during surgery. The study population included adults undergoing elective bariatric surgery at the University Hospital of Salamanca. Exclusion criteria were patients with a history of alcohol abuse or excessive alcohol consumption (> 30 g/day in men and > 20 g/day in women), chronic hepatitis C or B or diabetes. Data were analyzed using demographic information (age, sex, and ethnicity), anthropomorphic measurements (BMI), as well as smoking, alcohol history, coexisting medical conditions, and medication use. Fasting venous blood samples were collected, frozen and further measured using a Luminex assay. sWAT pieces, which were obtained during surgery, were frozen for further experiments.

### 2.2 Methods

#### 2.2.1 Mouse genotyping

##### 2.2.1.1 Isolation of genomic DNA from mouse tissue

Ear punches were lysed overnight at 55 °C in 500 µL lysis buffer containing 0.1 mg/mL Proteinase K and constantly shaken at 900 rpm on a thermomixer. 5 M NaCl (100 µL) was added to each sample in order to remove unwanted lipids and cellular fragments. Samples were shaken and centrifuged at 13000 rpm for 10 min at 4 °C. The aqueous nucleic acid containing upper phase (roughly 500 µL) was transferred into a new reaction tube added with 500 µL isopropanol and shaken thoroughly to precipitate the DNA/*ribonucleic acid* (RNA). Samples were placed at -20 °C for 20 min, followed by a centrifugation step at 13000 rpm for 10 min at 4 °C. The supernatant was discarded, and the nucleic acid pellet was washed with 70% ethanol and centrifuged again at 13000x *gravitation force* (g) for 10 min at 4 °C. The DNA pellet was dried for 15 min and solubilized in ultra-pure distilled water for 10 min at 55 °C under constant shaking. Genotyping was accomplished by a *polymerase chain reaction* (PCR) using a mixture of primers indicated below.

##### 2.2.1.2 Mouse genotyping by PCR

###### B6;129S-Prkd1<sup>tm1Eno</sup>/J

###### PCR mix for PKD1flox PCR (20 µL final volume):

1 µL	DNA
2 µL	Roche buffer + MgCl <sub>2</sub> (Roche Kit)
1 µL	forward primer (1:10 in H <sub>2</sub> O, stock: 1 µg/mL)
1 µL	reverse primer (1:10 in H <sub>2</sub> O, stock: 1 µg/mL)
0.5 µL	2'-deoxynucleoside 5'-triphosphates (dNTPs) (Roche Kit)
1 µL	<i>dimethylsulfoxid</i> (DMSO)
0.25 µL	Tag polymerase (Roche Kit)
13.25 µL	H <sub>2</sub> O

###### Primers for genotyping of PKD1flox mice:

PKD1flox fwd: 5' – AGC TTC ACT TGG AAT GAC AC – 3'

PKD1flox rev: 5' – GGT TGC ATG ATT TGT GAT AG – 3'

## RESULTS

---

### Resulting band size:

Mutant= ~300 bp

Heterozygote= ~300 bp and 152 bp

Wild type= 152 bp

### PCR program for PKD1flox:

Step 1	95 °C	3 min
Step 2	94 °C	45 seconds (s)
Step 3	52 °C	45 s
Step 4	72 °C	1 min 30 s
	→ go to step 2, 35x	
Step 5	72 °C	5 min
Step 6	4 °C	∞

### **B6;FVB-Tg(Adipoq-cre)1Evdr/J (adiponectin Cre)**

#### PCR mix for Adipoq-cre PCR (23 µL final volume):

2 µL	DNA
2.4 µL	Thermo buffer-MgCl <sub>2</sub>
1.92 µL	MgCl <sub>2</sub>
1.2 µL	forward primer (1:10 in H <sub>2</sub> O, stock: 1 µg/mL): transgene/internal positive control
1.2 µL	reverse primer (1:10 in H <sub>2</sub> O, stock: 1 µg/mL): transgene/internal positive control
0.5 µL	dNTPs (10 mM stock)
0.2 µL	Taq polymerase (5 U/µL)
13.58 µL	H <sub>2</sub> O

#### Primers for genotyping of Adipoq-cre PCR:

Transgene fwd: 5' – GGA TGT GCC ATG TGA GTC TG – 3'

Transgene rev: 5' – ACG GAC AGA AGC ATT TTC CA – 3'

Internal positive control fwd: 5' – CTA GGC CAC AGA ATT GAA AGA TCT – 3'

Internal positive control rev: 5' – GTA GGT GGA AAT TCT AGC ATC ATC C – 3'

### Resulting band sizes:

Transgene: ~200 bp

Internal positive control: 324 bp

## RESULTS

---

### PCR program for Adipoq-cre:

Step 1	94 °C	2 min
Step 2	94 °C	20 s
Step 3	56 °C	15 s
Step 4	68 °C	10 s
→ go to step 2, 10x		
Step 5	94 °C	15 s
Step 6	60 °C	15 s
Step 7	72 °C	10 s
→ go to step 6, 26x		
Step 8	72 °C	2 min
Step 9	4 °C	∞

### **Tg(Adipoq-cre/ERT2)1Soff**

#### PCR mix for Adipoq-cre/ERT2 PCR (23 µL final volume):

2 µL	DNA
2.4 µL	Thermo buffer-MgCl <sub>2</sub>
1.92 µL	MgCl <sub>2</sub>
1.2 µL	forward primer (1:10 in H <sub>2</sub> O, stock: 1 µg/mL): transgene/internal positive control
1.2 µL	reverse primer (1:10 in H <sub>2</sub> O, stock: 1 µg/mL): transgene/internal positive control
0.5 µL	dNTPs (10 mM stock)
0.2 µL	Taq polymerase (5 U/µL)
13.58 µL	H <sub>2</sub> O

#### Primers for genotyping of Adipoq-cre/ERT2 PCR:

Transgene fwd: 5' – GAG TCT GCC TTT CCC ATG AC – 3'

Transgene rev: 5' – TCC CTC ACA TCC TCA GGT TC – 3'

Internal positive control fwd: 5' – CCG CAT CTT CTT GTG CAG T – 3'

Internal positive control rev: 5' – ATC ACG TCC TCC ATC ATC C – 3'

#### Resulting band sizes:

Transgene: 272 bp

Internal positive control: 175 bp



## RESULTS

---

### PCR program for Adipoq-cre/ERT2:

Step 1	94 °C	2 min
Step 2	94 °C	20 s
Step 3	65 °C	15 s
	-0.5 °C per cycle	
Step 4	68 °C	10 s
	→ go to step 2, 10x	
Step 5	94 °C	15 s
Step 6	60 °C	15 s
Step 7	72 °C	10 s
	→ go to step 6, 28x	
Step 8	72 °C	2 min
Step 9	4 °C	∞

### **2.2.1.3 Agarose gel electrophoresis**

The PCR products after cloning or genotyping were separated on a 2% agarose gel. 5 g of agarose were added to 250 mL 1x *Tris-acetate-EDTA* (TAE) buffer and boiled in the microwave until the agarose was fully dissolved. To mark the DNA, Midori Green (15 µL) was added after the solution was cooled down. The gel was poured into a sleigh containing a comb and after polymerization laid into a chamber filled with TAE buffer. The PCR products were diluted in a 6 x Loading Dye and 20 µL of each sample were loaded onto the gel. In parallel, a marker with a range from 100 to 10,000 bp was loaded onto the gel to control the product size. The samples were separated for 40 min at 120 V. Finally, the DNA/Midori Green mix was visualized using a ultra violet light and pictures were taken.

## **2.2.2 Generation of stable cell lines**

### **2.2.2.1 Molecular cloning**

For the generation of stable cell lines standard cloning techniques were applied. In case of PKD1 knock-down, *small hairpin* (shRNA) was used for lentiviral transfection. The sequence and primers for cloning were synthesized by Eurofins. The insert was cloned into a pGIPZ shRNAmir (generous gift from Eilers lab, Biocenter, Würzburg) as previously described<sup>209</sup>. As a negative control, pGIPZ shNTC was used (whole plasmid sequences are described in the appendix under 7.1.6).

## RESULTS

---

### shPKD1:

5' tgctgttgacagtgagcgccccattgatagtggtgtgtatagtggaagccacagatgtatacaacaccactatcaatg  
ggatgcctactgcctcgga 3'

### Primers for cloning:

BE933 mirE Amp primer fwd:

5' – TGAACTCGAGAAGGTATATTGCTGTTGACAGTGAGCG – 3'

BE934 mirE Amp primer rev:

5' – TCTCGAATTCTAGCCCCTTGAAGTCCGAGGCAGTAGGC – 3'

100 ng template were used for PCR according to the PWO Master's instructions. Ligation of into the mir30 vector was performed between XhoI (5' CTCGAG 3') and EcoRI (5' GAATTC 3') cloning sites using the T4 DNA ligase from Thermo Fischer Scientific, following the manufacturer's protocol.

The retroviral pBabe-Puro system was used for expression of c-terminal Myc-tagged PKD1 *wild type* (wt) and *constitutive active* (ca) form (S744E/S748E), in which the two serines (S744/748) located on the kinase domain have been changed into *glutamic acid* (E). Both coding sequences were derived from the pcDNA5 vectors (Flag-PKD1 wt and 2S2E; generous gift from Ricci lab, IGBMC, Strassbourg) and introduced into a pBABEPuro vector according to the standard cloning procedures. The primers were synthesized by Eurofins. As a control cell line, the pBabePuro-Myc backbone has been used without the PKD1 sequences (whole plasmid sequences are described in the appendix under 7.1.6).

### Primers for cloning:

Pkd1Myc\_bamh1 fwd: 5'-CCTGGATCC ATGAGCGCCCCTCCGGTCC – 3'

Pkd1Myc\_EcoR1 rev:

5' – CTAGCGAATTCTTACAGATCCTCTTCTGAGATGAGTTTTTGTTCGAGGATGC  
TGACACGCTCACC – 3'

In brief, for DNA amplification, the PWO Master Kit was used and 10 ng of the plasmid DNA was added as described in the manufacturer's protocol. The inserts were introduced into a pBabePuro vector between BamHI (5' GGATCC 3') and EcoRI (5' GAATTC 3') restriction sites using T4 DNA ligase as described above.

## RESULTS

---

### 2.2.2.2 Transformation

Competent TOP10 *E. coli* bacteria have been used for transformation. The bacteria were incubated for 15 min on ice together with 10 ng of ligated vectors. 30 s heat shock at 42 °C triggered transformation, followed by a 2 min incubation on ice. Afterwards, 550 µL LB-medium were added to the bacteria and incubated for 1 h at 37 °C with shaking at 450 rpm. The transformation mixture was plated on LB-agar plates containing antibiotics and incubated at 37 °C overnight. Positive clones were picked and further cultured in LB-medium for Mini preps.

### 2.2.2.3 Mini and Midi preps

Clones were cultured in 5 mL LB-medium supplemented with antibiotics for overnight at 37 °C and 200 rpm. 4 mL of the culture was pelleted and further processed using the Mini Prep Kit (NucleoSpin® Plasmid) from Macherey-Nagel according to the manufacturer's protocol. Plasmids were confirmed by sequencing (Eurofins) and 1 mL from the positive Mini cultures was used to inoculate 200 mL Midi cultures as described in the NucleoBond Midi Kit from Macherey-Nagel.

### 2.2.2.4 Transfection

For lentiviral or retroviral transfection  $4 \times 10^6$  HEK or Plat-E cells were seeded per 6 cm dish and cultured overnight. Lentivirus was produced by transfection of HEK293T cells with a mixture of shRNA containing plasmids and the two packaging vectors, psPAX and pMD2.G, using Dharmafect Duo following the manufacturer's instructions. Briefly, 10 µg of shRNA were incubated with 10 µg psPAX and 4 µg pMD2.G in Optimem and incubated for 5 min. Additionally, 20 µL of Dharmafect Duo reagent were kept in Optimem for 5 min, followed by an incubation of the DNA/Dharmafect mix for 20 min. 200 µL of the transfection mix were added dropwise onto the cells cultured in 2 mL DMEM and 10% FCS without antibiotics. After an overnight incubation the transfection medium was replaced by DMEM supplemented with 10% FCS and 1% P/S and after another 24 and 48 h the supernatant containing viral particles was collected and cleared from the cell debris by filtration through a 0.40 µm filter. Retroviral particles were produced by transfection of Plat-E cells using 20 µg DNA following the same procedure as mentioned above.

## RESULTS

---

### 2.2.2.5 Transduction and selection

Transduction and selection of 3T3-L1 was carried out following the standard lentiviral and retroviral procedures. For generation of the stable cell lines, 3T3-L1 cells were transduced using lentiviral or retroviral particles. Therefore,  $6 \times 10^4$  3T3-L1 cells were seeded per well of a 6-well plate. Transduction was performed by adding the viral particle containing supernatant supplemented with polybrene (8  $\mu\text{g}/\text{mL}$ ) 48 and 72 h after transfection. Spinfection was conducted for 45 min at 32 °C and 1800 rpm. Afterwards, cells were selected by puromycin treatment (5  $\mu\text{g}/\text{mL}$ ) for up to one week. Stable cell lines were cultured, differentiated into adipocytes, and used for further experiments.

### 2.2.3 *In vitro* analysis

#### 2.2.3.1 Transient transfection with *small interfering RNA* (siRNA)

Fully differentiated SVC were transiently transfected with Dharmafect Duo transfection reagent and siRNA against AMPK $\alpha$ 1, AMPK $\alpha$ 2, CEBP $\alpha$ , CEBP $\delta$ , or NonTarget control (Dharmacon) according to the manufacturer's instructions.

siGenome SMARTPool Murine Prkaa1: #M-041035-02-0005

siGenome SMARTPool Murine Prkaa2: #M-040809-01-0005

siGenome SMARTPool Murine CEBP $\alpha$ : #M040561-01-0005

siGenome SMARTPool Murine CEBP $\delta$ : #M060294-01-0005

siGENOME Non-Targeting Control Pool Pool: #D001206-13-05

Briefly, wells were precoated with Matrigel (0.5% Matrigel in ice cold PBS) 1 h before transfection and washed with PBS before cell plating. Dharmafect and Optimem were mixed (2.1  $\mu\text{L}$  Dharmafect + 27.9  $\mu\text{L}$  Optimem per  $\text{cm}^2$ ) and incubated for 15 min. At the same time, 2  $\mu\text{M}$  siRNA was mixed with Optimem (14.48  $\mu\text{L}$  siRNA + 15.52  $\mu\text{L}$  Optimem per  $\text{cm}^2$ ) for 5 min. This was followed by a 20 min incubation of the Dharmafect/siRNA mix. In the meanwhile, Accutase was given onto the cells until fully detached. Cells were seeded in differentiation medium without antibiotics and siRNA

## RESULTS

---

mix was added dropwise. Generally, 48 h post transfection experiments were performed.

### **2.2.3.2 AMPK activity assay**

The CycLex AMPK Kinase Assay Kit is an immunoassay, which enables to measure AMPK activity in cell lysates. For this assay, differentiated 3T3L1 cells were stimulated with 100 nM Insulin for 10 min after 2 h of serum starvation. AMPK activity was measured in the collected cell lysates following the manufacturer's protocol. 100  $\mu$ L of the cell lysates were given to the wells and kept for 30 min at 30 °C, followed by washing steps. Primary antibody was added (100  $\mu$ L) and incubated for 30 min at room temperature. After washing, 100  $\mu$ L of *horseradish peroxidase* (HRP) conjugated anti-mouse *immunoglobulin G* (IgG) was added for 30 min at room temperature, followed by washing. Finally, 100  $\mu$ L of substrate reagent and 100  $\mu$ L of stop solution were placed onto the wells. A Spark 10 M microplate reader was used to read the absorbance at 450 nm/540 nm. After subtraction of the background, results were normalized to the protein content.

### **2.2.3.3 Quantification of TG accumulation**

The amount of TGs normalized to the DNA content of the cells was measured by double staining of AdipoRed reagent and Hoechst 33342 following the manufacturers' instructions. Briefly, cell were washed with PBS once and the final volume of PBS containing Hoechst 33342 (5  $\mu$ g/mL) was added depending on the well size. AdipoRed was added dropwise to the cells. After a 30 min incubation at 37 °C, the fluorescent intensity was measured using Spark 10 M microplate reader (AdipoRed: excitation at 485 nm; emission at 572 nm; Hoechst 33342: excitation at 361 nm; emission at 486 nm). The multiple intracellular lipid droplets in the cells were visualized by Oil-Red O staining. After full differentiation, cells were fixed with 10% formaldehyde for 30 min and stained with Oil Red O (0.375% Oil Red O solution (3:2 isopropanol:ddH<sub>2</sub>O, v/v; filtered through a filter paper before usage)) for 1 h. Cells were kept in ddH<sub>2</sub>O until pictures were taken. In indicated experiments, cells were either transiently transfected with siRNA against AMPK $\alpha$ 1/ $\alpha$ 2 subunits for 48 h or treated with 0.5 mM AICAR for 3 days.

## RESULTS

---

### **2.2.3.4 Lipolysis assay**

To assess the lipolysis rate, fully differentiated cells were serum starved for 2 h in phenol red-free DMEM supplemented with 0.5% BSA. After stimulation with 10  $\mu$ M isoproterenol for 2 h in fresh medium, FFA levels were measured in this medium by NEFA-reagents following the manufacturer's instructions. 200  $\mu$ L of Reagent A were added to 30  $\mu$ L of the collected medium and incubated for 5 min at 37 °C. Absorption at 550 nm and background absorption at 660 nm were assessed using Spark 10 M microplate reader. In the next step, 100  $\mu$ L of Reagent B were added and the measurement was repeated. Background absorption was subtracted from absorption at 550 nm. For the final calculation, values after the first measurement were subtracted from the second measures. Glycerol was quantified using free glycerol reagent according to the manufacturers' instructions. 200  $\mu$ L of the solution were added to 30  $\mu$ L medium and incubated for 5 min at 37 °C. Absorption was measured at 540 nm on a microplate reader.

### **2.2.3.5 Lipogenesis Assay**

*De novo* lipogenesis assay in explants or fully differentiated cells was determined according to the standard lab procedures. In detail, cells were serum starved for 3 h in DMEM supplemented with 0.5% BSA, followed by incubation in 1  $\mu$ Ci/mL D-[3-<sup>3</sup>H]-glucose for 3 h in the presence or absence of 100 nM insulin. Reaction was stopped by adding 230  $\mu$ L of NaOH to lyse the cells. Total intracellular lipids were extracted with a chloroform and methanol (2:1, v/v) mixture. To separate the phases, centrifugation at 3000x g for 10 min was performed and the chloroform phase was transferred into a scintillation vial. 4 mL scintillation liquid were added before counting. *De novo* lipogenesis rates were normalized to protein levels. Tritium incorporation into the lipid droplets was assessed in a liquid scintillation counter (measured in *disintegrations per minute* (dpm)). For certain experiments, cells were either treated with 2 mM AICAR for 2 h or transfected with siRNA against AMPK $\alpha$ 1/ $\alpha$ 2 subunits for 48 h.

## RESULTS

---

### 2.2.3.6 Mitochondrial respiration

Mitochondrial respiration was assessed using the Seahorse XF Cell Mito Stress Test and measuring OCR in the cells in a Seahorse XFe96 Analyzer following the manufacturer's instructions. In brief, 96 well Seahorse plates were precoated with 0.5% Matrigel in ice cold PBS. Cells were plated and fully differentiated in these wells. 1 day before each experiment, an Agilent Seahorse XFe96 Sensor Cartridge was hydrated with 200  $\mu$ L/well of XF calibrant solution overnight and kept in a non-CO<sub>2</sub> incubator at 37 °C. For the experimental assay, 75 mL of Seahorse assay medium supplemented with 1 mM sodium pyruvate, 2 mM glutamine and 5 mM glucose were prepared. pH was adjusted to 7.4 with 1 M NaOH in the prewarmed medium. Cells were washed two times with 180  $\mu$ L of the freshly prepared medium and incubated in 175  $\mu$ L of this medium per well in a non-CO<sub>2</sub> incubator at 37 °C for 1 h. Meanwhile, the Seahorse sensor cartridge ports were loaded with 25  $\mu$ L of inhibitors in a final concentration of 2  $\mu$ M oligomycin in port A, 1  $\mu$ M *carbonyl cyanide-4-(trifluoromethoxy) phenylhydrazone (FCCP)* in port B, and 0.75  $\mu$ M rotenone/antimycin A in port C. The experimental design was setup using the WAVE software program and measurements were conducted in the Seahorse XFe96 Analyzer. Normalization to the DNA content was performed by fixation of the cells in 75% ethanol, followed by Crystal Violet staining for 30 min and washing. Afterwards, air-dried Crystal Violet was dissolved in 10% acidic acid and absorption was determined at 590 nm in a Spark 10 M microplate reader. In indicated experiments, cells were either transfected with siRNA against AMPK $\alpha$ 1/ $\alpha$ 2 subunits for 48 h or treated with 0.5 mM AICAR for 3 days.

### 2.2.4 Biochemistry

#### 2.2.4.1 Immunoblotting

Proteins were extracted from cells or tissues in lysis buffer supplemented with a *protease and phosphatase inhibitor (PPI)* cocktail. In detail, cells were scraped from the tissue culture plates and tissue pieces were homogenized using a stick. Protein was extracted by pelleting the cell fragments in a centrifugation step (13000 rpm, 10 min at 4 °C). The Pierce BCA Protein Assay Kit was used to quantify proteins in the supernatant following the manufacturer's instructions. Concentrations were adjusted using lysis buffer, an equal volume of reducing 5 x Loading Dye was added to the

## RESULTS

---

samples, and boiled for 5 min at 95 °C. WB analysis was performed according to standard procedures by separating the proteins on an 10-12% *sodium dodecyl sulfate-polyacrylamide gel electrophoresis* (SDS-PAGE). The gel was blotted onto *polyvinylidene fluoride* (PVDF) membranes and the membrane was probed with primary antibodies (all antibodies used are listed in the appendix 7.1.2 and used in the concentrations indicated on the data sheets) overnight at 4 °C. After incubation with corresponding HRP-conjugated secondary antibodies, proteins were visualized by *enhanced chemiluminescence* (ECL) solution. Detection was performed using X-ray films. Actin, *glyceraldehyde 3-phosphate dehydrogenase* (GAPDH), and Tubulin were used as a loading control.

### **2.2.4.2 Immunoprecipitation (IP)**

Myc-tagged cells were lysed in an IP-buffer containing a freshly added PPI cocktail. Quantification of the protein content was determined as mentioned in section 2.2.4.1. Pierce Anti-c-Myc Magnetic beads at a concentration of 10 mg/mL were used to pull down Myc according to the standard procedure. The entire experiment was performed at 4 °C. Beads were gently mixed to ensure homogeneity and 250 µL of the beads were washed twice in IP-wash buffer supplemented with PPI cocktail. 10 mg protein (5 µg/µL protein concentration) in a total volume of 2 mL were mixed with the beads (beads/protein ratio 1:8) and vigorously shaken on a rotor for 2 h. Beads were collected on a magnetic rack and supernatant was collected for later analysis by WB. Beads were washed with IP-wash buffer twice for 5 min, followed by washing with 0.5% NP-40 two times, and three times with 0.1% NP-40. To elute the samples, 1 mM DTT was added to the Pierce™ Lane Marker Non-Reducing Sample Buffer and beads were incubated for 30 min at 37 °C. Beads were magnetically separated from the IP-product, which was further analyzed on a WB, Coomassie gel, or by Mass Spectrometry.

### **2.2.4.3 Coomassie gel**

Samples were quantified, prepared, and loaded on a SDS-PAGE as described in section 2.2.4.1. The gel was washed once in tap water and incubated in the Coomassie staining solution for 24 h. Coomassie destaining solution was used to wash the gel and exchanged several times over 48 h until gel was fully destained.



## RESULTS

---

### **2.2.4.4 Mass Spectrometry (MS) analysis**

MS analysis was performed in the working group of Prof. Dr. Schlosser. Gel electrophoresis and In-gel digestion were carried out according to the standard procedures. Protein precipitation was conducted overnight at -20 °C with acetone. NuPAGE® *lithium dodecyl sulfate* (LDS) sample buffer was used to dissolve samples. Proteins were reduced with 50 mM DTT for 10 min at 70 °C and alkylated using 120 mM Iodoacetamide for 20 min at room temperature. The samples were separated with a NuPAGE® Novex® 4-12% Bis-Tris gels using *3-(N-Morpholino) propanesulfonsäure* (MOPS) buffer following the manufacturer's guidelines. After washing and gel staining with Simply Blue™ Safe Stain, each gel band was cut into 16 slices. Destaining, shrinking, and drying was done for each lane, prior to overnight digestion at 37 °C using 0.1 µg trypsin in 0.1 M NH<sub>4</sub>HCO<sub>3</sub> (pH 8). Peptides were extracted and pooled with the supernatant. An Orbitrap Fusion, coupled to an EASY-nLC 1000 and equipped with a PicoView Ion Source was used for Nano *liquid chromatography* (LC)-MS/MS analyzes. Capillary columns self-packed with ReproSil-Pur 120 C18-AQ, 1.9 µm were used to load peptides. Separation took place with a 30-min linear gradient from 3-30% acetonitrile and 0.1% formic acid and a flow rate of 500 nl/min. MS and MS/MS scans were both obtained using an Orbitrap analyzer. The raw data were processed, analyzed and quantified using the MaxQuant version 1.6.2.2<sup>210</sup>. *Label-free quantification* (LFQ) intensities were used for protein quantification<sup>211</sup> and proteins were excluded with less than two identified razor and unique peptides.

### **2.2.4.5 RT-qPCR analysis**

Total RNA was extracted from tissue pieces and cells following the QIAzol Handbook guidelines using the RNeasy Plus Universal Tissue Mini Kit. In detail, cells were scraped with 1 mL QIAzol lysis reagent and tissues were homogenized using a bench-top homogenizer. Chloroform was added for subsequent phase separation. The upper, aqueous phase was mixed with an equal volume of 70% ethanol and transferred to an RNeasy Mini spin column. After centrifugation for 15 s at 8000x g and 4 °C, the column was washed with RW1 and RPE buffer. 40 µL of RNase free water were added and spun down (1 min, 8000x g) to elute the DNA. RNA concentration and quality were assessed using a NanoDrop spectral photometer.

## RESULTS

---

First strand *complementary DNA* (cDNA) was synthesized by First Strand cDNA Synthesis Kit according to the manufacturer's protocol. Two different master mix were prepared for cDNA synthesis.

### Master mix 1:

1 µg	RNA
1 µL	random hexamer primer
x µL	RNase-free water (up to a total volume of 10 µL)

Master mix 1 was heated up in a thermal cycler to 65 °C for 5 min for denaturation and cooled on ice afterwards.

### Master mix 2:

4 µL	5 x reaction buffer
1 µL	RiboLock RNase inhibitor (20 u/µL)
2 µL	10 mM dNTP mix
2 µL	M-MuLV reverse transcriptase (20 u/µL)

Master mix 2 was pooled with master mix 1 and incubated for 5 min at 25 °C in a thermal cycler, followed by 60 min at 37 °C. To terminate the reaction the samples were heated up for 5 min at 70 °C. cDNA of cells was diluted 1:5 in RNase-free water and from tissues 1:10.

RT-qPCR was performed using SYBR green Universal PCR master mix. The RT-qPCR samples and master mix were pipetted by a QIAgility and analyzed on a QuantStudio 5 Real Time PCR System.

### RT-qPCR mix:

2 µL	cDNA
5 µL	SYBR green
0.4 µL	forward primer (1:10 in H <sub>2</sub> O, stock: 1 µg/mL)
0.4 µL	reverse primer (1:10 in H <sub>2</sub> O, stock: 1 µg/mL)
2.2 µL	RNase-free water

## RESULTS

---

### RT-qPCR program:

Step 1	95 °C	10 min
Step 2	95 °C	15 sec
Step 3	60 °C	1 min

→ go to step 2, 40x

For melting curve (added to each RT-qPCR):

Step 4	95 °C	15 sec
Step 5	60 °C	1 min
Step 6	95 °C	15 sec

Expression of all genes (primers are listed in appendix 7.1.5) were normalized to the *ribosomal protein L13a (Rpl13a)* housekeeping gene measured in each sample (as listed in appendix 7.1.5).

Mitochondrial DNA (mtDNA) copy number was determined from total DNA isolated from snap frozen sWAT samples as well as differentiated SVC, following the manufacturer's guidelines. Briefly, the DNeasy Blood & Tissue Kit was used and Proteinase K was added to ATL buffer until cells or tissue were completely lysed. AL buffer and 100% ethanol were added to the samples and transferred into a DNeasy Mini spin column (1 min, 6000x g). The column was washed with AW1 (1 min, 6000x g) and AW2 (3 min, 20000x g) buffer. To elute the DNA, AE buffer was directly added onto the DNeasy membrane and incubated for 1 min (1 min, 6000g). mtDNA was normalized to genomic DNA (gDNA) (primers listed in appendix 7.1.5) performing RT-qPCR.

PKD1 expression in humans was conducted in the working group of Prof. Dr. Sabio. sWAT was obtained during surgery and frozen down further analysis. From this tissue, 1 mg of RNA was extracted with RNeasy Plus Universal Tissue Mini Kit according to the manufacturer's protocol as described above, and further transcribed to cDNA. Fast TaqMan probe (*PRKD1*) and the appropriate TaqMan Assay were used to perform RT-qPCR in a 7900 Fast Real Time thermocycler. Relative mRNA expression was normalized to *18s ribosomal 5 (18s)* mRNA levels assessed in each sample.

### **2.2.4.6 RNA sequencing**

RNA sequencing was performed with the help of the working group of Prof. Dr. Eilers. Total RNA was extracted from tissue samples using the RNeasy mini columns with

## RESULTS

---

on-column DNase I digestion, followed by PolyA<sup>+</sup>-RNA extraction from total RNA with the NEBNext® Poly(A) mRNA Magnetic Isolation Module. Sequencing libraries were prepared using the NEBNext® Ultra™ RNA Library Prep Kit for Illumina including the use of Agencourt AMPure XP Beads for size-selection and library purification following the manufacturer's guidelines. For library quality control and quantification, an Experion Automated Electrophoresis System was used. Sequencing of all samples was performed on a NextSeq500 System and an Illumina's FASTQ Generation software v1.0.0 was used for base calling. The overall sequencing quality was determined with a FastQC script. Fastq files were mapped to mm9 using Bowtie2 with default settings. To count reads per gene, the countOverlaps function from the R package GenomicRanges were applied. The differential expression of the remaining genes was called by EdgeR, to follow the removal of weakly expressed genes (mean CPM over all samples <1). *Gene set enrichment analysis* (GSEA)<sup>212</sup> was performed with Signal2noise metric, 1000 permutations, and the C2 gene set collection (v6.0) of MSigDB. When indicated, the C2 gene set collection was spiked with a gene signature of already published browning markers. The RNA-sequencing raw- and processed-datasets as well as information on data processing can be found under the accession number: GSE104797, in NCBI Gene Expression Omnibus.

### 2.2.4.7 DAG content

DAG content was measured in murine sWAT and BAT with the help of the working group of Prof. Dr. Schulze. Homogenization of 50 mg of tissue was performed in 7-fold volume of 1% acetic acid using a stirring plastic pistil. 280 µL of the homogenate, 70 µL methanol, 210 µL n-butanol and 20 µL 10 mM dioctanoylglycerol were mixed vigorously in n-butanol/methanol (3/1, v/v). 200 µL n-heptane and 100 µL acetic acid ethyl ester were added and centrifuged for 2 min at max rpm. The resulting upper phase was transferred to a new tube, the lower phase was extracted using another 200 µL n-heptane and 100 µL acetic acid ethyl ester. Evaporation of the combined upper phases were performed at 45 °C under a stream of *nitrogen* (N<sub>2</sub>).

For lipid class separation, the dried DAG extract was resuspended in 150 µL hexane and applied on a SilicaMatrix Column. By applying 750 µL hexane, 750 µL hexane/acetic acid ethyl ester (18/1, v/v) and 1.5 ml hexane/acetic acid ethyl ester (9/1,

## RESULTS

---

v/v) to the column, undesired lipids were washed out. DAGs were eluted with 750  $\mu$ L hexane/acetic acid ethyl ester (9/4, v/v). The eluate was collected and evaporated to dryness at 45 °C under a stream of N<sub>2</sub>.

LC/MS Analysis of DAGs was performed by dissolving the resulting residue in 250  $\mu$ L mobile phase A/mobile phase B (70/30, v/v) (mobile phase A: acetonitrile/water/formic acid (10/89.9/0.1, v/v/v)); mobile phase B: acetonitrile/water/formic acid (90/9.9/0.1, v/v/v)). For LC/MS analysis, a Thermo Scientific Dionex Ultimate 3000 UHPLC system hyphenated with a *Q exactive mass spectrometer* (QEMS) was used, equipped with a HESI probe and UPLCcolumn. 5  $\mu$ L of the sample were injected to the C8 column at 40 °C with the following gradient program:

### Gradient program:

20% solvent B	2 min
100% solvent B	5 min
100% solvent B	22 min
20% solvent B	1 min
20% solvent B	5 min (for column equilibration before each injection)

The flow rate was maintained at 350  $\mu$ L/min and the eluent was directed to the HESI source of the QEMS.

### MS parameters:

Heater temperature	120 °C
Sheath gas	30 L/min
Auxiliary gas	10 L/min
Sweep gas	3 L/min
Spray voltage	3.6 kV
Capillary temperature	320 °C
S-lens	55 (RF level)
Full scan range	300 to 700 (m/z) in positive ion mode
Resolution	70000 nm
Maximum injection time	200 <i>milliseconds</i> (ms)

For data evaluation, a TraceFinder software was used and peaks corresponding to the calculated DAG masses (MIMOH  $\pm$  2 mMU) were integrated.

### **2.2.5 Immunofluorescence (IF) and histological analysis**

#### **2.2.5.1 Mitochondrial staining**

Mitochondrial morphology was assessed in cells plated on a precoated cover slide (0.5% Matrigel in ice cold PBS) overnight. 150 nM MitoTracker Red were added in the suitable growth medium for 30 min at 37 °C for mitochondrial staining. Cells were fixed in 4% *paraformaldehyde* (PFA) for 20 min, washed in 1x PBS, and permeabilized in ice cold methanol for 5 min. ProLong Gold Antifade Mountant with DAPI was used to mount the cover slides. When treated with AICAR, 2 mM AICAR were added to the cells 2 h prior to fixation. A fluorescent microscope Leica DM5500 B was used to image the cells. Mitochondrial morphology in stained differentiated adipocytes was quantified blindly (independent of the genotype or the treatment) by grouping into different categories. Spherical mitochondria with no clear length or width were defined as *fragmented* (fragm.). Highly interconnected and elongated mitochondria were clustered as fused. All the other mitochondrial structures in between were counted as *intermediate* (interm.).

#### **2.2.5.2 IF staining of cells**

Fully differentiated cells were replated on precoated cover slides (with 0.5% Matrigel in ice cold PBS) for immunofluorescent staining, followed by fixation in 4% PFA for 10 min. Staining was conducted according to the standard procedures. To block the cells, PBS supplemented with 20% goat serum and 0.5% BSA was added for 1 h. Cells were further incubated with a primary antibody directed against ADRB3 (10 µg/mL – diluted in PBS containing 1% BSA) overnight in a humidified chamber at 4 °C. After intense washing with PBS a fluorophore-conjugated secondary antibody (Alexa 488 Anti-Chicken) was added for 2 h at 4 °C. Cells were mounted using ProLong Gold Antifade Mountant with DAPI. Cells were imaged with a fluorescent microscope Leica DM5500 B. ImageJ software was used to determine the fluorescent intensity of single cells (about 120 cells per genotype). The obtained average intensity was subtracted from the average background intensity around the cell.

## RESULTS

---

### **2.2.5.3 Histology – *hematoxylin and eosin (H&E)* staining of paraffin sections**

10% formaldehyde fixed adipose tissues were embedded in paraffin, sections (4-5  $\mu\text{m}$  thickness) were prepared, immobilized on glass slides, and dried overnight at 37 °C. Xylol (2 x 10 min), followed by an alcohol gradient (100% (2 x), 95%, 90%, 80%, 70%; and 50%; 5 min each) were used for deparaffinization and rehydration. After incubation in ddH<sub>2</sub>O for 5 min, slides were stained with hematoxylin for 10 min, rinsed in tap water for 10 min, and incubated in ddH<sub>2</sub>O for additional 5 min. Eosin (2 min) was used as counterstaining. Sections were dehydrated by a graded alcohol series (50%, 70%, 80%, 90%, 96%, and 100% (2 x; 2 min each)). After xylol incubation (2 x) for 10 min, slides were mounted using RotiMount, a xylene-based mounting medium. Analysis was performed with an inverted microscope Olympus CKX31.

### **2.2.5.4 Cell size quantification**

Pictures of H&E stained sections of gWAT and sWAT from HFD- or ND-fed mice were taken with a 20x magnification under the microscope. Four representative images of each sample were analyzed manually, measuring single cell areas in a total area of 0.6 mm<sup>2</sup>. The ImageJ tool, allowing manual encircling of each cell, and automatic measurement of the area, was used for this measurement.

### **2.2.5.5 Histology – *Immunohistochemistry (IHC)* on paraffin sections**

For IHC, adipose tissue was fixed in 10% formaldehyde and 4-5  $\mu\text{m}$  thick section were cut. After an overnight incubation at 37 °C, slides were deparaffinized with xylol (2 x for 15 min) and rehydrated with an alcohol gradient (100% (2 x), 95%, 90%, 80%, 70%; 2 min each). After an incubation for 1 min in ddH<sub>2</sub>O, blocking of endogenous peroxidases was performed for 15 min in 3% H<sub>2</sub>O<sub>2</sub>, followed by washing in ddH<sub>2</sub>O and PBS for 5 min each. For heat-induced antigen retrieval, 0.01M sodium citrate (pH 6) was used and samples were soaked in the boiling solution for 8 min in the microwave (low power), followed by a gradual cool down at room temperature for 1 h. After three washing steps in PBS for 5 min each, sections were blocked for 1 h at 37 °C in PBS supplemented with 10% goat serum. Primary antibody incubation of anti-heavy chain Myosin antibody or anti-UCP1 took place overnight at 4 °C (antibody dilution in PBS containing 1% BSA). Detection was conducted with SignalStain® (DAB substrate)

## RESULTS

---

according to the standard procedure. Hematoxylin was used for counterstaining (15 min, followed by 20 min under running tap water). Slides were dehydrated by a graded alcohol series (ddH<sub>2</sub>O, 70%, 80%, 90%, 95%; 2 min each – 100%; 2 x 10 min), followed by two incubations in xylol for 10 min each. Slides were covered in RotiMount and analysis was performed with an inverted microscope Olympus CKX31. Quadriceps sections served as positive controls in case of heavy chain Myosin staining.

### **2.2.5.6 Histology – Oil Red O staining of cryo sections**

Livers were embedded in OCT-Tissue-Tek. Frozen sections were stained according to the standard procedures. Briefly, 5 µm thick liver sections were cut and fixed in 10% formalin for 10 min. Slides were quickly washed in 60% isopropanol and stained in a 0.375% Oil Red O solution (3:2 isopropanol:ddH<sub>2</sub>O, v/v) for 10 min. Subsequently, slides were rinsed in 60% isopropanol as well as running tap water for 30 min and mounted with an aqueous mounting gel. Analysis was performed with an inverted microscope Olympus IX71 or CKX31.

### **2.2.6 *In vivo* analysis**

#### **2.2.6.1 Glucose and insulin tolerance and test**

After 18 and 20 weeks of HFD and ND feeding, glucose tolerance test (GTT) and insulin tolerance test (ITT) were performed in mice after 4 h fasting according to the standard procedures. In brief, defined doses of glucose (1 g/kg BW) or insulin (0.25 U/kg BW) were injected intraperitoneal. Glucose removal from the blood was assessed at defined time points (prior to the test as well as 15, 30, 60, 90 and 120 min after injection) measuring tail vein blood with an automated glucometer.

#### **2.2.6.2 Indirect calorimetry analysis**

Body weight gain of mice was followed up once every two weeks until the experiment was terminated. Indirect calorimetry was measured within the last two weeks of respective diets using an open-circuit, indirect calorimetry system (Phenomaster system), allowing constant and simultaneous measures of food intake, energy



## RESULTS

---

expenditure and voluntary movements. The mice housed in the metabolic cages at 23 or 30 °C as described before<sup>213</sup>. Training of the mice was started up to 4 days prior to the experiment using training bottles to adapt to the drinking dispenser in the cages. Afterwards, mice were kept in regular cages in the metabolic chamber with a predefined 12 h light/dark cycle and a constant temperature of 23 °C or 30 °C as indicated in the experiments. Mice had *ad libidum* access to food and water and were allowed to adapt for additional 3 days in the metabolic cage before data acquisition.

### **2.2.6.3 Body composition**

Body composition analysis was performed by either assessing different organ weights of the genotypes or measuring the mice in a *nuclear magnetic resonance* (NMR) analyser, which allows determining between fat mass, lean mass, and free fluids.

### **2.2.6.4 Liver TG Extraction**

Frozen liver pieces were homogenized in PBS and lipid extraction was performed with a 2:1 chloroform: methanol (v/v) mixture. The chloroform phase, which is containing the lipids, was dried under nitrogen flow. Lipids were re-solubilized using 15% Triton X-100. Liver triglycerides were measured with the commercial glycerol and TG reagents according to manufacturer's instructions. Glycerol (200 µL) was added to 5 µL of the lipid solution and incubated for 5 min at 37 °C. Absorption was measured at 540 nm on a microplate reader. 50 µL of the TG reagent was added, incubated for 5 min at 37 °C and absorbance was measured at 540 nm. The amount of TGs in liver was measured by subtracting the first measurement (amount of glycerol) from the second measurement (amount of total glycerides). Values were normalized to the total protein amount.

### **2.2.6.5 Analysis of blood samples in mice**

FFAs, glycerol and TGs were determined from serum of mice using NEFA, free glycerol and TG reagents according to the manufacturers' instructions. 5 µL serum were used for the assay and measurements were performed as described in section 2.2.3.4 and 2.2.6.4. Analysis of adiponectin, leptin, resistin and insulin were performed by a

## RESULTS

---

magnetic-bead based multiplex *enzyme-linked immunosorbent assay* (ELISA) assay on a MagPix Systems according to the manufacture's guidelines. In detail, standard and samples were prepared following the general guidelines. Magnetic beads were diluted and 50  $\mu$ L beads were transferred into each well of the assay plate. After two washing steps, 50  $\mu$ L standards, blanks, and samples were pipetted into the wells, followed by an incubation for 1 h at room temperature and 850 rpm. 25  $\mu$ L of the detection antibodies were added after three washing steps, protected from light, and incubated at 850 rpm for 30 min at room temperature. Washing was performed three times, followed by incubation of 50  $\mu$ L streptavidin for 10 min at room temperature under constant shaking. After washing, beads were resuspended in 125  $\mu$ L assay buffer for plate reading. A Bio-Plex MAGPIX was used to acquire the data using the default instrument settings.

### **2.2.6.6 Analysis of blood samples in humans**

Human blood samples were analyzed in the working group of Prof. Dr. Sabio. Blood was collected for measuring complete cell blood count (all parameters mentioned in Table 2) according to the standard procedures and glucose using a glucometer. After centrifugation of the blood, plasma was frozen to detect insulin with a Luminex assay. *homeostatic model assessment-insulin resistance* (HOMA-IR) was assessed from individually matched glucose and insulin levels according to the following calculations:  $\text{HOMA-IR} = [\text{glucose (mg/dl)} \times \text{insulin (mU/l)}] / 405$ .

### **2.2.7 Statistical analysis**

The results are presented as mean values  $\pm$  *standard error of the mean* (SEM), unless indicated otherwise. Determination of significances of more than two groups were assessed using one-way or two-way *analysis of variance* (ANOVA) followed by a *post hoc* Tukey test. Differences between two independent groups were statistically analyzed with an unpaired, two-tailed Student's t-test. P-values  $< 0.05$  were considered statistically significant (\*\* $p < 0.001$ ; \*\* $p < 0.01$ ; \* $p < 0.05$ ). P-values  $> 0.05$  were considered *non-significant* (ns). Each figure gives specific statistical indications.

### 3 RESULTS

#### 3.1 DAG-activated PKD1 promotes TG accumulation in adipocytes

##### 3.1.1 PKD1 is predominantly expressed in adipose tissue

PKD1 is the most studied of all three isoforms. It has been shown to be involved in many fundamental cellular processes, including signaling pathways involved in the development of metabolic diseases<sup>133,147,149-151,153-160</sup>. Therefore, the expression of *Pkd1* in different murine tissues, especially those that are involved in maintaining whole-body metabolism, was assessed. It was demonstrated that *Pkd1* is predominantly expressed in WAT as well as in isolated adipocytes (Figure 12). Therefore, the aim of this study was to identify its function in the regulation of adipose tissue.

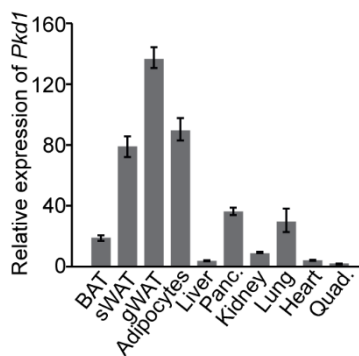


**Figure 12. PKD1 is predominantly expressed in adipose tissues.** (A) RT-qPCR analysis of *Pkd1* levels in different murine tissues. Data are presented as mean  $\pm$  standard deviation (SD) (number (n)=4 mice; representative of two individual experiments). *Protein kinase D* (PKD); *brown adipose tissue* (BAT); *subcutaneous white adipose tissue* (sWAT); *gonadal white adipose tissue* (gWAT); *pancreas* (Panc.); *quadriceps* (Quad.). (unpublished observation)

##### 3.1.2 ATP and DAG activate PKD1 in white adipocytes

The first aim was to identify potential PKD1 activators in adipocytes. Therefore, differentiated 3T3-L1 cells were stimulated with the major endocrine factors involved in the regulation of adipose tissue or those that were previously displayed to activate PKD1. Insulin, one of the major hormones regulating adipose tissue function<sup>214</sup>, did not show any activation of PKD1 in differentiated 3T3-L1 cells over the given time. Carbachol, to mimic parasympathetic stimulation of adipocytes, did only induce a minor activation of PKD1 after 2 min (Figure 13A). Furthermore,  $\beta$ -adrenergic stimulation with isoproterenol and serotonin, a recently identified hormone promoting lipolysis<sup>54</sup>, did not affect PKD1 activity *in vitro* (Figure 13B). Several studies have implied purinergic receptors in regulating adipose tissue function<sup>215-217</sup>. Moreover, activation of purinergic receptors results in PKD activation in other cell types<sup>218</sup>. Therefore, differentiated

## RESULTS

3T3-L1 cells were stimulated with ATP as well as ADP over 2, 5, and 15 min. At all three time points a robust activation of PKD1 was observed with both factors (Figure 13C). ATP was also stimulating PKD1 in gWAT fat pads (explants) at all given time points (Figure 13D). Altogether, PKD1 is activated in adipocytes to a minor extend through parasympathetic stimulation using carbachol, however, purinergic stimulation results in robust and specific activation of PKD1.

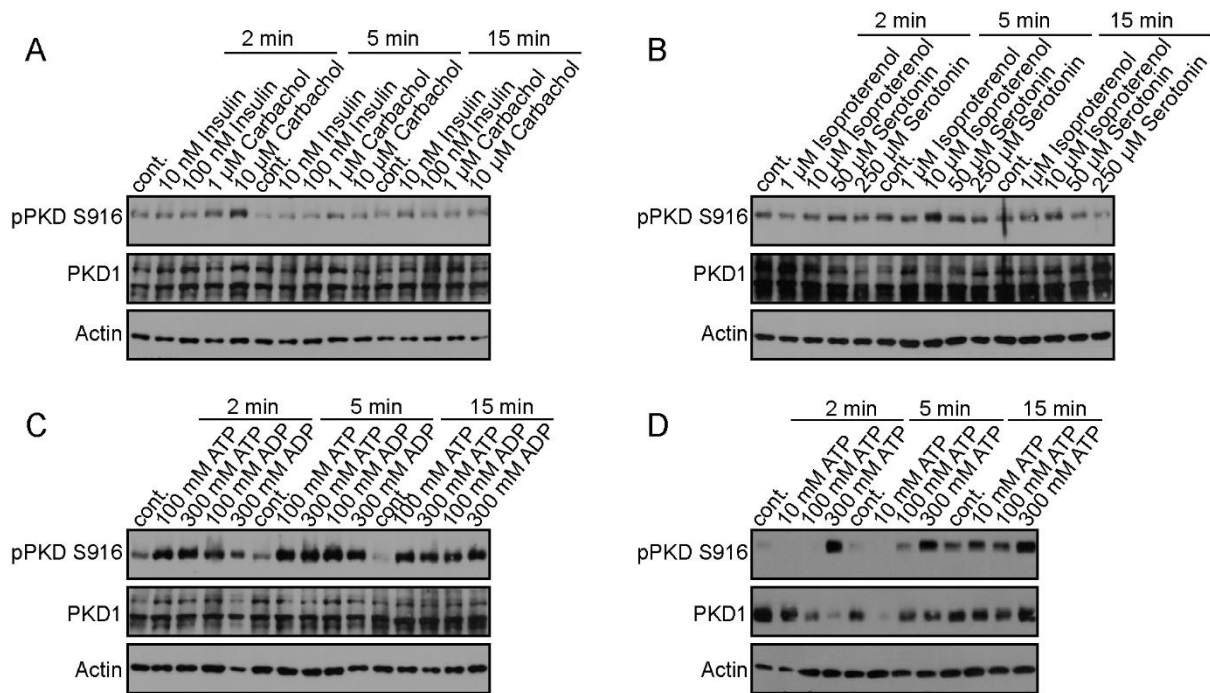


**Figure 13. PKD1 is activated upon purinergic stimulation in white adipocytes.** WB analysis was performed using antibodies against pPKD1 (S916) as well as PKD1 in 3T3-L1 cells, which were differentiated into adipocytes and stimulated with (A) insulin (10 nM, 100 nM), carbachol (1  $\mu$ M, 10  $\mu$ M), (B) isoproterenol (1  $\mu$ M, 10  $\mu$ M), serotonin (50  $\mu$ M, 250  $\mu$ M) or (C) ATP (100 mM, 300 mM) and ADP (100 mM, 300 mM) for 2, 5, and 15 min. Actin was used as a loading control. (D) WB analysis of pPKD1 (S916) and PKD1 expression in gonadal white adipose tissue fat pads stimulated with ATP (10 mM, 100 mM, 300 mM) for 2, 5, and 15 min. Actin served as a loading control. *Protein kinase D* (PKD); *phospho* (p); *serine* (S); *control* (cont.); *adenosine triphosphate* (ATP); *adenosine diphosphate* (ADP); *minutes* (min); *molar* (M) (Löffler *et al.*, 2018)<sup>219</sup>

Ligand-binding leads to a downstream signaling cascade activating PKD1, which still requires further investigation. PKD1 can sense 1,2-DAG levels in multiple cell types and is therefore activated in response to the stimulation of multiple cell surface receptors, which utilize DAG as a second messenger<sup>134</sup>. In addition, stimulation of purinergic receptors results in increased DAG levels<sup>220</sup>. It was further tested whether PKD1 activity can be directly induced by DAG, since in adipocytes large amounts of

## RESULTS

DAG are generated during TG synthesis<sup>221,222</sup>. To test this, the pre-adipocyte cell line 3T3-L1 was stimulated with a cell membrane permeable form of DAG, *1,2-dioctanoyl-sn-glycerol* (1,2-DAG). The results indicate that 1,2-DAG promotes PKD1 activity in undifferentiated as well as differentiated 3T3-L1 cells (Figure 14). This suggests that PKD1 activity in adipocytes might be induced by activation of other receptors utilizing DAG as secondary messenger and possibly by other sources of DAG.

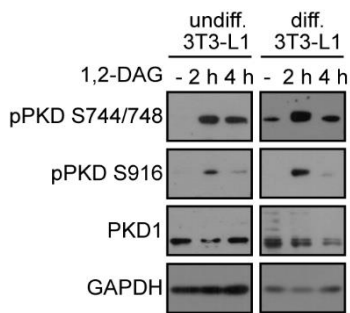


**Figure 14. DAG is directly activating PKD1 in white adipocytes.** WB analysis was performed in undifferentiated and differentiated 3T3-L1 cells stimulated with DAG (100  $\mu$ M) for 2 and 4 h, using antibodies against pPKD1 (S744/748), pPKD (S916), and PKD1. GAPDH was used as a loading control. Data are representative for two individual experiments. *Protein kinase D* (PKD); *phospho* (p); *serine* (S); *1,2-Dioctanoyl-sn-glycerol* (1,2-DAG); *glyceraldehyde 3-phosphate dehydrogenase* (GAPDH); *undifferentiated* (undiff.); *differentiated* (diff.); *hours* (h). (Löffler *et al.*, 2018)<sup>219</sup>

### 3.1.3 PKD1 is not primarily activated by purines in differentiated brown adipocytes

Furthermore, it was tested, whether brown adipocytes follow the same upstream activation pathway. In brown-like adipocytes, stimulation of differentiated T371 cells with insulin and carbachol increases activity of PKD1 (Figure 15A) as well as stimulation with isoproterenol and serotonin at the 5 min time point (Figure 15B). Extracellular purines also activate PKD1 at any time point (Figure 15C). However, stimulation with DAG directly only had a minor effect on the phosphorylation of PKD1 (Figure 15C). This indicates that in differentiated brown adipocytes, PKD1 is not only activated by paracrine factors, but also upon  $\beta$ -adrenergic as well as endocrine and autocrine stimulation.

## RESULTS

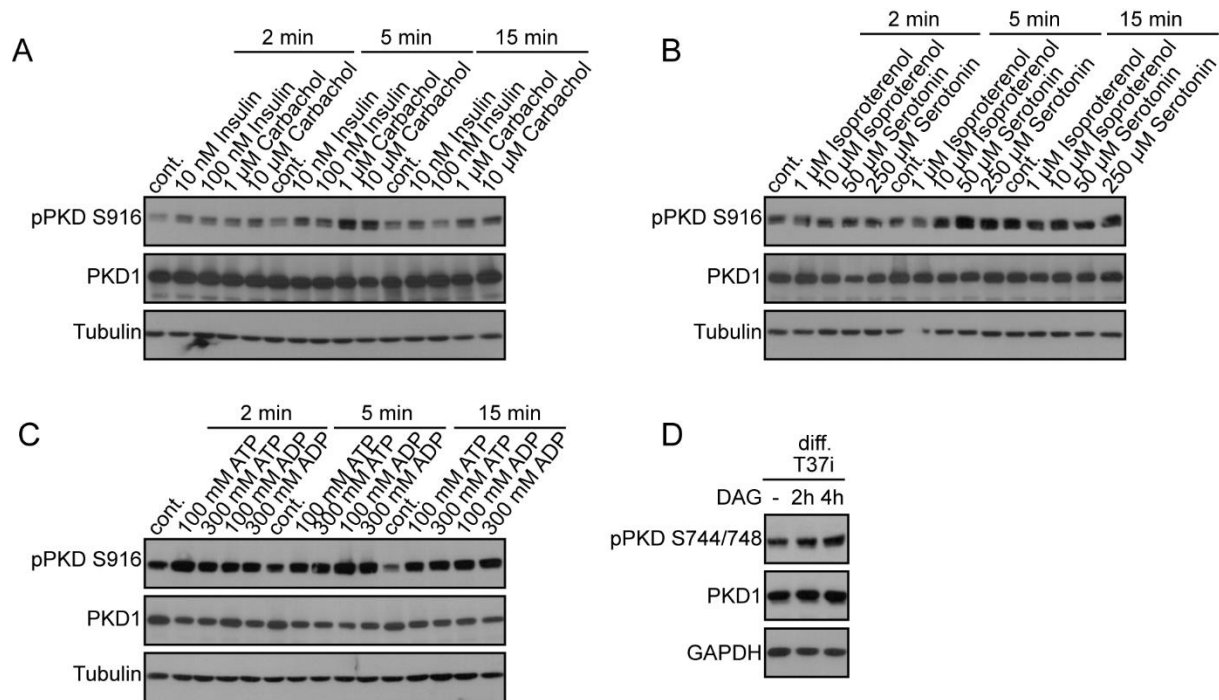


**Figure 15. PKD1 is activated upon stimulation with several endocrine factors in brown adipocytes.** WB analysis was performed using antibodies against pPKD1 (S916) as well as PKD1 in T371 cells, which were differentiated into adipocytes and stimulated with (A) insulin (10 nM, 100 nM), carbachol (1 μM, 10 μM), (B) isoproterenol (1 μM, 10 μM), serotonin (50 μM, 250 μM) or (C) ATP (100 mM, 300 mM) and ADP (100 mM, 300 mM) for 2, 5, and 15 min. Tubulin was used as a loading control. (D) WB analysis of pPKD1 (S744/748) and PKD1 expression in differentiated T371 cells stimulated with 1,2-DAG (100 μM) for 2 and 4 h. GAPDH served as a loading control. *Protein kinase D (PKD)*; *phospho (p)*; *serine (S)*; *control (cont.)*; *adenosine triphosphate (ATP)*; *adenosine diphosphate (ADP)*; *minutes (min)*; *molar (M)*; *1,2-dioctanoyl-sn-glycerol (DAG)*; *glyceraldehyde 3-phosphate dehydrogenase (GAPDH)*; *differentiated (diff.)*; *hours (h)*. ((A,B,C) Löffler *et al.*, 2018)<sup>219</sup>, (D) unpublished observation)

### 3.1.4 Deletion of PKD1 suppresses lipid accumulation in adipocytes

DAG is synthesized in the process of lipogenesis as an intermediate product and it has the potential to directly activate PKD1. Therefore, the impact of PKD1 during TG synthesis in adipocytes needs to be further studied. At first, 3T3-L1 cells were subjected to an adipocyte differentiation protocol in the presence of a specific PKD inhibitor: CID755673<sup>145</sup>. After 10 days of differentiation, 3T3-L1 cells, treated with different concentrations of CID755673, accumulated up to approximately 40% less of TGs than corresponding control cells as indicated by an AdipoRed assay (Figure 16A) and Oil-Red-O staining (Figure 16B). These results suggest that at least one of the PKD isoforms promotes TG accumulation.

## RESULTS

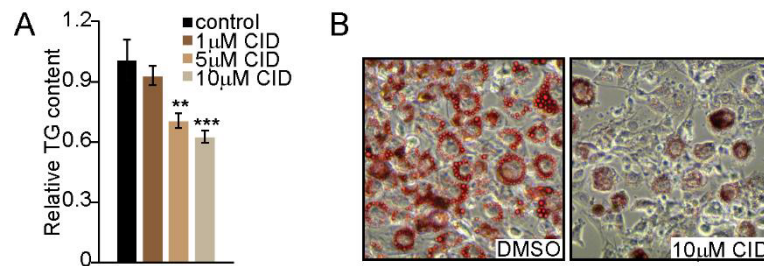


**Figure 16. Inhibition of PKD reduces TG accumulation in 3T3-L1 cells.** (A) Quantification of relative TG accumulation using AdipoRed reagent was conducted in 3T3-L1 cells treated with CID755673 (1  $\mu$ M, 5  $\mu$ M, 10  $\mu$ M) every other day during differentiation. (B) Images of Oil-Red-O staining for neutral lipids were performed in 3T3-L1 cells treated with CID755673 (10  $\mu$ M) every other day during differentiation. Cells were visualized using an inverted microscope Olympus IX71 at 20x magnification. Data are shown in mean  $\pm$  SEM (n=3). (A) One-way ANOVA with Tukey's multiple comparisons. For all data, \*\*p<0.01 and \*\*\*p<0.001. Triglyceride (TG); 2,3,4,5-tetrahydro-7-hydroxy-1H-benzofuro[2,3-c]azepin-1-one (CID); dimethylsulfoxid (DMSO); molar (M) . (unpublished observation)

To test whether deletion of PKD1 in pre-adipocytes might be sufficient to reduce TG accumulation, stable cell lines were generated, displaying an efficient shRNA-mediated PKD1 knockdown (*small hairpin PKD1* (shPKD1); controls (*small hairpin non-targeting control* (shNTC)) (Figure 17A). Moreover, 3T3-L1 cells with overexpression of a wild-type form of PKD1 (*PKD1 wild-type* (PKD1wt)) and a constitutively active form of PKD1 (*PKD1 constitutive active* (PKD1ca)) were generated (Figure 17B), to test whether PKD1 is not only required but also sufficient to induce lipid accumulation.

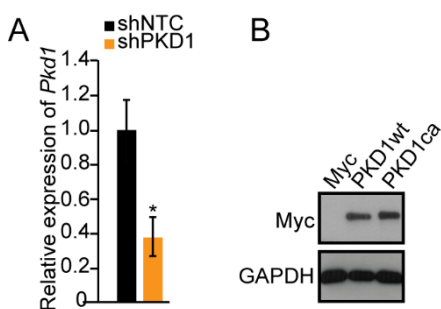


**Figure 17. Effective generation of stable cell lines.** (A) RT-qPCR analysis of *Pkd1* levels in 3T3-L1 cells stably transfected with shRNA against PKD1 and control cells. (B) WB analysis was performed with an anti-Myc antibody to detect exogenously expressed C-terminally Myc-tagged PKD1, in cells expressing Myc, PKD1wt, and PKD1ca. GAPDH was used as a loading control. Results are presented as mean  $\pm$  SEM (n=4; representative of three different experiments). (A) Unpaired, two-tailed Student's t-test. For all data, \*p<0.05. *Protein kinase D* (PKD); *small hairpin* (sh); *non-targeting control* (NTC); *wild type* (wt); *constitutive active* (ca); *glyceraldehyd-3-phosphat-dehydrogenase* (GAPDH). (Löffler *et al.*, 2018)<sup>219</sup>

## RESULTS

Indeed, cells lacking PKD1 demonstrated a significant decrease in the TG content after 10 days of differentiation compared to the corresponding control cells using an AdipoRed assay (Figure 18A). Oil-Red-O staining also revealed less TG accumulation as well as smaller lipid droplets within the cells (Figure 18B). Conversely, overexpression of PKD1ca in differentiated 3T3-L1 cells led to a more than 50% increased accumulation of TGs compared to control cells, whereas overexpression of PKD1wt did not lead to any changes (Figure 18C,D).

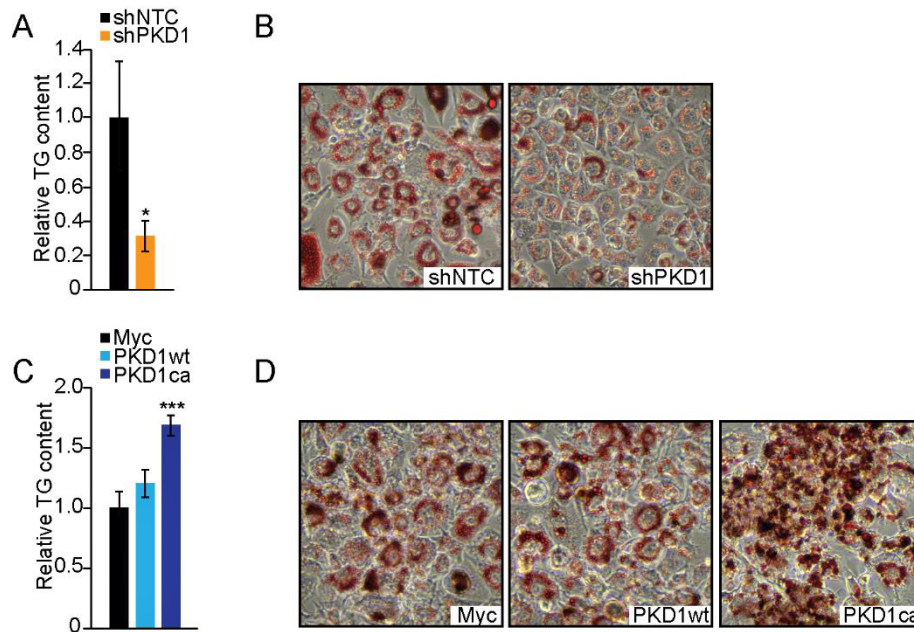


**Figure 18. PKD1 promotes TG accumulation in differentiated 3T3-L1 cells.** (A and C) Quantification of relative TG accumulation using AdipoRed reagent and (B and D) images of Oil-Red-O staining for neutral lipids was performed in (A and B) 3T3-L1 cells depleted of PKD1 using specific shRNA and in (C and D) 3T3-L1 cells overexpressing PKD1wt as well as PKD1ca. Cells were visualized using an inverted microscope Olympus IX71 at 20x magnification. Data are shown in mean  $\pm$  SEM (n=6; representative of three individual experiments). (A) Unpaired, two-tailed Student's t-test, (B) one-way ANOVA with Tukey's multiple comparisons post-test. For all data, \*p<0.05 and \*\*\*p<0.001. *Protein kinase D* (PKD); *small hairpin* (sh); *non-targeting control* (NTC); *triglyceride* (TG); *wild type* (wt); *constitutive active* (ca). (Löffler et al., 2018)<sup>219</sup>

The next step was to investigate whether the deletion of PKD1 has the same effect in primary cells isolated from fat tissue of mice and differentiated into adipocytes *in vitro*. To assess this, mice lacking PKD1 specifically in adipocytes (PKD1adipo. $\Delta/\Delta$ ) were generated using previously described PKD1 floxed mice<sup>150</sup> and a mouse strain expressing Cre recombinase under the control of an adiponectin promoter<sup>160</sup>. This resulted in a substantial reduction of PKD1 mRNA and protein levels in differentiated



## RESULTS

SVC isolated from sWAT of PKD1adipo. $\Delta/\Delta$  mice (Figure 19A,B). Importantly, AdipoRed assay and Oil-Red-O staining presented markedly lower TG content in these cells compared to corresponding controls (Figure 19C,D).

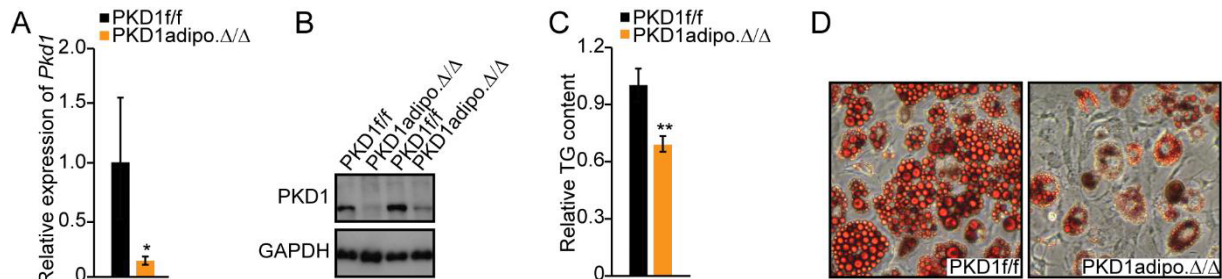


**Figure 19. Deletion of PKD1 reduces TG accumulation in differentiated SVF derived from mice.** (A) mRNA levels of *Pkd1* in SVC-derived adipocytes isolated from PKD1adipo. $\Delta/\Delta$  and control mice. (B) PKD1 levels defined by WB in SVC-derived adipocytes isolated from PKD1adipo. $\Delta/\Delta$  and control mice using an antibody against PKD1. GAPDH was used as a loading control. (C) Quantification of relative TG accumulation using AdipoRed reagent and (D) images of Oil-Red-O staining for neutral lipids was performed in PKD1-deficient SVC differentiated into adipocytes. Cells were visualized using an inverted microscope Olympus IX71 at 20x magnification. Data are shown as  $\pm$  SEM (n=4/genotype; representative for three individual experiments). (A,C) Unpaired, two-tailed Student's t-test. For all data, \*p<0.05 and \*\*p<0.01. *Protein kinase D* (PKD); *adiponectin* (adipo.); *flox/flox* (f/f); *triglycerides* (TG); *glyceraldehyd-3-phosphat-dehydrogenase* (GAPDH). (Löffler et al., 2018)<sup>219</sup>

### 3.2 PKD1 decreases mitochondrial respiration and promotes lipogenesis in adipocytes

#### 3.2.1 Changes in TG accumulation are not correlating with the adipocyte differentiation or their lipolysis rate

Several reasons might account for the decreased TG accumulation upon deletion of PKD1, such as changes in differentiation, alterations in lipolysis and/or lipogenesis, as well as changes in the energy homeostasis of the cells. Interestingly, adipocyte differentiation markers were not altered in PKD1-deficient SVC. Neither levels of PPAR $\gamma$ , the major transcription factor regulating terminal adipocyte differentiation, were affected (Figure 20A) nor levels of classical adipocyte structural proteins and enzymes (ATGL, HSL, and Perilipin) (Figure 20A). PPAR $\gamma$  was slightly upregulated in cells expressing PKD1ca but not altered in differentiated 3T3-L1 cells expressing PKD1wt. Adipocyte specific enzymatic proteins, like HSL or ATGL, were downregulated in PKD1ca as well as PKD1wt to some extent, whereas the structure protein Perilipin was not changed (Figure 20B). Overexpression of PKD1ca led to an increased

## RESULTS

accumulation of TGs in adipocytes (see Figure 18C,D), thus the downregulated expression of HSL and ATGL cannot be responsible for these changes. This indicates that PKD1 facilitates TG accumulation in adipocytes without affecting their differentiation.

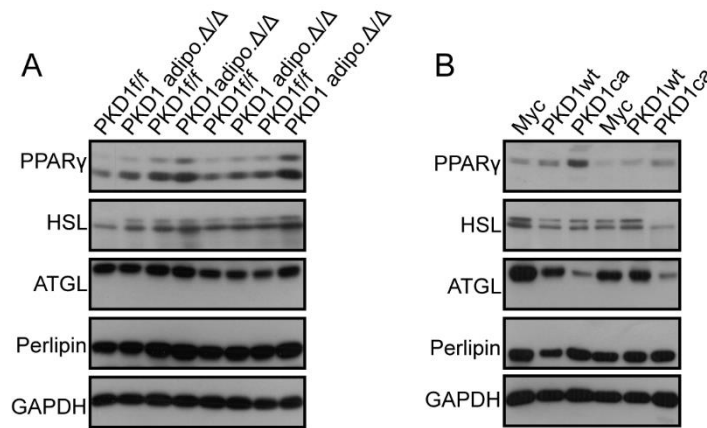


**Figure 20. PKD1 does not regulate adipocyte differentiation.** WB analysis of expression of indicated proteins, PPAR $\gamma$ , HSL, ATGL, and Perlipin in (A) SVC-derived adipocytes isolated from PKD1<sup>adipo. $\Delta/\Delta$</sup>  and control mice (n=4/genotype) and (B) differentiated 3T3-L1 cells overexpressing PKD1<sup>ca</sup> (n=2/cell line). GAPDH was used as a loading control. *Protein kinase D* (PKD); *adiponectin* (adipo.); *flox/flox* (f/f); *peroxisome proliferator-activated receptor* (PPAR); *hormone-sensitive lipase* (HSL); *adipose triglyceride lipase* (ATGL); *glyceraldehyd-3-phosphat-dehydrogenase* (GAPDH); *wild type* (wt); *constitutive active* (ca). ((A) Löffler *et al.*, 2018)<sup>219</sup>, ((B) unpublished observation)

In order to explain the altered TG accumulation, the regulation of PKD1 in the context of lipolysis in adipocytes was assessed. FFAs and glycerol, which are released from adipocytes during lipolysis, did not show any differences in the media compared to controls, neither unstimulated nor 2 h after stimulation with isoproterenol, the major factor inducing lipolysis. (Figure 21A-D). Since lipolysis is not affected by changes in PKD1 expression it cannot be responsible for the observed changes in TG accumulation.

## RESULTS

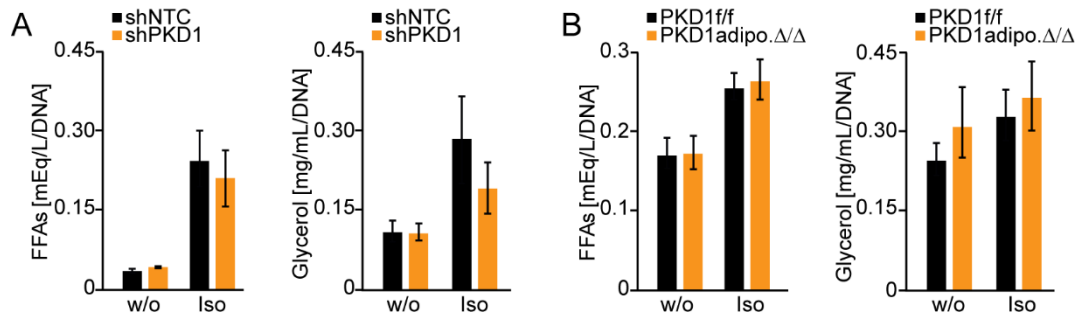


**Figure 21. Deletion of PKD1 does not affect lipolysis rate in adipocytes.** FFA and glycerol secretion from (A) differentiated control and PKD1-depleted 3T3-L1 cells stimulated with vehicle or 10  $\mu$ M isoproterenol for 2 h and (B) differentiated adipocytes derived from SVC of sWAT isolated from mice of indicated genotypes, which were either unstimulated or stimulated for 2 h with 10  $\mu$ M isoproterenol. Data are shown as  $\pm$  SEM (n=6; representative for three individual experiments). Unpaired, two-tailed Student's t-test. *Protein kinase D* (PKD); *small hairpin* (sh); *non-targeting control* (NTC); *free fatty acids* (FFAs); *isoproterenol* (Iso); *without* (w/o); *deoxyribonucleic acid* (DNA); *adiponectin* (adipo.); *flox/flox* (f/f). (Löffler *et al.*, 2018)<sup>219</sup>

### 3.2.2 PKD1 promotes lipogenesis in adipocytes

Since neither differentiation nor lipolysis rate in adipocytes were affected by PKD1, another explanation for the increased accumulation of TGs in PKD1ca and decreased content of lipids in cells lacking PKD1 could be an altered lipogenesis rate of the adipocytes. Indeed, differentiated 3T3-L1 cells lacking PKD1 showed a reduced lipogenesis rate compared to control cells under basal- and insulin-induced lipogenesis (Figure 22A). In primary adipocytes derived from SVC of PKD1adipo.Δ/Δ mice insulin-induced lipogenesis rate was even decreased by half (Figure 22B). In contrast, expression of PKD1ca led to an increased basal and insulin-stimulated lipogenesis rate in differentiated 3T3-L1 cells (Figure 22C). These results suggest that PKD1 affects lipogenesis in adipocytes leading to changes in TG accumulation.

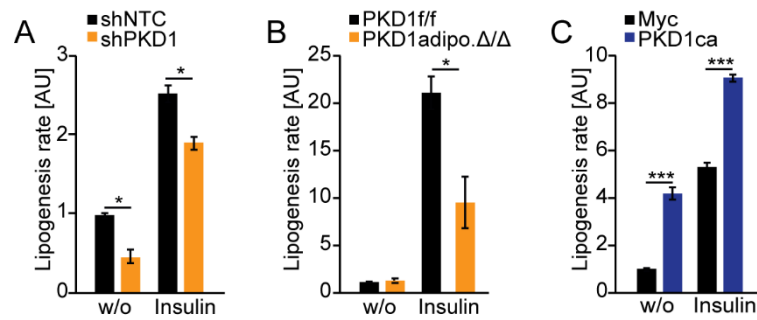


**Figure 22. PKD1 promotes lipogenesis rate in adipocytes.** Basal and 3 h insulin-induced (100 nM) lipogenesis rate in (A) differentiated 3T3-L1 with a PKD1 knockdown by shRNA, (B) differentiated SVC derived from sWAT of PKD1-deficient mice, and (C) 3T3-L1 cells expressing PKD1ca and their corresponding controls. Data are presented as mean  $\pm$  SEM (n=3; representative for three individual experiments). Unpaired, two-tailed Student's t-test. For all data, \* $p < 0.05$  and \*\*\* $p < 0.001$ . *Protein kinase D* (PKD); *small hairpin* (sh); *non-targeting control* (NTC); *arbitrary units* (AU); *without* (w/o); *adiponectin* (adipo.); *flox/flox* (f/f); *constitutive active* (ca). (Löffler *et al.*, 2018)<sup>219</sup>

### 3.2.3 PKD1 suppresses OCR in adipocytes

Another explanation for the reduced accumulation of fat could be changes in the energy homeostasis of these cells. Therefore, energy expenditure in these cells was studied by measuring the cellular respiration rate using a Seahorse analyzer. Deletion of PKD1 in differentiated 3T3-L1 resulted in an elevated OCR during basal respiration, as well as in response to oligomycin (inhibition of the mitochondrial ATP-synthase), and FCCP (stimulation of maximal respiration rate). Upon stimulation with antimycin-A/rotenone (inhibitor of mitochondrial respiration), OCR was decreasing in both PKD1-deficient and control adipocytes (Figure 23A). Proton leak is a physiological process in which protons travel across the mitochondrial inner membrane, mainly driven by UCP1, without contributing to ATP synthesis<sup>223,224</sup>. As indicated by the increased OCR in the presence of oligomycin, this process was also increased in adipocytes lacking PKD1 (Figure 23A). These data indicate that adipocytes lacking PKD1 increase energy dissipation and mitochondrial activity. On the other hand, PKD1ca expressing 3T3-L1 cells displayed a reduced OCR and mitochondrial decoupling activity (Figure 23B), suggesting that, in white adipocytes, PKD1 promotes lipid storage and suppresses energy dissipation.

## RESULTS

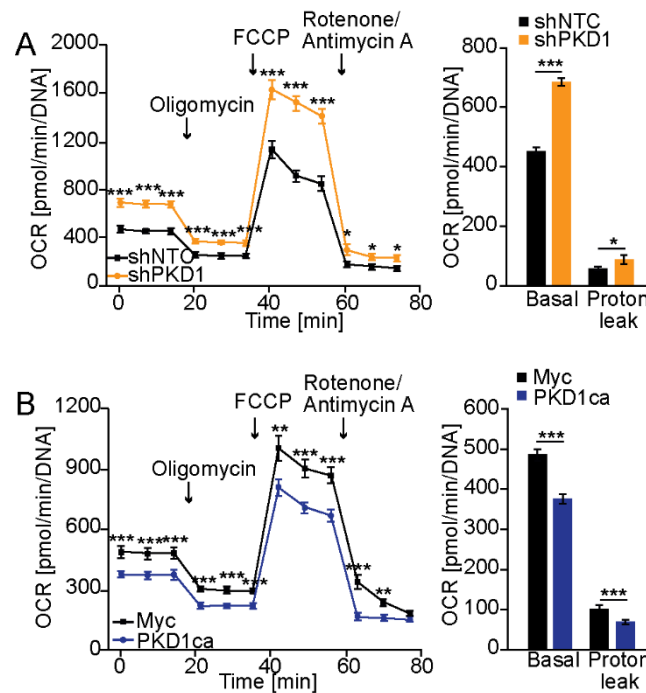


**Figure 23. PKD1 suppresses energy dissipation in adipocytes.** (A) Oxygen consumption rate (OCR) was measured under basal conditions and after stimulation with oligomycin (2  $\mu$ M), FCCP (2  $\mu$ M) and rotenone/antimycin A (1.5  $\mu$ M) in differentiated 3T3-L1 cells lacking PKD1 and corresponding controls over the given time points as well as average of basal OCR and level of proton leak (calculated by deducting the last measurement after rotenone/antimycin A treatment from the last measurement after oligomycin stimulation) assessed in PKD1 deleted adipocytes and controls. (B) OCR in response to indicated substances as well as OCR annotated to the indicated cellular such as basal respiration and proton leak were measured in PKD1ca expressing 3T3-L1 cells and corresponding controls. Data are presented as mean  $\pm$  SEM (n=30; representative of three individual experiments). For all data, \*p<0.05, \*\*p<0.01, and \*\*\*p<0.001. Unpaired, two-tailed Student's t-test. *Protein kinase D* (PKD); *small hairpin* (sh); *non-targeting control* (NTC); *oxygen consumption rate* (OCR); *minutes* (min); *carbonyl cyanide-4-(trifluoromethoxy) phenylhydrazine* (FCCP); *deoxyribonucleic acid* (DNA); *constitutive active* (ca). (Löffler et al., 2018)<sup>219</sup>

A similar phenotype was observed in adipocytes isolated from PKD1adipo. $\Delta/\Delta$ , which showed an increased basal OCR as well as an increase upon oligomycin and FCCP stimulation. Here, proton leak was also increased in PKD1-deficient adipocytes derived from SVC (Figure 24A). Consistently, an increased mitochondrial content was measured in adipocytes lacking PKD1 (Figure 24B). As mentioned before, proton leak is mainly driven by UCP1 and leads to an oxidative phosphorylation uncoupled from ATP synthesis in which energy is dissipated as heat<sup>223,224</sup>. This phenomenon in addition to an increased mitochondrial content are usually typical for brown adipocytes, but can also be found during beiging of adipocytes that develop within white adipose tissue depots<sup>225</sup>. To test if beiging occurs in white adipocytes RT-qPCR analyses were

## RESULTS

performed, in which all the classical browning markers, especially UCP1, were tested. There was no difference in *Ucp1* expression between adipocytes lacking PKD1 and their controls. Neither were any other classical browning genes (*cell death-inducing DNA fragmentation factor,  $\alpha$  subunit-like effector (Cide) a*, *Prdm16*, *bone morphogenic protein 7 (Bmp7)*, *Cideb*, *solute carrier family (Slc) 27a1*, *Slc27a2* (both FA transporter), and *Ucp3*) differently expressed (Figure 24C). This indicates that there must be an additional mechanism regulating increased energy dissipation and mitochondrial content in PKD1-deficient adipocytes.

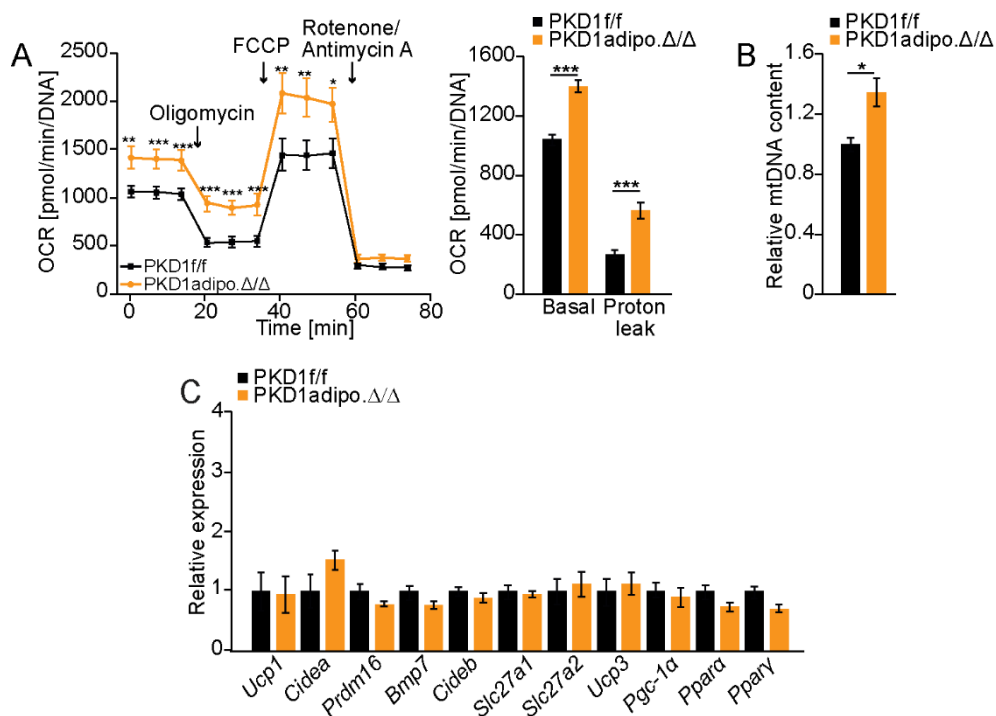


**Figure 24. Deletion of PKD1 increases OCR and mitochondrial content in adipocytes.** OCR was measured under basal conditions and after stimulation with oligomycin (2  $\mu$ M), FCCP (2  $\mu$ M) and rotenone/antimycin A (1.5  $\mu$ M) in differentiated SVC derived from sWAT of PKD1<sup>adipo.Δ/Δ</sup> mice and corresponding controls over the given time points as well as basal respiration and proton leak of these cells (n=14). (B) Ratio of mitochondrial DNA and genomic DNA in SVC-derived adipocytes with deletion of PKD1 and control cells (n=5/genotype). (C) mRNA levels of indicated genes in SVC-derived adipocytes isolated from sWAT of PKD1<sup>adipo.Δ/Δ</sup> and control mice (n=7/genotype). Data are presented as mean  $\pm$  SEM (representative of three individual experiments). Unpaired, two-tailed Student's t-test. For all data, \*p<0.05, \*\*p<0.01 and \*\*\*p<0.001. *Protein kinase D (PKD)*; *adiponectin (adipo.)*; *flox/flox (f/f)*; *oxygen consumption rate (OCR)*; *minutes (min)*; *deoxyribonucleic acid (DNA)*; *carbonyl cyanide-4-(trifluoromethoxy) phenylhydrazine (FCCP)*; *mitochondrial DNA (mtDNA)*; *uncoupling protein (UCP)*; *cell death-inducing DNA fragmentation factor,  $\alpha$  subunit-like effector (CIDE)*; *PR domain containing 16 (PRDM16)*; *bone morphogenic protein 7 (BMP7)*; *solute carrier family (SLC)*; *proliferator-activated receptor  $\gamma$  coactivator 1 $\alpha$  (PGC1 $\alpha$ )*; *peroxisome proliferator-activated receptor (PPAR)*. (Löffler et al., 2018)<sup>219</sup>

### 3.2.4 PKD1 mainly affects white adipose tissue, without changing energy metabolism in brown adipocytes

Since brown adipocytes belong to the metabolically more active adipose tissue, the idea was to assess whether PKD1 also affects the energy homeostasis in brown adipocytes. First, lipogenesis rate was examined in differentiated SVC derived from brown adipose tissue of PKD1<sup>adipo.Δ/Δ</sup> mice. Indeed, lipogenesis was reduced by more than 60% in PKD1-depleted adipocytes after insulin stimulation (Figure 25A). On the other hand, apart from a minor decrease in maximal respiration after stimulation with FCCP in PKD-deficient adipocytes, OCR was not changed upon any other treatment or time point in SVC lacking PKD1 compared to their controls (Figure 25B). In conclusion, PKD1 primarily affects white adipocytes without changing the energy metabolism of brown adipose tissue. This is consistent with the findings that brown adipocytes are also regulated by different upstream stimuli (see Figure 15A-D).

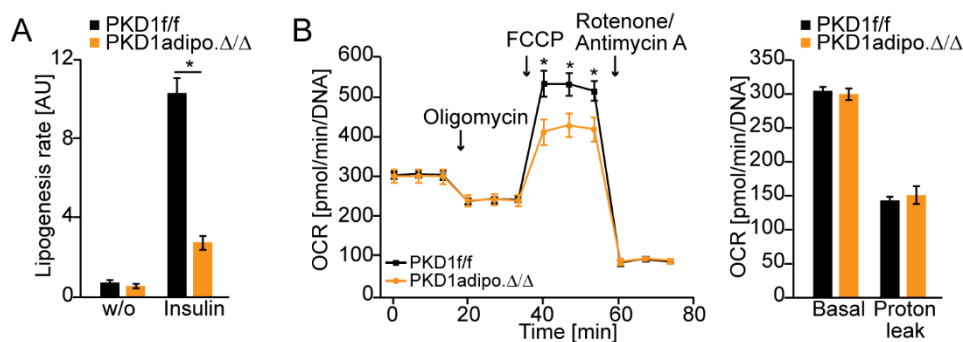


**Figure 25. Deletion of PKD1 in BAT decreases lipogenesis rate in adipocytes without affecting their OCR.** Basal and 3 h insulin-induced (100 nM) lipogenesis rate in adipocytes isolated from SVC of BAT of indicated genotypes. (B) OCR was measured under basal conditions and after stimulation with oligomycin (2  $\mu$ M), FCCP (2  $\mu$ M) and rotenone/antimycin A (1.5  $\mu$ M) in differentiated SVC derived from BAT of PKD1<sup>adipo.Δ/Δ</sup> mice and corresponding controls over the given time points. (C) Basal respiration and proton leak were measured in SVC lacking PKD1. Data are presented as mean  $\pm$  SEM (representative of three individual experiments). Unpaired, two-tailed Student's t-test. For all data, \* $p$ <0.05. *Protein kinase D* (PKD); *adiponectin* (adipo.); *flox/flox* (f/f); *arbitrary units* (AU); *without* (w/o); *oxygen consumption rate* (OCR); *minutes* (min); *deoxyribonucleic acid* (DNA); *carbonyl cyanide-4-(trifluoromethoxy) phenylhydrazone* (FCCP); (Löffler et al., 2018)<sup>219</sup>

### 3.2.5 PKD1 suppresses gene expression of the creatine metabolism and mitochondrial fragmentation

The increase in energy dissipation of adipocytes lacking PKD1 could not be explained by changes in UCP1 or any of the other classical browning markers, meaning there must be an additional explanation for this phenotype. Recently, an alternative

## RESULTS

mechanism of energy dissipation by beige adipocytes has been proposed. Creatine-driven substrate cycle can increase energy expenditure of adipocytes independently of UCP1 expression<sup>17</sup>. Interestingly, expression of most of the creatine metabolism related genes (*myosin heavy polypeptide (Myh) 1*, *Myh2*, *creatine kinase muscle (Ckm)*, *creatine kinase mitochondrial (Ckmt) 1*, *Ckmt2*, and *melanocyte proliferating gene (Myg)*) were markedly up regulated in adipocytes lacking PKD1 (Figure 26), suggesting that creatine-dependent energy dissipation is enhanced in the absence of PKD1.

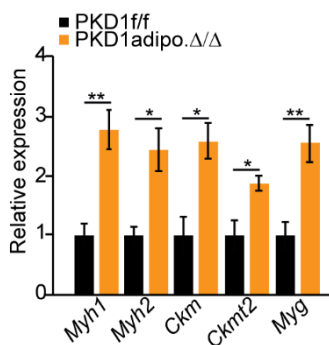


**Figure 26. Deletion of PKD1 enhances expression of genes involved in the creatine metabolism.** mRNA levels of indicated genes in SVC-derived adipocytes isolated from sWAT of PKD1<sup>adipo.Δ/Δ</sup> and control mice. Data are presented as mean ± SEM (representative of three individual experiments). Unpaired, two-tailed Student's t-test. For all data, \* $p < 0.05$  and \*\* $p < 0.01$ . *Protein kinase D* (PKD); *adiponectin* (adipo.); *flox/flox* (f/f); *myosin heavy polypeptide* (MYH); *creatine kinase muscle* (CKM); *creatine kinase mitochondrial* (CKMT); *melanocyte proliferating gene* (MYG). (Löffler et al., 2018)<sup>219</sup>

Another recently shown explanation for changes in energy dissipation would be alterations in mitochondrial dynamics. In order to sustain their optimal bioenergetics, the highly dynamic mitochondria undergo constant fission and fusion<sup>123</sup>. Fragmentation of mitochondria was previously shown to increase energy expenditure in adipocytes by supporting uncoupled respiration<sup>67,129</sup>. Consistently, deletion of PKD1 in differentiated 3T3-L1 cells as well as SVC increased mitochondrial fragmentation, shown by representative IF images and respective quantifications of fragmented, intermediate, and fused cells per genotype (Figure 27A,B). In contrast, more fused mitochondria were found in PKD1<sup>ca</sup> expressing 3T3-L1 cells (Figure 27C), indicating that PKD1 suppresses mitochondrial fragmentation or promotes mitochondrial fusion to reduce energy dissipation in adipocytes.



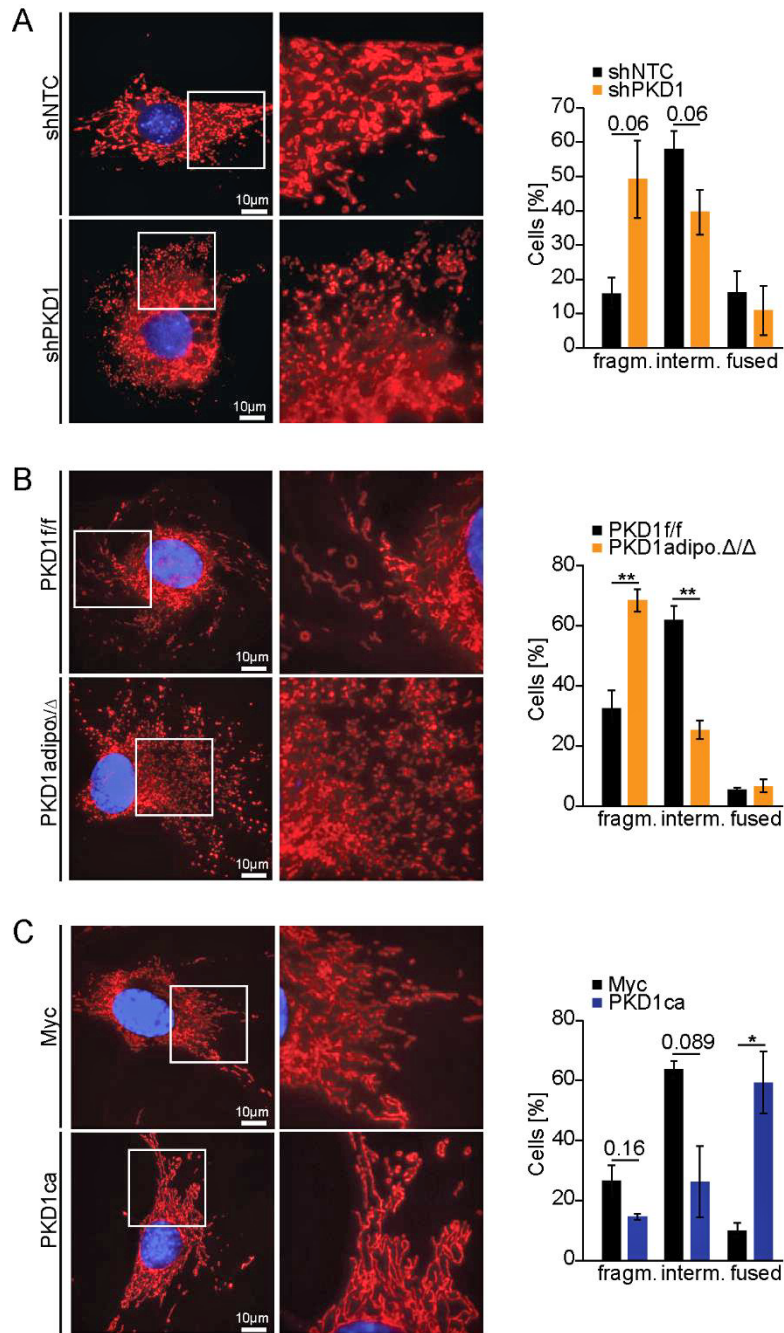


**Figure 27. PKD1 suppresses mitochondrial fragmentation.** Representative microscopy images of the mitochondrial morphology and its respective quantification of fragmented, intermediate and fused cells in (A) differentiated 3T3-L1 cells lacking PKD1, (B) PKD1-deficient adipocytes derived from SVC of sWAT, and (C) differentiated 3T3-L1 cells expressing PKD1ca and corresponding controls. Cells were stained with 150 nM MitoTracker Red for 30 min at 37 °C and subsequently fixed with 4% PFA. Nuclei were stained using DAPI. Cells were visualized under a fluorescent microscope Leica DM5500 B at 63x magnification. Quantitative data are shown as the mean  $\pm$  SEM of three independent experiments with 200 cells counted for each replicate. Unpaired, two-tailed Student's t-test. For all data, \* $p < 0.05$  and \*\* $p < 0.01$ . *Protein kinase D* (PKD); *small hairpin* (sh); *non-targeting control* (NTC); *fragmented* (fragm.); *intermediate* (interm.); *adiponectin* (adipo.); *flox/flox* (f/f); *constitutive active* (ca). (Löffler et al., 2018)<sup>219</sup>

### 3.3 PKD1 regulates adipocyte function by targeting AMPK- and possibly mTORC signaling

#### 3.3.1 Rictor is a possible interaction partner of PKD1 in adipocytes

To further investigate the molecular mechanism through which PKD1 regulates the adipose tissue, an unbiased approach was applied to identify possible interaction partners. To this end, an IP was performed in cells overexpressing Myc-tagged PKD1ca. Successful pull-down of Myc was achieved and confirmed using WB analysis and Coomassie blue staining (Figure 28A,B).

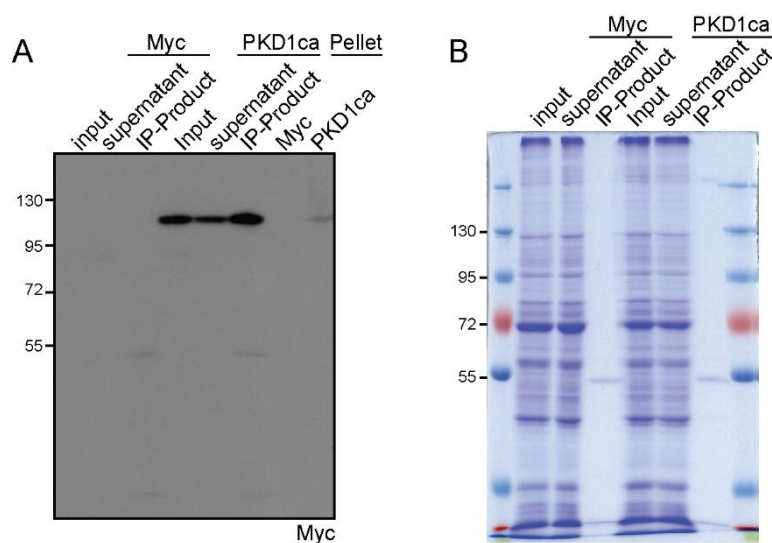


**Figure 28. Pull-down of Myc in differentiated 3T3-L1 cells.** IP was performed using magnetic Myc beads to pull-down Myc-tagged PKD1ca and corresponding controls in differentiated 3T3-L1 cells and confirmed using lysates from the input, supernatant and IP-product for (A) WB analysis or (B) Coomassie staining (representative of three individual experiments). *Protein kinase D* (PKD); *constitutive active* (ca); *immunoprecipitation* (IP). (unpublished observation)

The IP-products were analyzed by mass spectrometry to identifying Rictor as one likely interaction partner of PKD1 in adipocytes. Rictor is part of the mTORC2 complex and has been shown to play an important role in the lipid metabolism<sup>226-231</sup>. *Cullin 7* (CUL7), mediating ubiquitination and degradation of the IRS1 in an mTOR-dependent manner<sup>232</sup> or *AT-rich interaction domain 5b* (ARID5B), also known as modulator recognition factor 2 (MRF2), which was shown to be required for adipogenesis by regulating TG metabolism in adipocytes through the regulation of adipogenic gene expression<sup>233-235</sup>, were also identified. PKD2, another PKD isoform, was shown to dimerize with PKD1<sup>236</sup>, thus appearing in the list of possible interaction partners (Table

## RESULTS

1). Since Rictor was the top hit and mTORC2 has previously been shown to be involved in adipocyte regulation, a possible interaction of PKD1 and Rictor was confirmed by WB after IP in differentiated PKD1ca 3T3-L1 cells (Figure 29).

**Table 1. PKD1 interaction partners identified through mass spec analysis.** (A) IP was performed in differentiated 3T3-L1 cells overexpressing PKD1ca using Myc-tagged beads. The IP-product was analyzed via mass spectrometry and candidate proteins are displayed below. This experiment was conducted in collaboration with the working group of Dr. Schlosser. *Protein kinase D* (PKD); *cullin 7* (CUL7); *AT-rich interaction domain 5b* (ARID5B); *synaptopodin* (SNYPO); *light-free quantification* (LFQ); immunoprecipitation (IP). (unpublished observation)

	Gene names	Razor and unique peptides	log10 LFQ intensity_ctrl	log10 LFQ intensity_IP
1	PKD1ca	126	7.68	11.90
2	Rictor	38	7.48	9.17
3	CUL7	26	7.98	9.02
4	ARID5B	24	6.95	9.09
5	SNYPO	24	7.54	8.96
6	PKD2	22	6.89	10.40

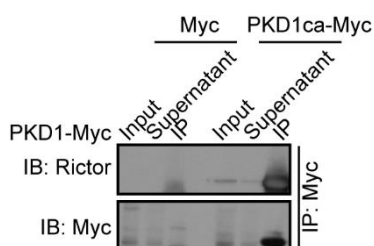


**Figure 29. PKD1 interacts with Rictor in differentiated 3T3-L1 cells.** Immunoblots using antibodies against Rictor and Myc were performed after pulling down overexpressed Myc-tagged PKD1ca in differentiated 3T3-L1 cells (representative of three individual experiments). *Protein kinase D* (PKD); *constitutive active (ca)*; *immunoprecipitation* (IP); *immunoblot* (IB). (unpublished observation)

### 3.3.2 PKD1 possibly regulates adipocyte function through the phosphorylation of Akt, a downstream target of mTOR

The mTOR signaling network plays an important role in the central regulation of cell growth and metabolism and is regulated by amino acids and growth factors, such as insulin. Several studies implied the role of mTORC1 and mTORC2 complexes in the regulation of adipose tissue function<sup>226-231,237-239</sup>. Furthermore, dysfunctions of the

## RESULTS

mTORC2 signaling have been implicated in the development of insulin resistance and diabetes<sup>240</sup>. Since Rictor, as part of the mTORC2 complex, was identified as a possible interaction partner of PKD1 in adipocytes, further investigations were conducted to identify whether downstream targets of the mTORC2 complex are regulated by PKD1. One of the downstream targets is Akt, which is usually found in an inactive conformation in the cytosol. Upon PI3K activation, e.g. through insulin, Akt is translocated and phosphorylated on the T308, which is the phosphorylation site independently of the mTORC2 complex. Full activation of Akt is achieved by phosphorylation of S473, which is catalyzed by the mTORC2 complex<sup>241</sup>. WB analysis revealed that upon inhibition of PKD1 with CID755673 there was a clear upregulation of pAkt S473 after treatment with insulin, whereas pAkt T308 was only mildly changed (Figure 30). This result shows that PKD1 regulates the mTORC2 complex and its downstream targets most likely through an inhibitory phosphorylation of Rictor.

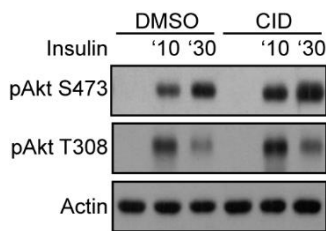


**Figure 30. Inhibition of PKD1 results in an upregulation of Akt activity.** WB analysis using antibodies against pAkt S473 and pAkt T308 in differentiated 3T3-L1 cells treated with CID755673 (10  $\mu$ M) during differentiation and stimulated with insulin (100 nM) for 10 and 30 min. Actin was used as a loading control. *Protein kinase B (Akt); phospho (p); serine (S); threonine (T); dimethylsulfoxid (DMSO); 2,3,4,5 tetrahydro-7-hydroxy-1H-benzofuro[2,3-c] azepin-1-one (CID);*. (unpublished observation)

To further examine the role of PKD1 in the mTORC signaling pathway, cells were incubated in medium supplemented with amino acids and glucose or without, since mTORC is regulated by nutrients and growth factors<sup>241,242</sup>. In contrast to PKD1 inhibition, overexpression of PKD1ca in differentiated 3T3-L1 cells led to a downregulation of pAkt S473, especially after nutrients were removed from the medium and cells were stimulated with insulin, whereas activity of Akt on its phosphorylation site T308 was even slightly increased, especially when nutrients were removed from the medium (Figure 31A). According to the literature, increased activity of mTORC2 is also upregulating the mTORC1 signaling pathway by inhibition of TSC1/2 through Akt<sup>227</sup>. In case of differentiated cells overexpressing PKD1ca, an upregulation of mTORC1 could be observed via WB after nutrient deprivation and even more after insulin stimulation, seen by the mTORC1 specific phosphorylation site S2448. S6K activity, a substrate downstream of mTORC1, was also upregulated in PKD1ca cells

## RESULTS

compared to controls upon nutrient deprivation in addition to insulin stimulation (Figure 31A). Expression of Raptor or Rictor itself were not changed due to PKD1 under any of the growth conditions (Figure 31B). Taken together, these findings show that PKD1 inhibits downstream targets of the mTORC2 complex by inhibiting the mTORC2 complex possibly through an interaction with Rictor. Nevertheless, mTORC1 and its downstream targets are still upregulated, suggesting that there might be another regulator of the mTORC1 complex, which is also controlled by PKD1.

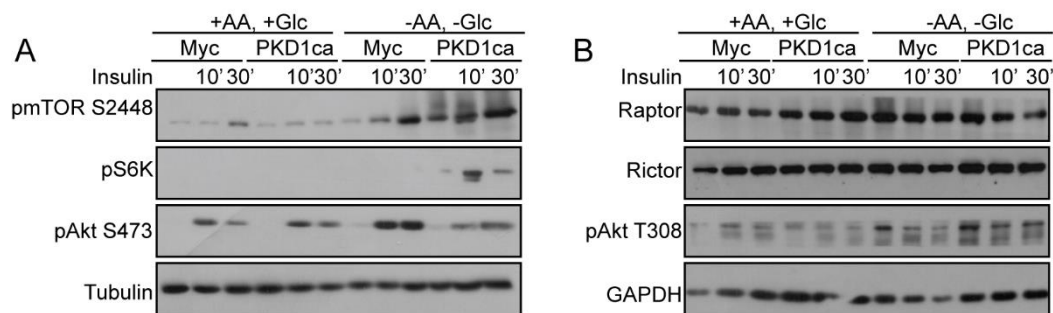


**Figure 31. PKD1 is impeding mTORC2 signaling, while it is upregulating the mTORC1 complex and its downstream targets.** WB analysis using antibodies targeting mTORC1 specific phosphorylation site S2448, pAkt S473, pAkt T308 and pS6K in differentiated 3T3-L1 cells overexpressing PKD1ca, which were either grown in medium supplemented with amino acids and glucose or without and treated with insulin (100 nM) for 10 and 30 minutes. Tubulin was used as a loading control. (B) WB analysis using antibodies against Raptor, Rictor and pAkt T308 in PKD1ca cells kept in medium with or without amino acids and glucose. GAPDH was used as a loading control. *Protein kinase D* (PKD); *phospho* (p); *serine* (S); *threonine* (T); *constitutive active* (ca); *amino acids* (AA); *glucose* (Glc); *mammalian target of rapamycin* (mTOR); *ribosomal protein S6 kinase* (S6K); *glyceraldehyd-3-phosphat-dehydrogenase* (GAPDH). ((part of A) Löffler *et al.*, 2018)<sup>219</sup>, ((A,B) unpublished observation)

### 3.3.3 PKD1 regulates adipocyte function mainly by suppressing AMPK activity

The underlying molecular mechanism of PKD1-dependent regulation of adipocyte function was further unraveled, using a targeted approach. So far, it was shown that PKD1 promotes lipogenesis, suppresses OCR, and is involved in the regulation of mitochondrial biogenesis. AMPK is a multi-subunit enzyme, which regulates several processes of energy homeostasis in adipocytes<sup>182,243</sup>. It was previously demonstrated to mediate inhibitory phosphorylation of ACC that reduces malonyl-CoA leading to inhibition of CPT1 to promote FAO and suppress FA synthesis<sup>188</sup>. AMPK was further revealed to regulate mitochondrial homeostasis through MFF<sup>130</sup> and to inhibit mTOCR1 by raptor phosphorylation<sup>187</sup>. Importantly, recent studies indicate that in

## RESULTS

---

muscle cells PKD1 phosphorylates AMPK $\alpha$  subunits, leading to inactivation of the kinase activity of the whole complex<sup>185</sup>. Therefore, the influence of PKD1 on AMPK in adipocytes was tested. Interestingly, AMPK $\alpha$  phosphorylation at putative PKD1 sites (S485/S491) was reduced in PKD1-deficient adipocytes, whereas total AMPK levels remained unchanged. Additionally, AMPK $\alpha$  phosphorylation site T172, which is a good indicator for the general activity of the protein, showed an enhanced phosphorylation in PKD1-deficient cells (Figure 32A,B). On the other hand, differentiated 3T3-L1 cells expressing PKD1ca presented the opposite (Figure 32C). These results demonstrate that PKD1 inhibits AMPK activity in adipocytes. Consistently, classical AMPK targets, ACC1/ACC2 at S79/S221<sup>182</sup>, displayed an increased phosphorylation in adipocytes lacking PKD1 and reduced in PKD1ca cells, whereas total ACC levels were not altered. Densitometric analysis was conducted for each of the given proteins (Figure 32A,B,C). These results are a good indication that PKD1 regulates adipocyte function in an AMPK-dependent manner by inhibitory phosphorylation of AMPK $\alpha$  at S485/491, leading to a decreased phosphorylation of ACC at S79.

## RESULTS

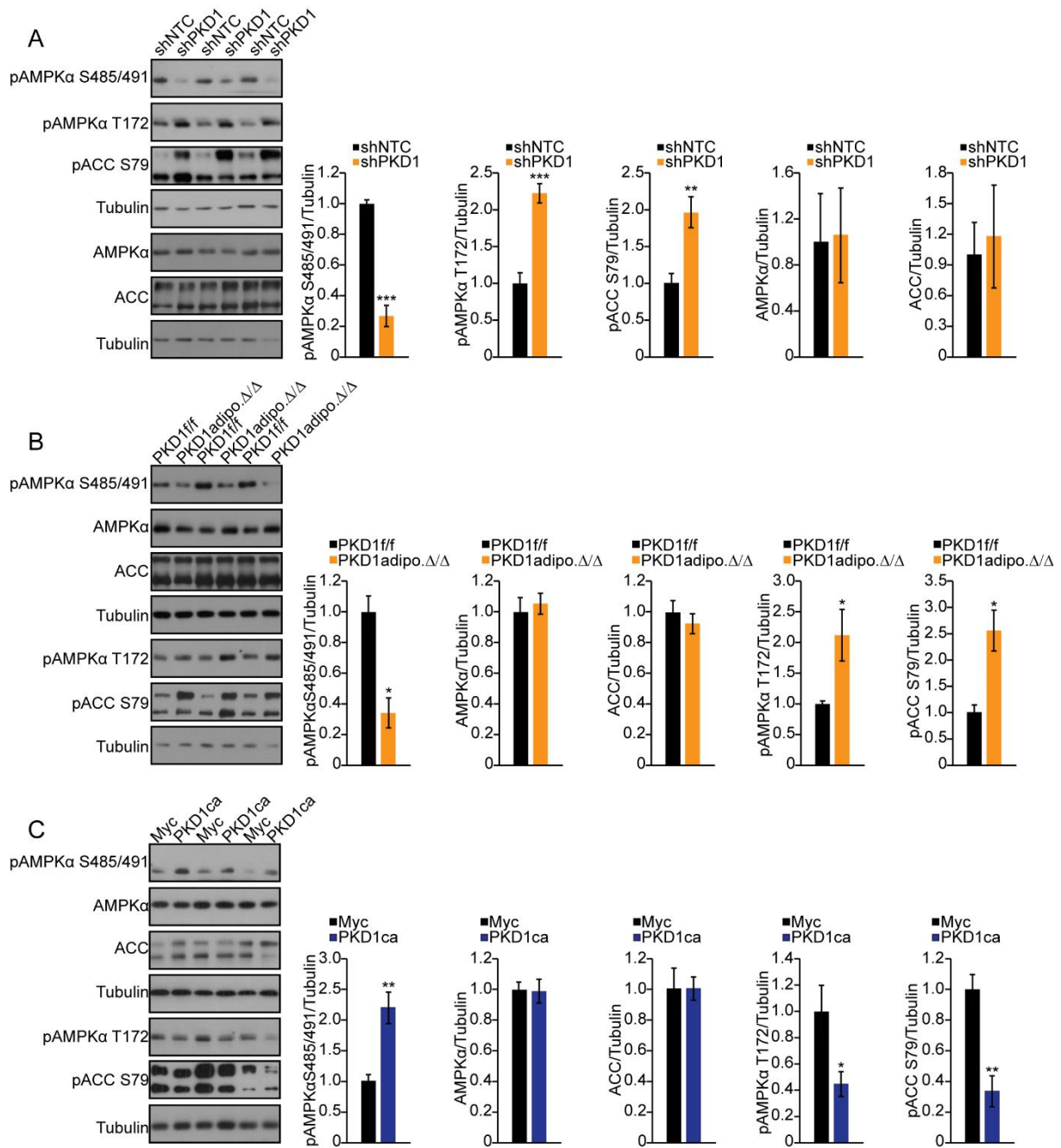


**Figure 32. PKD1 regulates adipocyte function in an AMPK-dependent manner.** WB analysis using antibodies against AMPKα phosphorylation site S485/491, AMPKα, ACC, pAMPKα T172, and pACC S79 in (A) differentiated 3T3-L1 cells lacking PKD1, (B) differentiated SVC isolated from sWAT of PKD1adipo.Δ/Δ mice as well as (C) differentiated 3T3-L1 cells overexpressing PKD1ca and their corresponding controls including densitometric analysis of four replicates each. Tubulin was used as a loading control. Data are presented as mean ± SEM. Unpaired, two-tailed Student's t-test. For all data, \*p<0.05, \*\*p<0.01 and \*\*\*p<0.001. *Protein kinase D* (PKD); *phospho* (p); *serine* (S); *threonine* (T); *small hairpin* (sh); *non-targeting control* (NTC); *AMP-activated protein kinase* (AMPK); *acetyl-CoA carboxylase* (ACC); *adiponectin* (adipo.); *flox/flox* (f/f); *constitutive active* (ca). (Löffler et al., 2018)<sup>219</sup>

## RESULTS

To further test whether AMPK is more active upon deletion of PKD1 in adipocytes a phospho-AMPK substrate motif antibody was used, which preferentially recognizes endogenous proteins and peptides containing the LXRXXpS/pT motif. Indeed, more AMPK substrates could be detected in cells lacking PKD1, whereas 3T3-L1 cells expressing PKD1ca showed the opposite (Figure 33A,C). Since the PKD1 motif antibody recognizes the same consensus sequence, this antibody was tested on the same lysates to exclude overlapping of the same substrates. It is clearly visible that PKD1 substrate recognition is reduced in cells lacking PKD1 and shows a completely different pattern compared to the AMPK motif antibody and the opposite can be seen in PKD1ca cells (Figure 33B,D).

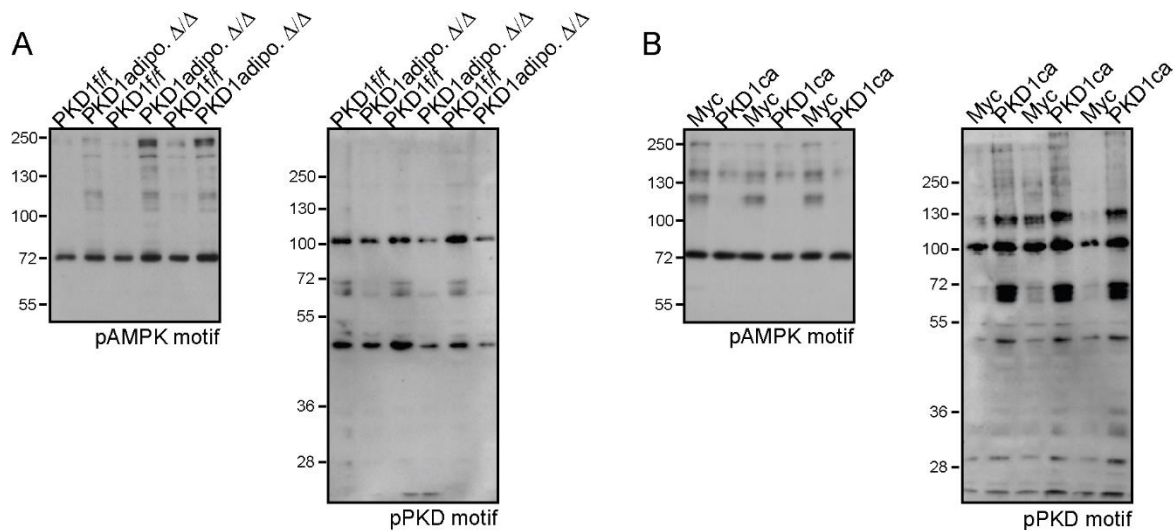


**Figure 33. AMPK substrate recognition is PKD1-dependent.** WB analysis using antibodies against a phospho-AMPK substrate motif as well as a phospho-PKD substrate in (A,B) differentiated SVC isolated from sWAT of PKD1adipo.Δ/Δ mice and (C,D) differentiated 3T3-L1 cells expressing PKD1ca including their corresponding controls. *Protein kinase D* (PKD); *phospho* (p); *adiponectin* (adipo.); *flox/flox* (f/f); *constitutive active* (ca); *AMP-activated protein kinase* (AMPK). (unpublished observation)

Additionally, AMPK activity was assessed using an ELISA-based AMPK kinase assay. Consistently, AMPK activity was increased in differentiated adipocytes lacking PKD1 (Figure 34A). As a negative control cell lysates were treated with compound C during the assay, which completely abolished AMPK activity (Figure 34A). In contrast, decreased AMPK activity was observed in differentiated 3T3-L1 cells expressing PKD1ca (Figure 34B). This clearly shows that activity of AMPK is regulated by PKD1 abundance and expression.



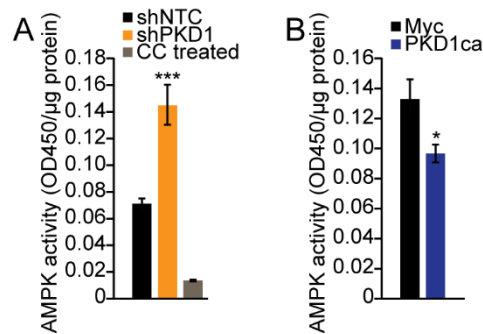


**Figure 34. PKD1 regulates AMPK activity in adipocytes.** AMPK kinase assay was used to measure activity of AMPK in (A) cells lacking PKD1 and (B) differentiated 3T3-L1 cells expressing PKD1ca. Compound C treatment (250  $\mu$ M) of cell lysates during the assay was used as a negative control. Data are presented as mean  $\pm$  SEM (n=5; average of two individual experiments). (A) One-way ANOVA with Tukey's multiple comparisons post-test, (B) unpaired, two-tailed Student's t-test. For all data, \*p<0.05 and \*\*\*p<0.001. *Protein kinase D* (PKD); *small hairpin* (sh); *non-targeting control* (NTC); *AMP-activated protein kinase* (AMPK); *compound C* (CC); *optical density* (OD); *constitutive active* (ca). (Löffler *et al.*, 2018)<sup>219</sup>

### 3.3.4 AMPK deletion or activation can reverse the phenotype caused by altered PKD1 activity

Since adipose tissue is regulated by PKD1 in an AMPK-dependent manner, it was tested whether the previously observed phenotypes could be reversed either by silencing or chemically activating AMPK. Therefore, cells lacking PKD1 and corresponding controls were differentiated and successfully transfected with siRNA against AMPK $\alpha$ 1 and  $\alpha$ 2 subunits, as seen by the reduced AMPK $\alpha$  protein levels (Figure 35A,B). Chemical activation of AMPK using AICAR led to an increased AMPK activity in 3T3-L1 cells expressing PKD1ca and their controls, shown by enhanced phosphorylation of the downstream target ACC at S79 (Figure 35C).

## RESULTS

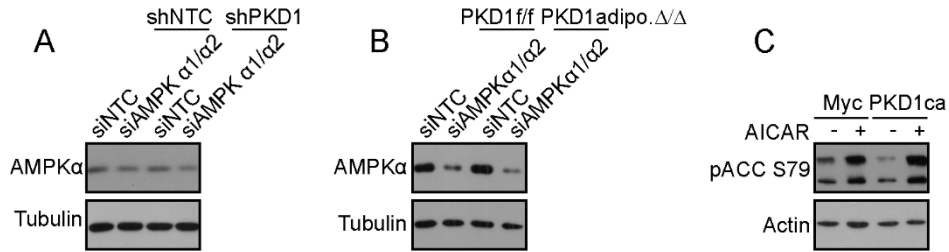


**Figure 35. Successful silencing or activation of AMPK.** WB analysis using an AMPK $\alpha$  antibody in (A) 3T3-L1 cells lacking PKD1 and (B) SVC isolated from sWAT of PKD1adipo. $\Delta/\Delta$  mice and corresponding controls, which have been transfected with siRNA against AMPK $\alpha$ 1/ $\alpha$ 2 or control siRNA. Tubulin was used as a loading control. (C) WB analysis using an antibody against phosphorylation of ACC at S79 in differentiated 3T3-L1 cells expressing PKD1ca including their corresponding controls, which have been treated with AICAR (2 mM) for 2 h. Actin was used as a loading control. *Protein kinase D* (PKD); *phospho* (p); *serine* (S); *small hairpin* (sh); *non-targeting control* (NTC); *small interfering* (si); *AMP-activated protein kinase* (AMPK); *acetyl-CoA carboxylase* (ACC); *5-aminoimidazole-4-carboxamide 1- $\beta$ -D-ribofuranoside* (AICAR). (Löffler *et al.*, 2018)<sup>219</sup>

Phosphorylation of ACC at S79 through AMPK suppresses lipogenesis<sup>182</sup>. Since PKD1-dependent phosphorylation was shown to inhibit AMPK $\alpha$ , the PKD1 regulation of adipocyte function in an AMPK-dependent manner was further analyzed. First, effects on TG accumulation were assessed. Deletion of AMPK $\alpha$  subunits in differentiated 3T3-L1 cells increased the TG content and lipid accumulation, which were reduced in PKD1-depleted adipocytes transfected with control siRNA (Figure 36A,B). On the other hand, activation of AMPK by AICAR treatment reduced TG content and lipid accumulation in differentiated adipocytes expressing PKD1ca to the level observed in control cells (Figure 36D,E).

## RESULTS

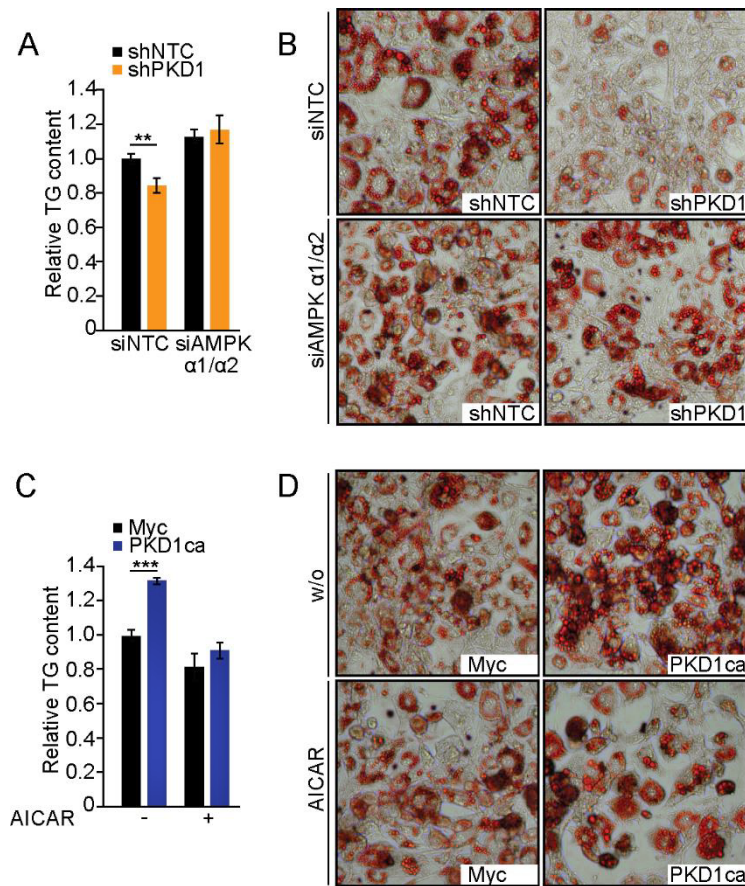


**Figure 36. PKD1 regulates TG accumulation in adipocytes in an AMPK-dependent manner.** (A and C) Quantification of relative TG accumulation using AdipoRed reagent and (B and D) images of Oil-Red-O staining for neutral lipids was performed in (A and B) PKD1-depleted 3T3-L1 cells, which were transfected with control siRNA or siRNA against AMPK $\alpha$ 1/ $\alpha$ 2 or (C and D) 3T3-L1 cells expressing PKD1ca treated with AICAR (0.5 mM) for 3 days. Cells were visualized under an inverted microscope Olympus IX71 at 20x magnification. Data are shown in mean  $\pm$  SEM (n=3; representative of three individual experiments). One-way ANOVA with Tukey's multiple comparisons post-test. For all data, \*\*p<0.01 and \*\*\*p<0.001. *Protein kinase D* (PKD); *small hairpin* (sh); *non-targeting control* (NTC); *small interfering* (si); *triglyceride* (TG); *AMP-activated protein kinase* (AMPK); *constitutive active* (ca); *5-aminoimidazole-4-carboxamide 1- $\beta$ -d-ribofuranoside* (AICAR); *without* (w/o). (Löffler et al., 2018)<sup>219</sup>

In line with these findings, silencing of AMPK $\alpha$  subunits in differentiated 3T3-L1 cells lacking PKD1 increased the lipogenesis rate to the same level as seen in control cells (Figure 37A). Consistently, in explants that have been treated with Compound C in order to chemically inhibit AMPK activity, lipogenesis rate was increased in both, control and PKD1-deficient adipocyte pieces, compared to the observed reduction in explants lacking PKD1 in the absence of Compound C (Figure 37B). In contrast, PKD1-induced lipogenesis in adipocytes could be blocked by inducing AMPK activity. Therefore, AMPK signaling was chemically activated by AICAR in cells expressing

## RESULTS

PKD1ca. This led to a reduction in the lipogenesis rate to the levels observed in control cells (Figure 37C).

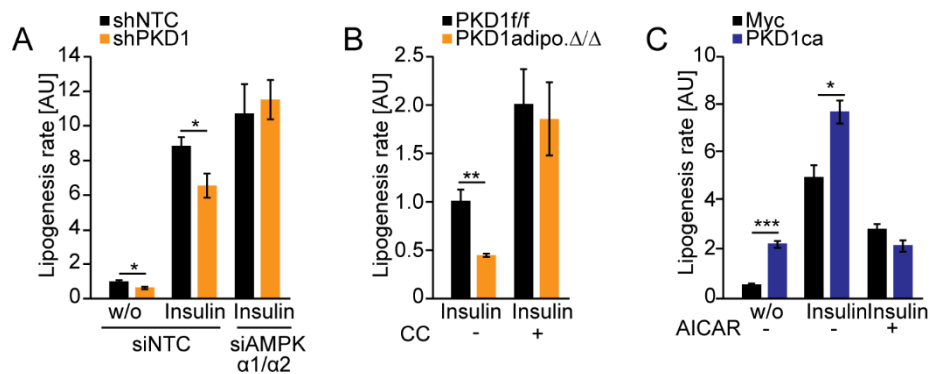


**Figure 37. PKD1 regulates lipogenesis rate in adipocytes through AMPK.** (A) Basal- and insulin-induced (100 nM for 3 h) lipogenesis rate was assessed in differentiated 3T3-L1 cells lacking PKD1, which were transfected with control siRNA or siRNA against siAMPK $\alpha$ 1 and  $\alpha$ 2 subunits for 48 h. (B) Insulin-induced (100 nM for 3 h) lipogenesis rate was measured in explants from sWAT of PKD1adipo. $\Delta/\Delta$  and control mice treated with Compound C (5  $\mu$ M) for 4 h. (C) Basal- and insulin-induced (100 nM for 3 h) lipogenesis rate of differentiated 3T3-L1 cells expressing control vector and PKD1ca, treated with 2 mM AICAR for 1 h. Data are presented as mean  $\pm$  SEM (n=3; representative of three individual experiments). One-way ANOVA with Tukey's multiple comparisons post-test. For all data, \* $p$ <0.05, \*\* $p$ <0.01, and \*\*\* $p$ <0.001. *Protein kinase D* (PKD); *small hairpin* (sh); *non-targeting control* (NTC); *small interfering* (si); *AMP-activated protein kinase* (AMPK); *arbitrary units* (AU); *without* (w/o); *compound C* (CC); *adiponectin* (adipo.); *flox/flox* (f/f); *constitutive active* (ca); *5-aminoimidazole-4-carboxamide 1- $\beta$ -d-ribofuranoside* (AICAR). (Löffler et al., 2018)<sup>219</sup>

AMPK was also shown to induce energy dissipation in the cells<sup>244</sup>. Since deletion of PKD1 increases OCR in adipocytes, it was assessed if deletion of AMPK $\alpha$  subunits would reverse this phenotype. Therefore, differentiated 3T3-L1 cells as well as SVC lacking PKD1 were transfected with control siRNA or siRNA against AMPK  $\alpha$ 1/ $\alpha$ 2 subunits and OCR was measured. Indeed, previously enhanced OCR in PKD1-deficient cells led to a decreased basal energy dissipation as well as proton leak of 3T3-L1 cells lacking PKD1 after knock-down of AMPK $\alpha$  subunits, even to a lower extend than measured in control cells in case of PKD1-deficient 3T3-L1 cells (Figure 38A,B). Similarly, it also normalized enhanced basal respiration and proton leak of PKD1-deficient cells (Figure 38C).

## RESULTS

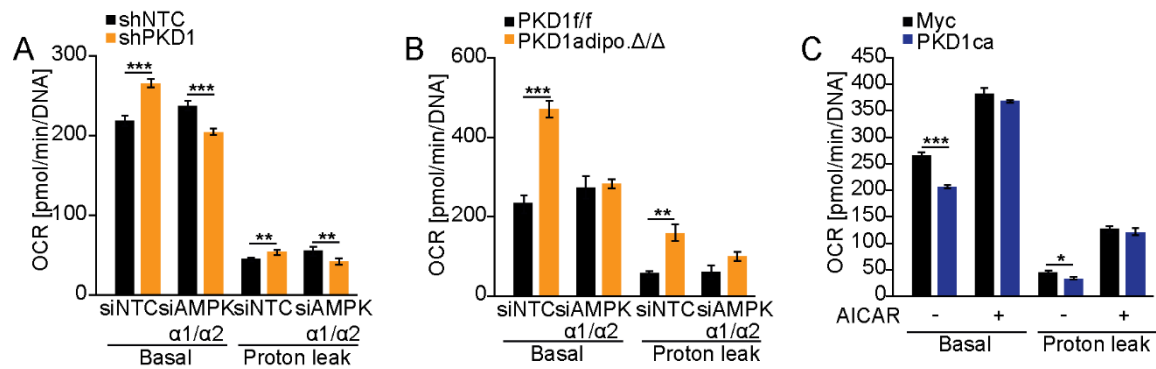


**Figure 38. PKD1 regulates OCR in adipocytes through AMPK.** Basal respiration and proton leak were measured in (A) differentiated 3T3-L1 cells lacking PKD1 and (B) SVC derived from control and PKD1-deficient adipocytes, which were transfected with control siRNA and siRNA against AMPK  $\alpha 1$  and  $\alpha 2$  subunits. (C) OCR required for indicated processes in PKD1ca expressing 3T3L1 cells treated with AICAR (0.5 mM) for 3 days. Data are presented as mean  $\pm$  SEM (n=22; representative of two individual experiments). One-way ANOVA with Tukey's multiple comparisons post-test. For all data, \*\*p<0.01 and \*\*\*p<0.001. *Protein kinase D* (PKD); *small hairpin* (sh); *non-targeting control* (NTC); *small interfering* (si); *oxygen consumption rate* (OCR); *minute* (min); *deoxyribonucleic acid* (DNA); *adiponectin* (adipo.); *flox/flox* (f/f); *constitutive active* (ca); *5 aminoimidazole-4-carboxamide 1- $\beta$ -d-ribofuranoside* (AICAR). ((A) unpublished observation), ((B,C) Löffler *et al.*, 2018)<sup>219</sup>

Finally, it was tested if mitochondrial fragmentation in adipocytes was also regulated by PKD1 in an AMPK-dependent manner. Indeed, silencing of AMPK $\alpha$  subunits in differentiated 3T3-L1 cells resulted in a shift towards more intermediated mitochondria in cells lacking PKD1 (Figure 39A). In contrast, mitochondrial fusion was reversed upon activation of AMPK in PKD1ca expressing cells (Figure 39B). Taken together, these results show that PKD1 regulates TG accumulation, lipogenesis, respiration rate, and mitochondrial fragmentation of adipocyte primarily by suppressing AMPK.

## RESULTS

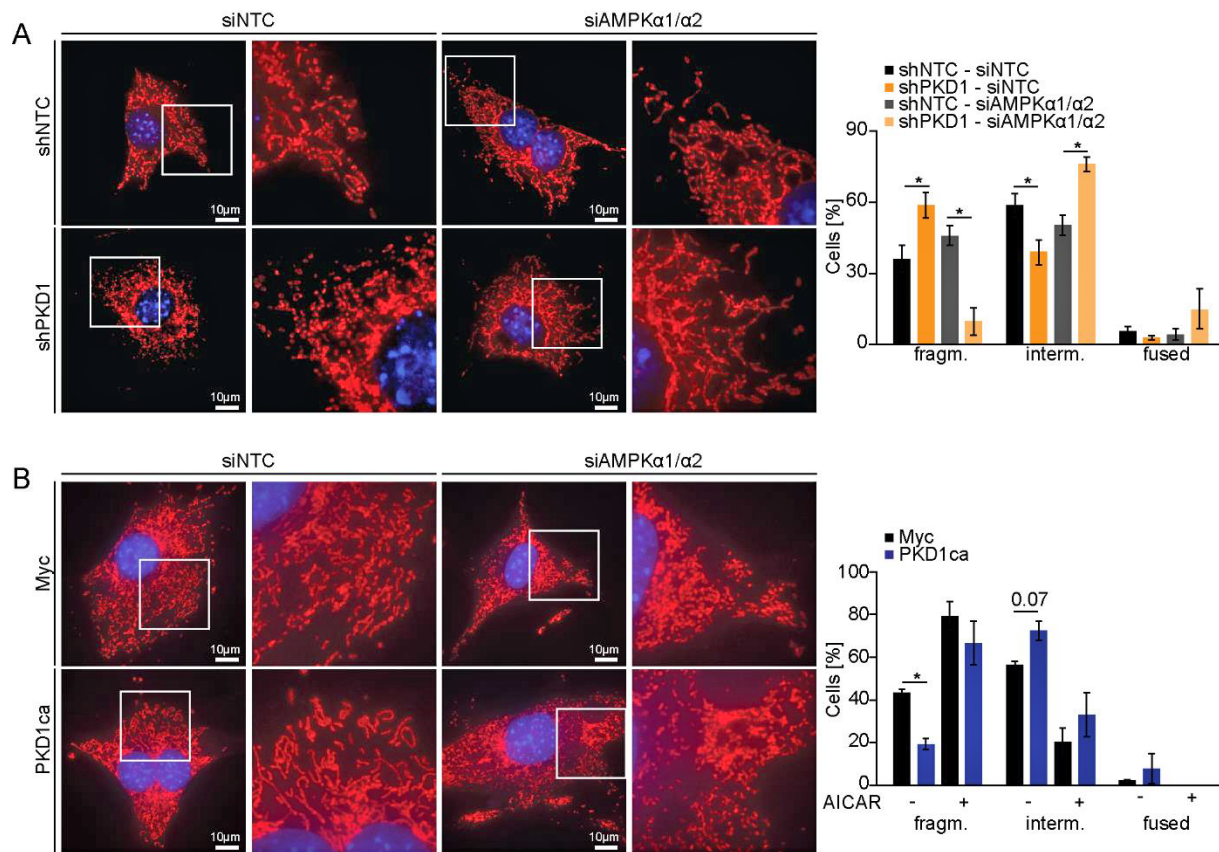


**Figure 39. PKD1 regulates mitochondrial fragmentation in adipocytes in an AMPK-dependent manner.** Representative microscopy images of the mitochondrial morphology and its respective quantification of fragmented, intermediate and fused cells in (A) differentiated 3T3-L1 cells lacking PKD1, which have been transfected with control siRNA and siRNA against AMPK  $\alpha$ 1 and  $\alpha$ 2 subunits as well as (B) differentiated 3T3-L1 cells expressing PKD1ca and corresponding controls treated with AICAR (2 mM) for 2 h. Cells were stained with 150 nM MitoTracker Red for 30 min at 37 °C and subsequently fixed with 4% PFA. Nuclei were stained using DAPI. Cells were visualized under a fluorescent microscope Leica DM5500 B at 63x magnification. Quantitative data are shown as the mean  $\pm$  SEM of three independent experiments with 200 cells counted for each replicate. Unpaired, two-tailed Student's t-test. For all data, \* $p$ <0.05. *Protein kinase D* (PKD); *small hairpin* (sh); *non-targeting control* (NTC); *small interfering* (si); *AMP-activated protein kinase* (AMPK); *fragmented* (fragm.); *intermediate* (interm.); *constitutive active* (ca); *5 aminoimidazole-4-carboxamide 1- $\beta$ -d-ribofuranoside* (AICAR). ((A) unpublished observation), ((B) Löffler *et al.*, 2018)<sup>219</sup>

### 3.4 Mice lacking PKD1 in adipocytes are protected against the development of diet-induced obesity, diabetes, and liver steatosis

#### 3.4.1 DAG levels are independent of the diet

Since an increased lipogenic rate in adipocytes is associated with adiposity, there is the possibility that the intermediate product of lipogenesis, DAG, accumulates in

## RESULTS

adipose tissue of mice during obesity. Therefore, steady state levels of DAG in white and brown adipose tissue of lean mice fed ND and obese mice fed HFD were measured. However, neither the diet nor the degree of obesity changed the DAG levels in both tissues (Figure 40).

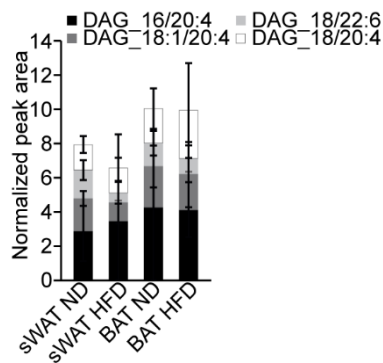


**Figure 40. DAG levels are not influenced by the diet.** DAG content measured in sWAT and BAT of wild-type mice fed HFD or ND. Data are presented as mean  $\pm$  SEM (n=6/group). Unpaired, two-tailed Student's t-test. *Subcutaneous white adipose tissue (sWAT); brown adipose tissue (BAT); normal diet (ND); high-fat diet (HFD); diacylglycerol (DAG).* This experiment has been performed in collaboration with the working group of Prof. Dr. Schulze. (Löffler *et al.*, 2018)<sup>219</sup>

### 3.4.2 PKD1 is upregulated upon feeding

Since PKD1 was shown to induce lipid accumulation and lipogenesis *in vitro*, it was tested, whether PKD1 is regulated in adipocytes in response to feeding *in vivo*. To examine this, groups of mice were compared, which were *ad libitum* fed, fasted for 24 h, or refed for 24 h after 24 h fasting. Indeed, activation, abundance, and expression of PKD1 in adipocytes were induced upon *ad libitum* feeding and after refeeding, while a downregulation occurred in the fasted state. This can be seen on the protein level, when activity of PKD1 was measured using antibodies against PKD1 phosphorylation site S916. Similarly, total PKD1 expression was induced in the fed state and upon refeeding on protein level seen by WB (Figure 41A) as well as transcriptionally on mRNA levels (Figure 41B). This suggests that PKD1 might promote adiposity *in vivo*.

## RESULTS

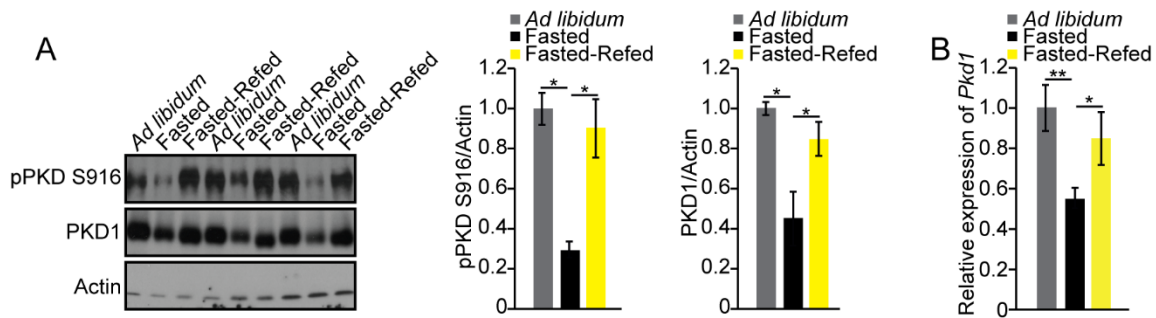


**Figure 41. PKD1 expression and activity is induced upon feeding.** WB analysis using antibodies against PKD phosphorylation site S916, and PKD1 (Actin as loading control) as well as (B) RT-qPCR analysis of *Pkd1* was conducted in sWAT of *ad libidum*, 24 h fasted, and 24 h fasted-refed mice. Data are presented as mean  $\pm$  SEM ( $n=3$ /group; representative for three individual experiments). Unpaired, two-tailed Student's t-test. For all data, \* $p < 0.05$  and \*\* $p < 0.01$ . Protein kinase D (PKD); phospho (p); serine (S). ((in parts) Löffler *et al.*, 2018)<sup>219</sup>

### 3.4.3 PKD1 deletion in adipocytes protects against diet-induced obesity

To understand the physiological consequence of PKD1-mediated regulation of AMPK-dependent and independent aspects of adipocyte biology, mice were generated lacking PKD1 specifically in adipocytes. PKD1*adipo*. $\Delta/\Delta$  mice were born at normal Mendelian ratio and displayed no gross abnormalities compared to their littermates. When analyzed by immunoblotting, a substantial reduction of PKD1 protein levels was observed in all adipose tissue depots, but not in the other organs tested (Figure 42A). Consistently, *Pkd1* mRNA levels were markedly reduced in primary adipocytes. Due to the generation of the PKD1*f/f* mice in which the loxP sites were inserted in the introns flanking exons 12 and 14 in the N-terminal region of the kinase domain (see Figure 11)<sup>150</sup>, two different primers have been used. One of them is located at exon 16 and 17, the region directly after the loxP site, which is removed by the Cre recombinase. The other one is located at exon 1 and 2, to test if the entire mRNA is degraded after the Cre recombinase was removing parts of the catalytic domain (Figure 42B). Specific deletion of PKD1 in adipocytes did not affect the other isoforms (PKD2, PKD3). There was no effect observed, neither on protein level in the different fat depots nor on mRNA level of isolated adipocytes (Figure 42C,D). This is an important result, since PKD1 and PKD2 isoforms have previously been shown to dimerize<sup>236</sup>, and any effects of the PKD1 deletion on the expression of the other isoforms was to be excluded.



## RESULTS

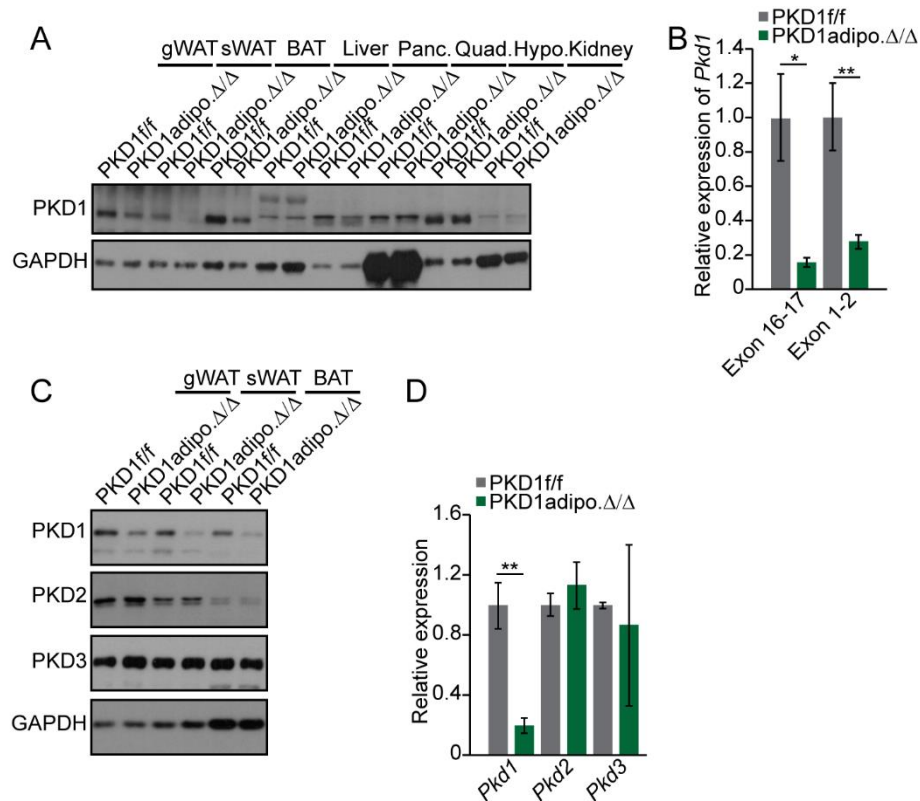


**Figure 42. PKD1 is effectively and specifically deleted in adipocytes.** (A) WB analysis of different murine tissues of PKD1adipo.Δ/Δ and control mice using an antibody against PKD1. (B) RT-qPCR analysis of *Pkd1* expression using primers located in exon 16 and 17 as well as exon 1 and 2 of the *Pkd1* gene in isolated adipocytes of sWAT from PKD1adipo.Δ/Δ and control mice. (C) WB analysis of different murine fat depots of PKD1adipo.Δ/Δ and control mice using an antibody against PKD1, PKD2, PKD3. GAPDH was used as a loading control. (D) RT-qPCR analysis of *Pkd1*, *Pkd2* and *Pkd3* in isolated adipocytes of sWAT from mice lacking PKD1 and controls. Data are presented as mean ± SEM (n=4/genotype). Unpaired, two-tailed Student's t-test. For all data, \*p<0.05 and \*\*p<0.01. *Protein kinase D* (PKD); *adiponectin* (adipo.); *flox/flox* (f/f); *gonadal white adipose tissue* (gWAT); *subcutaneous white adipose tissue* (sWAT); *brown adipose tissue* (BAT); *pancreas* (Panc.); *quadriceps* (Quad.); *hypothalamus* (Hypo.); *glyceraldehyd-3-phosphat-dehydrogenase* (GAPDH). (Löffler et al., 2018)<sup>219</sup>

Since PKD1 was increasingly expressed and activated in the fed stage, it was tested whether PKD1 promotes adiposity in response to high-caloric HFD as well as ND. To this end, mice lacking PKD1 in adipocytes and controls were monitored for 24 weeks on HFD and ND. Weight gain was assessed every other week. Mice lacking PKD1 displayed significantly reduced weight gain during a HFD challenge starting directly after weaning at the age of 3 weeks and continued for 24 weeks. On the other hand, ND feeding did not reveal any differences regarding body weight gain between genotypes (Figure 43A). Body composition analysis after 24 weeks of HFD feeding showed markedly reduced fat tissue and liver weight, while the other organs did not differ (Figure 43B).

## RESULTS

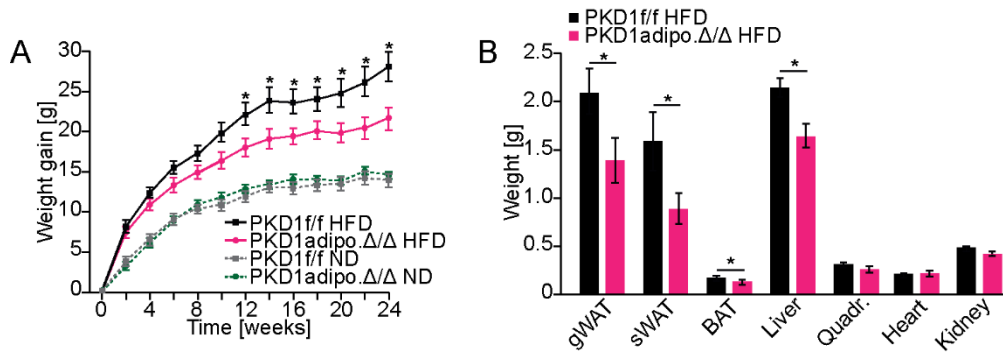


**Figure 43. Deletion of PKD1 reduces body weight gain in mice on HFD.** (A) Body weight evolution was monitored every other week over 24 weeks in control and PKD1adipo.Δ/Δ mice fed HFD and ND. (B) Organ weight of control and PKD1adipo.Δ/Δ mice fed HFD. Data are presented as mean  $\pm$  SEM (n=6-11/genotype). Unpaired, two-tailed Student's t-test. For all data, \*p<0.05. *Protein kinase D* (PKD); *adiponectin* (adipo.); *flox/flox* (f/f); *high-fat diet* (HFD); *normal diet* (ND); *gonadal white adipose tissue* (gWAT); *subcutaneous white adipose tissue* (sWAT); *brown adipose tissue* (BAT); *quadriceps* (Quadr.). (Löffler et al., 2018)<sup>219</sup>

Although overall weight gain was not changed in mice lacking PKD1 compared to their controls when fed ND, there was still a reduction upon PKD1 deletion gWAT weight even upon ND feeding (Figure 44A). When mice were measured in an NMR analyzer, which enables whole body composition acquisition (lean mass, fat mass and free fluids) of the mice, a decrease in fat mass was observed in PKD1-depleted mice. Lean mass and body fluids on the other hand were not differing between mice lacking PKD1 and their littermates indicating specific function of PKD1 in regulation of adiposity (Figure 44B,C,D).

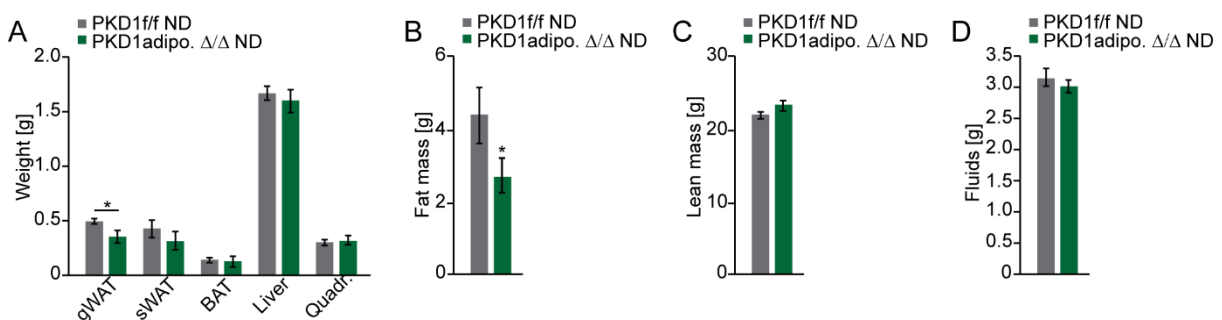


**Figure 44. Deletion of PKD1 reduces overall fat mass in mice on ND.** (A) Organ weight of control and PKD1adipo.Δ/Δ mice fed ND. NMR analysis of mice with PKD1 depletion and their controls showing (B) fat mass, (C) lean mass, and (D) fluids after 24 weeks of ND feeding. Data are presented as mean  $\pm$  SEM (n=6-10/genotype). Unpaired, two-tailed Student's t-test. For all data, \*p<0.05. *Protein kinase D* (PKD); *adiponectin* (adipo.); *flox/flox* (f/f); *normal diet* (ND); *gonadal white adipose tissue* (gWAT); *subcutaneous white adipose tissue* (sWAT); *brown adipose tissue* (BAT); *quadriceps* (Quadr.). (Löffler et al., 2018; A)<sup>219</sup>, (unpublished observation; B,C,D)

### **3.4.4 PKD1 suppresses activity of AMPK in murine adipose tissue**

Moreover, it was tested, if PKD1 is also regulating adipose tissue in an AMPK-dependent manner *in vivo*. Indeed, in adipose tissue of mice lacking PKD1, which were fed ND, decreased AMPK $\alpha$  phosphorylation at S485/S491, enhanced phosphorylation of AMPK $\alpha$  subunit at T172, and increased phosphorylation of the AMPK downstream target ACC at S79 were observed (Figure 45A). This suggests that PKD1 inhibits AMPK activity *in vitro* and *in vivo*. AMPK is known to induce autophagy<sup>245</sup>. Interestingly, increased *light chain 3* (LC3) cleavage observed in adipose tissue of PKD1-deficient mice fed ND proposes enhanced autophagy (Figure 45A). Consistently with these findings, a reduced phosphorylation at S485/S491 of AMPK $\alpha$  as well as an enhanced phosphorylation of ACC at S79 in sWAT isolated from PKD1-deficient mice fed HFD could be seen (Figure 45B). However, no alterations in the phosphorylation of AMPK $\alpha$  at T172 were observed in sWAT of mice fed 24 weeks HFD feeding (Figure 45B).

## RESULTS

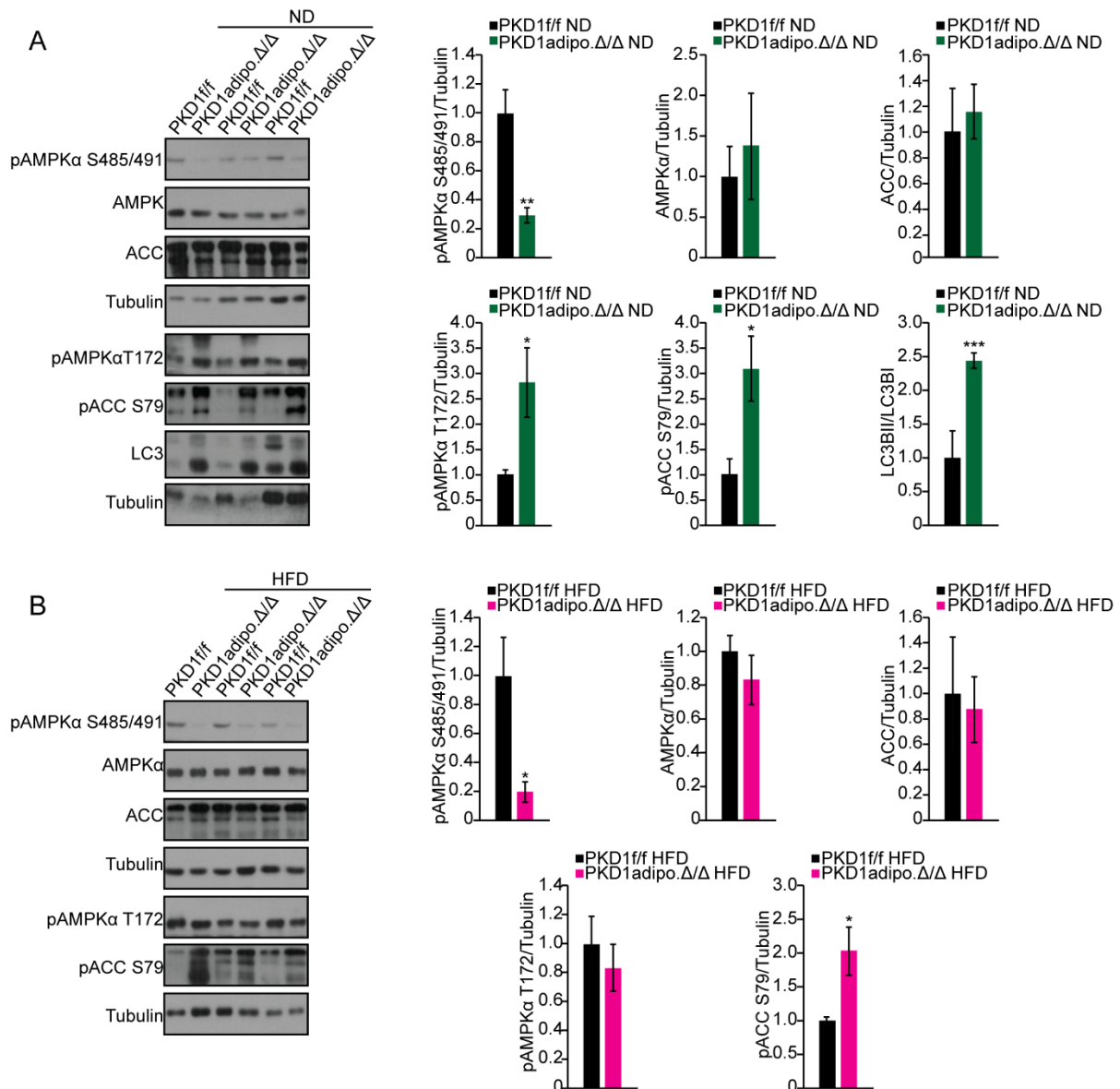


**Figure 45. PKD1 regulates white adipose tissue in an AMPK-dependent manner also *in vivo*.** WB analysis using antibodies against AMPKα phosphorylation site S485/491, AMPKα, ACC, pAMPKα T172, and pACC S79 in protein lysates of sWAT derived from PKD1adipo.Δ/Δ and control mice fed (A) ND and (B) HFD including densitometric analysis of four replicates each. Tubulin was used as a loading control. Data are presented as mean ± SEM. Unpaired, two-tailed Student's t-test. For all data, \*p<0.05, \*\*p<0.01 and \*\*\*p<0.001. *Protein kinase D* (PKD); *phospho* (p); *serine* (S); *threonine* (T); *adiponectin* (adipo.); *flox/flox* (f/f); *AMP-activated protein kinase* (AMPK); *acetyl-CoA carboxylase* (ACC); *light chain 3* (LC3); *normal diet* (ND); *high-fat diet* (HFD). (Löfller *et al.*, 2018)<sup>219</sup>

In BAT, PKD1 deletion did not lead to changes in phosphorylation of AMPKα at S485/S49, T172, or ACC at S79, regardless of the diet (Figure 46A). Furthermore, PKD1-deficient SVC isolated from BAT had no alterations in phosphorylation of AMPKα at S485/S49, T172 and ACC at S79 (Figure 46B). These data suggest that

## RESULTS

PKD1 only affects phosphorylation and activity of AMPK in white but not in brown adipose tissue.

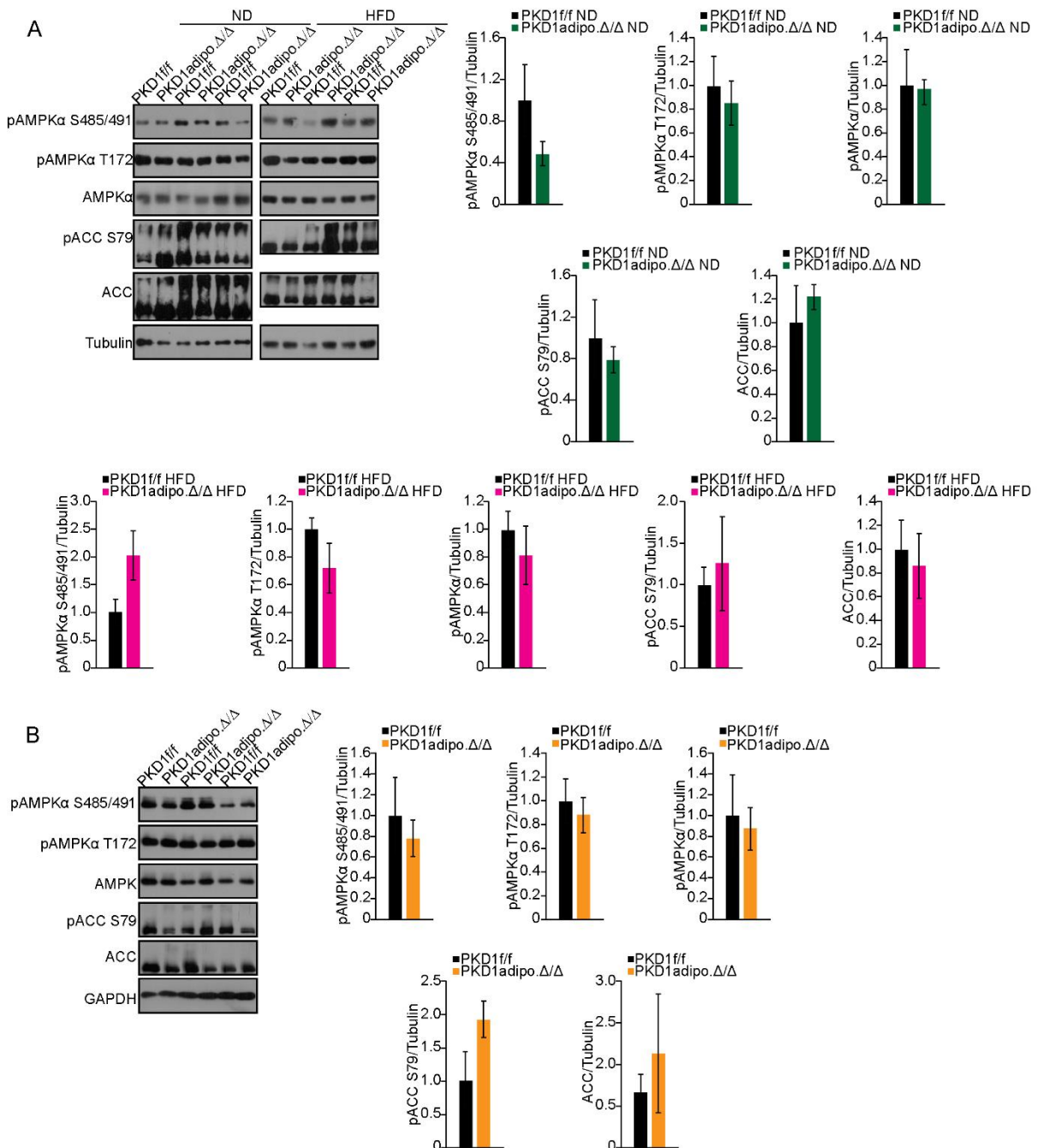


**Figure 46. PKD1 does not affect AMPK phosphorylation in brown adipose tissue.** WB analysis using antibodies against AMPK $\alpha$  phosphorylation site S485/491, pAMPK $\alpha$  T172, AMPK $\alpha$ , pACC S79, and ACC in protein lysates of (A) BAT derived from PKD1adipo. $\Delta/\Delta$  and control mice fed ND and HFD as well as (B) SVC isolated from BAT of mice lacking PKD1 including densitometric analysis of three replicates each. Tubulin or GAPDH were used as a loading control. Data are presented as mean  $\pm$  SEM. Unpaired, two-tailed Student's t-test. *Protein kinase D* (PKD); *phospho* (p); *serine* (S); *threonine* (T); *adiponectin* (adipo.); *flox/flox* (f/f); *AMP-activated protein kinase* (AMPK); *acetyl-CoA carboxylase* (ACC); *glyceraldehyd-3-phosphat-dehydrogenase* (GAPDH); *high-fat diet* (HFD); *normal diet* (ND). (Löffler *et al.*, 2018)<sup>219</sup>

## RESULTS

### 3.4.5 Deletion of PKD1 alters AMPK activity in response to refeeding

Since fasting and fasting-refeeding experiments influenced PKD1 expression (see Figure 41A), it was tested whether there was any effect between mice lacking PKD1 and controls. Therefore, mice lacking PKD1 and control animals were fasted for 24 h, followed by 24 h refeeding. The FFAs, glycerol, total TGs, and glucose levels did not differ between PKD1adipo. $\Delta/\Delta$  and control mice, neither at the fasted nor fasted-refed stage (Figure 48A-D).

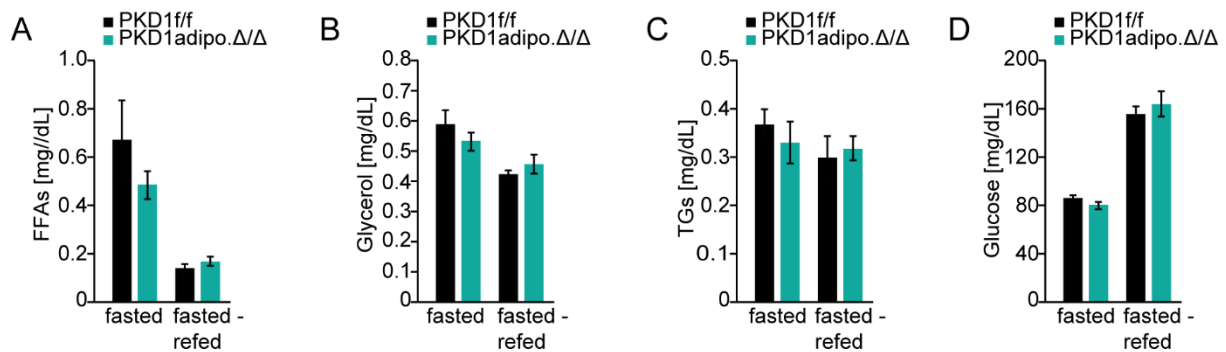


**Figure 47. Deletion of PKD1 does not affect lipolysis or glucose levels in young mice upon fasting.** (A) FFA, (B) glycerol, (C) TG, and (D) glucose levels in blood of PKD1adipo. $\Delta/\Delta$  and control mice, which were subjected to either 24 h fasting or 24 h fasting followed by 24 h refeeding. Indicated parameters were measured in the serum of these mice at the age of 8 weeks. For all data, n=5-9/group. Data are presented as mean  $\pm$  SEM. Unpaired, two-tailed Student's t-test. *Protein kinase D* (PKD); *adiponectin* (adipo.); *flox/flox* (f/f); *free fatty acids* (FFAs); *triglycerides* (TGs). (Löffler *et al.*, 2018)<sup>219</sup>

In addition, the levels of AMPK $\alpha$  subunit phosphorylation at S485/S491, T172, and ACC phosphorylation at S79 did not differ upon PKD1 deletion during fasting (Figure 48A). However, less phosphorylation of AMPK $\alpha$  at S485/S491 was observed in PKD1-deficient adipose tissue of fasted-refed mice, while phosphorylation of AMPK $\alpha$  at T172 and ACC at S79 was enhanced (Figure 48B), indicating that PKD1 promotes adiposity *in vivo*.

## RESULTS

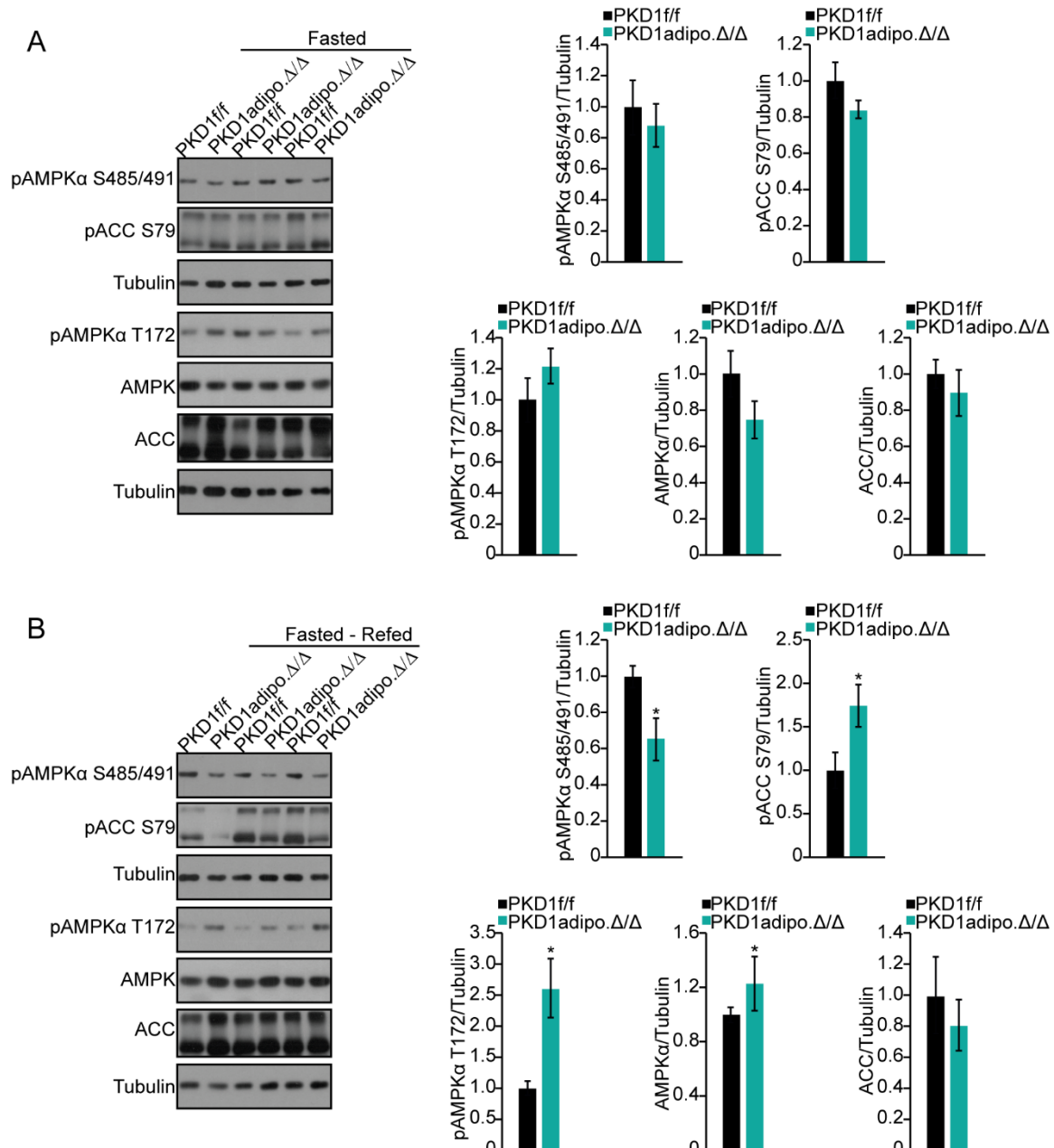


**Figure 48. Deletion of PKD1 affects AMPK phosphorylation in the fasted-refed stage.** WB analysis using antibodies against AMPKα phosphorylation site S485/491, pACC S79, pAMPKα T172, AMPKα, and ACC in protein lysates of sWAT derived from PKD1adipo.Δ/Δ and control mice, which were (A) fasted for 24 h or (B) fasted and refed for 24 h, including densitometric analysis of four replicates each. Tubulin was used as a loading control. Data are presented as mean ± SEM. Unpaired, two-tailed Student's t-test. For all data, \*p<0.05. *Protein kinase D* (PKD); *phospho* (p); *serine* (S); *threonine* (T); *adiponectin* (adipo.); *flox/flox* (f/f); *AMP-activated protein kinase* (AMPK); *acetyl-CoA carboxylase* (ACC). (Löffler *et al.*, 2018)<sup>219</sup>

### 3.4.6 Deletion of PKD1 protects against diet-induced obesity by enhancing energy expenditure

Differences in body weight gain are caused by an imbalance between energy intake and energy expenditure. PKD1-depleted mice might eat less, move more, or show

## RESULTS

changes in their energy expenditure independent of the motoric activity. To simultaneously measure all the metabolically important parameters, mice were kept in a metabolic cage for several days. Metabolic analysis of mice lacking PKD1 depicted no differences in food intake, activity, or *respiratory exchange ratio* (RER) compared to control animals upon HFD feeding (Figure 49A-C). There were also no changes in any of the above-mentioned parameters in mice lacking PKD1 and their littermates when fed with ND (Figure 49D-F).

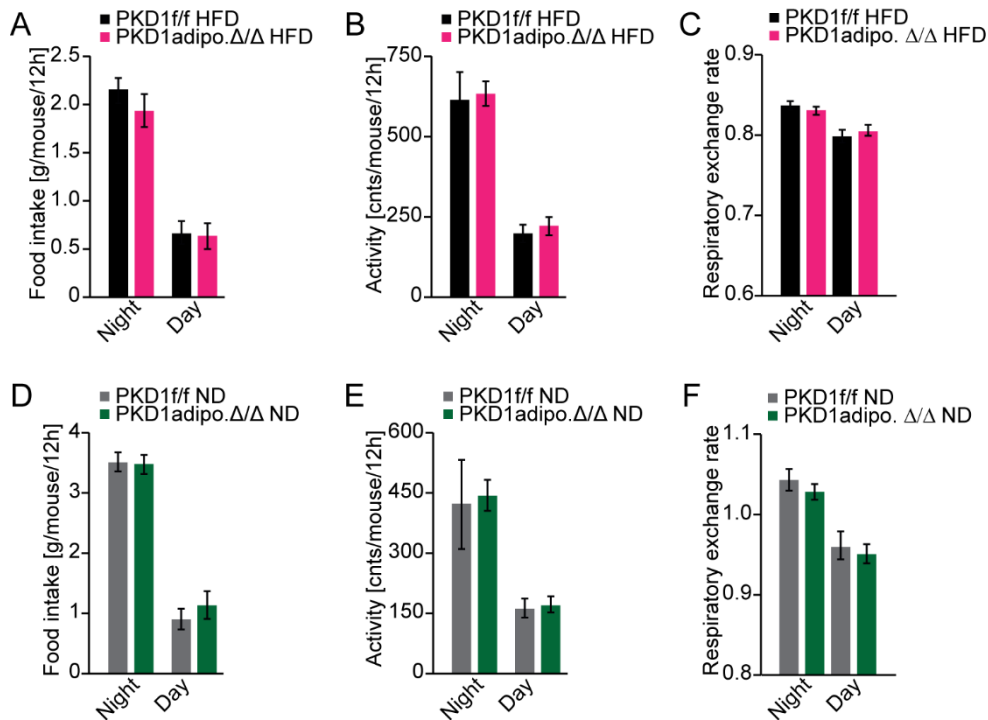


**Figure 49. PKD1 deletion does not affect food intake, activity, or respiratory exchange ratio.** PKD1-depleted mice and their controls were measured in a metabolic cage for 1 week after 24 weeks of HFD feeding and (A) food intake, (B) voluntary movement, and (C) respiratory exchange ratio (RER) were measured. (D) Food intake, (E) voluntary movement, and (F) respiratory exchange ratio were measured in ND-fed mice lacking PKD1 and their controls. Data are presented as mean  $\pm$  SEM (n=6-11/genotype). Unpaired, two-tailed Student's t-test. *Protein kinase D* (PKD); *adiponectin* (adipo.); *flox/flox* (f/f); *high-fat diet* (HFD); *normal diet* (ND); *hours* (h). ((A,B,D,E) Löffler *et al.*, 2018)<sup>219</sup>, ((C,F) unpublished observation)

Energy expenditure is another parameter measured in the metabolic cages. Indeed, PKD1<sup>adipo.Δ/Δ</sup> mice fed HFD displayed an enhanced energy expenditure compared to the corresponding controls (Figure 50A). Similar effects could be seen in ND-fed PKD1<sup>adipo.Δ/Δ</sup> mice (Figure 50B). These data correlate to the *in vivo* findings showing an increased OCR in SVC derived from sWAT of PKD1<sup>adipo.Δ/Δ</sup> mice. Therefore,



## RESULTS

specific deletion of PKD in adipocytes is protective against diet-induced obesity in mice due to an increased energy expenditure.

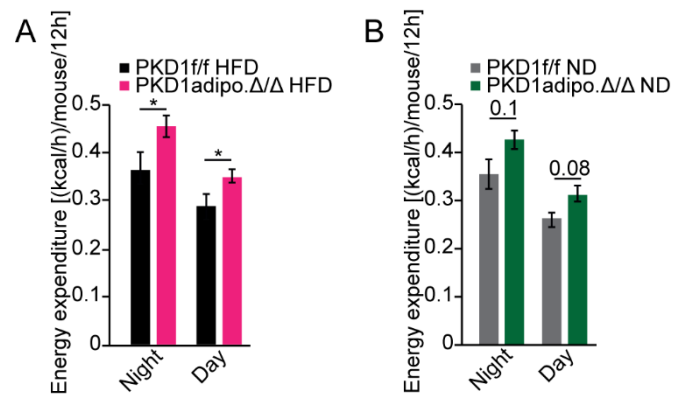


**Figure 50. PKD1 promotes obesity by suppressing energy dissipation in adipocytes.** Energy expenditure of mice lacking PKD1 and their littermates, which were measured in a metabolic cage for 1 week after (A) HFD or (B) ND feeding for 24 weeks. Data are presented as mean  $\pm$  SEM (n=6-11/genotype). Unpaired, two-tailed Student's t-test. For all data, \*p<0.05. *Protein kinase D* (PKD); *adiponectin* (adipo.); *flox/flox* (f/f); *high-fat diet* (HFD); *normal diet* (ND); *hours* (h). (Löffler *et al.*, 2018)<sup>219</sup>

### 3.4.7 PKD1 deletion reduces overall adipocyte size

Consistent with the previous results, increased energy expenditure of PKD1adipo.Δ/Δ mice had a profound effect on adipose tissue morphology. As seen in the histological analysis by H&E staining, adipocyte size was largely reduced in all three fat depots, gWAT, BAT, and sWAT (Figure 51A,C,D). The overall adipocyte size was additionally quantified using an imaging software. Indeed, smaller adipocytes were measured in PKD1adipo.Δ/Δ mice as compared to control animals when fed HFD (Figure 51B,E).

## RESULTS

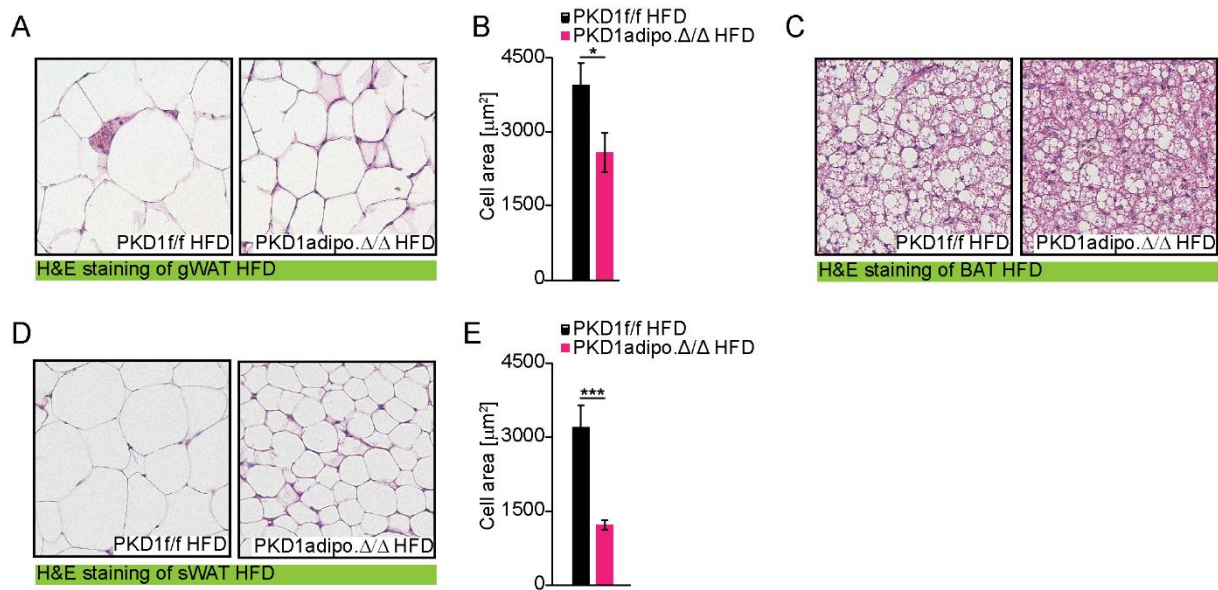


**Figure 51. Deletion of PKD1 decreases overall adipocyte size in mice fed HFD.** Representative H&E staining of (A) gWAT, (C) BAT, and (D) sWAT from PKD1<sup>adipo.Δ/Δ</sup> and control mice fed HFD for 24 weeks. Average adipocytes size was analyzed using the ImageJ software in (B) gWAT and (E) sWAT of indicated mice. Data are presented as mean  $\pm$  SEM (n=8/genotype). Stainings were visualized using an inverted microscope Olympus CKX31 at 20x magnification. Unpaired, two-tailed Student's t-test. For all data, \*p<0.05 and \*\*\*p<0.001. *Protein kinase D* (PKD); *adiponectin* (adipo.); *flox/flox* (f/f); *high-fat diet* (HFD); *gonadal white adipose tissue* (gWAT); *subcutaneous white adipose tissue* (sWAT); *brown adipose tissue* (BAT); *hematoxylin and eosin* (H&E). (Löffler et al., 2018)<sup>219</sup>

On normal diet however, different types of adipose tissue did not show any changes in mice fed ND over 24 weeks, neither in the H&E staining of the three adipose tissue depots (Figure 52A,C,D), nor after quantitative analysis (Figure 52B,E). In case of gWAT, H&E staining and graph show some mild tendency towards decreased adipocyte size (Figure 52A,B). In BAT the same trend can be observed (Figure 52C), while no difference was visible in sWAT of mice lacking PKD1 in adipocytes compared to their littermates (Figure 52D,E). This is in line with the observation that only minor differences were detected between the genotypes in mice on ND feeding, when looking at their body weight gain, different fat depot weights, as well as their energy expenditure.

## RESULTS

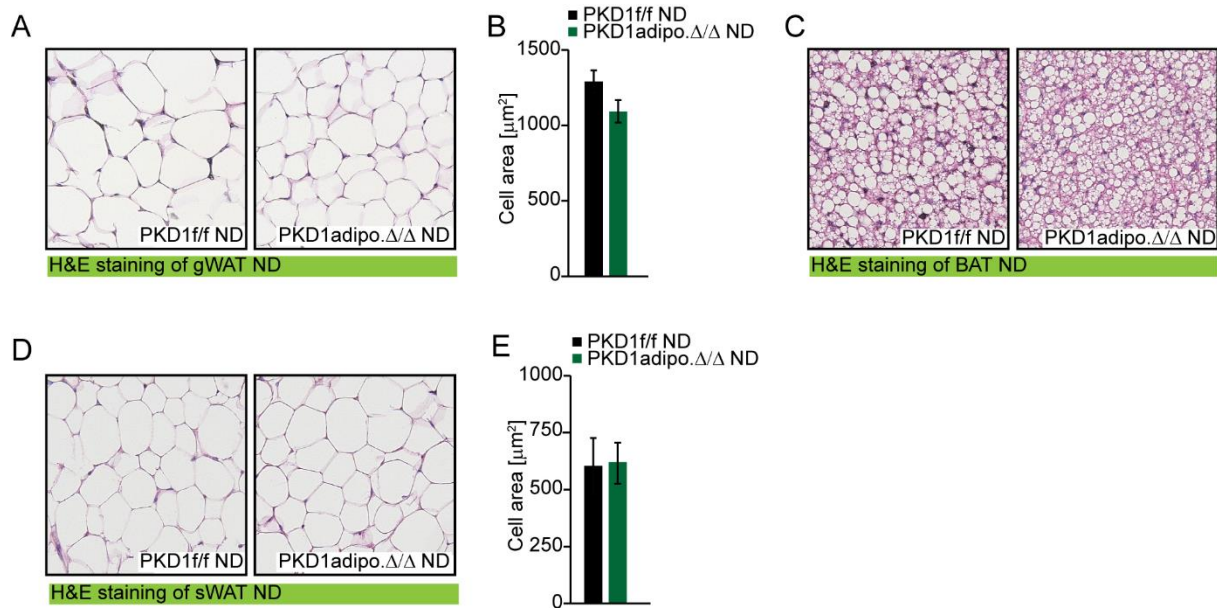


**Figure 52. PKD1 deletion in adipocytes does not change adipocyte size in mice fed ND.** Representative H&E staining of (A) gWAT, (C) BAT, and (D) sWAT from PKD1<sup>adipo.Δ/Δ</sup> and control mice fed ND for 24 weeks. Average adipocytes size was analyzed using the ImageJ software in (B) gWAT and (E) sWAT of indicated mice. Data are presented as mean  $\pm$  SEM (n=6/genotype). Stainings were visualized using an inverted microscope Olympus CKX31 at 20x magnification. Unpaired, two-tailed Student's t-test. *Protein kinase D* (PKD); *adiponectin* (adipo.); *flox/flox* (f/f); *normal diet* (ND); *gonadal white adipose tissue* (gWAT); *subcutaneous white adipose tissue* (sWAT); *brown adipose tissue* (BAT); *hematoxylin and eosin* (H&E). (Löffler et al., 2018)<sup>219</sup>

### 3.4.8 Deletion of PKD1 induces beiging of white adipocytes in mice

Induced energy expenditure triggered by adipocytes requires a reprogramming of expression patterns in these cells. To further investigate the molecular mechanisms regulating adipocyte function in the absence of PKD1 leading to a reduced weight, cell size, and overall increased energy expenditure, RNA sequencing was performed using gWAT of mice lacking PKD1 in adipocytes and their littermates after 24 weeks of HFD feeding. With this analysis, changes in specific genes or gene clusters can be identified, which could explain the observed phenotype. gWAT was chosen for the first analysis, since this was the only fat depot with a reduced weight, as well as some tendencies towards a reduced adipocyte size in mice lacking PKD1 even on ND feeding. Importantly, genes involved in beiging of white adipocytes were upregulated in this tissue of PKD1<sup>adipo.Δ/Δ</sup> mice, including gene clusters shown in classical browning, as well as genes involved in the creatine metabolism (Figure 53). This gives the conclusion that there is an increased beiging in adipocytes leading to enhanced energy dissipation in these mice.

## RESULTS

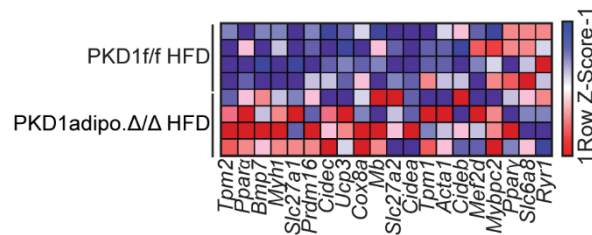


**Figure 53. RNA sequencing of gWAT revealed an upregulation of browning genes in PKD1-deleted mice.** RNA-sequencing based heat map of the expression patterns of browning-related genes in gWAT from mice lacking PKD1 in adipocytes and their controls (GSE analysis software<sup>209</sup>). For all data, n=4/genotype. *Protein kinase D* (PKD); *adiponectin* (adipo.); *flox/flox* (f/f); *high-fat diet* (HFD); *tropomyosin* (TPM); *peroxisome proliferator-activated receptor* (PPAR); *bone morphogenic protein 7* (BMP7); *myosin heavy polypeptide* (MYH); *solute carrier family* (SLC); *PR domain containing 16* (PRDM16); *cell death-inducing DFFA-like effector c* (CIDEC); *uncoupling protein* (UCP); *cytochrome c oxidase, subunit* (COX); *myoglobin* (MB); *cell death-inducing DNA fragmentation factor,  $\alpha$  subunit-like effector* (CIDE); *actinin  $\alpha$  1* (ACTA1); *myocyte enhancer factor 2D* (MEF2D); *myosin binding protein C, fast-type* (MYBPC2); *ryanodine receptor 1* (RYR1). This experiment has been performed in collaboration with the working group of Prof. Dr. Eilers. (unpublished observation)

Since browning of white adipocytes usually rather occurs in the more metabolically active sWAT, a second RNA sequencing analysis was performed using sWAT depots of PKD1adipo. $\Delta/\Delta$  mice and their controls, which have been kept on HFD for 24 weeks. Indeed, RNA sequencing revealed that genes promoting browning of white adipocytes were also increased in sWAT of mice lacking PKD1. GSEA further showed an elevated expression of genes related to the creatine-driven substrate cycle in addition to the genes generally known to be characteristic for beige adipocytes (Figure 54A,B). Upregulation of the creatine kinase and genes involved in the creatine metabolism have recently been proposed to promote energy expenditure in adipocytes<sup>17</sup>. GSEA also revealed an increased expression of genes related to the AMPK-stimulated FFA oxidation as well as a downregulation of genes related to obesity in sWAT lacking PKD1 (Figure 54C,D).

## RESULTS

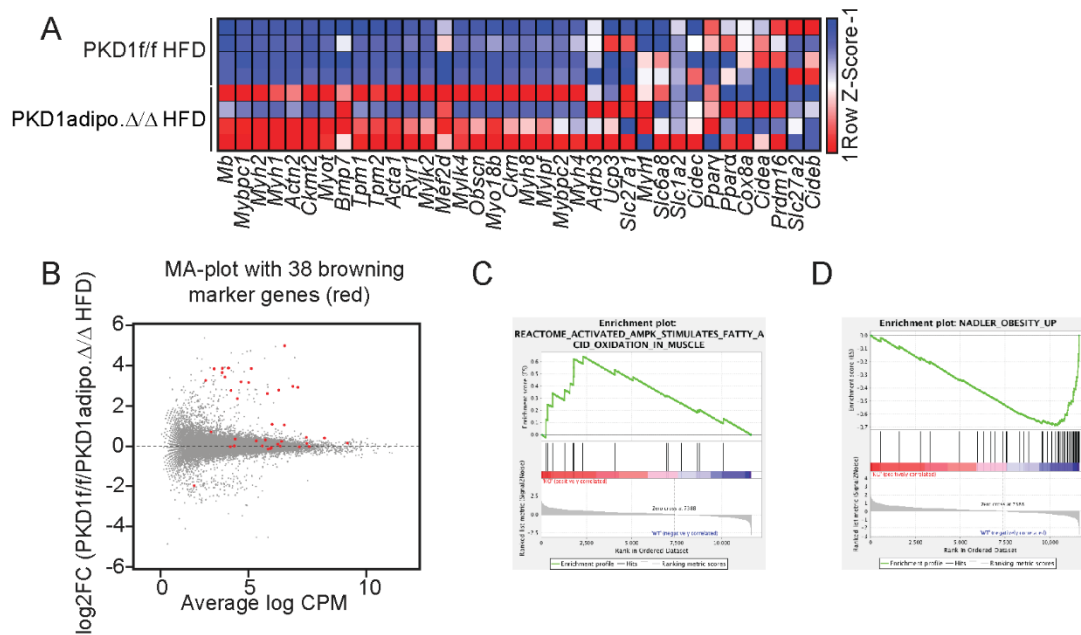


**Figure 54. Increased expression of browning genes in sWAT shown by RNA sequencing analysis.** (A) RNA-sequencing based heat map of the expression patterns of browning-related genes in sWAT from mice of the indicated genotypes (GSE analysis software<sup>209</sup>). (B) MA-plot showing RNA-sequencing results. Differential expression and average abundance (indicated as log<sub>2</sub> fold-change (FC) and log counts-per-million (CPM)) of all genes was calculated with EdgeR. Beiging related genes are highlighted in red. (C and D) GSEA gene sets enriched among genes up- or down regulated in RNA sequencing of sWAT derived from PKD1adipo.Δ/Δ mice. (GSE analysis software<sup>209</sup>). For all data, n=4/genotype. *Protein kinase D* (PKD); *adiponectin* (adipo.); *flox/flox* (f/f); *high-fat diet* (HFD); *myoglobin* (MB); *myosin binding protein C, slow-type* (MYBPC2); *myosin heavy polypeptide* (MYH); *actinin α 2* (ACTN2); *creatine kinase mitochondrial* (CKMT); *myotilin* (Myot); *bone morphogenic protein 7* (BMP7); *tropomyosin* (TPM); *actinin α 1* (ACTA1); *ryanodine receptor 1* (RYR1); *myosin light chain kinase* (MYLK); *myocyte enhancer factor 2D* (MEF2D); *obscurin, cytoskeletal calmodulin and titin-interacting RhoGEF* (OBSCN); *myosin XVIIIb* (MYO18B); *creatine kinase muscle* (CKM); *myosin light chain, phosphorylatable, fast skeletal muscle* (MYLPF); *myosin binding protein C* (MYBPC); *β<sub>3</sub> adrenergic receptor* (ADRB3); *uncoupling protein* (UCP); *solute carrier family* (SLC); *cell death-inducing DFFA-like effector c* (CIDEA); *peroxisome proliferator-activated receptor* (PPAR); *cytochrome c oxidase, subunit* (COX); *cell death-inducing DNA fragmentation factor, α subunit-like effector* (CIDE); *PR domain containing 16* (PRDM16); *fold change* (FC); *counts per million* (CPM). This experiment has been performed in collaboration with the working group of Prof. Dr. Eilers. ((A,B) Löffler *et al.*, 2018)<sup>219</sup>, ((C,D) unpublished observation)

RT-qPCR analysis of the same samples confirmed an enhanced expression of these genes promoting energy expenditure by inducing beiging of white adipocytes in sWAT upon deletion of PKD1<sup>17</sup>, including *Ucp1*, *Ucp3*, and *Pgc1a*. Moreover, sWAT of PKD1adipo.Δ/Δ showed increased expression of genes involved in the creatine cycle such as, *Myh1*, *Myh2*, *Ckm*, *Ckmt1*, *Ckmt2*, and *myogenic factor 5* (*Myf5*). On the other hand, expression of *Pparγ*, the major transcription factor regulating adipocyte differentiation, was not changed (Figure 55A). In gWAT of mice lacking PKD1,

## RESULTS

---

upregulation of the same set of genes was observed, with some alteration in significances. *Ucp1*, *Cidea*, *Slc27a2*, *Myh2*, and *Ckm* were highly enhanced (Figure 55B). However, in intra-scapular brown adipose tissue expression of these genes was not altered upon deletion of PKD1 and in some cases, like *Bmp7*, *Cideb*, *Slc27a1*, *Ucp3*, *Cidec*, and *Slc6a8*, a downregulation could even be observed (Figure 55C). These results indicate that deletion of PKD1 in adipocytes leads to changes in gene expression resulting in a beiging phenotype and enhancement of the overall energy dissipation by gWAT and sWAT without affecting brown adipocyte gene expression.

## RESULTS

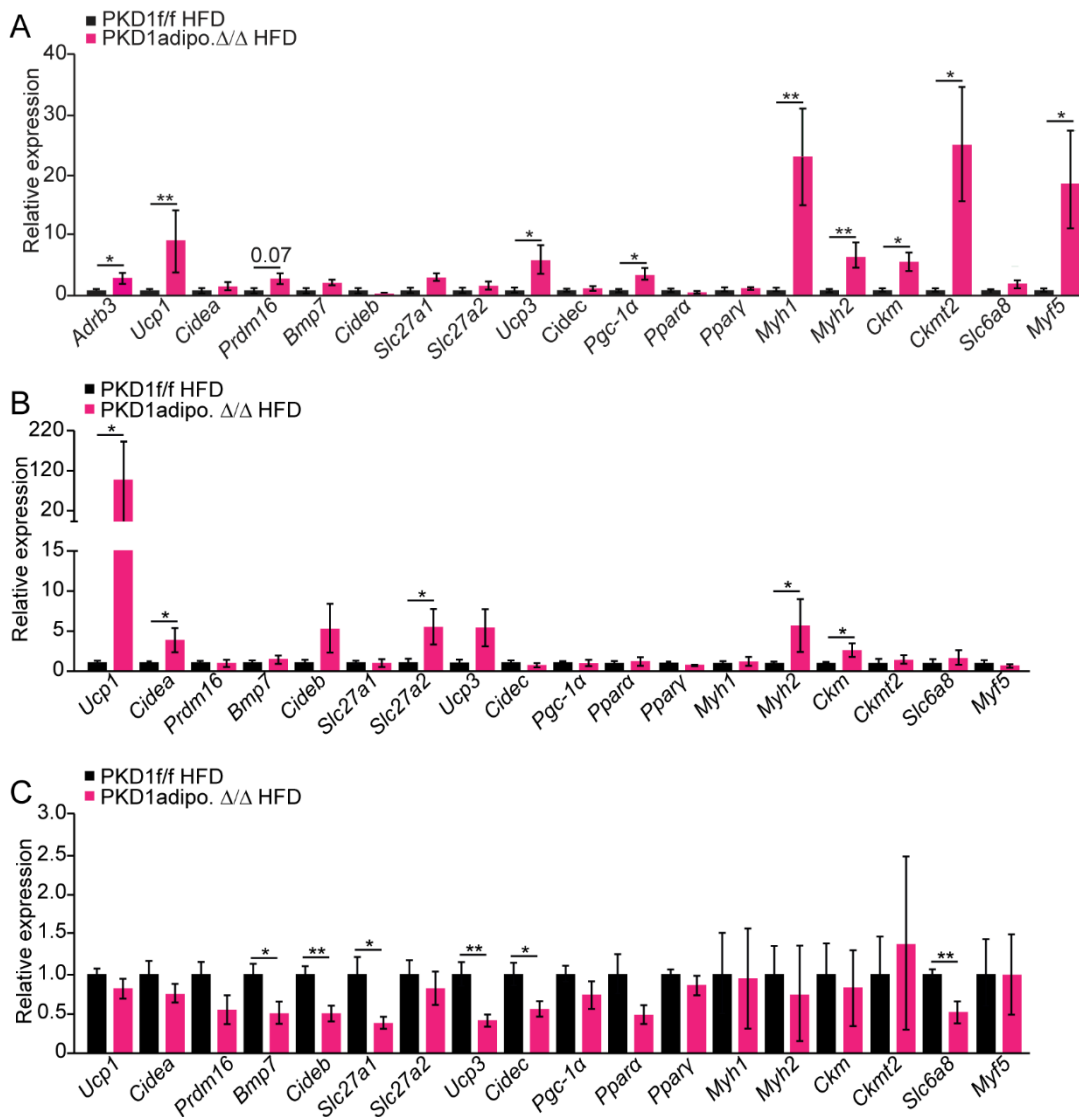


**Figure 55. PKD1 suppresses expression of genes characteristic for being.** RT-qPCR analyses of expression of indicated genes in (A,B) sWAT, (C) gWAT, and (D) BAT from control and PKD1-deficient mice fed HFD for 24 weeks. Data are presented as mean  $\pm$  SEM (n=6/genotype). Unpaired, two-tailed Student's t-test. For all data, \*p<0.05 and \*\*p<0.01. *Protein kinase D* (PKD); *adiponectin* (adipo.); *flox/flox* (f/f);  $\beta$ 3 *adrenergic receptor* (ADRB3); *uncoupling protein* (UCP); *cell death-inducing DNA fragmentation factor,  $\alpha$  subunit-like effector* (CIDE); *PR domain containing 16* (PRDM16); *bone morphogenetic protein 7* (BMP7); *solute carrier family* (SLC); *proliferator-activated receptor  $\gamma$  coactivator 1 $\alpha$*  (PGC1 $\alpha$ ); *peroxisome proliferator-activated receptor* (PPAR); *myosin heavy polypeptide* (MYH); *creatine kinase muscle* (CKM); *creatine kinase mitochondrial* (CKMT); myogenic factor 5 (MYF5); *high-fat diet* (HFD). ((A,B,C) Löffler et al., 2018)<sup>219</sup>, ((C) unpublished observation)

Since PPAR $\gamma$  was not changed in sWAT of PKD1-deficient mice (see Figure 55A), expression of the major lipolytic or lipogenic genes in adipocytes (*Fas*, *diacylglycerol-O-acyltransferase* (*Dgat*), *lipoprotein lipase* (*Lpl*), *Acc*, *Srebp1*, *Srebp2*, *Creb*, and *carbohydrate-responsive element-binding protein* (*Chrebp*)) were measured. None of the tested genes determining lipid metabolism were altered by PKD1 deletion (Figure

## RESULTS

56). This suggests that PKD1 affects beiging of white adipocytes without changing overall lipid metabolism of adipocytes.

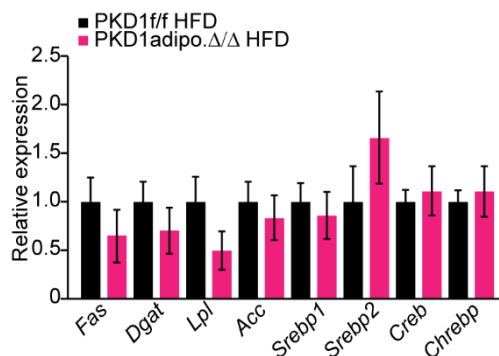


**Figure 56. PKD1 does not affect lipid metabolism.**

RT-qPCR analyses of expression of indicated genes in sWAT of control and PKD1-deficient mice fed HFD for 24 weeks. Data are presented as mean  $\pm$  SEM (n=6/genotype). Unpaired, two-tailed Student's t-test. *Protein kinase D* (PKD); *adiponectin* (adipo.); *flox/flox* (f/f); *high-fat diet* (HFD); *fatty acid synthase* (FAS); *diacylglycerol-O-acyltransferase* (DGAT); *lipoprotein lipase* (LPL); *acetyl-CoA carboxylase* (ACC); *sterol regulatory element-binding protein* (SREBP); *cAMP-response element-binding protein* (CREB); *carbohydrate-responsive element-binding protein* (CHREBP). (Löffler *et al.*, 2018)<sup>219</sup>

Beige adipocytes are not just characterized by an enhanced expression of UCP1 and other related genes, but also by an increased mitochondrial content. In SVC of PKD1-depleted adipocytes, both upregulation of genes promoting energy metabolism as well as increased mitochondrial content could be observed. Therefore, in addition to the RT-qPCR analysis, mitochondrial content in sWAT from PKD1<sup>adipo.Δ/Δ</sup> and control mice after 24 weeks on HFD was also measured. Consistently, it was markedly increased in PKD1<sup>adipo.Δ/Δ</sup> mice (Figure 57A). There was no clear correlation between appearance of multilocular adipocytes and PKD1 deletion in sWAT of PKD1-deficient mice (see Figure 51A). Nevertheless, increased UCP1 staining was observed in these tissues compared to littermates, when analyzed with IHC (Figure 57B). Furthermore, protein levels of UCP1 were enhanced in sWAT of mice lacking PKD1 (Figure 57C). Altogether, these results suggest that PKD1 deficiency promotes beiging of white adipocytes, elevating whole-body energy dissipation and protecting against diet-induced obesity.



## RESULTS

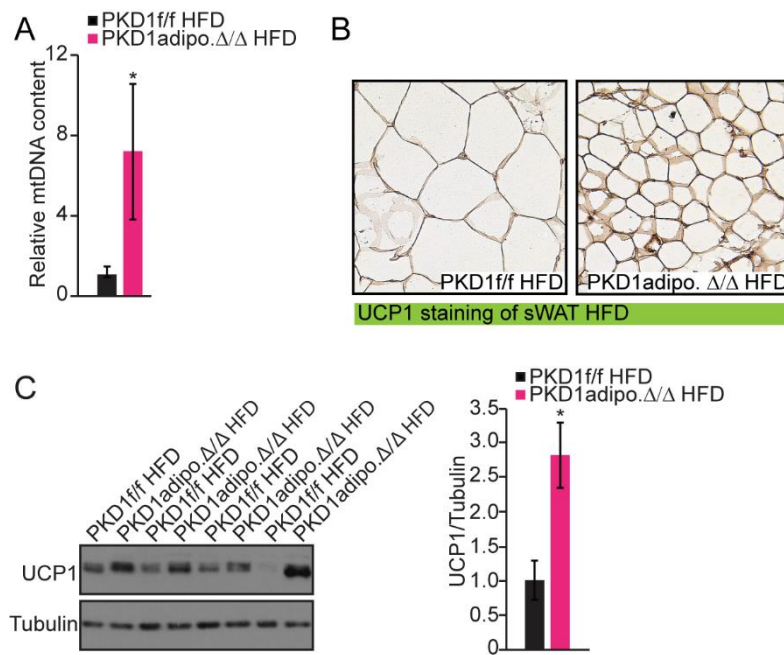


**Figure 57. PKD1adipo.Δ/Δ mice show an increased mitochondrial content and increased UCP1 levels in their sWAT.** (A) Ratio of mitochondrial DNA and genomic DNA in sWAT of mice lacking PKD1 and controls after 24 weeks of HFD feeding. (B) IHC staining for UCP1 in sWAT of mice lacking PKD1 in adipocytes and controls. Stainings were visualized using an inverted microscope Olympus CKX31 at 20x magnification. (C) WB analysis using an antibody against UCP1 in sWAT of mice lacking PKD1 and their controls including densitometric analysis of four replicates each. Tubulin was used as a loading control. Data are presented as mean  $\pm$  SEM (n=6/genotype). Unpaired, two-tailed Student's t-test. For all data, \*p<0.05. *Protein kinase D* (PKD); *adiponectin* (adipo.); *flox/flox* (f/f); *high-fat diet* (HFD); *uncoupling protein* (UCP); *mitochondrial DNA* (mtDNA); *subcutaneous white adipose tissue* (sWAT). ((A,B) unpublished observation), ((C) Löffler *et al.*, 2018)<sup>219</sup>

So far, all the observed changes occurring during HFD could also be mildly seen in mice fed ND. Genes enhancing energy expenditure were upregulated in white adipocytes of PKD1-depleted mice after 24 weeks on HFD. Therefore, it was examined whether some of these genes are also upregulated in fat depots of ND-fed mice upon deletion of PKD1. In contrast to HFD-fed mice, PKD1 deletion in adipocytes of mice fed ND did not lead to any changes in gene expression, regarding the ones responsible for promotion of energy expenditure, in none of the fat depots. In sWAT of PKD1adipo.Δ/Δ some mild, but not significantly upregulated genes could be observed, whereas in gWAT or BAT no alterations in expression were detectable (Figure 58A-C).

## RESULTS

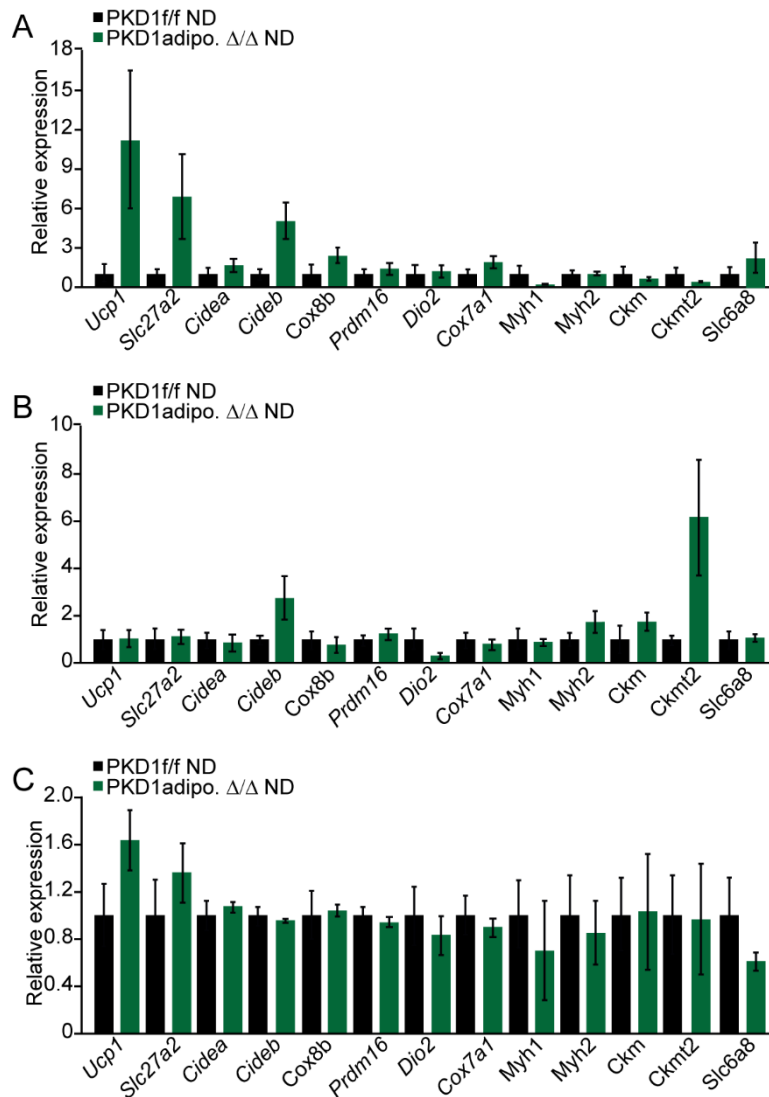


**Figure 58. Deletion of PKD1 does not alter gene expression in mice fed ND.** RT-qPCR analyses of expression of indicated genes in (A) sWAT, (B) gWAT, and (C) BAT from control and PKD1-deficient mice fed ND for 24 weeks. Data are presented as mean  $\pm$  SEM (n=5/genotype). Unpaired, two-tailed Student's t-test. For all data, \*p<0.05. Normal diet (ND). *Protein kinase D* (PKD); *adiponectin* (adipo.); *flox/flox* (f/f); *uncoupling protein* (UCP); *solute carrier family* (SLC); *cell death-inducing DNA fragmentation factor,  $\alpha$  subunit-like effector* (CIDE); *cytochrome c oxidase, subunit* (COX); *PR domain containing 16* (PRDM16); *iodothyronine deiodinase 2* (DIO2); *myosin heavy polypeptide* (MYH); *creatine kinase muscle* (CKM); *creatine kinase mitochondrial* (CKMT); *normal diet* (ND). (unpublished observation)

Due to the fact that muscle related markers like *Ckm* and *Myh* showed an enhanced expression in sWAT of HFD-fed mice lacking PKD1, it was further investigated, whether ectopic myofiber formation could be found within sWAT of these mice. Staining for MYH1 revealed that there is no formation of myofibers sWAT of mice lacking PKD1, neither on HFD nor on ND (Figure 59A,B).

## RESULTS

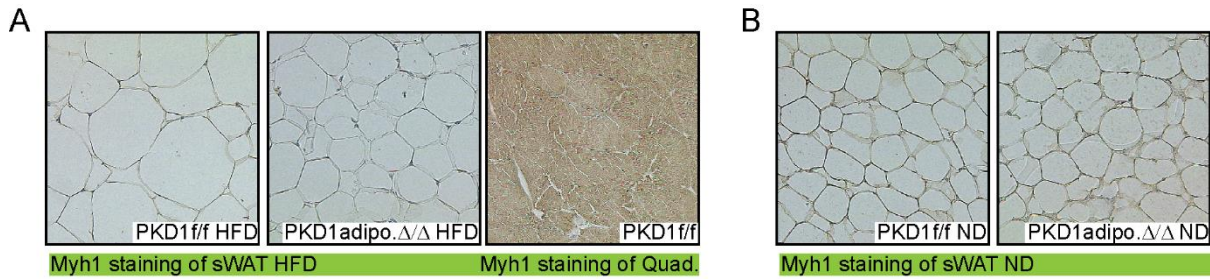


**Figure 59. Deletion of PKD1 does not show formation of ectopic myofibers.** IHC staining for MYH1 in sWAT of mice lacking PKD1 in adipocytes and controls fed (A) HFD and (B) ND. Quadriceps of a control mouse fed HFD diet was used for a positive MYH1 staining (representative pictures of n=4/genotype). Stainings were visualized using an inverted microscope Olympus CKX31 at 20x magnification. *Protein kinase D* (PKD); *adiponectin* (adipo.); *flox/flox* (f/f); *myosin heavy polypeptide* (MYH); *high-fat diet* (HFD); *normal diet* (ND); *subcutaneous white adipose tissue* (sWAT); *quadriceps* (Quad.). (Löffler et al., 2018)<sup>219</sup>

### 3.4.9 Effects on energy expenditure are abolished under thermoneutral conditions

Beige adipocyte acquisition is largely suppressed in the thermoneutral environment<sup>246</sup>. Indeed, housing at 30 °C resulted in normalization of elevated energy expenditure in PKD1-deficient mice (Figure 60A) as well as normalization of the reduction in body weight gain in PKD1<sup>adipo.Δ/Δ</sup> mice (Figure 60B). This indicates that the observed changes in energy dissipation can be abolished under thermoneutral conditions.

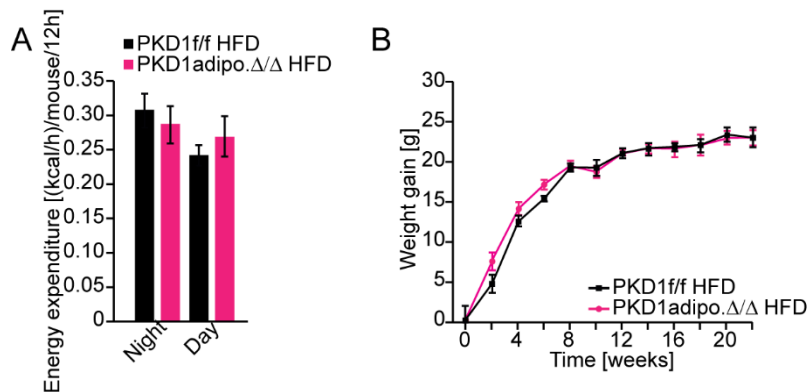


**Figure 60. Effects on energy expenditure are abolished under thermoneutral conditions.** (A) Energy expenditure of mice lacking PKD1 and their littermates, which were measured in a metaboli<sup>o</sup>cage for 1 week after HFD feeding under thermoneutral conditions for 22 weeks. (B) Body weight gain over 22 weeks of HFD-feeding at thermoneutral temperature. Data are presented as mean  $\pm$  SEM (n=6-8/genotype). Unpaired, two-tailed Student's t-test. *Protein kinase D* (PKD); *adiponectin* (adipo.); *flox/flox* (f/f); *high-fat diet* (HFD). (Löffler et al., 2018)<sup>219</sup>

### 3.4.10 PKD1 suppresses ADRB3 expression in an AMPK-C/EBP- $\alpha$ /C/EBP- $\delta$ -dependent manner

Creatin kinase cycle-related genes and selected muscle markers were previously shown to be increased in differentiated SVC of PKD1adipo. $\Delta/\Delta$  mice (see Figure 26A), without changes in gene expression of the classical browning markers (see Figure 24C). On the other hand, RNA sequencing revealed an upregulation of the gene encoding for ADRB3 (see Figure 54A). *Adrb3* expression was further enhanced in differentiated adipocytes lacking PKD1 (Figure 61A). Consistently, ADRB3 staining displayed elevated levels on the surface of PKD1-depleted adipocytes (Figure 61B).  $\beta$ -adrenergic stimulation induces UCP1 in adipocytes<sup>17</sup>. In fact,  $\beta$ -adrenergic stimulation of adipocytes lacking PKD1 and control cells led to an enhanced *Ucp1* expression in the absence of PKD1 (Figure 61C). These data indicate that PKD1 regulates expression of *Ucp1* in adipose tissue in an ADRB3-dependent manner. However, the transcription factor mediating this whole process remains unknown.

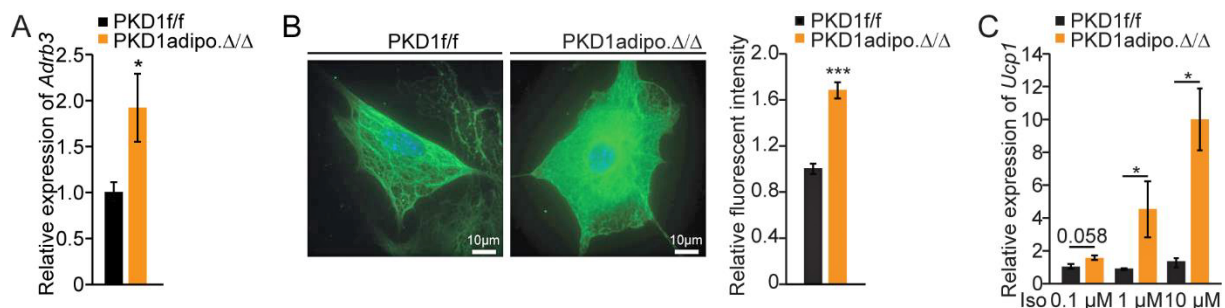


**Figure 61. UCP1 expression is regulated by the ADRB3 in PKD1-deficient adipocytes.** (A) Relative gene expression of *Adrb3* in differentiated SVC derived from SWAT of PKD1-deficient and control mice (n=5). (B) Representative immunofluorescent images of ADRB3 staining and quantification of fluorescent intensity in PKD1-deficient and control adipocytes derived from SVC (n=7). Cells were visualized under a fluorescent microscope Leica DM5500 B at 63x magnification. (C) RT-qPCR analyzes of *Ucp1* in differentiated SVC of indicated genotypes after 24 h stimulation with Isoproterenol at indicated concentrations (n=5). Data are presented as mean  $\pm$  SEM (representative of two individual experiments). Unpaired, two-tailed Student's t-test. For all data, \*p<0.05 and \*\*\*p<0.001. *Protein kinase D* (PKD); *adiponectin* (adipo.); *flox/flox* (f/f);  $\beta$ 3 *adrenergic receptor* (ADRB3); *uncoupling protein* (UCP); *isoproterenol* (Iso); *molar* (M). (Löffler *et al.*, 2018)<sup>219</sup>

There are several transcription factors mediating beige adipocyte function<sup>204</sup>. Therefore, protein abundance and/or phosphorylation of a number of these transcription factors was measured in PKD1ca expressing 3T3-L1 cells (*C-terminal binding protein* (CtBP) 1/2, PGC-1 $\alpha$ , C/EBP- $\alpha$ , C/EBP- $\delta$ , *retinoblastoma protein* (Rb),

## RESULTS

*forkhead box protein O1* (FoxO1), C/EBP- $\beta$ , *estrogen-related receptor  $\alpha$*  (ERR $\alpha$ ), *activating transcription factor 2* (ATF2), CREB, and PRDM16) (Figure 62A). Interestingly, expression of PKD1ca resulted in a reduction of C/EBP- $\alpha$  and C/EBP- $\delta$  protein levels, whereas all the other transcription factors tested were not altered (Figure 62).

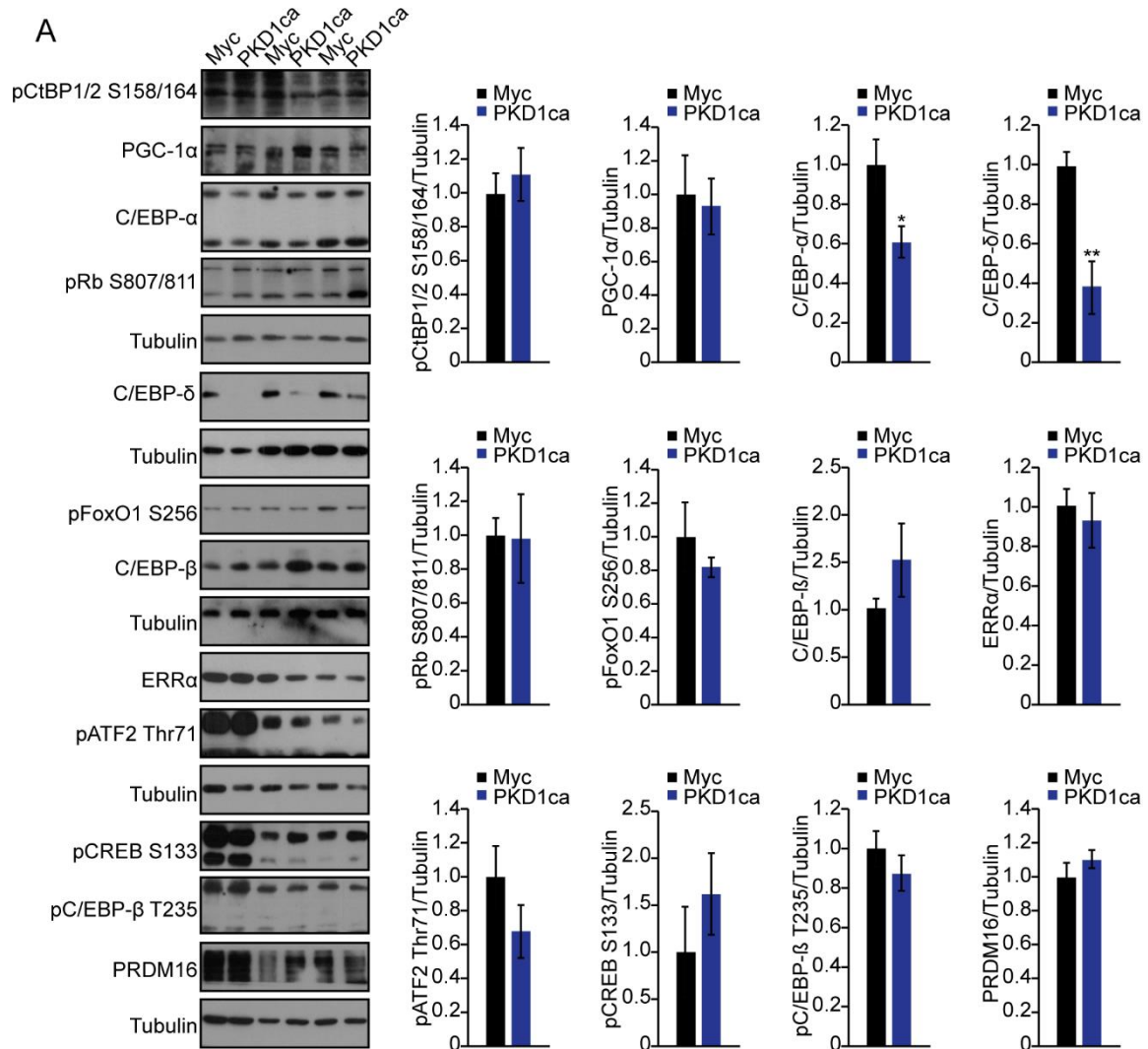


**Figure 62. PKD1 suppresses ADRB3 expression in an AMPK-C/EBP- $\alpha$ /C/EBP- $\delta$ -dependent manner.** WB analysis using antibodies against CtBP1/CtBP2, PGC-1 $\alpha$ , C/EBP- $\alpha$ , C/EBP- $\delta$ , Rb, FoxO1, C/EBP- $\beta$ , ERR $\alpha$ , ATF2, CREB, and PRDM16 in differentiated 3T3-L1 cells expressing PKD1ca and corresponding controls including densitometric analysis of four replicates each. Tubulin was used as a loading control. Data are presented as mean  $\pm$  SEM. Unpaired, two-tailed Student's t-test. For all data, \* $p < 0.05$  and \*\* $p < 0.01$ . *Protein kinase D* (PKD); *constitutive active* (ca); *C-terminal binding protein* (CtBP); *proliferator-activated receptor  $\gamma$  coactivator 1 $\alpha$*  (PGC1 $\alpha$ ); *CCAAT/enhancer-binding protein* (C/EBP); *retinoblastoma protein* (Rb); *forkhead box protein O1* (FoxO1); *estrogen-related receptor  $\alpha$*  (ERR $\alpha$ ); *activating transcription factor 2* (ATF2); *cAMP-response element-binding protein* (CREB); *PR domain containing 16* (PRDM16); *phospho* (p). (Löffler *et al.*, 2018)<sup>219</sup>

## RESULTS

---

Conversely, depleting PKD1 in adipocytes resulted in increased C/EBP- $\alpha$  and C/EBP- $\delta$  levels (Figure 63A,B), whereas mRNA expression of both transcription factors was not altered (Figure 63E,F). Of note, AICAR stimulation of adipocytes expressing PKD1ca led to elevated C/EBP- $\alpha$  and C/EBP- $\delta$  levels in control and PKD1ca cells (Figure 63C). Previous studies demonstrate that C/EBP- $\alpha$  and possibly C/EBP- $\delta$  are necessary for expression of ADRB3 in adipocytes<sup>201</sup>. Furthermore, mice lacking C/EBP- $\alpha$  and C/EBP- $\delta$  showed reduced UCP1 expression in adipose tissue<sup>202</sup>. To test whether PKD1 regulates ADRB3 in a C/EBP- $\alpha$  and/or C/EBP- $\delta$ -dependent manner, silencing of these transcription factors was performed in SVC of PKD1adipo. $\Delta/\Delta$  mice. Successful silencing of both C/EBP- $\alpha$  and C/EBP- $\delta$  was achieved (Figure 63E,F) and was sufficient to normalize increased ADRB3 expression in cells lacking PKD1 (Figure 63D). Altogether, these results demonstrate that PKD1 inhibits C/EBP- $\alpha$  and C/EBP- $\delta$  abundance in an AMPK-dependent manner. Full induction of beige/brown gene expression on the other hand require ADRB3 and its expression is promoted by both transcription factors.

## RESULTS

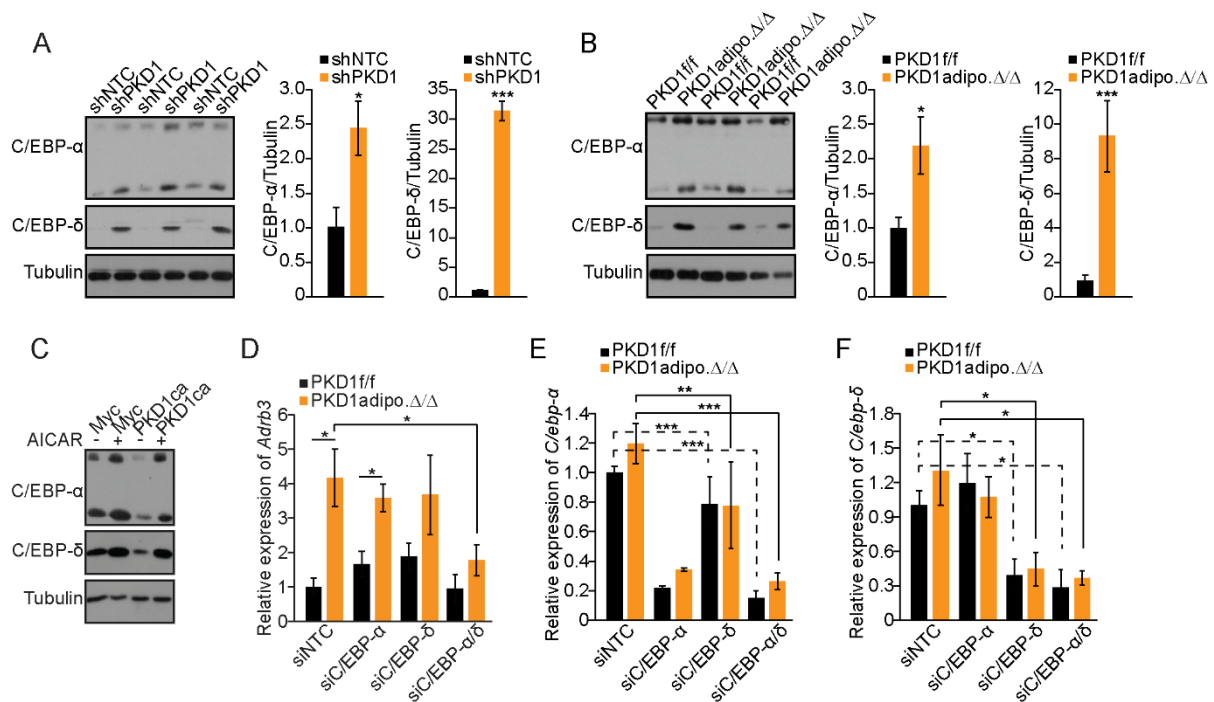


**Figure 63. PKD1 suppresses C/EBP- $\alpha$  and C/EBP- $\delta$  abundance in an AMPK-dependent manner in order to regulate ADRB3 expression.** WB analysis using antibodies against C/EBP- $\alpha$  and C/EBP- $\delta$  in (A) differentiated 3T3-L1 cells lacking PKD1 and (B) SVF cells derived from PKD1-deficient mice including densitometric analysis of triplicates each. (C) WB analysis of C/EBP- $\alpha$  and C/EBP- $\delta$  in differentiated 3T3-L1 expressing PKD1ca, which were treated with AICAR (2 mM) for 2 h. RT-qPCR analysis of (D) *Adrb3*, (E) *C/ebp- $\alpha$* , and (F) *C/ebp- $\delta$*  in SVC derived from sWAT of control and PKD1-deficient mice transfected with control siRNA, siRNA against C/EBP- $\alpha$  and/or C/EBP- $\delta$  (n=4). Data are presented as mean  $\pm$  SEM. (A,B) Unpaired, two-tailed Student's t-test, (D,E,F) one-way ANOVA with Tukey's multiple comparisons post-test. For all data, \*p<0.5, \*\*p<0.01, and \*\*\*p<0.001. *Protein kinase D* (PKD); *small hairpin* (sh); *non-targeting control* (NTC); *CCAAT/enhancer-binding protein* (C/EBP); *adiponectin* (adipo.); *flox/flox* (f/f); *constitutive active* (ca);  $\beta$ 3 *adrenergic receptor* (ADRB3). (Löffler *et al.*, 2018)<sup>219</sup>

### 3.4.11 PKD1 deletion in adipocytes protects against the development of type 2 diabetes and diet-induced fatty liver disease

AMPK signaling is protective against fatty liver disease and insulin resistance. Its activation was shown to control adipokine levels in the circulation<sup>191,192</sup>. Therefore, an *in vivo* analysis was performed in mice lacking PKD1 specifically in adipocytes.

Neither levels of adiponectin nor resistin in the blood of PKD1-deficient mice were changed as compared to control animals upon HFD or ND feeding for 24 weeks (Figure 64A,B). However, leptin levels were decreased PKD1-deficient mice fed ND, whereas HFD feeding did not alter leptin levels significantly (p=0.18) (Figure 64C).

## RESULTS

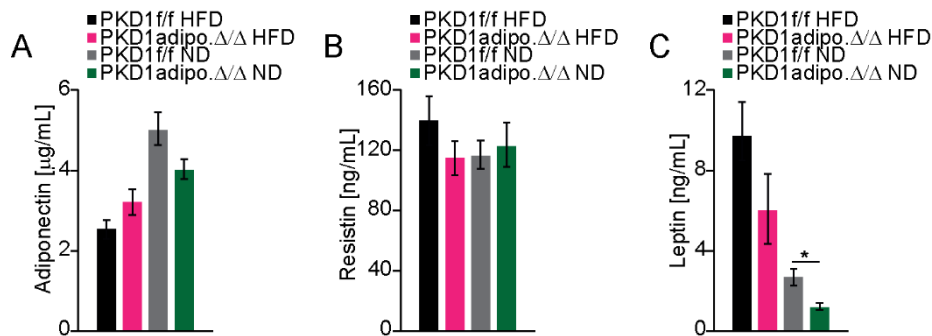


**Figure 64. Deletion of PKD1 reduces leptin levels but does not affect any of the other adipokines.** (A) Adiponectin, (B) resistin, and (C) leptin levels in blood of PKD1adipo. $\Delta/\Delta$  and control mice fed ND and HFD for 24 weeks. Blood was drawn from mice and parameters have been analyzed in the serum using a multiplex ELISA. For all data,  $n=6-11/\text{genotype}$ . Data are presented as mean  $\pm$  SEM. One way ANOVA with Tukey's multiple comparisons post test. For all data,  $*p<0.05$ . *Protein kinase D* (PKD); *adiponectin* (adipo.); *flox/flox* (f/f); *high-fat diet* (HFD), *normal diet* (ND). (Löffler et al., 2018)<sup>219</sup>

Consistently with the fact that mice lacking PKD1 showed decreased adipose tissue content, FFA levels in the blood were markedly lower in PKD1adipo. $\Delta/\Delta$  mice compared to controls during HFD feeding. PKD1-depleted mice fed ND presented only moderately reduced FFA levels in the blood ( $p=0.13$ ) (Figure 65A). Importantly, other lipolysis products, glycerol and TGs, did not display any alterations between genotypes (Figure 65B,C).

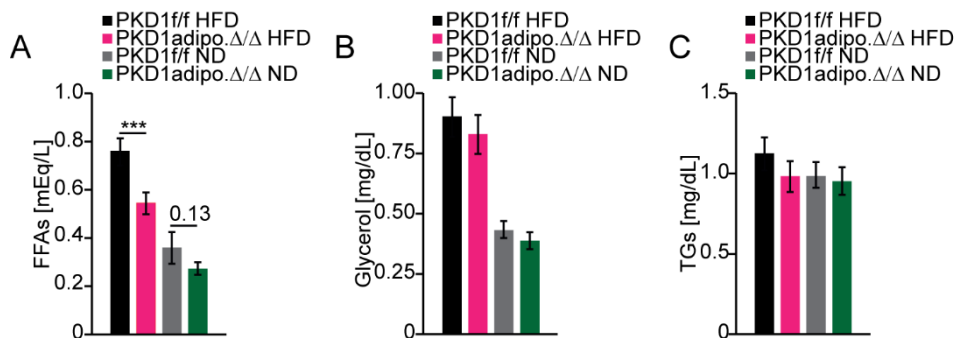


**Figure 65. FFA levels are reduced in mice lacking PKD1 in adipocytes.** (A) FFA, (B) glycerol, and (C) TG levels in blood of PKD1adipo. $\Delta/\Delta$  and control mice fed ND and HFD. Indicated parameters were measured in the serum of these mice after 16 weeks of HFD or ND feeding. For all data,  $n=6-11/\text{genotype}$ . Data are presented as mean  $\pm$  SEM. One way ANOVA with Tukey's multiple comparisons post test. For all data,  $***p<0.001$ . *Protein kinase D* (PKD); *adiponectin* (adipo.); *flox/flox* (f/f); *free fatty acids* (FFAs); *triglycerides* (TGs); *high-fat diet* (HFD), *normal diet* (ND). (Löffler et al., 2018)<sup>219</sup>

Increased FFA levels are one major link between obesity, insulin resistance and the development of T2D<sup>247</sup>. Therefore, it was tested whether mice lacking PKD1 respond



## RESULTS

better to insulin as predicted by the reduced FFA levels by performing an ITT as well as a GTT. PKD1adipo. $\Delta/\Delta$  mice and their controls were challenged with a defined dose of insulin and glucose removal from the blood was measured over 2 h. On HFD, PKD1adipo. $\Delta/\Delta$  mice presented lower glucose levels compared to controls at all indicated time points. PKD1-deficient mice fed ND displayed a moderate but significant improvement of insulin action (Figure 66A). In line with these data, HFD-fed mice lacking PKD1 showed an improved glucose tolerance at all times, after glucose was injected intraperitoneal. In case of ND-fed mice, glucose injection had no impact on the blood glucose levels in mice with a PKD1 deletion compared to their controls (Figure 66B). Similarly, PKD1 deletion had no impact on glucose tolerance in the same HFD-fed mice after a shorter period of 8 weeks (Figure 66C), suggesting that improved glucose tolerance is secondary to the decreased adiposity in mice fed HFD for 24 weeks.

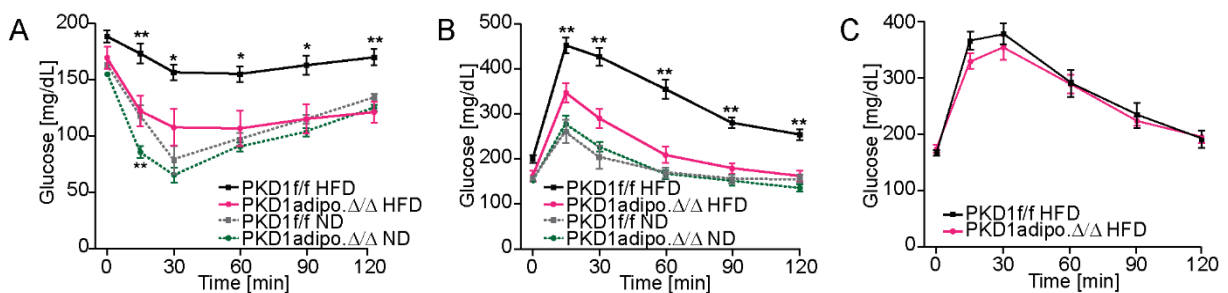


**Figure 66. PKD1 deletion protects against insulin resistance and type 2 diabetes.** (A) Insulin tolerance test was performed in PKD1adipo. $\Delta/\Delta$  and control mice after 20 weeks of HFD or ND feeding by intraperitoneal injection of insulin (0.25 U/kg BW) after a fasting period of 4 h. Glucose levels in the blood were measured in the fasting state and at 15, 30, 60, 90, and 120 minutes after injection. Glucose tolerance test was performed in PKD1adipo. $\Delta/\Delta$  and control mice after (B) 18 weeks of HFD or ND feeding or (C) 8 weeks of HFD feeding by intraperitoneal injection of glucose (1 g/kg BW) after 4 h fasting. Glucose levels in the blood were measured in the fasting state and at 15, 30, 60, 90, and 120 minutes after injection. For all data,  $n=8-11$ /genotype. (A,B) One way ANOVA with Tukey's multiple comparisons post test, (C) unpaired, two-tailed Student's t-test. Data are presented as mean  $\pm$  SEM ( $n=6-11$ /genotype). For all data, \* $p<0.05$ , \*\* $p<0.01$ , and \*\*\* $p<0.001$ . *Protein kinase D* (PKD); *adiponectin* (adipo.); *flox/flox* (f/f); *high-fat diet* (HFD), *normal diet* (ND). (Löffler *et al.*, 2018)<sup>219</sup>

Better peripheral insulin sensitivity specifically improved glucose tolerance in PKD1-deficient mice, since insulin levels in the circulation were not altered in the absence of PKD1, regardless of the diet (Figure 67A). Consistently, activation of Akt, a key regulator in the insulin pathway, was enhanced in differentiated SVC derived from

## RESULTS

sWAT of PKD1adipo. $\Delta/\Delta$  mice and decreased in cells with elevated PKD1-dependent signaling (Figure 67B,C).

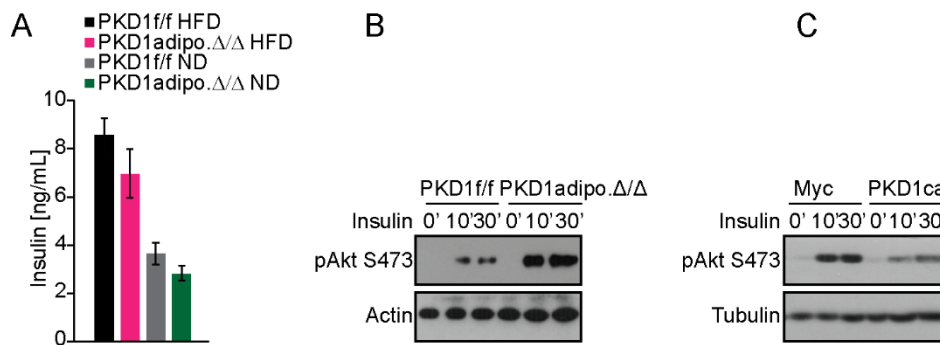


**Figure 67. Impaired insulin sensitivity, but not insulin secretion, is the major cause for the reduced glucose tolerance.** (A) Insulin levels in blood of PKD1adipo. $\Delta/\Delta$  and control mice fed ND and HFD for 24 weeks. Blood was drawn from mice and insulin was measured in the serum using a multiplex ELISA. For all data, n=8-11/genotype. WB analysis using an antibody against phosphorylation site of Akt at S473 in (B) differentiated SVC isolated from sWAT of mice lacking PKD1 and controls and (C) differentiated 3T3-L1 cells overexpressing PKD1ca (part of the WB from Figure 19). The cells were incubated in medium deprived from amino acids and glucose and stimulated with insulin (100 nM) for 10 and 30 minutes. Actin or Tubulin were used as a loading control. Data are presented as mean  $\pm$  SEM. (A) One way ANOVA with Tukey's multiple comparisons post test. For all data, n=6-11/genotype). *Protein kinase D* (PKD); *adiponectin* (adipo.); *flox/flox* (f/f); *high-fat diet* (HFD), *normal diet* (ND); *phospho* (p). (Löffler *et al.*, 2018)<sup>219</sup>

Diet-induced fatty liver disease often occurs upon obesity. Indeed, a reduced liver weight was observed in PKD1adipo. $\Delta/\Delta$  mice fed HFD (see Figure 43B), which could be explained by a lower TG content, assessed by an Oil Red O staining of liver sections or by measuring the overall TG content in liver samples from mice lacking PKD1 and controls (Figure 68A,B).

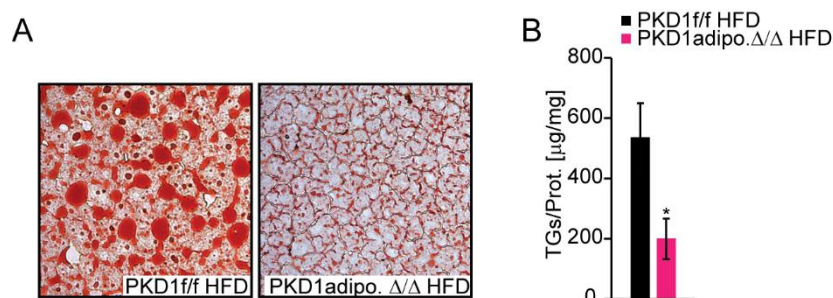


**Figure 68. PKD1 deletion protects against diet-induced fatty liver disease.** (A) Oil-Red-O staining of liver sections and (B) liver TG content from PKD1adipo. $\Delta/\Delta$  and control mice fed HFD for 24 weeks. Stainings were visualized using an inverted microscope Olympus CKX31 at 20x magnification. Data are presented as mean  $\pm$  SEM (n=6-11/genotype). (B) Unpaired, two-tailed Student's t-test. For all data, \*p<0.1. *Protein kinase D* (PKD); *adiponectin* (adipo.); *flox/flox* (f/f); *high-fat diet* (HFD); *triglycerides* (TGs). (Löffler *et al.*, 2018)<sup>219</sup>

### 3.4.12 PKD1 also regulates human adipose tissue function

To test whether PKD1 is also involved in the regulation of insulin sensitivity in humans, multiple parameters were assessed in human subjects (Table 2). Furthermore, expression of PKD1 in sWAT of control and insulin resistant patients was examined. PKD1 levels positively correlated with HOMA-IR (the major parameter for insulin resistance in humans), suggesting that PKD1 regulates insulin sensitivity also in human adipose tissue (Figure 69A). PKD1 also positively correlates with levels of insulin in these patients (Figure 69B), whereas all the other measured parameters, such as glucagon, *glucagon-like peptide-1* (GLP-1), IL-6, ghrelin, leptin, resistin, and adiponectin were not changed (Table 3).

**Table 2. Characteristics of human subjects and blood analysis.** Demographic informations, anthropomorphic measurements, and blood analysis of obese, insulin resistant patients and controls were assessed. Variables are presented as mean (SD) or absolute frequency (percentage). This experiment has been performed in collaboration with the working group of Dr. Sabio. *Body mass index* (BMI); *homeostatic model assessment-insulin resistance* (HOMA-IR). (Löffler *et al.*, 2018)<sup>219</sup>

Variables	Obese patients (n=41)	Controls non-obese (n=20)	P
Age (year)	44.2 (12.1)	52 (16.4)	0.1
Female:male ratio	31:10	11:9	0.103
Hypertension (n)	16 (39)	5 (25)	0.279
BMI (kg/m <sup>2</sup> )	48.6 (7.3)	25.4 (3.4)	<0.001
Fasting blood sugar	97.4 (18.3)	93.3 (13.9)	0.535
Triglycerides (mg/dL)	145.5 (89.8)	117.6 (50.7)	0.311
Insulin (mIU/L)	3.5 (3.3)	2.2 (3)	0.014
HOMA-IR	14.4 (12.6)	8.8 (11)	0.011

## RESULTS

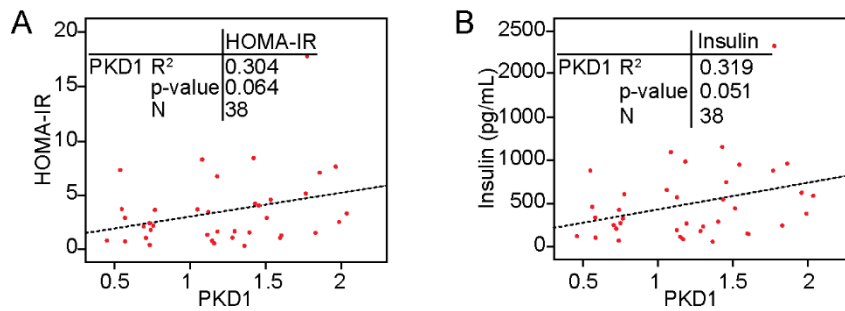


**Figure 69. PKD1 positively correlates with HOMA-IR.** Correlation between PKD1 expression and (A) HOMA-IR levels or (B) insulin levels in human sWAT. Blood samples were taken to measure glucose using a standard glucometer. Blood samples were also centrifuged, and plasma was frozen to detect insulin by Luminex assay. Individually matched glucose and insulin levels were used to assess HOMA-IR using the following calculations:  $HOMA-IR = \frac{\text{glucose (mg/dl)} \times \text{insulin (mU/l)}}{405}$ . This experiment has been performed in collaboration with the working group of Dr. Sabio. *Protein kinase D (PKD)*; *homeostatic model assessment-insulin resistance (HOMA-IR)*. ((A) Löffler *et al.*, 2018)<sup>219</sup>, (B) unpublished observation)

**Table 3.Characteristics of human blood samples.** Blood analysis of obese, insulin resistant patients and controls were assessed by collection of blood followed by a Luminex assay. This experiment has been performed in collaboration with the working group of Dr. Sabio. *glucagon-like peptide-1 (GLP-1)*; *interleukin-6 (IL-6)*. (unpublished observation)

	Glucagon	GLP-1	IL-6	Grelin	Leptin	Resistin	Adiponectin
PKD1 R <sup>2</sup>	0.275	-0.002	-0.148	0.202	0.210	0.097	0.054
p-value	0.094	0.992	0.375	0.223	0.206	0.562	0.748
N	38	38	38	38	38	38	38

Moreover, in human adipocytes, which were treated with a PKD-inhibitor, a reduced lipogenesis rate was shown (Figure 70A). Consistently with previous findings, PKD inhibition resulted in higher oxygen consumption in human adipocytes, at basal conditions and upon stimulation with oligomycin (oxygen consumption caused by the decoupling activity) (Figure 70B). Altogether, absence of PKD1 specifically in adipocytes protects against diet-induced T2D and lipid accumulation in the liver. Moreover, these data suggest that the proposed mechanisms might not only apply to rodents but also to humans.

## RESULTS

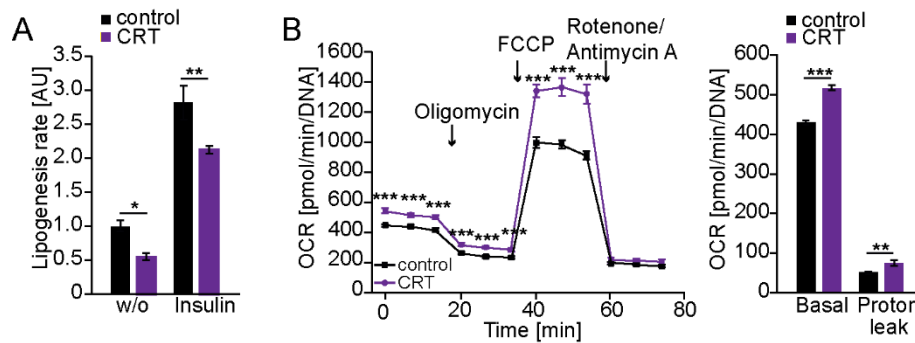


**Figure 70. PKD1 inhibition reduces lipogenesis rate and increases OCR also in human adipocytes.** (A) Basal and insulin-induced lipogenesis rate in differentiated human subcutaneous preadipocytes treated with CRT 0066101 (3  $\mu$ M) or vehicle for 3 days (n=4). (B) OCR in response to indicated substances as well as OCR annotated to the indicated cellular processes in differentiated human subcutaneous preadipocytes treated with CRT 0066101 (3  $\mu$ M) for 3 days (n=19). Data are presented as mean  $\pm$  SEM (representative of two individual experiments). Unpaired, two-tailed Student's t-test. For all data, \*\*p<0.01 and \*\*\*p<0.001. 2-[4-[[[(2R)-2-aminobutyl]amino]-2-pyrimidinyl]-4-(1-methyl-1H-pyrazol-4-yl)phenol] dihydrochloride (CRT 0066101); arbitrary units (AU); without (w/o); minutes (min); oxygen consumption rate (OCR); deoxyribonucleic acid (DNA). (Löffler et al., 2018)<sup>219</sup>

### 3.4.13 Abrogation of PKD1-dependent signalling in adipose tissue can attenuate the course of the disease

Next, it was tested whether the course of this disease in adipose tissue of obese mice can be attenuated by abrogating PKD1-dependent signaling. Therefore, a mouse line was generated in which PKD1 can be specifically deleted in adipocytes (PKD1ind.adipo $\Delta/\Delta$ ) by tamoxifen administration after 10 weeks of HFD. PKD1ind.adipo $\Delta/\Delta$  mice were born at normal Mendelian ratio and showed no gross abnormalities compared to their littermates. When analyzed by WB, substantial reduction of PKD1 protein levels were observed in sWAT (Figure 71A). Of note, upon PKD1 deletion, mice did not further gain body weight compared to their littermates (Figure 71B). Similarly, the fat mass gain was almost completely abolished upon deletion of PKD1 while control animals continued accumulating fat (Figure 71C).

## RESULTS

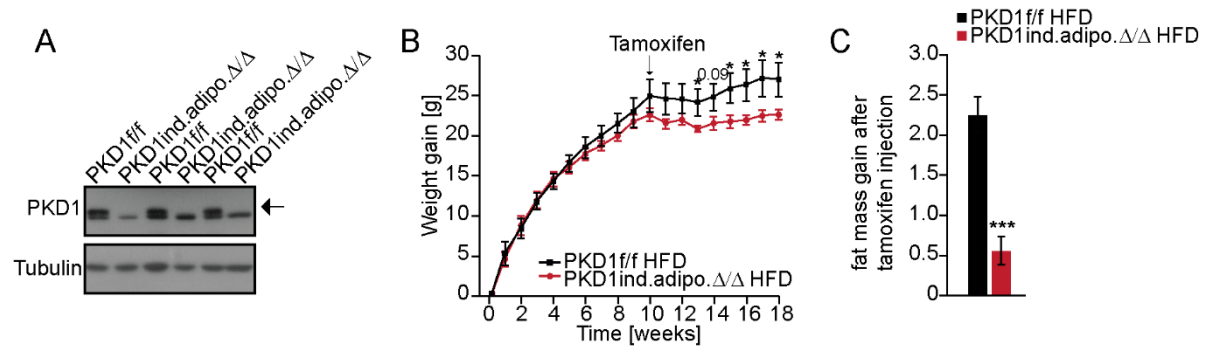


**Figure 71. Inactivation of PKD1 in obese mice prevents further body weight gain.** (A) WB analysis using an antibody against PKD1 in lysates of sWAT derived from PKD1ind.adipoΔ/Δ mice in which PKD1 deletion was induced upon injection of 100 mg/kg Tamoxifen for 5 consecutive days. (B) Body weight evolution was monitored every other week over 18 weeks in control and PKD1ind.adipoΔ/Δ mice fed HFD. (C) Fat mass gain after tamoxifen injection in control and PKD1ind.adipoΔ/Δ mice fed HFD for 22 weeks. Data are presented as mean ± SEM (n=9-10/genotype). (B,C) Unpaired, two-tailed Student's t-test. For all data, \*p<0.05 and \*\*\*p<0.001. *Protein kinase D* (PKD); *inducible* (ind.); *adiponectin* (adipo.); *flox/flox* (f/f); *high-fat diet* (HFD). (Löffler *et al.*, 2018)<sup>219</sup>

It was further assessed in which way metabolic parameters are affected in these mice. In line with the previous findings, deletion of PKD1 in obese mice further resulted in an enhanced energy expenditure (Figure 72BA) without affecting their activity or food intake (Figure 72B,C). These results indicate that inactivation of PKD1 even in already obese mice prevents mice from further body weight gain due to an increased energy dissipation.

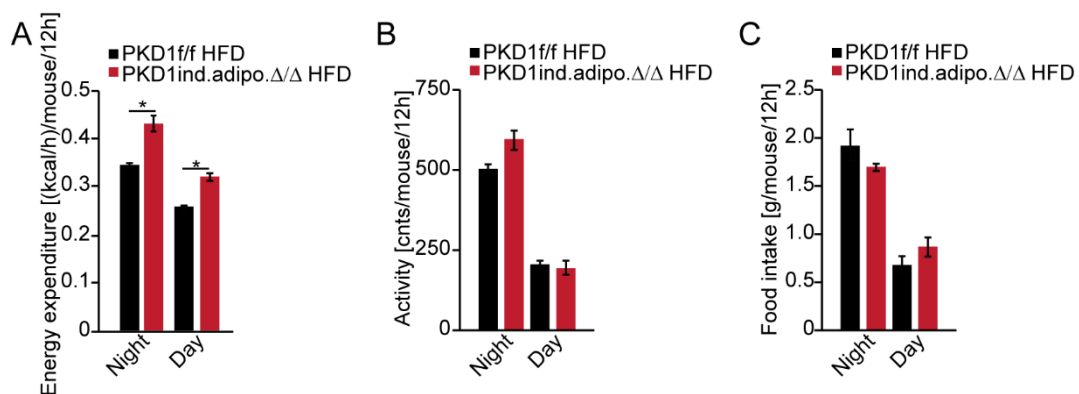


**Figure 72. PKD1 deletion in obese mice increases energy expenditure.** (A) Energy expenditure, (B) activity, and (C) food intake of PKD1ind.adipoΔ/Δ mice and their littermates, which were measured in a metabolic cage for 1 week after 18 weeks of HFD feeding. Data are presented as mean ± SEM (n=9-10/genotype). Unpaired, two-tailed Student's t-test. For all data, \*p<0.05. *Protein kinase D* (PKD); *inducible* (ind.); *adiponectin* (adipo.); *flox/flox* (f/f); *high-fat diet* (HFD). (Löffler *et al.*, 2018)<sup>219</sup>

## RESULTS

Finally, absence of PKD1 in adipocytes of obese mice presented improved glucose tolerance (Figure 73), suggesting that these mice are protected from the development of T2D upon induced deletion of PKD1 in the obese state.

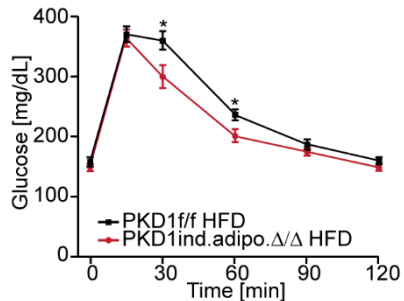


**Figure 73. Inactivation of PKD1 in obese mice protects against development of diabetes.** Glucose tolerance test was performed in PKD1ind.adipo $\Delta/\Delta$  and control mice after 17 weeks of HFD by intraperitoneal injection of glucose (1 g/kg BW) after 4 h fasting. Glucose levels in the blood were measured in the fasting state and at 15, 30, 60, 90, and 120 minutes after injection. For all data, n=9-10/genotype. Data are presented as mean  $\pm$  SEM. Unpaired, two-tailed Student's t-test. For all data, \*p<0.05. *Protein kinase D* (PKD); *inducible* (ind.); *adiponectin* (adipo.); *flox/flox* (f/f); *high-fat diet* (HFD). (Löffler *et al.*, 2018)<sup>219</sup>

In conclusion, the results of this thesis demonstrate that deletion of PKD1 induces the transition of white into beige adipocytes mainly in an AMPK-dependent manner. This results in an increased whole-body energy expenditure and protects against diet-induced obesity, development of T2D as well as liver steatosis (Figure 74). Therefore, PKD1 could be a new therapeutic target in the treatment of obesity.

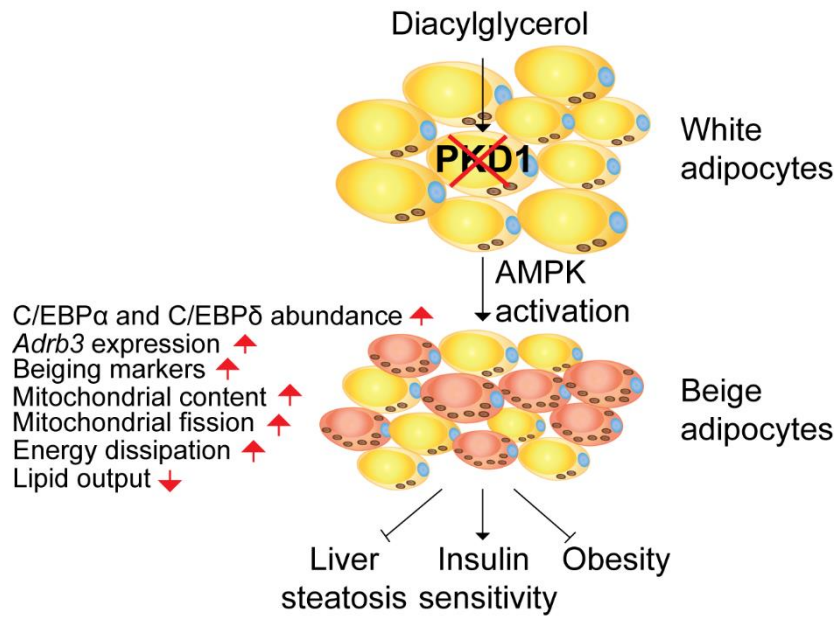


**Figure 74. Loss of PKD1 promotes AMPK activity, mitochondrial function and beiging of white adipocytes.** Deletion of PKD1 promotes beiging in white adipose tissue through activation of AMPK and subsequent induction of mitochondrial fragmentation and content, as well as expression of thermogenic markers. Expression of thermogenic genes in PKD1-deficient adipocytes is mediated by C/EBP- $\alpha$  and C/EBP- $\delta$  driven *Adrb3* expression, which increases sensitivity of cells to  $\beta$ -agonists. This results in an elevated whole-body energy expenditure and decreased lipid accumulation, which further protects against the development of diet-induced obesity, development of T2D as well as liver steatosis. *Protein kinase D* (PKD); *AMP-activated protein kinase* (AMPK); *CCAAT/enhancer-binding protein* (C/EBP);  $\beta 3$  *adrenergic receptor* (ADRB3). (Löffler *et al.*, 2018)<sup>219</sup>



## 4 DISSCUSSION

Adipocytes fulfil a pivotal function in the regulation of the metabolic homeostasis, as they have the ability to adapt quickly to alterations in energy demand by releasing or storing nutrients<sup>13</sup>. Due to the life style and dietary habits in the western society, the trend is shifted to an increased fat mass to store excess nutrients. This abnormal and excessive lipid accumulation in white adipocytes are hallmarks of obesity and associated with life threatening complications, such as T2D, cancer, and cardiovascular diseases. Its epidemic rate has been increasing tremendously over the last three decades<sup>73</sup>.

Over the past years, major focus was put on different strategies to increase energy consumption, since obesity arises due to an imbalance in the energy homeostasis. Importantly, formation of metabolically active beige adipocytes within the white adipose tissue is one way to protect individuals from obesity<sup>17</sup>.

Adiposity-related metabolic overload results in the accumulation of different species of lipids, including DAG in multiple tissues<sup>118</sup>. The impact of DAG-evoked signaling on adipocyte function are still poorly characterized. PKD1 is one of the kinases activated by DAG and PKCs<sup>133</sup>. PKD1-mediated signaling emerges as a master regulator of nutrient and energy homeostasis in health and disease<sup>133</sup>. It has been shown before to play a central role in the regulation of insulin secretion and survival of pancreatic  $\beta$  cells<sup>156</sup>. Its expression was found to be even higher in all adipose tissue depots (see Figure 12). But up to now, the physiological role of PKD1 in adipose tissue and its role in the relevant human diseases remains elusive.

Therefore, the aim of this study was to investigate the role of PKD1 in the regulation of adipose tissue function under physiological and pathophysiological conditions. The results in this thesis reveal that PKD1 expressed in adipocytes is involved in the regulation of the whole-body energy homeostasis, opening new insights into possible mechanisms how to increase energy dissipation in order to develop new anti-obesity therapeutics.

#### 4.1 PKD1 activation through DAG and extracellular purines

PKD1 is classically activated upon ligand binding to a GPCR, leading to the activation of DAG and recruitment of PKD1 to the plasma membrane, where it is phosphorylated by PKC<sup>163</sup>. Indeed, activation of PKD1 upon DAG treatment occurred in differentiated and undifferentiated 3T3-L1 cells (see Figure 14) suggesting that any signaling pathway involving DAG, and possibly DAG itself, also serves as a potent PKD activator especially in the context of increased DAG accumulation during obesity. Nevertheless, *in vivo* no difference in DAG content was observed in fat tissues of HFD- or ND-fed mice (see Figure 40). Since DAG can be very rapidly metabolized<sup>248</sup>, the measurement of DAG content in this study might not be the most suitable, as it cannot be seen if the tissues also convert the same amount of DAG upon different diets. Instead of only measuring the steady-state concentrations of DAG, one could analyze the DAG turnover using isotopic labelling or flux-measurements. Furthermore, the total amount of the four most abundant DAG classes was measured in the entire adipose tissue. Studies revealed that membrane and especially the cytosolic DAG is responsible for induction of muscle insulin resistance in humans<sup>249</sup>. Therefore, it might also be necessary to do cell fractionation in order to measure DAG content depending on the cellular localization. Another possible explanation for this could be the fact that DAG is not the only driving upstream factor regulating PKD activity during excessive lipid accumulation in adipocytes. Therefore, the direct impact of DAG-signaling on PKD1 activation and further upstream targets still needs to be studied in more detail. Ligand binding to purinergic receptors have been shown to result in increased DAG levels<sup>220</sup>. In this thesis, it was shown that PKD1 is specifically activated through purinergic stimulation upon treatment with extracellular ATP and ADP in white adipocytes (see Figure 13). Indeed, a previous study confirmed that potent stimulation of purinergic receptors results in activation of PKD in astrocytes<sup>218</sup>. In addition, several studies have implicated the role of purinergic receptor stimulation in the regulation of lipogenesis, lipolysis, and adipokine secretion<sup>215-217</sup>. Nevertheless, these studies are often contradicting each other. Therefore, the role of PKD1 in the purinergic-mediated signaling in adipocytes requires further investigation. Moreover, specific purinergic receptors responsible for PKD1 activation need to be identified and further insights into the mechanism by which DAG and extracellular purines might activate PKD1 in adipocytes is required, including the potential role of PKC in this process.

On the other hand, brown and white adipocytes do not seem to follow the same upstream mechanism regarding the activation of PKD1. DAG and purinergic stimulation occur to be specific PKD1 activators in white adipocytes (see Figure 13, Figure 14). This process seems to be less specific in brown adipocytes, since every endocrine factor tested had an effect on PKD1 activation in brown adipocytes (see Figure 15). Possible explanations for this are the different anatomical locations, morphological structures, functions, and regulations of both tissues, as well as the different original precursor cells from which both tissues derive<sup>250,251</sup>. Therefore, it is quite likely that also upstream stimuli differ between both tissues, leading to a different mechanism of PKD1 activation and function.

### **4.2 The impact of PKD1 on lipolysis, lipogenesis, OCR, and mitochondrial fragmentation**

DAG is synthesized in the process of lipogenesis as an intermediate product and its potential to activate PKD1 was shown<sup>118,166,252</sup>. Therefore, one aim of this study was to investigate the role of PKD1 during lipid accumulation in adipocytes. Inhibition of PKD1, using either pharmacological or genetic means, was effectively reducing TG formation in 3T3-L1 cells and SVC (see Figure 16, Figure 18, Figure 19), whereas overexpression of a constitutive active form of PKD1 led to the opposite effect (see Figure 18). Excessive lipid accumulation is associated with the development of obesity and further insulin resistance<sup>3</sup>. DAG was previously shown to stimulate PKC activity subsequently impairing insulin signaling by inhibitory serine phosphorylation of IRS in muscle<sup>253,254</sup>. It needs to be assessed, if DAG is the driving force behind the PKD1 driven lipid accumulation.

PKD1 dependent changes in TG formation might be explained in several ways. Activation of PPAR $\gamma$ , the major transcription factor, for instance was shown to promote FFA influx into adipose tissue<sup>255</sup>. On the other hand, deletion of Perlipin, a lipid droplet structure protein, promotes a lean phenotype due to smaller adipocytes<sup>256,257</sup>. However, PKD1 deletion did neither affect PPAR $\gamma$  or Perlipin nor any of the lipolytic proteins like HSL or ATGL (see Figure 20). In cells expressing PKD1ca, PPAR $\gamma$  was upregulated, whereas HSL and ATGL were downregulated (see Figure 20). Differentiated 3T3-L1 cells expressing PKD1ca even demonstrated and increased TG accumulation, thus

## DISCUSSION

---

the reduced protein levels of HSL and ATGL cannot be the appropriate explanation for this, since ATGL or HSL deletion in mice rather reduced fat accumulation<sup>42-44</sup>. Furthermore, reduction of ATGL and HSL in PKD1ca expressing cells might lead to a lower lipolysis rate. However, lipolysis, assessed by the release of FFAs and glycerol, was not changed regardless of the PKD1 expression (see Figure 21), indicating that neither differentiation nor lipolysis are affected by the expression of PKD1. Conversely, lipogenesis rate was reduced in cells lacking PKD1 and increased upon overexpressing PKD1ca (see Figure 22). PKD1 deletion did not only result in reduced rate of lipogenesis, but also in less TG accumulation in PKD1-deficient adipocytes (see Figure 16, Figure 18, Figure 19). Circulating levels of FFAs are reduced due to an increased catabolism preventing adipocyte hypertrophy and lipid accumulation<sup>258</sup>. Indeed, the results shown in this thesis also demonstrate an increased energy expenditure (Figure 23, Figure 24) as well as an increased mitochondrial content (Figure 24) in cells lacking PKD1, which both indicate a switch to a rather beige phenotype of these cells. A beige phenotype indicates a switch of the white adipocytes into brown-like adipocytes with an increased number of mitochondria and thermogenic gene expression, such as UCP1<sup>66</sup>. Both were shown to be upregulated in PKD1-deficient adipocytes (see Figure 24, Figure 57, Figure 54, Figure 61). UCP is used for FAO and therefore plays an important role in energy expenditure and lowering mitochondrial membrane potential in order to dissipate metabolic energy as heat (thermogenesis)<sup>140</sup>.

Whether in this study the increased energy expenditure is caused due to an increased  $\beta$ -oxidation, still needs to be tested by measuring FAO of the cells.

Since adipocytes store TGs in their lipid droplets, the lipogenic and lipolytic rate within the adipocytes are associated with changes in the volume of the lipid droplets. For instance, FFAs released during lipolysis could be directly used for other metabolic pathways, such as re-esterification, mitochondrial oxidation, or mitochondrial uncoupling. A study revealed that treatment of 3T3-L1 cells with palmitoleic acid boosts mitochondrial bioenergetics in combination with an increased lipolysis rate and FA re-esterification leading to an enhanced energy metabolism in the adipocytes due to the stimulation of the TG/FFA futile cycle<sup>259</sup>. Therefore, another possible mechanism, which requires further testing, is the effect of PKD1 on the *in situ* re-esterification of FFAs and the activation of a futile cycle of lipogenesis/lipolysis consuming ATP further

leading to increased oxygen consumption. Since lipolysis was not changed in PKD1-deficient adipocytes and lipogenesis rate was reduced (see Figure 21, Figure 22), this mechanism most likely cannot be the reason for the increased energy expenditure in this study. Nevertheless, FFA levels were reduced in the circulation of mice lacking PKD1 (see Figure 65) and therefore, this possibility needs to be tested.

In addition, these data indicate an alternative way to promote uncoupling respiration by regulating mitochondrial dynamics and content in adipocytes. Mitochondria, as the major site of ATP production, FAO, and oxygen consumption play an important role in the regulation of energy expenditure<sup>260,261</sup>. A recent study revealed that mitochondrial fission in brown adipocytes is increased upon  $\beta$ -adrenergic stimulation leading to thermogenic activation and enhanced oxygen consumption<sup>67</sup>. Moreover, deletion of the PPAR $\gamma$  target Bnip3 was shown to support mitochondrial fusion in white adipocytes which suppresses energy dissipation<sup>129</sup>. Indeed, ablation of PKD1 increases mitochondrial fragmentation, which positively correlates with the enhanced energy expenditure in adipocytes (see Figure 23, Figure 24, Figure 27). Thus, PKD1 displays the first identified signaling module (kinase) repressing mitochondrial fragmentation to reduce energy dissipation in adipocytes. Furthermore, not only mitochondrial dynamics were changed, but also the mitochondrial content was increased in differentiated SVF lacking PKD1 (see Figure 24), as well as in sWAT of PKD1-deficient mice (see Figure 57). To test whether mitochondrial bioenergetics are changed upon PKD1 deletion, citrate synthase activity, as well as ATP content should be measured. In addition, electron microscopy could reveal changes in mitochondrial morphology and size. Further, changes in protein content of mitochondrial oxidative phosphorylation complexes should be measured, in order to fully analyze mitochondrial activity and its impact on the increased energy expenditure.

### **4.3 PKD1 regulates adipose tissue function in an AMPK-dependent manner**

Importantly, the data shown in this study link PKD1 signaling to AMPK, a key regulator of adipocyte function. A previous study displayed that PKD1 inhibits AMPK activity by phosphorylating the AMPK $\alpha$  subunit in muscle cells *in vitro*<sup>185</sup>. In this thesis, PKD1 also suppressed AMPK activity in adipocytes by affecting phosphorylation of AMPK and its

downstream target ACC (see Figure 32) as well as overall AMPK kinase activity (see Figure 33, Figure 34). Furthermore, deletion of PKD1 in mice resulted in an increased AMPK signaling in sWAT derived from HFD- or ND-fed mice (Figure 45). However, unlike other markers of AMPK activation, T172 phosphorylation of the AMPK $\alpha$  subunit was not clearly enhanced in PKD1-deficient adipose tissue of mice fed HFD for 24 weeks (see Figure 45), suggesting that prolonged HFD feeding induces additional signaling pathways partially masking the effect of PKD1 deletion. AMPK supports mitochondrial biogenesis and the expression of genes, which are involved in energy dissipation of adipocytes as well as genes suppressing lipogenesis<sup>182,191,192</sup>. Consistently, PKD1 drives lipogenesis, reduces mitochondrial content, and lowers energy dissipation in adipocytes *in vitro* (see Figure 22, Figure 23, Figure 24) and *in vivo* (see Figure 43, Figure 50, Figure 57). Similarly to the deletion of PKD1, a number of studies revealed that elevation of AMPK signaling in adipocytes ameliorates diet-induced obesity, insulin resistance and hepatic steatosis by enhancing energy expenditure of animals<sup>191,262,263</sup>. Indeed, silencing of AMPK or pharmacological activation of the kinase normalized the effects on TG accumulation, lipogenesis, as well as OCR in PKD1 modified adipocytes to the level observed in control cells (see Figure 36, Figure 37, Figure 38). Additionally, AMPK further promotes mitochondrial fragmentation in other cell types<sup>264</sup>, while the results in this study demonstrate that PKD1 suppresses this process (see Figure 39). Moreover, manipulation of AMPK activity fully reversed the effects of PKD1ca on mitochondrial aggregation (see Figure 39).

Numerous studies aimed to define the impact of AMPK on the regulation of lipolysis. Both, pro- and anti-lipolytic effects of AMPK have been described<sup>182,265</sup>. A genetic study revealed that  $\beta$ -adrenergic-induced lipolysis in mice is not affected by the loss of AMPK activity in adipocytes<sup>192</sup>. However, during cancer-associated cachexia, ablation of AMPK activity enhances both lipolysis and lipogenesis resulting in increased energy dissipation in adipocytes<sup>266</sup>. The results in this thesis suggest that PKD1 neither affects basal nor  $\beta$ -adrenergic-induced lipolysis in isolated adipocytes (see Figure 21). Also, the levels of FFAs and glycerol of fasted young-adult mice (8 weeks old) lacking PKD1 were not altered (see Figure 47). However, it is shown that FFA levels were reduced in PKD1-deficient mice (see Figure 65), which is probably caused by the reduced adipose tissue content.

## DISCUSSION

---

AMPK suppresses lipogenesis by phosphorylating and inhibiting the action of ACC<sup>182</sup>. Indeed, the ACC phosphorylation of S79 was increased in the absence of PKD1, but the expression of genes involved in lipid synthesis was not changed (see Figure 45, Figure 55). Activation of AMPK in multiple cell lines induces autophagy in a mTORC1-dependent and independent manner<sup>267</sup>. In line with these data, PKD1 deletion increases autophagy marker-LC3 cleavage (see Figure 45). Beige to white adipocyte transition is promoted through the induction of autophagy<sup>22</sup>. Moreover, deletion of ATG7, which is required to induce autophagy, results in a beige-like phenotype<sup>268,269</sup>. However, activation of AMPK in adipocytes induces energy expenditure and is protective against obesity<sup>191,262,263</sup>. Therefore, the data in this thesis provide evidence that AMPK promotes energy expenditure in adipocytes utilizing autophagy-independent mechanisms.

Furthermore, the data in this study indicate that ADRB3 expression is regulated through PKD1 by targeting C/EBP- $\alpha$  and C/EBP- $\delta$  in an AMPK-dependent manner. ADRB3 was shown to regulate lipolysis and non-shivering thermogenesis<sup>17,198-200</sup> and C/EBP- $\alpha$  was demonstrated to regulate ADRB3 during adipogenesis<sup>201</sup>. In this study, adipose tissue as well as differentiated SVC of PKD1-deficient mice show enhanced expression of ADRB3 (see Figure 54, Figure 61). Indeed, no changes could be observed in the expression of thermogenic genes such as UCP1 in PKD1-deficient SVC under normal culturing conditions. Only upon  $\beta$ -adrenergic stimulation UCP1 was enhanced in cells lacking PKD1 (see Figure 61). Furthermore, receptor abundance on the surface was increased in adipocytes lacking PKD1 (see Figure 61). All these data suggest that induction of UCP1 expression by PKD1 deletion requires the presence of the ligand for  $\beta$ 3-adrenergic receptor. Moreover, UCP1 expression in adipocytes was shown to be reduced upon deletion of C/EBP- $\alpha$  and C/EBP- $\delta$ <sup>202</sup>. Here, it is shown that deletion of C/EBP- $\alpha$  and C/EBP- $\delta$  in PKD1-deficient cells reduce ADRB3 expression to the same level as previously seen in control cells (see Figure 63). In addition, C/EBP- $\alpha$  and C/EBP- $\delta$  were both upregulated in PKD1-deficient cells and downregulated in cells expressing PKD1ca (see Figure 62, Figure 63). Moreover, protein content of C/EBP- $\alpha$  and C/EBP- $\delta$  was not just altered between cells expressing PKD1ca and controls, but even increased upon stimulation with AICAR (see Figure 63). Taken together, all the data suggest that C/EBP- $\alpha$  and C/EBP- $\delta$  are regulated

## DISCUSSION

---

through PKD1 in an AMPK-dependent manner and further influence ADRB3 expression to control the thermogenic programming.

Furthermore, Rictor, part of the mTORC2 complex and shown to play an important role in the lipid metabolism<sup>220-225</sup>, was identified as a potential interaction partner of PKD1 (see Figure 29, Table 1). In addition, Akt phosphorylation on S473, which is a downstream target of the mTORC2 complex<sup>241</sup>, was increased upon chemical inactivation of PKD, using a PKD inhibitor (see Figure 30), and downregulated in cells expressing PKD1ca (see Figure 31). Indeed, several studies linked mTORC1 and mTORC2 complex to the regulation of adipose tissue function<sup>226-231,237-239</sup>. One study showed that mice with a specific deletion of Rictor in adipose tissue are not able to maintain their core body temperature and showed a decreased oxygen consumption<sup>228</sup>. This is consistent with the fact that PKD1 reduced mTORC2 downstream signaling (see Figure 31) leading to a decreased oxygen consumption observed in differentiated 3T3-L1 cells expressing PKD1ca (see Figure 23). Moreover, mTORC is involved in the insulin signaling. Dysfunction of mTORC2 signaling has been implicated in the development of insulin resistance and diabetes<sup>270</sup>. In this study phosphorylation of Akt at S473 is downregulated in cells expressing PKD1ca (see Figure 31) and upregulated upon inhibition of PKD or PKD1 deletion in adipocytes (see Figure 30, Figure 67). In addition, insulin sensitivity was improved in mice lacking PKD1 (see Figure 66). Therefore, PKD1 dependent regulation of mTORC2 signaling might define insulin sensitivity of adipocytes. On the other hand, according to the literature, increased activity of mTORC2 is also upregulating the mTORC1 signaling pathway by inhibition of *tuberous sclerosis complex* (TSC) 1/2 through Akt<sup>227</sup>. This is not the case in this study, since the downstream target of mTORC1, S6K, are upregulated in PKD1ca cells, and even mTOR phosphorylation at S2448, which binds to raptor and rictor<sup>271</sup>, are upregulated in these cells (see Figure 30). The fact that mTORC1 complex was more active in PKD1ca cells is in line with a study, showing that deletion of raptor increases energy expenditure and protects mice from obesity<sup>238</sup>. Furthermore, over-activation of mTORC1 was shown to promote adipogenesis<sup>272</sup>. A possible explanation for this might be the fact that AMPK regulates mTORC activity, which independently of PKD1 leads to an activation of the mTORC1 complex. AMPK is known to inhibit mTORC1 via TSC<sup>273</sup>. This is in agreement with the data observed in this study, showing that PKD1 inhibits AMPK signaling, leading to an increased activity of mTORC. Nevertheless,



detailed regulation of mTORC2 through PKD1 and mTORC1 through AMPK is still unclear and needs further investigation.

### **4.4 PKD1 deletion induces beiging of white adipocytes and increases energy expenditure**

In this thesis, PKD1-induced browning of sWAT in mice increases energy expenditure and protects against diet-induced obesity. Therefore, PKD1 expressed in adipocytes plays a crucial role in the whole-body energy homeostasis, since PKD1<sup>adipo.Δ/Δ</sup> mice were resistant to diet-induced obesity (see Figure 43). Mice fed HFD over 24 weeks present an increase in energy expenditure, a reduced content of adipose tissue, as well as smaller adipocytes (see Figure 50, Figure 43, Figure 51). Moreover, sWAT depots contained more mitochondria and displayed enhanced expression of genes responsible for energy dissipation (see Figure 57, Figure 54, Figure 55). Since mice lacking UCP1 can survive cold temperatures upon gradual acclimatisation<sup>70,274</sup> and  $\beta$ -adrenergic stimulation showed a similar thermogenic response in UCP1 knockout and wild-type mice<sup>275</sup>, this implies the existence of UCP1 independent thermogenic mechanisms. Indeed, one study showed that creatine kinase increases energy metabolism of adipocytes, independently of UCP1<sup>17</sup>. Interestingly, data presented here revealed an increased expression of typical thermogenic genes (e.g. *Adrb3*, *Ucp1*, *Pgc-1 $\alpha$* , and *Ucp3*) but also genes involved in the creatine-driven substrate cycle (*Ckm*, *Ckmt2*) (see Figure 54, Figure 55, Figure 26), suggesting that PKD1 represses energy dissipation in adipocytes using various complementary mechanisms. Although, no clear correlation between the appearance of multilocular cells within sWAT and the absence of PKD1 could be shown (see Figure 51), UCP1 levels were clearly elevated in adipose tissue lacking PKD1 (see Figure 57). Of note, several other mouse models observed an increased UCP1 abundance also in unilocular adipocytes<sup>276-278</sup>. Although genes involved in the creatin-driven cycle were increased (see Figure 55), no formation of ectopic myofibers was observed (see Figure 59).

Keeping mice at room temperature induced mild cold stress in these mice, which stimulated the energy expenditure in order to maintain the core body temperature, whilst for housing at thermoneutrality no extra energy was required<sup>246</sup>. Furthermore, it was shown that thermoneutrality negatively regulated the thermogenic program

## DISCUSSION

---

including formation of beige adipocytes<sup>246</sup>. Indeed, in this study it is shown that the effects on energy metabolism and body weight gain are abrogated when mice were housed at 30°C (see Figure 60). This shows that PKD1 promotes beiging of white adipocytes and its effect is abrogated upon thermoneutrality. Furthermore, adipose tissue is highly innervated by the sympathetic nervous system and  $\beta$ -adrenergic stimulation of the cells is also known to increase mitochondrial content, expression of the thermogenic genes, and further energy dissipation<sup>279-281</sup>. Thus, an increased innervation of the ADRB3 during housing at room temperature might increase the beiging phenotype due to an upregulated expression of the receptor in PKD1-depleted mice. Whether stimulation of the ADRB3 is abrogated during thermoneutrality or if the receptor expression itself is reduced still needs to be tested.

In addition, the ADRB3 is nearly exclusively expressed in white and brown adipocytes<sup>197,199,282,283</sup> and is important for energy storage and energy expenditure, respectively. Indeed, in isolated adipocytes lacking PKD1 increased levels of *Adrb3* were measured, whereas *Ucp1* gene expression was not changed in unstimulated conditions (see Figure 61, Figure 24). Only muscle related genes were highly upregulated already at basal conditions (see Figure 26). These data suggest that inducing UCP1 expression by deleting PKD1 requires the presence of the ligand for  $\beta$ 3-adrenergic receptor, as  $\beta$ -agonist stimulation of cultured adipocytes lead to an increased expression of *Ucp1* in the absence of PKD1 (see Figure 61). However, enhanced expression of thermogenic genes could not be demonstrated in BAT of PKD1adipo. $\Delta/\Delta$  mice (see Figure 55). Moreover, AMPK-dependent signaling was not altered in BAT of PKD1-deficient mice (see Figure 46). This result is in line with the fact that isolated brown adipocytes lacking PKD1 did not show any changes in basal respiration and energy dissipation (see Figure 25). Taken together, these data suggest that PKD1 deletion supports beiging in WAT without affecting brown adipocytes. One possible explanation for this, could be the different origins of the two fat depots and their functional roles<sup>250,251</sup>, which can explain the discrepancies between PKD1 effects on energy metabolism and thermogenic gene expression in white, but not in brown adipocytes. Furthermore, one study revealed an increase oxygen consumption upon  $\beta$ -adrenergic stimulation in white and brown adipocytes with transgenic re-expression of adrenergic receptors, whilst stimulation of re-expressed adrenergic receptors in BAT alone only had minor effect on energy metabolism, suggesting that the presence of

## DISCUSSION

---

adrenergic receptors in white adipose tissue is required<sup>200</sup>. This could also explain the fact that thermogenic gene expression and energy expenditure was only increased in white adipocytes through the PKD1 mediated regulation of ADRB3. Another study revealed a close relationship of smooth muscle-like cells and beige fat cells but not classical brown adipocytes<sup>284</sup>, which could explain the differential expression of genes involved in the creatine-driven cycle.

Furthermore, the thermogenic gene expression pattern not only varies between white and brown adipocytes, but is also different between white adipose tissue depots. Whilst a number of thermogenic genes and genes involved in the creatine kinase metabolism are highly upregulated in sWAT of PKD1-deficient mice, only a few of these genes are upregulated in gWAT of mice lacking PKD1 (see Figure 53, Figure 54, Figure 55). This could be explained due to the fact that sWAT has been shown to “brown” more easily upon cold or  $\beta$ -adrenergic stimulation<sup>66,285</sup>. Browning also occurred in gWAT<sup>286</sup>, but this phenomenon is much less common, suggesting an increased beiging in sWAT. Furthermore, one study revealed that beiging markers, such as UCP1 or PRDM16, are generally less expressed in gWAT compared to sWAT<sup>287</sup>. To analyze the exact differences of gWAT and sWAT regarding the beiging gene expression pattern, influences on energy expenditure of both tissues should be measured using fat tissue explants or isolated adipocytes. In this way, one could identify, which of the tissues is contributing more to the increased energy expenditure in mice lacking PKD1.

In addition, ADRB2 was downregulated in human visceral fat compared to subcutaneous fat<sup>288</sup>, which means that expression of other adrenergic receptors could also be downregulated in visceral fat, leading to a reduced expression of thermogenic genes in this tissue. In this case, expression of ADRB3 should be compared within both white fat tissue depots, as well as in BAT, to see if there is a differential expression in these tissues. At the same time, differences between PKD1-depleted and control mice should be assessed in BAT and gWAT. Furthermore, it could be measured whether  $\beta$ -adrenergic stimulation also increases UCP1 in PKD1-deficient SVC isolated from BAT or gWAT.

#### 4.5 The role of PKD1 in adipocytes under physiological and pathophysiological conditions

The final aim of this study was to identify the role of PKD1 under physiological and pathophysiological conditions. First, it was shown that levels and activity of this kinase are induced in adipose tissue upon feeding (see Figure 41). Since PKD1 is induced upon feeding and it regulates adipose tissue function in an AMPK dependent manner, it is not surprising that phosphorylation of AMPK and downstream target ACC are only changed upon refeeding in mice lacking PKD1 (see Figure 48). According to the data in this study, PKD1 is downregulated upon fasting, suggesting that the inhibitory effects of PKD1 on AMPK signaling are abolished in wild type mice during fasting. This shows an important role of PKD1 in the fasting and refeeding response of mice and can go along with the data showing that PKD1 is activated by DAG, accumulating during the process of lipogenesis. It further suggests that PKD1 can drive adiposity *in vivo*.

Consistently with the fact that PKD1<sup>adipo.Δ/Δ</sup> mice presented decreased adipose tissue content (see Figure 43), blood FFA levels were observed to be markedly lower in HFD-fed mice lacking PKD1 in adipocytes compared to control animals. PKD1<sup>adipo.Δ/Δ</sup> mice fed ND showed moderately reduced FFA levels in the circulation ( $p=0.13$ ) (see Figure 65). Importantly, deletion of PKD1 did not alter levels of TGs and glycerol, another lipolytic product (see Figure 65). Lipolysis rate *in vitro* was not changed (see Figure 21). Nevertheless, reduced FFA levels were observed in mice lacking PKD1, especially when fed HFD (see Figure 65). The reduced fat mass observed during HFD in mice lacking PKD1 (see Figure 43) could be one possible explanation. Furthermore, mice lacking PKD1 also showed increased energy expenditure (see Figure 50), suggesting that FFA levels in the circulation are directly consumed by increased  $\beta$ -oxidation due to the increased energy demand<sup>289</sup>, leading to less plasma FFA levels in mice lacking PKD1. Increased FFA levels in the circulation occur upon obesity, due to inflammatory processes leading to increased release of FFAs<sup>290</sup>. This could explain that FFAs are only highly reduced in PKD1-deficient mice upon HFD, when mice are protected from obesity and demonstrate much smaller adipocyte size (see Figure 43, Figure 51), leading to less FFA release due to reduced inflammation. Whether mice lacking PKD1 have less inflammation in their adipose tissue needs to be further investigated. Moreover, increased plasma FFA

## DISCUSSION

---

concentrations led to intracellular accumulation of several metabolites of the esterification pathway including DAG in muscle and liver<sup>291</sup>. As mentioned before, DAG activates PKC leading to insulin resistance by inhibitory phosphorylation of IRS<sup>253</sup>. Indeed, as predicted by lower FFA levels, mice lacking PKD1 presented improved insulin sensitivity and glucose tolerance when fed HFD (see Figure 66), suggesting that expression of PKD1 in adipocytes promotes insulin resistance. Only minor effects of PKD1 deletion were observed in mice fed ND (see Figure 66). Importantly, improved glucose tolerance in PKD1adipo. $\Delta/\Delta$  mice was specifically caused by better peripheral insulin sensitivity, since insulin levels were not altered in the absence of PKD1 (see Figure 67). Consistently, activation of Akt kinase, a key signaling molecule in the insulin pathway, was markedly enhanced in adipocytes depleted of PKD1 and reduced in adipocytes with elevated PKD1-dependent signaling (see Figure 67). However, PKD1 in cardiomyocytes rather promotes insulin sensitivity<sup>292</sup>. In pancreatic  $\beta$  cells PKD1 was also shown to promote insulin secretion<sup>156</sup>, indicating that the impact of PKD1 on insulin signaling is highly dependent on the cellular context. Alternatively, improved insulin sensitivity in the absence of PKD1 in adipocytes might be secondary to the reduced lipid accumulation.

Similarly to the ablation of PKD1, promoting AMPK signaling in adipocytes by pharmacological interventions or genetic manipulations ameliorates diet-induced obesity, insulin resistance and hepatic steatosis by enhancing energy expenditure of animals<sup>191,262,263</sup>. In fact, PKD1 expression in adipocytes promoted insulin resistance and PKD1-deficient mice presented improved insulin sensitivity, glucose tolerance, and were protected against liver steatosis when fed HFD (see Figure 66, Figure 67, Figure 68). However, PKD1 in cardiomyocytes was shown to rather increase insulin sensitivity<sup>292</sup>, suggesting that the impact of PKD1 on insulin signalling depends on the cellular context. Alternatively, improved insulin sensitivity upon PKD1 deletion in adipocytes might be secondary due to less lipid accumulation. In addition, mice lacking PKD1 have reduced adipocyte size when fed HFD (see Figure 51) and are protected against diet-induced obesity (see Figure 43), which can be explained due to the increase in energy expenditure and thermogenic gene expression (see Figure 50, Figure 55). On the other hand, insulin sensitivity was only mildly improved in PKD1-deficient mice fed ND, whereas body weight gain was not changed at all (Figure 43, Figure 66). Furthermore, no changes in adipocyte size were observed (see Figure 52)

## DISCUSSION

---

and only mild reduction in overall fat mass was seen (see Figure 44). There is a small reduction in circulating FFAs (see Figure 65). Similarly, mice lacking PKD1 show some tendency to improved glucose tolerance and increased levels of thermogenic genes, as well as energy expenditure when fed ND, but the effects are very mild (see Figure 66, Figure 58, Figure 50). One possible explanation for the increased effects of the phenotype on HFD diet could be an increased lipogenic rate during obesity, which in turn forms DAG as an intermediate product activating PKD1. Further, purinergic signaling was shown to be increased during obesity due to chronic local inflammations<sup>293,294</sup>, increasing PKD1 activation upon HFD directly or indirectly by DAG, which was revealed to be enhanced upon stimulation of purinergic receptors<sup>220</sup>. Therefore, the effects are much more diminished during ND, when the overall lipogenic rate and chronic inflammation are lower. This possibility needs to be further analysed. A closer look into the obesity-induced inflammatory processes is necessary. Additionally, adipose tissue is highly challenged and remodeled upon HFD<sup>295</sup>, which could be another explanation for the more pronounced phenotype upon HFD feeding in mice due to the dietary induction.

Energy expenditure was increased in mice lacking PKD1 especially during HFD feeding and to a minor extent during ND, without affecting food intake or activity of these mice (see Figure 50, Figure 49). This could be explained due to the beige phenotype occurring in PKD1adipo. $\Delta/\Delta$  mice.

Besides, adipose tissue does not just store and release but it also actively regulates the whole body energy homeostasis by secreting multiple hormones, which regulate processes such as food intake (leptin) or peripheral insulin sensitivity (adiponectin and resistin), levels of these hormones was also checked<sup>46,280</sup>. Adiponectin and resistin were not altered between control and PKD1-deficient mice. However, upon ND feeding Adiponectin levels were increased compared to HFD-fed mice and a tendency towards increased levels could also be observed in HFD-fed mice lacking PKD1 (see Figure 63). This is consistent with the literature, showing reduced adiponectin levels the higher the state of obesity and insulin resistance and increased levels were observed upon weight loss<sup>59</sup>. Resistin, on the other hand has been demonstrated to be elevated upon obesity and insulin resistance in mice<sup>60</sup>, and therefore shows some tendency towards decreased levels upon ND feeding, as well as in PKD1adipo. $\Delta/\Delta$  mice fed HFD (see Figure 63). Leptin is secreted during food intake and suppresses appetite. In

## DISCUSSION

---

animals and humans with mutations in either leptin or the leptin receptor present increased appetite, are obese and insulin resistant<sup>58</sup>. Therefore, it has a primary role as an anti-obesity hormone, although high concentrations of leptin in the blood circulation are associated with obesity, which is due to the presence of leptin resistance similar to insulin resistance<sup>296,297</sup>. Of note, excessive energy intake and body fat deposition as a response to HFD revealed the acquisition of resistance to leptin<sup>298</sup>. It is also known that leptin expression and levels increase as the size of the adipose tissue TG stores increase<sup>299,300</sup>. Additionally, a strong positive correlation is observed between serum leptin levels and the amount of body fat and adipocyte leptin mRNA expression<sup>301,302</sup>. This could explain the reduced leptin levels observed in PKD1adipo.Δ/Δ mice when fed ND or HFD and when comparing both diets in general. The fact that on HFD reduction of leptin levels did not reach significance (p=0.18) (see Figure 63) could most probably be explained due to the high variations observed upon HFD feeding. Furthermore, since HFD also induces a mild state of obesity even in knock-out mice, a starting leptin resistance in these mice could be another explanation for the reduced leptin secretion. The reduced adipocyte mass and cell size in mice lacking PKD1 could also be possible explanations for the reduced leptin levels. Nevertheless, further investigations are needed to elucidate the potential function of PKD1 signaling in leptin production *in vivo*.

Besides, the protective role of PKD1 deletion against obesity and insulin resistance, it was shown that inducible deletion of PKD1 in mice with already established obesity attenuates the course of this disease, since body weight gain was stopped upon deletion and an increased energy expenditure occurred (see Figure 71, Figure 72). Moreover, improved glucose tolerance in these mice was observed (see Figure 73). Strikingly, this study also indicates that expression of PKD1 in human adipose tissue correlates with insulin sensitivity, seen by the correlation of PKD1 with insulin levels and HOMA-IR (see Figure 69, Table 2). Moreover, in agreement with the data obtained in rodents, it was presented that inhibition of PKD in human adipocytes increases energy dissipation and suppresses lipogenesis (see Figure 70), which rises evidences that the shown mechanisms are conserved in humans.

Taken together, these data provide evidence for the important role of PKD1 signaling in fat tissue and energy homeostasis *in vivo*. Thus, the development of precision medicine to ablate PKD1 specifically in adipocytes represents an attractive strategy to

## DISCUSSION

---

treat obesity and diabetes in the future. If the regulation of adipose tissue through PKD1 plays a substantial role also in the thermogenesis in humans, as the data in this thesis suggest, new possibilities to manipulate energy expenditure in obese patients with metabolic diseases by new drugs could be opened.



## 5 CLOSING REMARKS AND FUTURE PERSPECTIVES

Adipocytes are key regulators of metabolic homeostasis. Abnormal lipid accumulation within the white adipose tissue is a hallmark of obesity and leads to obesity-related disorders. Importantly, formation of beige adipocytes within the white adipose tissue is protective against obesity due to their higher metabolic activity<sup>17</sup>. Up to now, the physiological role of PKD1 in adipose tissue and relevant human diseases remained elusive. The findings summarized in this thesis shed new light on the mechanisms involved in the regulation of the PKD1 signaling cascade in adipose tissue. PKD1 expressed in adipocytes plays a crucial role in the whole-body energy homeostasis. It further promotes lipogenesis, inhibits mitochondrial fission, and OCR in adipocytes in an AMPK-dependent manner. *In vivo* deletion of PKD1 results in smaller adipocytes and increases energy expenditure. Moreover, sWAT depots contain higher numbers of mitochondria and show increased expression of genes responsible for the energy dissipation in these mice due to beiging of white adipocytes. Altogether, this is protective against diet-induced obesity and resulting complications, such as insulin resistance and NAFLD. Although caution is required, regarding the direct translation of the findings obtained in the mouse model lacking PKD1 to the human system, the data present good evidence that PKD1 is involved in the regulation of insulin sensitivity in humans. Thus, approaches to reduce PKD1 activity in adipocytes might be beneficial in the prevention of obesity and T2D. However, further studies are required to better characterize the mechanisms regulating PKD1 activity and to evaluate the suitability of the kinase as a pharmacological target. Notably, such modulation of PKD1 expression and activity may have important implications also during targeted overexpression of the kinase. Especially during cancer-associated cachexia upregulation of PKD1 activity could be beneficial to prevent weight loss.

## 6 REFERENCES

- 1 Frayn, K., Karpe, F., Fielding, B., Macdonald, I. & Coppack, S. Integrative physiology of human adipose tissue. *International journal of obesity* **27**, 875-888 (2003).
- 2 Cannon, B. & Nedergaard, J. Brown adipose tissue: function and physiological significance. *Physiological reviews* **84**, 277-359 (2004).
- 3 Rosen, E. D. & Spiegelman, B. M. What we talk about when we talk about fat. *Cell* **156**, 20-44 (2014).
- 4 Frontini, A. & Cinti, S. Distribution and development of brown adipocytes in the murine and human adipose organ. *Cell metabolism* **11**, 253-256 (2010).
- 5 Jonckheere, A. I., Smeitink, J. A. & Rodenburg, R. J. Mitochondrial ATP synthase: architecture, function and pathology. *Journal of inherited metabolic disease* **35**, 211-225 (2012).
- 6 Busiello, R. A., Savarese, S. & Lombardi, A. Mitochondrial uncoupling proteins and energy metabolism. *Frontiers in physiology* **6** (2015).
- 7 Huttunen, P., Hirvonen, J. & Kinnula, V. The occurrence of brown adipose tissue in outdoor workers. *European journal of applied physiology and occupational physiology* **46**, 339-345 (1981).
- 8 Virtanen, K. A. *et al.* Functional brown adipose tissue in healthy adults. *New England Journal of Medicine* **360**, 1518-1525 (2009).
- 9 Cypess, A. M. *et al.* Identification and importance of brown adipose tissue in adult humans. *New England Journal of Medicine* **360**, 1509-1517 (2009).
- 10 van Marken Lichtenbelt, W. D. *et al.* Cold-activated brown adipose tissue in healthy men. *New England Journal of Medicine* **360**, 1500-1508 (2009).
- 11 Lee, M.-J., Wu, Y. & Fried, S. K. Adipose tissue heterogeneity: implication of depot differences in adipose tissue for obesity complications. *Molecular aspects of medicine* **34**, 1-11 (2013).
- 12 Tran, T. T. & Kahn, C. R. Transplantation of adipose tissue and stem cells: role in metabolism and disease. *Nature Reviews Endocrinology* **6**, 195-213 (2010).
- 13 Trayhurn, P. & Beattie, J. H. Physiological role of adipose tissue: white adipose tissue as an endocrine and secretory organ. *Proceedings of the Nutrition Society* **60**, 329-339 (2001).
- 14 Galic, S., Oakhill, J. S. & Steinberg, G. R. Adipose tissue as an endocrine organ. *Molecular and cellular endocrinology* **316**, 129-139 (2010).
- 15 Yu, Y.-H. & Ginsberg, H. N. Adipocyte signaling and lipid homeostasis. *Circulation research* **96**, 1042-1052 (2005).
- 16 Wu, J. *et al.* Beige adipocytes are a distinct type of thermogenic fat cell in mouse and human. *Cell* **150**, 366-376 (2012).
- 17 Kazak, L. *et al.* A creatine-driven substrate cycle enhances energy expenditure and thermogenesis in beige fat. *Cell* **163**, 643-655, doi:10.1016/j.cell.2015.09.035 (2015).
- 18 Xue, B. *et al.* Genetic variability affects the development of brown adipocytes in white fat but not in interscapular brown fat. *Journal of lipid research* **48**, 41-51 (2007).
- 19 Barbatelli, G. *et al.* The emergence of cold-induced brown adipocytes in mouse white fat depots is determined predominantly by white to brown adipocyte

## REFERENCES

---

- transdifferentiation. *American Journal of Physiology-Endocrinology and Metabolism* **298**, E1244-E1253 (2010).
- 20 Cousin, B. *et al.* Occurrence of brown adipocytes in rat white adipose tissue: molecular and morphological characterization. *Journal of cell science* **103**, 931-942 (1992).
- 21 Cinti, S., Zingaretti, M. C., Cencello, R., Ceresi, E. & Ferrara, P. Morphologic techniques for the study of brown adipose tissue and white adipose tissue. *Adipose Tissue Protocols*, 21-51 (2001).
- 22 Altshuler-Keylin, S. *et al.* Beige adipocyte maintenance is regulated by autophagy-induced mitochondrial clearance. *Cell metabolism* **24**, 402-419 (2016).
- 23 Kajimura, S. & Saito, M. A new era in brown adipose tissue biology: molecular control of brown fat development and energy homeostasis. *Annu Rev Physiol* **76**, 225-249, doi:10.1146/annurev-physiol-021113-170252 (2014).
- 24 Muller, T. D. *et al.* p62 links beta-adrenergic input to mitochondrial function and thermogenesis. *J Clin Invest* **123**, 469-478, doi:10.1172/JCI64209 (2013).
- 25 Cinti, S. White, brown and pink adipocytes: the extraordinary plasticity of the adipose organ. *Italian Journal of Anatomy and Embryology* **120**, 28 (2015).
- 26 Morroni, M. *et al.* Reversible transdifferentiation of secretory epithelial cells into adipocytes in the mammary gland. *Proceedings of the National Academy of Sciences of the United States of America* **101**, 16801-16806 (2004).
- 27 Smith-Kirwin, S. M. *et al.* Leptin expression in human mammary epithelial cells and breast milk. *The Journal of Clinical Endocrinology & Metabolism* **83**, 1810-1810 (1998).
- 28 Palou, A., Sánchez, J. & Picó, C. in *Early Nutrition Programming and Health Outcomes in Later Life* 95-104 (Springer, 2009).
- 29 Gaggini, M., Saponaro, C. & Gastaldelli, A. Not all fats are created equal: adipose vs. ectopic fat, implication in cardiometabolic diseases. *Hormone molecular biology and clinical investigation* **22**, 7-18 (2015).
- 30 Kersten, S. Mechanisms of nutritional and hormonal regulation of lipogenesis. *EMBO reports* **2**, 282-286 (2001).
- 31 Lodhi, I. J. *et al.* Inhibiting adipose tissue lipogenesis reprograms thermogenesis and PPAR $\gamma$  activation to decrease diet-induced obesity. *Cell metabolism* **16**, 189-201 (2012).
- 32 Park, K. & Kim, K.-H. Regulation of acetyl-CoA carboxylase gene expression. Insulin induction of acetyl-CoA carboxylase and differentiation of 30A5 preadipocytes require prior cAMP action on the gene. *Journal of Biological Chemistry* **266**, 12249-12256 (1991).
- 33 Oh, W. *et al.* Glucose and fat metabolism in adipose tissue of acetyl-CoA carboxylase 2 knockout mice. *Proceedings of the National Academy of Sciences of the United States of America* **102**, 1384-1389 (2005).
- 34 Choi, C. S. *et al.* Continuous fat oxidation in acetyl-CoA carboxylase 2 knockout mice increases total energy expenditure, reduces fat mass, and improves insulin sensitivity. *Proceedings of the National Academy of Sciences* **104**, 16480-16485 (2007).
- 35 Zechner, R. *et al.* FAT SIGNALS-lipases and lipolysis in lipid metabolism and signaling. *Cell metabolism* **15**, 279-291 (2012).
- 36 Nielsen, T. S., Jessen, N., Jørgensen, J. O. L., Møller, N. & Lund, S. Dissecting adipose tissue lipolysis: molecular regulation and implications for metabolic disease. *Journal of molecular endocrinology* **52**, R199-R222 (2014).

## REFERENCES

---

- 37 Haemmerle, G. *et al.* Defective lipolysis and altered energy metabolism in mice lacking adipose triglyceride lipase. *Science* **312**, 734-737 (2006).
- 38 Haemmerle, G. *et al.* Hormone-sensitive lipase deficiency in mice causes diglyceride accumulation in adipose tissue, muscle, and testis. *Journal of Biological Chemistry* **277**, 4806-4815 (2002).
- 39 Osuga, J.-i. *et al.* Targeted disruption of hormone-sensitive lipase results in male sterility and adipocyte hypertrophy, but not in obesity. *Proceedings of the National Academy of Sciences* **97**, 787-792 (2000).
- 40 Taschler, U. *et al.* Monoglyceride lipase deficiency in mice impairs lipolysis and attenuates diet-induced insulin resistance. *Journal of Biological Chemistry* **286**, 17467-17477 (2011).
- 41 Schweiger, M., Lass, A., Zimmermann, R., Eichmann, T. O. & Zechner, R. Neutral lipid storage disease: genetic disorders caused by mutations in adipose triglyceride lipase/PNPLA2 or CGI-58/ABHD5. *American Journal of Physiology-Endocrinology and Metabolism* **297**, E289-E296 (2009).
- 42 Sekiya, M. *et al.* Absence of hormone-sensitive lipase inhibits obesity and adipogenesis in Lepob/ob mice. *Journal of Biological Chemistry* **279**, 15084-15090 (2004).
- 43 Schreiber, R. *et al.* Hypophagia and metabolic adaptations in mice with defective ATGL-mediated lipolysis cause resistance to HFD-induced obesity. *Proceedings of the National Academy of Sciences* **112**, 13850-13855 (2015).
- 44 Schweiger, M. *et al.* Pharmacological inhibition of adipose triglyceride lipase corrects high-fat diet-induced insulin resistance and hepatosteatosis in mice. *Nature communications* **8**, 14859 (2017).
- 45 Schoenborn, V. *et al.* The ATGL gene is associated with free fatty acids, triglycerides, and type 2 diabetes. *Diabetes* **55**, 1270-1275 (2006).
- 46 Rosen, E. D. & Spiegelman, B. M. Adipocytes as regulators of energy balance and glucose homeostasis. *Nature* **444**, 847-853, doi:10.1038/nature05483 (2006).
- 47 Kahn, S. E., Hull, R. L. & Utzschneider, K. M. Mechanisms linking obesity to insulin resistance and type 2 diabetes. *Nature* **444**, 840 (2006).
- 48 Ashcroft, F. M. & Rorsman, P. Diabetes mellitus and the  $\beta$  cell: the last ten years. *Cell* **148**, 1160-1171 (2012).
- 49 Andrews, R. C. & Walker, B. R. Glucocorticoids and insulin resistance: old hormones, new targets. *Clinical science* **96**, 513-523 (1999).
- 50 Vegiopoulos, A. & Herzig, S. Glucocorticoids, metabolism and metabolic diseases. *Molecular and cellular endocrinology* **275**, 43-61 (2007).
- 51 Thompson, B. R., Lobo, S. & Bernlohr, D. A. Fatty acid flux in adipocytes: the in's and out's of fat cell lipid trafficking. *Molecular and cellular endocrinology* **318**, 24-33 (2010).
- 52 Perea, A., Clemente, F., Martinell, J., Villanueva-Peñacarrillo, M. L. & Valverde, I. Physiological effect of glucagon in human isolated adipocytes. *Hormone and metabolic research* **27**, 372-375 (1995).
- 53 Longuet, C. *et al.* The glucagon receptor is required for the adaptive metabolic response to fasting. *Cell metabolism* **8**, 359-371 (2008).
- 54 Sumara, G., Sumara, O., Kim, J. K. & Karsenty, G. Gut-derived serotonin is a multifunctional determinant to fasting adaptation. *Cell metabolism* **16**, 588-600 (2012).

## REFERENCES

---

- 55 Inagaki, T. *et al.* Endocrine regulation of the fasting response by PPAR $\alpha$ -mediated induction of fibroblast growth factor 21. *Cell metabolism* **5**, 415-425 (2007).
- 56 Kershaw, E. E. & Flier, J. S. Adipose tissue as an endocrine organ. *The Journal of Clinical Endocrinology & Metabolism* **89**, 2548-2556 (2004).
- 57 Coelho, M., Oliveira, T. & Fernandes, R. Biochemistry of adipose tissue: an endocrine organ. *Archives of medical science: AMS* **9**, 191 (2013).
- 58 Friedman, J. M. & Halaas, J. L. Leptin and the regulation of body weight in mammals. *Nature* **395**, 763-770 (1998).
- 59 Ryo, M. *et al.* Adiponectin as a biomarker of the metabolic syndrome. *Circulation journal* **68**, 975-981 (2004).
- 60 Steppan, C. M. *et al.* The hormone resistin links obesity to diabetes. *Nature* **409**, 307-312 (2001).
- 61 Banerjee, R. R. *et al.* Regulation of fasted blood glucose by resistin. *Science* **303**, 1195-1198 (2004).
- 62 Krauss, S., Zhang, C.-Y. & Lowell, B. B. The mitochondrial uncoupling-protein homologues. *Nature reviews Molecular cell biology* **6**, 248 (2005).
- 63 Fedorenko, A., Lishko, P. V. & Kirichok, Y. Mechanism of fatty-acid-dependent UCP1 uncoupling in brown fat mitochondria. *Cell* **151**, 400-413 (2012).
- 64 Klingenspor, M. Cold-induced recruitment of brown adipose tissue thermogenesis. *Experimental physiology* **88**, 141-148 (2003).
- 65 Kajimura, S., Spiegelman, B. M. & Seale, P. Brown and beige fat: physiological roles beyond heat generation. *Cell metabolism* **22**, 546-559 (2015).
- 66 Wu, J., Cohen, P. & Spiegelman, B. M. Adaptive thermogenesis in adipocytes: is beige the new brown? *Genes & development* **27**, 234-250 (2013).
- 67 Wikstrom, J. D. *et al.* Hormone-induced mitochondrial fission is utilized by brown adipocytes as an amplification pathway for energy expenditure. *EMBO J* **33**, 418-436, doi:10.1002/embj.201385014 (2014).
- 68 Golozoubova, V. *et al.* Only UCP1 can mediate adaptive nonshivering thermogenesis in the cold. *The FASEB Journal* **15**, 2048-2050 (2001).
- 69 de Meis, L., Arruda, A. P., da Costa, R. M. & Benchimol, M. Identification of a Ca<sup>2+</sup>-ATPase in brown adipose tissue mitochondria regulation of thermogenesis by Atp and Ca<sup>2+</sup>. *Journal of Biological Chemistry* **281**, 16384-16390 (2006).
- 70 Ukropec, J., Anunciado, R. P., Ravussin, Y., Hulver, M. W. & Kozak, L. P. UCP1-independent thermogenesis in white adipose tissue of cold-acclimated Ucp1<sup>-/-</sup> mice. *Journal of Biological Chemistry* **281**, 31894-31908 (2006).
- 71 GONG, D.-W., BI, S., WEINTRAUB, B. D. & REITMAN, M. Rat mitochondrial glycerol-3-phosphate dehydrogenase gene: multiple promoters, high levels in brown adipose tissue, and tissue-specific regulation by thyroid hormone. *DNA and cell biology* **17**, 301-309 (1998).
- 72 Flachs, P. *et al.* Synergistic induction of lipid catabolism and anti-inflammatory lipids in white fat of dietary obese mice in response to calorie restriction and n-3 fatty acids. *Diabetologia* **54**, 2626 (2011).
- 73 Finucane, M. *et al.* Global Burden of Metabolic Risk Factors of Chronic Diseases Collaborating Group (Body Mass Index) National, regional, and global trends in body-mass index since 1980: systematic analysis of health examination surveys and epidemiological studies with 960 country-years and 9.1 million participants. *Lancet* **377**, 557-567 (2011).

## REFERENCES

---

- 74 Spiegelman, B. M. & Flier, J. S. Obesity and the regulation of energy balance. *Cell* **104**, 531-543 (2001).
- 75 Organization, W. H. *Obesity and overweight. (World Health Organization 2016).* <http://www.who.int/mediacentre/factsheets/fs311/en/>, checked on 12.02.2018.
- 76 Qi, L. & Cho, Y. A. Gene-environment interaction and obesity. *Nutrition reviews* **66**, 684-694 (2008).
- 77 Kaila, B. & Raman, M. Obesity: a review of pathogenesis and management strategies. *Canadian Journal of Gastroenterology and Hepatology* **22**, 61-68 (2008).
- 78 Zhang, Y. & Scarpace, P. J. The role of leptin in leptin resistance and obesity. *Physiology & behavior* **88**, 249-256 (2006).
- 79 Organization, W. H. *Global health risks: mortality and burden of disease attributable to selected major risks.* (World Health Organization, 2009).
- 80 Langin, D. In and out: adipose tissue lipid turnover in obesity and dyslipidemia. *Cell metabolism* **14**, 569-570 (2011).
- 81 Choe, S. S., Huh, J. Y., Hwang, I. J., Kim, J. I. & Kim, J. B. Adipose tissue remodeling: its role in energy metabolism and metabolic disorders. *Frontiers in endocrinology* **7**, 30 (2016).
- 82 Sun, K., Tordjman, J., Clément, K. & Scherer, P. E. Fibrosis and adipose tissue dysfunction. *Cell metabolism* **18**, 470-477 (2013).
- 83 Hotamisligil, G. S., Shargill, N. S. & Spiegelman, B. M. Adipose expression of tumor necrosis factor- $\alpha$ : direct role in obesity-linked insulin resistance. *Science* **259**, 87-91 (1993).
- 84 Weisberg, S. P. *et al.* Obesity is associated with macrophage accumulation in adipose tissue. *The Journal of clinical investigation* **112**, 1796-1808 (2003).
- 85 Xu, H. *et al.* Chronic inflammation in fat plays a crucial role in the development of obesity-related insulin resistance. *The Journal of clinical investigation* **112**, 1821-1830 (2003).
- 86 Kanda, H. *et al.* MCP-1 contributes to macrophage infiltration into adipose tissue, insulin resistance, and hepatic steatosis in obesity. *The Journal of clinical investigation* **116**, 1494-1505 (2006).
- 87 Fried, S. K., Bunkin, D. A. & Greenberg, A. S. Omental and subcutaneous adipose tissues of obese subjects release interleukin-6: depot difference and regulation by glucocorticoid. *The Journal of Clinical Endocrinology & Metabolism* **83**, 847-850 (1998).
- 88 Fain, J. N., Madan, A. K., Hiler, M. L., Cheema, P. & Bahouth, S. W. Comparison of the release of adipokines by adipose tissue, adipose tissue matrix, and adipocytes from visceral and subcutaneous abdominal adipose tissues of obese humans. *Endocrinology* **145**, 2273-2282 (2004).
- 89 Canello, R. *et al.* Increased infiltration of macrophages in omental adipose tissue is associated with marked hepatic lesions in morbid human obesity. *Diabetes* **55**, 1554-1561 (2006).
- 90 Yolanda, S. M. o. A. D. S. G. S. R. P. r. s. j. a. n. M. R. M. W. P. G. D. E. v. d. G. Ultrasound measurements of intraabdominal fat estimate the metabolic syndrome better than do measurements of waist circumference. *The American journal of clinical nutrition* **77**, 857-860 (2003).
- 91 DiPietro, L., Katz, L. & Nadel, E. Excess abdominal adiposity remains correlated with altered lipid concentrations in healthy older women. *International journal of obesity* **23**, 432 (1999).

## REFERENCES

---

- 92 Morinaga, H., Talukdar, S., Bae, E. J. & Olefsky, J. M. Increased macrophage migration into adipose tissue in obese mice. *Diabetes* **61**, 346-354 (2012).
- 93 Lumeng, C. N., Bodzin, J. L. & Saltiel, A. R. Obesity induces a phenotypic switch in adipose tissue macrophage polarization. *Journal of Clinical Investigation* **117**, 175 (2007).
- 94 Cummins, T. D. *et al.* Metabolic remodeling of white adipose tissue in obesity. *American Journal of Physiology-Endocrinology and Metabolism* **307**, E262-E277 (2014).
- 95 Wellen, K. E. & Hotamisligil, G. S. Inflammation, stress, and diabetes. *The Journal of clinical investigation* **115**, 1111-1119 (2005).
- 96 Shoelson, S. E., Lee, J. & Goldfine, A. B. Inflammation and insulin resistance. *The Journal of clinical investigation* **116**, 1793-1801 (2006).
- 97 Randle, P., Garland, P., Hales, C. & Newsholme, E. The glucose fatty-acid cycle its role in insulin sensitivity and the metabolic disturbances of diabetes mellitus. *The Lancet* **281**, 785-789 (1963).
- 98 Shulman, G. I. Cellular mechanisms of insulin resistance. *The Journal of clinical investigation* **106**, 171-176 (2000).
- 99 Kim, J. K., Gavrilova, O., Chen, Y., Reitman, M. L. & Shulman, G. I. Mechanism of insulin resistance in A-ZIP/F-1 fatless mice. *Journal of Biological Chemistry* **275**, 8456-8460 (2000).
- 100 Summers, S. A., Garza, L. A., Zhou, H. & Birnbaum, M. J. Regulation of insulin-stimulated glucose transporter GLUT4 translocation and Akt kinase activity by ceramide. *Molecular and cellular biology* **18**, 5457-5464 (1998).
- 101 Blagosklonny, M. TOR-centric view on insulin resistance and diabetic complications: perspective for endocrinologists and gerontologists. *Cell death & disease* **4**, e964 (2013).
- 102 Ruderman, N. B., Carling, D., Prentki, M. & Cacicedo, J. M. AMPK, insulin resistance, and the metabolic syndrome. *The Journal of clinical investigation* **123**, 2764-2772 (2013).
- 103 Mohanty, P. *et al.* Both lipid and protein intakes stimulate increased generation of reactive oxygen species by polymorphonuclear leukocytes and mononuclear cells. *The American journal of clinical nutrition* **75**, 767-772 (2002).
- 104 Shoelson, S. E., Herrero, L. & Naaz, A. Obesity, inflammation, and insulin resistance. *Gastroenterology* **132**, 2169-2180 (2007).
- 105 Furukawa, S. *et al.* Increased oxidative stress in obesity and its impact on metabolic syndrome. *The Journal of clinical investigation* **114**, 1752-1761 (2017).
- 106 Özcan, U. *et al.* Endoplasmic reticulum stress links obesity, insulin action, and type 2 diabetes. *Science* **306**, 457-461 (2004).
- 107 Summers, S. A. Ceramides in insulin resistance and lipotoxicity. *Progress in lipid research* **45**, 42-72 (2006).
- 108 Hirosumi, J. *et al.* A central role for JNK in obesity and insulin resistance. *Nature* **420**, 333 (2002).
- 109 Aguirre, V., Uchida, T., Yenush, L., Davis, R. & White, M. F. The c-Jun NH<sub>2</sub>-terminal kinase promotes insulin resistance during association with insulin receptor substrate-1 and phosphorylation of Ser307. *Journal of Biological Chemistry* **275**, 9047-9054 (2000).
- 110 Engelman, J. A., Berg, A. H., Lewis, R. Y., Lisanti, M. P. & Scherer, P. E. Tumor necrosis factor  $\alpha$ -mediated insulin resistance, but not dedifferentiation, is

## REFERENCES

---

- abrogated by MEK1/2 inhibitors in 3T3-L1 adipocytes. *Molecular endocrinology* **14**, 1557-1569 (2000).
- 111 Ahmad, F. & Goldstein, B. J. Effect of tumor necrosis factor -  $\alpha$  on the phosphorylation of tyrosine kinase receptors is associated with dynamic alterations in specific protein - tyrosine phosphatases. *Journal of cellular biochemistry* **64**, 117-127 (1997).
- 112 Silswal, N. *et al.* Human resistin stimulates the pro-inflammatory cytokines TNF- $\alpha$  and IL-12 in macrophages by NF- $\kappa$ B-dependent pathway. *Biochemical and biophysical research communications* **334**, 1092-1101 (2005).
- 113 Hardy, O. T., Czech, M. P. & Corvera, S. What causes the insulin resistance underlying obesity? *Current opinion in endocrinology, diabetes, and obesity* **19**, 81 (2012).
- 114 Kasuga, M. Insulin resistance and pancreatic  $\beta$  cell failure. *The Journal of clinical investigation* **116**, 1756-1760 (2006).
- 115 Guilherme, A., Virbasius, J. V., Puri, V. & Czech, M. P. Adipocyte dysfunctions linking obesity to insulin resistance and type 2 diabetes. *Nature reviews Molecular cell biology* **9**, 367 (2008).
- 116 Lowell, B. B. & Shulman, G. I. Mitochondrial dysfunction and type 2 diabetes. *Science* **307**, 384-387 (2005).
- 117 Barroso, I. Genetics of type 2 diabetes. *Diabetic Medicine* **22**, 517-535 (2005).
- 118 Samuel, V. T. & Shulman, G. I. Mechanisms for insulin resistance: common threads and missing links. *Cell* **148**, 852-871, doi:10.1016/j.cell.2012.02.017 (2012).
- 119 Leung, N. *et al.* Prolonged increase of plasma non-esterified fatty acids fully abolishes the stimulatory effect of 24 hours of moderate hyperglycaemia on insulin sensitivity and pancreatic beta-cell function in obese men. *Diabetologia* **47**, 204-213 (2004).
- 120 Prentki, M., Joly, E., El-Assaad, W. & Roduit, R. Malonyl-CoA signaling, lipid partitioning, and glucolipotoxicity: role in  $\beta$ -cell adaptation and failure in the etiology of diabetes. *Diabetes* **51**, S405-S413 (2002).
- 121 Zhou, Y.-P. & Grill, V. E. Long-term exposure of rat pancreatic islets to fatty acids inhibits glucose-induced insulin secretion and biosynthesis through a glucose fatty acid cycle. *The Journal of clinical investigation* **93**, 870-876 (1994).
- 122 Westermann, B. Bioenergetic role of mitochondrial fusion and fission. *Biochimica et Biophysica Acta (BBA)-Bioenergetics* **1817**, 1833-1838 (2012).
- 123 Twig, G., Hyde, B. & Shirihai, O. S. Mitochondrial fusion, fission and autophagy as a quality control axis: the bioenergetic view. *Biochim Biophys Acta* **1777**, 1092-1097, doi:10.1016/j.bbabi.2008.05.001 (2008).
- 124 Youle, R. J. & Van Der Bliek, A. M. Mitochondrial fission, fusion, and stress. *Science* **337**, 1062-1065 (2012).
- 125 Benard, G. & Karbowski, M. in *Seminars in cell & developmental biology*. 365-374 (Elsevier).
- 126 Beraud, N. *et al.* Mitochondrial dynamics in heart cells: very low amplitude high frequency fluctuations in adult cardiomyocytes and flow motion in non beating HL-1 cells. *Journal of bioenergetics and biomembranes* **41**, 195-214 (2009).
- 127 Saotome, M. "Mitochondrial remodeling" in coronary heart disease. (2014).
- 128 Otera, H. *et al.* Mff is an essential factor for mitochondrial recruitment of Drp1 during mitochondrial fission in mammalian cells. *The Journal of cell biology* **191**, 1141-1158 (2010).



## REFERENCES

---

- 129 Tol, M. J. *et al.* A PPAR $\gamma$ -Bnip3 Axis Couples Adipose Mitochondrial Fusion-Fission Balance to Systemic Insulin Sensitivity. *Diabetes* **65**, 2591-2605, doi:10.2337/db16-0243 (2016).
- 130 Toyama, E. Q. *et al.* AMP-activated protein kinase mediates mitochondrial fission in response to energy stress. *Science* **351**, 275-281 (2016).
- 131 Johannes, F.-J., Prestle, J., Eis, S., Oberhagemann, P. & Pfizenmaier, K. PKC $\alpha$  is a novel, atypical member of the protein kinase C family. *Journal of Biological Chemistry* **269**, 6140-6148 (1994).
- 132 Valverde, A. M., Sinnett-Smith, J., Van Lint, J. & Rozengurt, E. Molecular cloning and characterization of protein kinase D: a target for diacylglycerol and phorbol esters with a distinctive catalytic domain. *Proceedings of the National Academy of Sciences* **91**, 8572-8576 (1994).
- 133 Rozengurt, E. Protein kinase D signaling: multiple biological functions in health and disease. *Physiology (Bethesda)* **26**, 23-33, doi:10.1152/physiol.00037.2010 (2011).
- 134 Rozengurt, E., Rey, O. & Waldron, R. T. Protein kinase D signaling. *Journal of Biological Chemistry* **280**, 13205-13208 (2005).
- 135 Wang, Q. J. PKD at the crossroads of DAG and PKC signaling. *Trends in pharmacological sciences* **27**, 317-323 (2006).
- 136 Fu, Y. & Rubin, C. S. Protein kinase D: coupling extracellular stimuli to the regulation of cell physiology. *EMBO reports* **12**, 785-796 (2011).
- 137 Pi, M., Wu, Y. & Quarles, L. D. GPRC6A mediates responses to osteocalcin in beta-cells in vitro and pancreas in vivo. *Journal of bone and mineral research : the official journal of the American Society for Bone and Mineral Research* **26**, 1680-1683, doi:10.1002/jbmr.390 (2011).
- 138 Bradford, M. D. & Soltoff, S. P. P2X7 receptors activate protein kinase D and p42/p44 mitogen-activated protein kinase (MAPK) downstream of protein kinase C. *Biochem J* **366**, 745-755, doi:10.1042/BJ20020358 (2002).
- 139 Baron, C. L. & Malhotra, V. Role of diacylglycerol in PKD recruitment to the TGN and protein transport to the plasma membrane. *Science* **295**, 325-328 (2002).
- 140 Rousset, S. *et al.* The biology of mitochondrial uncoupling proteins. *Diabetes* **53**, S130-S135 (2004).
- 141 Jacamo, R., Sinnett-Smith, J., Rey, O., Waldron, R. T. & Rozengurt, E. Sequential Protein Kinase C (PKC)-dependent and PKC-independent Protein Kinase D Catalytic Activation via Gq-coupled Receptors DIFFERENTIAL REGULATION OF ACTIVATION LOOP SER744 AND SER748 PHOSPHORYLATION. *Journal of Biological Chemistry* **283**, 12877-12887 (2008).
- 142 Sinnett-Smith, J. *et al.* Protein kinase D mediates mitogenic signaling by Gq-coupled receptors through protein kinase C-independent regulation of activation loop Ser744 and Ser748 phosphorylation. *Journal of Biological Chemistry* **284**, 13434-13445 (2009).
- 143 Matthews, S. A., Rozengurt, E. & Cantrell, D. Characterization of Serine 916 as an in Vivo Autophosphorylation Site for Protein Kinase D/Protein Kinase C $\alpha$ . *Journal of Biological Chemistry* **274**, 26543-26549 (1999).
- 144 Rybin, V. O., Guo, J. & Steinberg, S. F. Protein Kinase D1 Autophosphorylation via Distinct Mechanisms at Ser<sup>744</sup>/Ser<sup>748</sup> and Ser<sup>916</sup>. *Journal of biological chemistry* (2009).

## REFERENCES

---

- 145 Sharlow, E. R. *et al.* Potent and selective disruption of protein kinase D functionality by a benzoxoloazepinolone. *Journal of Biological Chemistry* **283**, 33516-33526 (2008).
- 146 Harikumar, K. B. *et al.* A novel small-molecule inhibitor of protein kinase D blocks pancreatic cancer growth in vitro and in vivo. *Molecular cancer therapeutics* **9**, 1136-1146 (2010).
- 147 Kleger, A. *et al.* Protein kinase D2 is an essential regulator of murine myoblast differentiation. *PloS one* **6**, e14599, doi:10.1371/journal.pone.0014599 (2011).
- 148 Steiner, T. S., Ivison, S. M., Yao, Y. & Kifayet, A. Protein kinase D1 and D2 are involved in chemokine release induced by toll-like receptors 2, 4, and 5. *Cellular immunology* **264**, 135-142, doi:10.1016/j.cellimm.2010.05.012 (2010).
- 149 Konopatskaya, O. *et al.* Protein kinase C mediates platelet secretion and thrombus formation through protein kinase D2. *Blood* **118**, 416-424, doi:10.1182/blood-2010-10-312199 (2011).
- 150 Fielitz, J. *et al.* Requirement of protein kinase D1 for pathological cardiac remodeling. *Proceedings of the National Academy of Sciences of the United States of America* **105**, 3059-3063, doi:10.1073/pnas.0712265105 (2008).
- 151 Kim, M. S. *et al.* Protein kinase D1 stimulates MEF2 activity in skeletal muscle and enhances muscle performance. *Molecular and cellular biology* **28**, 3600-3609, doi:10.1128/MCB.00189-08 (2008).
- 152 Li, C. *et al.* Protein kinase D3 is a pivotal activator of pathological cardiac hypertrophy by selectively increasing the expression of hypertrophic transcription factors. *The Journal of biological chemistry* **286**, 40782-40791, doi:10.1074/jbc.M111.263046 (2011).
- 153 Matthews, S. A. *et al.* Essential role for protein kinase D family kinases in the regulation of class II histone deacetylases in B lymphocytes. *Molecular and cellular biology* **26**, 1569-1577, doi:10.1128/MCB.26.4.1569-1577.2006 (2006).
- 154 Ittner, A. *et al.* Regulation of PTEN activity by p38delta-PKD1 signaling in neutrophils confers inflammatory responses in the lung. *J Exp Med* **209**, 2229-2246, doi:10.1084/jem.20120677 (2012).
- 155 Ferdaoussi, M. *et al.* G protein-coupled receptor (GPR)40-dependent potentiation of insulin secretion in mouse islets is mediated by protein kinase D1. *Diabetologia* **55**, 2682-2692, doi:10.1007/s00125-012-2650-x (2012).
- 156 Sumara, G. *et al.* Regulation of PKD by the MAPK p38delta in insulin secretion and glucose homeostasis. *Cell* **136**, 235-248, doi:10.1016/j.cell.2008.11.018 (2009).
- 157 Gehart, H. *et al.* The BAR domain protein Arfaptin-1 controls secretory granule biogenesis at the trans-Golgi network. *Dev Cell* **23**, 756-768, doi:10.1016/j.devcel.2012.07.019 (2012).
- 158 Goginashvili, A. *et al.* Insulin granules. Insulin secretory granules control autophagy in pancreatic beta cells. *Science* **347**, 878-882, doi:10.1126/science.aaa2628 (2015).
- 159 Bergeron, V. *et al.* Deletion of protein kinase D1 in pancreatic beta cells impairs insulin secretion in high-fat fed mice. *Diabetes*, db170982 (2017).
- 160 Eguchi, J. *et al.* Transcriptional control of adipose lipid handling by IRF4. *Cell Metab* **13**, 249-259, doi:10.1016/j.cmet.2011.02.005 (2011).
- 161 Storz, P. & Toker, A. Protein kinase D mediates a stress-induced NF-kappaB activation and survival pathway. *EMBO J* **22**, 109-120, doi:10.1093/emboj/cdg009 (2003).

## REFERENCES

---

- 162 Asaithambi, A., Kanthasamy, A., Saminathan, H., Anantharam, V. & Kanthasamy, A. G. Protein kinase D1 (PKD1) activation mediates a compensatory protective response during early stages of oxidative stress-induced neuronal degeneration. *Mol Neurodegener* **6**, 43, doi:10.1186/1750-1326-6-43 (2011).
- 163 Rykx, A. *et al.* Protein kinase D: a family affair. *FEBS letters* **546**, 81-86 (2003).
- 164 Matthews, S. A., Iglesias, T., Rozengurt, E. & Cantrell, D. Spatial and temporal regulation of protein kinase D (PKD). *The EMBO journal* **19**, 2935-2945 (2000).
- 165 Spitaler, M., Emslie, E., Wood, C. D. & Cantrell, D. Diacylglycerol and protein kinase D localization during T lymphocyte activation. *Immunity* **24**, 535-546 (2006).
- 166 Cowell, C. F. *et al.* Mitochondrial diacylglycerol initiates protein-kinase-D1-mediated ROS signaling. *Journal of cell science* **122**, 919-928 (2009).
- 167 Liljedahl, M. *et al.* Protein kinase D regulates the fission of cell surface destined transport carriers from the trans-Golgi network. *Cell* **104**, 409-420 (2001).
- 168 Yeaman, C. *et al.* Protein kinase D regulates basolateral membrane protein exit from trans-Golgi network. *Nature cell biology* **6**, 106 (2004).
- 169 Ghanekar, Y. & Lowe, M. Signalling for secretion. *Nature cell biology* **7**, 851 (2005).
- 170 Bankaitis, V. A. Slick recruitment to the Golgi. *Science* **295**, 290-291 (2002).
- 171 Hausser, A. *et al.* Protein kinase D regulates vesicular transport by phosphorylating and activating phosphatidylinositol-4 kinase III $\beta$  at the Golgi complex. *Nature cell biology* **7**, 880 (2005).
- 172 Sinnott-Smith, J., Zhukova, E., Hsieh, N., Jiang, X. & Rozengurt, E. Protein kinase D potentiates DNA synthesis induced by Gq-coupled receptors by increasing the duration of ERK signaling in swiss 3T3 cells. *Journal of Biological Chemistry* **279**, 16883-16893 (2004).
- 173 Wang, Q. J. PKD at the crossroads of DAG and PKC signaling. *Trends Pharmacol Sci* **27**, 317-323, doi:10.1016/j.tips.2006.04.003 (2006).
- 174 Johannessen, M. *et al.* Protein kinase D induces transcription through direct phosphorylation of the cAMP-response element-binding protein. *The Journal of biological chemistry* **282**, 14777-14787, doi:10.1074/jbc.M610669200 (2007).
- 175 Ozgen, N. *et al.* Protein kinase D links Gq-coupled receptors to cAMP response element-binding protein (CREB)-Ser133 phosphorylation in the heart. *The Journal of biological chemistry* **283**, 17009-17019, doi:10.1074/jbc.M709851200 (2008).
- 176 Steinberg, S. F. Regulation of protein kinase D1 activity. *Molecular pharmacology* **81**, 284-291, doi:10.1124/mol.111.075986 (2012).
- 177 Mihaylova, M. M. *et al.* Class IIa histone deacetylases are hormone-activated regulators of FOXO and mammalian glucose homeostasis. *Cell* **145**, 607-621, doi:10.1016/j.cell.2011.03.043 (2011).
- 178 Altarejos, J. Y. & Montminy, M. CREB and the CRTC co-activators: sensors for hormonal and metabolic signals. *Nature reviews. Molecular cell biology* **12**, 141-151, doi:10.1038/nrm3072 (2011).
- 179 Locke, A. E. *et al.* Genetic studies of body mass index yield new insights for obesity biology. *Nature* **518**, 197-206 (2015).
- 180 Davies, S. P. *et al.* Purification of the AMP - activated protein kinase on ATP -  $\gamma$  - Sepharose and analysis of its subunit structure. *The FEBS Journal* **223**, 351-357 (1994).

## REFERENCES

---

- 181 Jeon, S.-M. Regulation and function of AMPK in physiology and diseases. *Experimental & molecular medicine* **48**, e245 (2016).
- 182 Bijland, S., Mancini, S. J. & Salt, I. P. Role of AMP-activated protein kinase in adipose tissue metabolism and inflammation. *Clin Sci (Lond)* **124**, 491-507, doi:10.1042/CS20120536 (2013).
- 183 Hardie, D. G., Ross, F. A. & Hawley, S. A. AMPK: a nutrient and energy sensor that maintains energy homeostasis. *Nature reviews Molecular cell biology* **13**, 251 (2012).
- 184 Hawley, S. A. *et al.* Phosphorylation by Akt within the ST loop of AMPK- $\alpha$ 1 down-regulates its activation in tumour cells. *Biochemical Journal* **459**, 275-287 (2014).
- 185 Coughlan, K. A. *et al.* PKD1 Inhibits AMPK $\alpha$ 2 through Phosphorylation of Serine 491 and Impairs Insulin Signaling in Skeletal Muscle Cells. *The Journal of biological chemistry* **291**, 5664-5675, doi:10.1074/jbc.M115.696849 (2016).
- 186 Daval, M., Foufelle, F. & Ferré, P. Functions of AMP - activated protein kinase in adipose tissue. *The Journal of physiology* **574**, 55-62 (2006).
- 187 Gwinn, D. M. *et al.* AMPK phosphorylation of raptor mediates a metabolic checkpoint. *Molecular cell* **30**, 214-226 (2008).
- 188 Hardie, D. & Pan, D. (Portland Press Limited, 2002).
- 189 Li, Y. *et al.* AMPK phosphorylates and inhibits SREBP activity to attenuate hepatic steatosis and atherosclerosis in diet-induced insulin-resistant mice. *Cell metabolism* **13**, 376-388 (2011).
- 190 Jäger, S., Handschin, C., Pierre, J. S.-. & Spiegelman, B. M. AMP-activated protein kinase (AMPK) action in skeletal muscle via direct phosphorylation of PGC-1 $\alpha$ . *Proceedings of the National Academy of Sciences* **104**, 12017-12022 (2007).
- 191 Zhu, Q. *et al.* Adipocyte-specific deletion of Ip6k1 reduces diet-induced obesity by enhancing AMPK-mediated thermogenesis. *J Clin Invest* **126**, 4273-4288, doi:10.1172/JCI85510 (2016).
- 192 Mottillo, E. P. *et al.* Lack of Adipocyte AMPK Exacerbates Insulin Resistance and Hepatic Steatosis through Brown and Beige Adipose Tissue Function. *Cell Metab* **24**, 118-129, doi:10.1016/j.cmet.2016.06.006 (2016).
- 193 Gauthier, M.-S. *et al.* Decreased AMP-activated protein kinase activity is associated with increased inflammation in visceral adipose tissue and with whole-body insulin resistance in morbidly obese humans. *Biochemical and biophysical research communications* **404**, 382-387 (2011).
- 194 Viollet, B. *et al.* The AMP-activated protein kinase  $\alpha$ 2 catalytic subunit controls whole-body insulin sensitivity. *The Journal of clinical investigation* **111**, 91-98 (2003).
- 195 Villena, J. A. *et al.* Induced adiposity and adipocyte hypertrophy in mice lacking the AMP-activated protein kinase- $\alpha$ 2 subunit. *Diabetes* **53**, 2242-2249 (2004).
- 196 Dasgupta, B. *et al.* The AMPK  $\beta$ 2 subunit is required for energy homeostasis during metabolic stress. *Molecular and cellular biology* **32**, 2837-2848 (2012).
- 197 Nahmias, C. *et al.* Molecular characterization of the mouse beta 3 - adrenergic receptor: relationship with the atypical receptor of adipocytes. *The EMBO Journal* **10**, 3721-3727 (1991).
- 198 Collins, S. *et al.* Impaired expression and functional activity of the beta 3-and beta 1-adrenergic receptors in adipose tissue of congenitally obese (C57BL/6J ob/ob) mice. *Molecular endocrinology* **8**, 518-527 (1994).

## REFERENCES

---

- 199 Muzzin, P. *et al.* An adipose tissue-specific beta-adrenergic receptor. Molecular cloning and down-regulation in obesity. *Journal of Biological Chemistry* **266**, 24053-24058 (1991).
- 200 Grujic, D. *et al.*  $\beta$ 3-Adrenergic Receptors on White and Brown Adipocytes Mediate  $\beta$ 3-Selective Agonist-induced Effects on Energy Expenditure, Insulin Secretion, and Food Intake A STUDY USING TRANSGENIC AND GENE KNOCKOUT MICE. *Journal of Biological Chemistry* **272**, 17686-17693 (1997).
- 201 Dixon, T. M., Daniel, K. W., Farmer, S. R. & Collins, S. CCAAT/Enhancer-binding Protein  $\alpha$  Is Required for Transcription of the  $\beta$ 3-Adrenergic Receptor Gene during Adipogenesis. *Journal of Biological Chemistry* **276**, 722-728 (2001).
- 202 Tanaka, T., Yoshida, N., Kishimoto, T. & Akira, S. Defective adipocyte differentiation in mice lacking the C/EBP $\beta$  and/or C/EBP $\delta$  gene. *The EMBO journal* **16**, 7432-7443 (1997).
- 203 Cao, Z., Umek, R. M. & McKnight, S. L. Regulated expression of three C/EBP isoforms during adipose conversion of 3T3-L1 cells. *Genes & development* **5**, 1538-1552 (1991).
- 204 Inagaki, T., Sakai, J. & Kajimura, S. Transcriptional and epigenetic control of brown and beige adipose cell fate and function. *Nature reviews Molecular cell biology* **17**, 480 (2016).
- 205 Kajimura, S., Seale, P. & Spiegelman, B. M. Transcriptional control of brown fat development. *Cell metabolism* **11**, 257-262 (2010).
- 206 Sassmann, A., Offermanns, S. & Wettschureck, N. Tamoxifen - inducible Cre - mediated recombination in adipocytes. *Genesis* **48**, 618-625 (2010).
- 207 Cai, K., El-Merahbi, R., Loeffler, M., Mayer, A. E. & Sumara, G. Ndrp1 promotes adipocyte differentiation and sustains their function. *Sci Rep* **7**, 7191, doi:10.1038/s41598-017-07497-x (2017).
- 208 Zennaro, M.-C. *et al.* Hibernoma development in transgenic mice identifies brown adipose tissue as a novel target of aldosterone action. *The Journal of clinical investigation* **101**, 1254-1260 (1998).
- 209 Fellmann, C. *et al.* An optimized microRNA backbone for effective single-copy RNAi. *Cell Rep* **5**, 1704-1713, doi:10.1016/j.celrep.2013.11.020 (2013).
- 210 Cox, J. & Mann, M. MaxQuant enables high peptide identification rates, individualized ppb-range mass accuracies and proteome-wide protein quantification. *Nature biotechnology* **26**, 1367 (2008).
- 211 Cox, J. *et al.* MaxLFQ allows accurate proteome-wide label-free quantification by delayed normalization and maximal peptide ratio extraction. *Molecular & cellular proteomics*, mcp. M113. 031591 (2014).
- 212 Subramanian, A. *et al.* Gene set enrichment analysis: a knowledge-based approach for interpreting genome-wide expression profiles. *Proceedings of the National Academy of Sciences of the United States of America* **102**, 15545-15550, doi:10.1073/pnas.0506580102 (2005).
- 213 Trujillo Viera, J., El-Merahbi, R., Nieswandt, B., Stegner, D. & Sumara, G. Phospholipases D1 and D2 Suppress Appetite and Protect against Overweight. *PLoS One* **11**, e0157607, doi:10.1371/journal.pone.0157607 (2016).
- 214 Guerre-Millo, M. Adipose tissue hormones. *Journal of endocrinological investigation* **25**, 855-861 (2002).
- 215 Laplante, M.-A., Monassier, L., Freund, M., Bousquet, P. & Gachet, C. The purinergic P2Y1 receptor supports leptin secretion in adipose tissue. *Endocrinology* **151**, 2060-2070 (2010).

## REFERENCES

---

- 216 Lee, H. *et al.* Dual roles of P2 purinergic receptors in insulin-stimulated leptin production and lipolysis in differentiated rat white adipocytes. *Journal of Biological Chemistry* **280**, 28556-28563 (2005).
- 217 Schödel, J., Weise, I., Klinger, R. & Schmidt, M. Stimulation of lipogenesis in rat adipocytes by ATP, a ligand for P2-receptors. *Biochemical and biophysical research communications* **321**, 767-773 (2004).
- 218 Carrasquero, L. M. G., Delicado, E. G., SÁnchez - Ruiloba, L., Iglesias, T. & Miras - Portugal, M. T. Mechanisms of protein kinase D activation in response to P2Y2 and P2X7 receptors in primary astrocytes. *Glia* **58**, 984-995 (2010).
- 219 Löffler, M. C. *et al.* Protein kinase D1 deletion in adipocytes enhances energy dissipation and protects against adiposity. *The EMBO journal* **37**, e99182 (2018).
- 220 Pfielschifter, J. Extracellular ATP stimulates polyphosphoinositide hydrolysis and prostaglandin synthesis in rat renal mesangial cells: involvement of a pertussis toxin-sensitive guanine nucleotide binding protein and feedback inhibition by protein kinase C. *Cellular signalling* **2**, 129-138 (1990).
- 221 Ahmadian, M., E Duncan, R., Jaworski, K., Sarkadi-Nagy, E. & Sul, H. S. Triacylglycerol metabolism in adipose tissue. (2007).
- 222 Weiss, S. B., Kennedy, E. P. & Kiyasu, J. Y. The enzymatic synthesis of triglycerides. *Journal of Biological Chemistry* **235**, 40-44 (1960).
- 223 Stuart, J. A., Brindle, K. M., Harper, J. A. & Brand, M. D. Mitochondrial proton leak and the uncoupling proteins. *Journal of bioenergetics and biomembranes* **31**, 517 (1999).
- 224 Ricquier, D. & Bouillaud, F. Mitochondrial uncoupling proteins: from mitochondria to the regulation of energy balance. *The Journal of physiology* **529**, 3-10 (2000).
- 225 Rui, L. Brown and Beige Adipose Tissues in Health and Disease. *Comprehensive Physiology* (2017).
- 226 Cybulski, N., Polak, P., Auwerx, J., Rüegg, M. A. & Hall, M. N. mTOR complex 2 in adipose tissue negatively controls whole-body growth. *Proceedings of the National Academy of Sciences* **106**, 9902-9907 (2009).
- 227 Lamming, D. W. & Sabatini, D. M. A central role for mTOR in lipid homeostasis. *Cell metabolism* **18**, 465-469 (2013).
- 228 Albert, V. *et al.* mTORC2 sustains thermogenesis via Akt - induced glucose uptake and glycolysis in brown adipose tissue. *EMBO molecular medicine*, e201505610 (2016).
- 229 Hung, C.-M. *et al.* Rictor/mTORC2 loss in the Myf5 lineage reprograms brown fat metabolism and protects mice against obesity and metabolic disease. *Cell reports* **8**, 256-271 (2014).
- 230 Kumar, A. *et al.* Fat cell-specific ablation of rictor in mice impairs insulin-regulated fat cell and whole-body glucose and lipid metabolism. *Diabetes* **59**, 1397-1406 (2010).
- 231 Tang, Y. *et al.* Adipose tissue mTORC2 regulates ChREBP-driven de novo lipogenesis and hepatic glucose metabolism. *Nature communications* **7** (2016).
- 232 Xu, X. *et al.* The CUL7 E3 ubiquitin ligase targets insulin receptor substrate 1 for ubiquitin-dependent degradation. *Molecular cell* **30**, 403-414 (2008).
- 233 Yamakawa, T., Sugimoto, K., Whitson, R. H. & Itakura, K. Modulator recognition factor-2 regulates triglyceride metabolism in adipocytes. *Biochemical and biophysical research communications* **391**, 277-281 (2010).

## REFERENCES

---

- 234 Yamakawa, T., Whitson, R. H., Li, S.-L. & Itakura, K. Modulator recognition factor-2 is required for adipogenesis in mouse embryo fibroblasts and 3T3-L1 cells. *Molecular Endocrinology* **22**, 441-453 (2008).
- 235 Whitson, R. H., Tsark, W., Huang, T. H. & Itakura, K. Neonatal mortality and leanness in mice lacking the ARID transcription factor Mrf-2. *Biochemical and biophysical research communications* **312**, 997-1004 (2003).
- 236 Aicart-Ramos, C., He, S. D. Q., Land, M. & Rubin, C. S. A Novel Conserved Domain Mediates Dimerization of Protein Kinase D (PKD) Isoforms DIMERIZATION IS ESSENTIAL FOR PKD-DEPENDENT REGULATION OF SECRETION AND INNATE IMMUNITY. *Journal of Biological Chemistry* **291**, 23516-23531 (2016).
- 237 Wullschleger, S., Loewith, R. & Hall, M. N. TOR signaling in growth and metabolism. *Cell* **124**, 471-484 (2006).
- 238 Polak, P. *et al.* Adipose-specific knockout of raptor results in lean mice with enhanced mitochondrial respiration. *Cell metabolism* **8**, 399-410 (2008).
- 239 Laplante, M. & Sabatini, D. M. mTOR signaling in growth control and disease. *Cell* **149**, 274-293 (2012).
- 240 Wang, R.-H. *et al.* Hepatic Sirt1 deficiency in mice impairs mTORC2/Akt signaling and results in hyperglycemia, oxidative damage, and insulin resistance. *The Journal of clinical investigation* **121**, 4477 (2011).
- 241 Tato, I., Bartrons, R., Ventura, F. & Rosa, J. L. Amino acids activate mammalian target of rapamycin complex 2 (mTORC2) via PI3K/Akt signaling. *Journal of Biological Chemistry* **286**, 6128-6142 (2011).
- 242 Sengupta, S., Peterson, T. R. & Sabatini, D. M. Regulation of the mTOR complex 1 pathway by nutrients, growth factors, and stress. *Molecular cell* **40**, 310-322 (2010).
- 243 Mihaylova, M. M. & Shaw, R. J. The AMPK signalling pathway coordinates cell growth, autophagy and metabolism. *Nature cell biology* **13**, 1016-1023 (2011).
- 244 Gaidhu, M. P. *et al.* Prolonged AICAR-induced AMP-kinase activation promotes energy dissipation in white adipocytes: novel mechanisms integrating HSL and ATGL. *Journal of lipid research* **50**, 704-715 (2009).
- 245 Kim, J., Kundu, M., Viollet, B. & Guan, K.-L. AMPK and mTOR regulate autophagy through direct phosphorylation of Ulk1. *Nature cell biology* **13**, 132 (2011).
- 246 Cui, X. *et al.* Thermoneutrality decreases thermogenic program and promotes adiposity in high - fat diet - fed mice. *Physiological reports* **4**, e12799 (2016).
- 247 Boden, G. Free fatty acids, insulin resistance, and type 2 diabetes mellitus. *Proceedings of the Association of American Physicians* **111**, 241-248 (1999).
- 248 Berridge, M. J. Inositol trisphosphate and diacylglycerol as second messengers. *Biochemical Journal* **220**, 345 (1984).
- 249 Szendroedi, J. *et al.* Role of diacylglycerol activation of PKC $\theta$  in lipid-induced muscle insulin resistance in humans. *Proceedings of the National Academy of Sciences*, 201409229 (2014).
- 250 Giralt, M. & Villarroya, F. White, brown, beige/brite: different adipose cells for different functions? *Endocrinology* **154**, 2992-3000 (2013).
- 251 Park, A., Kim, W. K. & Bae, K.-H. Distinction of white, beige and brown adipocytes derived from mesenchymal stem cells. *World journal of stem cells* **6**, 33 (2014).

## REFERENCES

---

- 252 Peterson, D. B. *et al.* Comparative proteomic analysis of PAI-1 and TNF-alpha-derived endothelial microparticles. *Proteomics* **8**, 2430-2446, doi:10.1002/pmic.200701029 (2008).
- 253 Itani, S. I., Ruderman, N. B., Schmieder, F. & Boden, G. Lipid-induced insulin resistance in human muscle is associated with changes in diacylglycerol, protein kinase C, and I $\kappa$ B- $\alpha$ . *Diabetes* **51**, 2005-2011 (2002).
- 254 Szendroedi, J. *et al.* Role of diacylglycerol activation of PKC $\theta$  in lipid-induced muscle insulin resistance in humans. *Proceedings of the National Academy of Sciences* **111**, 9597-9602 (2014).
- 255 Yamauchi, T. *et al.* The mechanisms by which both heterozygous peroxisome proliferator-activated receptor  $\gamma$  (PPAR $\gamma$ ) deficiency and PPAR $\gamma$  agonist improve insulin resistance. *Journal of Biological Chemistry* **276**, 41245-41254 (2001).
- 256 Martinez-Botas, J. *et al.* Absence of perilipin results in leanness and reverses obesity in *Lepr* db/db mice. *Nature genetics* **26**, 474 (2000).
- 257 Tansey, J. *et al.* Perilipin ablation results in a lean mouse with aberrant adipocyte lipolysis, enhanced leptin production, and resistance to diet-induced obesity. *Proceedings of the National Academy of Sciences* **98**, 6494-6499 (2001).
- 258 Wang, Y.-X. *et al.* Peroxisome-proliferator-activated receptor  $\delta$  activates fat metabolism to prevent obesity. *Cell* **113**, 159-170 (2003).
- 259 Cruz, M. M. *et al.* Palmitoleic acid (16: 1n7) increases oxygen consumption, fatty acid oxidation and ATP content in white adipocytes. *Lipids in health and disease* **17**, 55 (2018).
- 260 Lanza, I. R. & Nair, K. S. Functional assessment of isolated mitochondria in vitro. *Methods in enzymology* **457**, 349-372 (2009).
- 261 Duchen, M. R. Mitochondria in health and disease: perspectives on a new mitochondrial biology. *Molecular aspects of medicine* **25**, 365-451 (2004).
- 262 Zhang, Z. *et al.* Berberine activates thermogenesis in white and brown adipose tissue. *Nat Commun* **5**, 5493, doi:10.1038/ncomms6493 (2014).
- 263 Gaidhu, M. P. *et al.* Chronic AMP-kinase activation with AICAR reduces adiposity by remodeling adipocyte metabolism and increasing leptin sensitivity. *J Lipid Res* **52**, 1702-1711, doi:10.1194/jlr.M015354 (2011).
- 264 Toyama, E. Q. *et al.* Metabolism. AMP-activated protein kinase mediates mitochondrial fission in response to energy stress. *Science* **351**, 275-281, doi:10.1126/science.aab4138 (2016).
- 265 Djouder, N. *et al.* PKA phosphorylates and inactivates AMPK $\alpha$  to promote efficient lipolysis. *EMBO J* **29**, 469-481, doi:10.1038/emboj.2009.339 (2010).
- 266 Rohm, M. *et al.* An AMP-activated protein kinase-stabilizing peptide ameliorates adipose tissue wasting in cancer cachexia in mice. *Nat Med* **22**, 1120-1130, doi:10.1038/nm.4171 (2016).
- 267 Roach, P. J. AMPK $\rightarrow$  uLK1 $\rightarrow$  autophagy. *Molecular and cellular biology* **31**, 3082-3084 (2011).
- 268 Zhang, Y. *et al.* Adipose-specific deletion of autophagy-related gene 7 (*atg7*) in mice reveals a role in adipogenesis. *Proceedings of the National Academy of Sciences* **106**, 19860-19865 (2009).
- 269 Singh, R. *et al.* Autophagy regulates adipose mass and differentiation in mice. *The Journal of clinical investigation* **119**, 3329-3339 (2009).



## REFERENCES

---

- 270 Wang, R.-H. *et al.* Hepatic Sirt1 deficiency in mice impairs mTorc2/Akt signaling and results in hyperglycemia, oxidative damage, and insulin resistance. *The Journal of clinical investigation* **121** (2011).
- 271 Rosner, M., Siegel, N., Valli, A., Fuchs, C. & Hengstschläger, M. mTOR phosphorylated at S2448 binds to raptor and rictor. *Amino acids* **38**, 223-228 (2010).
- 272 Zhang, H. H. *et al.* Insulin stimulates adipogenesis through the Akt-TSC2-mTORC1 pathway. *PloS one* **4**, e6189 (2009).
- 273 Wang, C. *et al.* Adiponectin sensitizes insulin signaling by reducing p70 S6 kinase-mediated serine phosphorylation of IRS-1. *Journal of Biological Chemistry* (2007).
- 274 Meyer, C. W. *et al.* Adaptive thermogenesis and thermal conductance in wild-type and UCP1-KO mice. *American Journal of Physiology-Regulatory, Integrative and Comparative Physiology* **299**, R1396-R1406 (2010).
- 275 Granneman, J., Burnazi, M., Zhu, Z. & Schwamb, L. White adipose tissue contributes to UCP1-independent thermogenesis. *American Journal of Physiology-Endocrinology and Metabolism* **285**, E1230-E1236 (2003).
- 276 Schneider, K. *et al.* Increased energy expenditure, Ucp1 expression, and resistance to diet-induced obesity in mice lacking nuclear factor-erythroid-2-related transcription factor-2 (Nrf2). *Journal of Biological Chemistry* **291**, 7754-7766 (2016).
- 277 Zheng, Q. *et al.* Reconstitution of UCP1 using CRISPR/Cas9 in the white adipose tissue of pigs decreases fat deposition and improves thermogenic capacity. *Proceedings of the National Academy of Sciences* **114**, E9474-E9482 (2017).
- 278 Rossmesl, M. *et al.* Expression of the uncoupling protein 1 from the aP2 gene promoter stimulates mitochondrial biogenesis in unilocular adipocytes in vivo. *The FEBS Journal* **269**, 19-28 (2002).
- 279 Landsberg, L. & Young, J. B. in *Mammalian thermogenesis* 99-140 (Springer, 1983).
- 280 Cohen, P. & Spiegelman, B. M. Cell biology of fat storage. *Molecular biology of the cell* **27**, 2523-2527 (2016).
- 281 Kajimura, S., Spiegelman, B. M. & Seale, P. Brown and Beige Fat: Physiological Roles beyond Heat Generation. *Cell Metab* **22**, 546-559, doi:10.1016/j.cmet.2015.09.007 (2015).
- 282 Emorine, L. J. *et al.* Molecular characterization of the human beta 3-adrenergic receptor. *Science* **245**, 1118-1121 (1989).
- 283 Granneman, J. G., Lahners, K. N. & Chaudhry, A. Molecular cloning and expression of the rat beta 3-adrenergic receptor. *Molecular Pharmacology* **40**, 895-899 (1991).
- 284 Long, J. Z. *et al.* A smooth muscle-like origin for beige adipocytes. *Cell metabolism* **19**, 810-820 (2014).
- 285 Vitali, A. *et al.* The adipose organ of obesity-prone C57BL/6J mice is composed of mixed white and brown adipocytes. *Journal of lipid research*, jlr. M018846 (2012).
- 286 Kiefer, F. W. *et al.* Retinaldehyde dehydrogenase 1 regulates a thermogenic program in white adipose tissue. *Nature medicine* **18**, 918 (2012).
- 287 Cohen, P. *et al.* Ablation of PRDM16 and beige adipose causes metabolic dysfunction and a subcutaneous to visceral fat switch. *Cell* **156**, 304-316 (2014).

## REFERENCES

---

- 288 Vohl, M. C. *et al.* A survey of genes differentially expressed in subcutaneous and visceral adipose tissue in men. *Obesity research* **12**, 1217-1222 (2004).
- 289 Kemp, B. E. *et al.* Dealing with energy demand: the AMP-activated protein kinase. *Trends in biochemical sciences* **24**, 22-25 (1999).
- 290 Sears, B. & Perry, M. The role of fatty acids in insulin resistance. *Lipids in health and disease* **14**, 121 (2015).
- 291 Boden, G., Lebed, B., Schatz, M., Homko, C. & Lemieux, S. Effects of acute changes of plasma free fatty acids on intramyocellular fat content and insulin resistance in healthy subjects. *Diabetes* **50**, 1612-1617 (2001).
- 292 Dirkx, E. *et al.* Protein kinase-D1 overexpression prevents lipid-induced cardiac insulin resistance. *J Mol Cell Cardiol* **76**, 208-217, doi:10.1016/j.yjmcc.2014.08.017 (2014).
- 293 Pandolfi, J. *et al.* Purinergic signaling modulates human visceral adipose inflammatory responses: implications in metabolically unhealthy obesity. *Journal of leukocyte biology* **97**, 941-949 (2015).
- 294 Pandolfi, J. B. *et al.* ATP-induced inflammation drives tissue-resident Th17 cells in metabolically unhealthy obesity. *The Journal of Immunology*, 1502506 (2016).
- 295 Sun, K., Kusminski, C. M. & Scherer, P. E. Adipose tissue remodeling and obesity. *The Journal of clinical investigation* **121**, 2094-2101 (2011).
- 296 Van Heek, M. *et al.* Diet-induced obese mice develop peripheral, but not central, resistance to leptin. *The Journal of clinical investigation* **99**, 385-390 (1997).
- 297 El-Haschimi, K., Pierroz, D. D., Hileman, S. M., Bjørnbæk, C. & Flier, J. S. Two defects contribute to hypothalamic leptin resistance in mice with diet-induced obesity. *The Journal of clinical investigation* **105**, 1827-1832 (2000).
- 298 Mori, H. *et al.* Socs3 deficiency in the brain elevates leptin sensitivity and confers resistance to diet-induced obesity. *Nature medicine* **10**, 739 (2004).
- 299 Mantzoros, C. S. *et al.* Leptin concentrations in relation to body mass index and the tumor necrosis factor- $\alpha$  system in humans. *The Journal of Clinical Endocrinology & Metabolism* **82**, 3408-3413 (1997).
- 300 Tritos, N. & Mantzoros, C. Leptin: its role in obesity and beyond. *Diabetologia* **40**, 1371-1379 (1997).
- 301 Caro, J. F., Sinha, M. K., Kolaczynski, J. W., Zhang, P. L. & Considine, R. V. Leptin: the tale of an obesity gene. *Diabetes* **45**, 1455-1463 (1996).
- 302 Maffei, M. *et al.* Leptin levels in human and rodent: measurement of plasma leptin and ob RNA in obese and weight-reduced subjects. *Nature medicine* **1**, 1155 (1995).

## 7 APPENDIX

### 7.1 Materilas and Reagents

#### 7.1.1 Appliances and consumables

REAGENT or RESOURCE	SPECIFICATION	SOURCE
Appliances		
Animal ear punch	2 mM whole size	VWR
Autoclave	VX-120	Systec
Autoclave sterilizer	DX-100	Systec
Bench-top homogenizer	PT 1600E	Polytron
Centrifuge	Multifuge X3R Rotor: TX-750 4 x 750 mL Insert: PA75003638; PA75003639; PA75003617	Eppendorf
Centrifuge	5424 R	Eppendorf
Centrifuge	5810 R Rotor: A-4-62	Eppendorf
Cryostat	CM1900	Leica
Dionex Ultimate 3000 UHPLC system	hyphenated with a Q <i>exactive mass spectrometer</i> (QEMS) equipped with a HESI probe	Thermo Fisher Scientific
Easy-nLC 1000		Thermo Fisher Scientific
Electrophoresis cell	Sub-Cell GT	Bio-Rad
Erlenmeyer flask	1000 mL	Simax
Gas burner	Type CFH	A. Hartenstein
FastQC script		Babraham Bioinformatics
Fine tweezer	Tip: 0.8 mM x 0.7 mM	Fine Science Tools

APPENDIX

REAGENT or RESOURCE	SPECIFICATION	SOURCE
Fluorescence microscope	DM5500 B Illuminator: X-Cite 200DC Camera: Leica DFC365 FX Power supply: CTR HS	Leica
Freezer (-20 °C)	profi line GG4310	Liebherr
Freezer (-20 °C)	Comfort	Liebherr
Freezer (-80 °C)	HERAfreeze HFU666 basic	Thermo Fisher Scientific
Freezing chamber		Thermo Fisher Scientific
Fridge	profi line FKS5000	Liebherr
Fridge + freezer	CP3523-21	Liebherr
Glass bottles	2000 mL; 1000 mL; 500 mL; 250 mL; 100 mL	Duran
Glucometer	Accu-Chek	Roche
Homogeniser stick	PP-pestle; cone-shaped; 70 mM	Roth
Ice machine		Ziegra
Incubator	Heracell 240	Heraeus
Incubator	C150	Binder
Incubator shaker	ISF-1-W	Kuhner
Inverted microscope	CKX31	Olympus
Inverted microscope	IX71	Olympus
Laminar flow cabinet	SB-1200	BDK Luft- und Reinraumtechnik GmbH
Liquid scintillation counter	Tri-Carb 2910 TR	Perkin Elmer
Magnetic rack		Alpaqua
Magnetic stirrer	MR Hei-Standard	Heidolph
Mechanical counter	T120	IVO
Metabolic cage	Indirect calorimetry system PhenoMaster	TSE systems GmbH, Germany

APPENDIX

REAGENT or RESOURCE	SPECIFICATION	SOURCE
Mice cage	GM500PFS Lid: for water bottles Water bottle: 300 mL Lid: full length	Tecniplast
Mice cage rack system	Green Line IVC	Tecniplast
Microcentrifuge	Galaxy Ministar	VWR
Micro scales	AB265-S	Mettler Toledo
Microwave		Dynamic
MilliQ water purification system	X-CAD	Millipore
Multi-channel pipette	Transferpette S12; 20 – 200 µL	Brand
Multimode microplate reader	Spark™ 10M	Tecan
Multiplex ELISA reader	Bio-Plex® MAGPIX™ Multiplex reader	Bio-Rad
Neubauer chamber	0.1 mM Depth	Hecht-Assistant
NextSeq500 system		Illumina
Nitrogen cell storage tank	Cryosystem 4000	MVE
Nitrogen storage tank	Cryotherm	Apollo
<i>nuclear magnetic resonance</i> (NMR) analyzer	The minispec; LF50	Bruker
Orbitrap analyzer	Orbitrap LC-MS	Thermo Fisher Scientific
Orbitrap fusion	Orbitrap Fusion™ Tribrid™ Mass spectrometer	Thermo Fisher Scientific
pH-meter	FiveEasy	Mettler Toledo
Photometer	BioPhotometer	Eppendorf
PicoView® ion source		New Objective
Pipette	Transferpette S; 0.5 – 10 µL	Brand
Pipette controller	Accu-Jet Pro	Brand

APPENDIX

REAGENT or RESOURCE	SPECIFICATION	SOURCE
Power supply	PowerPac HC	Bio-Rad
QIAgility	Version 4.13.5	Qiagen
Real-time PCR system	QuantStudio 5 real-time PCR system	Thermo Fisher Scientific
Repetitive pipet	Repetman	Gilson
Seahorse	Seahorse XFe96 analyzer	Agilent Technologies
Standard tweezer	15.5 cm	Fine Science Tools
Standard scissor	Blunt; 13 cm	Fine Science Tools
Thermal cycler	T100	Bio-Rad
Thermo block	Thermomixer Comfort	Eppendorf
Thermocycler	7900 Fast Real Time thermocycler	Thermo Fisher Scientific
Tissue scissors	Spiky; 10.5 cm	Fine Science Tools
UV-transilluminator	UVT-28 ME Camera: EASY 440K	Herolab
UV-/Vis-spectral photometer	Nanodrop 2000c	Thermo Fisher Scientific
Vacuum concentrator	Concentrator 5301	Eppendorf
Vacuum pump	BVC 21	Vacuubrand
Volumetric flask	2000 mL; 1000 mL; 250 mL; 100 mL	Vitlab
Vortexer	RS-VA 10	Phoenix Instrument
Water bath	TW8	Julabo
Water bath	WB20	P-D Industriegesellschaft
X-ray film processor	Cawomat 2000 IR	CAWO
REAGENT or RESOURCE	SPECIFICATION	SOURCE
Disposables		
Aluminium foil	15 µm	A. Hartenstein
Adhesive film	PCR compatible	Thermo Fisher Scientific
Blotting and chromatography papers	Grade 3 mM CHR; 46 x 57 cm	Whatman

## APPENDIX

REAGENT or RESOURCE	SPECIFICATION	SOURCE
Capillary columns	PicoFrit, 30 cm x 150 µm ID	New Objective
Cell culture dish	10 cm; 6 cm Cell+ coating	Sarstedt
Cell culture microplate	Seahorse plates (96-well)	Seahorse
Cell scraper	24 cm	Techno Plastic Products
Cell strainer	40 µm	Thermo Fisher Scientific
Cover slips	Round; Diameter: 20 mM	Roth
Cover slips	24 x 60 mM	Roth
Cryo tube	1.8 mL	Sarstedt
Cryomold	Intermediate; Standard	Tissue Tek
Cuvette	10x 4 x 45 mM	Sarstedt
Falcon tube	Plastic; 15 mL; 50 mL	Sarstedt
Filter papers	185 mM	Macherey-Nagel
Filtropur	S 0.45/S 0.2	Sarstedt
Glucometer stripes	ACCU-CHEK Inform II test strips (50)	Roche
Microscope slide	Superfrost; 26 x 76 mM	Thermo Fisher Scientific
Microscope slide	26 x 76 mM	Roth
Needle	26 gauge (G) x 3/8"; 0.45 mM x 10 mM	BD Microlane™ 3
Needle	25 G x 5/8"; 0.5 x 16 mM	Neobject
Pipette	Serological; 2 mL; 5 mL; 10 mL; 25 mL	Sarstedt
Pipette boy		Gilson
Pipette filter tips	Biosphere; 20 µL; 200 µL; 1250 µL	Sarstedt
Pipette tips	20 µL; 200 µL; 1000 µL	Sarstedt
Pipette syringes	500 µL; 1250 µL; 2500 µL	VWR

APPENDIX

REAGENT or RESOURCE	SPECIFICATION	SOURCE
Immobilon-P transfer membrane ( <i>polyvinylidene fluoride</i> (PVDF))	0.45 $\mu\text{m}$	Millipore
Reaction tube	15 mL, 50 mL	Sarstedt
Reaction tube	1500 $\mu\text{L}$ , 2000 $\mu\text{L}$	Sarstedt
Reaction tube	200 $\mu\text{L}$ ; Multiply- $\mu\text{Strip}$ Pro8-Strip	Sarstedt
Reagent reservoir	50 mL; Disposable; Pre-sterile	VWR
Repetative pipette tips	(0.1, 0.5, 1.25, 2.5, 5.0 ml)	VWR
Scintillation tial	Miniature size	Perkin Elmer
Seal foil	Parafilm	Roth
Silica-matrix columns	Strata SI-1 Silica 100 mg/1 ml tubes	Phenomenex
Sterile filter	Pore size: 0.2 $\mu\text{m}$ ; 0.45 $\mu\text{m}$	Sarstedt
Super RX medical x-ray		Fujifilm
Syringe	Tuberculin; 1 mL	Chirana T. Injecta
Syringe	Omnifix; 1 mL; 5 mL; 10 mL; 20 mL	B. Braun
Syringe (ITT, GTT)	Omnican; U-100 Insulin; 1 mL/100 I.U.; 30 G x 1/2"; 0.3 mM x 12 mM	Braun
Tissue culture dishes (6 cm, 10 cm)	Cell, Cell+ coating	Sarstedt
Tissue culture flasks	Cell Coating; (T25/75)	Sarstedt
UPLC-column	Acclaim RSLC 120 C8 reversed-phase column (2.2 $\mu\text{m}$ particles, 50 x 2.1 mm)	Thermo Fisher Scientific
Well plates (6-well, 12-well)	Cell, Cell+ coating	Sarstedt



## APPENDIX

REAGENT or RESOURCE	SPECIFICATION	SOURCE
96-well plate	Nunc-Immuno; MaxiSorp	Thermo Fisher Scientific
384-well plate	MicroAmp Optical	Thermo Fisher Scientific

### 7.1.2 Reagents

REAGENT or RESOURCE	SOURCE	IDENTIFIER
Reagents and Chemicals		
Acetic acid	Roth	#3738.1
Acetonitrile	Sigma-Aldrich	#271004
Acrylamide	AppliChem	#A4989
AdipoRed dye	Lonza	#PT-7009
Agar	Sigma-Aldrich	#A1296
Agarose	Roth	#2267.4
Agencourt AMPure XP beads	Beckman Coulter	#A63881
<i>5-Aminoimidazole-4-carboxamide ribonucleotide (AICAR)</i>	Sigma-Aldrich	#A9978
Albumin fraction V	Roth	#8076.2
<i>Adenosine monophosphate (AMP)</i>	Sigma-Aldrich	#A1752
AMPK active enzyme	CycLex	#CY-SEA11
Ampicillin	Sigma-Aldrich	#A0166
Antimycin A	Sigma-Aldrich	#A8674
<i>Ammonium peroxodisulphate (APS)</i>	Roth	#9592.2
<i>Bovine serum albumin (BSA)</i>	Sigma-Aldrich	#A7030
Bromophenol blue	Roth	#A512.1
<i>Calcium chloride (CaCl<sub>2</sub>)</i>	Roth	#CN93.1
<i>Potassium acetate (CH<sub>3</sub>COOK)</i>	Sigma-Aldrich	#P1190
Chloroform	Roth	#Y015.1
Citric acid	Sigma-Aldrich	#C0759
Collagenase D	Roche	#11088858001
Coomassie brilliant blue	Sigma-Aldrich	#B0770
Crystal violet	Sigma-Aldrich	#C0775
1,2-Dioctanoyl-sn-glycerol	Sigma-Aldrich	#D5156

## APPENDIX

REAGENT or RESOURCE	SOURCE	IDENTIFIER
<i>4',6-diamidino-2-phenylindole</i> (DAPI) mounting reagent	Thermo Fisher Scientific	#P36931
D-[3-3H]-glucose	Perkin Elmer	#NET331C005 MC
DharmaFECT duo	Thermo Fisher Scientific	#T-2010-03
Distilled water (UltraPure)	Thermo Fisher Scientific	#10977-035
DNA loading dye solution, 6x	Sigma-Aldrich	#G2526
<i>2'-deoxynucleoside 5'-triphosphate</i> (dNTP) mix (100 mM each):	Thermo Fisher Scientific	
<i>2'-deoxyadenosine-5'-triphosphate</i> (dATP)		#R0142
<i>2'-deoxycytidin-5'-triphosphate</i> (dCTP)		#R0152
<i>2'-deoxyguanosine-5'-triphosphate</i> (dGTP)		#R0162
<i>2'-deoxythymidin-5'-triphosphate</i> (dTTP)		#R0172
Dry milk; fat-free	Roth	#T145.4
<i>1,4-Dithiothreitol</i> (DTT)	Sigma-Aldrich	#10197777001
1,2-Dioctanoyl-sn-glycerol	Enzo Life Sciences	#BML-DG112- 0020
<i>Enhanced chemiluminescence</i> (ECL)	Bio-Rad	#170-5061
<i>Ethylenediaminetetraacetic acid</i> (EDTA)	Roth	#8040.1
Eosin G solution	Roth	#3139.2
Ethanol; absolute	Roth	#5054.1
Ethanol; denatured	Roth	#K928.3
<i>Carbonyl cyanide-4-</i> <i>(trifluoromethoxy)phenylhydrazone</i> (FCCP)	Sigma-Aldrich	#C2920
<i>Free fatty acid</i> (FFA) standard	Wako Diagnostics	276-76491
Formalin	Sigma-Aldrich	#HT501128
Formic acid	Sigma-Aldrich	#106526

## APPENDIX

REAGENT or RESOURCE	SOURCE	IDENTIFIER
Free glycerol reagent	Sigma-Aldrich	#F6428
Gel Mount™ aqueous mounting medium	Sigma-Aldrich	#G0918
GeneRuler 100 bp DNA ladder	Thermo Fisher Scientific	#SM0241
GeneRuler 1 kp DNA ladder	Thermo Fisher Scientific	#SM0311
Glucose	Roth	#X997.2
Glycerol	Roth	#3783.1
Glycerol standard	Sigma-Aldrich	#G7793
Glycine	Roth	#3790.3
Goat serum	Sigma-Aldrich	#G9023
H <sub>2</sub> O, <i>diethylpyrocarbonate</i> (DEPC)	Thermo Fisher Scientific	#10977-035
<i>Hydrogen peroxide</i> (H <sub>2</sub> O <sub>2</sub> )	Sigma-Aldrich	#31642
<i>Hydrochloric acid</i> (HCl)	Sigma Aldrich	#30721
<i>N-2-Hydroxyethylpiperazine-N'-2-ethanesulfonic acid</i> (HEPES)	Roth	#HN78.1
Hoechst 33342 dye	Thermo Fisher Scientific	#62249
HPLC-MS solvents	Sigma-Aldrich	
Hydrophobic pen; Roti®-Liquid barrier marker	Roth	#AN91.1
Immersion liquid type G	Leica	#11513910
Insulin (100 I.E./mL)	Sanofi Aventis	Insuman rapid
Iodoacetamide	Sigma Aldrich	#144489
Isopropanol	Roth	#CP41.3
Kanamycin sulfate	Sigma-Aldrich	#K1377
<i>Potassium chloride</i> (KCl)	Sigma-Aldrich	#P9333
<i>Potassium bicarbonate</i> (KHCO <sub>3</sub> )	Sigma-Aldrich	#237205
LC-MS formic acid (98-100%)	Sigma-Aldrich	#5.33002
Mayer's hematoxylin solution	Sigma-Aldrich	#MHS16
<i>Magnesium chloride</i> (MgCl <sub>2</sub> )	Roth	#KK36.1
<i>Magnesium sulfate</i> (MgSO <sub>4</sub> )	Sigma-Aldrich	#M2643
Methanol	Roth	#4627.3
Midori green advanced DNA stain	Nippon Genetics	#MG04

## APPENDIX

REAGENT or RESOURCE	SOURCE	IDENTIFIER
MitoTracker red CMXRos	Thermo Fisher Scientific	#M7512
Mounting medium; Roti®-Mount	Roth	#HP68.1
<i>Sodium chloride</i> (NaCl)	Roth	#3957.1
<i>Sodium citrate</i> (Na <sub>3</sub> C <sub>6</sub> H <sub>5</sub> O <sub>7</sub> )	Sigma-Aldrich	#W302600
<i>Sodium azide</i> (NaN <sub>3</sub> )	Roth	#4221.1
<i>Sodium hydroxide</i> (NaOH)	Roth	#P031.1
NEBNext multiplex oligos for Illumina	NEB	#E7335
<i>Ammonium chloride</i> (NH <sub>4</sub> Cl)	Sigma-Aldrich	#A9434
<i>Ammonium bicarbonate</i> (NH <sub>4</sub> HCO <sub>3</sub> )	Sigma-Aldrich	#09830
<i>Nonidet P-40</i> (NP-40)	Sigma-Aldrich	#74385
NuPAGE® <i>lithium dodecyl sulfate</i> (LDS) sample buffer	Thermo Fisher Scientific	#NP0007
NuPAGE™ MOPS SDS running buffer (20X)	Thermo Fisher Scientific	#NP0001
NuPAGE® Novex® 4-12% Bis-Tris gels	Thermo Fisher Scientific	#NP0321PK2
O.C.T compound	Tissue Tek	#4583
Oil Red O	Sigma-Aldrich	#O0625
Oligomycin	Calbiochem	#495455
PageRuler® prestained protein ladder	Thermo Fischer Scientific	#26619
<i>Phosphate-buffered saline</i> (PBS)	Sigma-Aldrich	#P3813
PCR buffer	Sigma-Aldrich	#P2192
<i>Paraformaldehyde</i> (PFA)	Roth	#0335.2
Pierce anti-c-Myc magnetic beads	Thermo Fisher Scientific	#88842
Pierce™ lane marker non-reducing Sample buffer	Thermo Fisher Scientific	#39001
Polybrene	Sigma-Aldrich	#H9268
PowerUp™ SYBR™ green master mix	Thermo Fischer Scientific	#A25742
<i>Protease phosphatase inhibitor</i> (PPI) cocktail (100x)	Thermo Fisher Scientific	#1861281

## APPENDIX

REAGENT or RESOURCE	SOURCE	IDENTIFIER
Proteinase K	Thermo Fisher Scientific	#EO0491
QIAzol lysis reagent	Qiagen	#79306
Quick start Bradford protein assay	Bio-Rad	#5000201
ReproSil-Pur 120 C18-AQ, 1.9 $\mu$ m	Dr. Maisch	#r119.b9
Rotenone	Sigma-Aldrich	#R8875
Scintillation fluid	Zinsser Analytic	#1008000
<i>Sodium dodecyl sulfate</i> (SDS) pellets	Roth	#CN30.2
Simply Blue™ safe stain	Thermo Fisher Scientific	#LC6060
Taq DNA polymerase	Thermo Fisher Scientific	#EP0282
<i>Tetramethylethylenediamine</i> (TEMED)	Carl Roth	#2367.1
Trichloromethan/Chloroform	Roth	#Y015.1
Triglyceride reagent	Sigma-Aldrich	#T2449
TRIS base	Roth	#AE15.4
Triton X	Roth	#3051.3
Trypton/Pepton aus casein	Roth	#8952.2
Tween 20	Roth	#9127.1
UltraPure™ distilled water (Dnase/Rnase Free)	Thermo Fisher Scientific	#10977-035
Xylol	Roth	#9713.3
Yeast extract	AppliChem	#A1552.1
$\beta$ -mercaptoethanol	Sigma-Aldrich	#M3148
<b>Cell Culture materials</b>		
Accutase	Sigma-Aldrich	#A6946
<i>Adenosine diphosphate</i> (ADP)	Sigma-Aldrich	#01905
<i>Adenosine triphosphate</i> (ATP)	Sigma-Aldrich	#A2383
Blastcidin	InvivoGen	#ant-bl-1
<i>Bovine serum albumine</i> (BSA)	Sigma-Aldrich	#A8806
Carbachol	Tocris	#2810
CID 755673	Tocris	#3327
CRT 0066101	Tocris	#4975
Dexamethasone	Sigma-Aldrich	#D2915

APPENDIX

REAGENT or RESOURCE	SOURCE	IDENTIFIER
<i>Dulbecco's modified eagle media</i> (DMEM) (-glucose, -glutamine, -phenol red)	Thermo Fisher Scientific	#A1443001
DMEM (1 g/L D-glucose, -glutamine, -phenol red)	Thermo Fisher Scientific	#11880-028
DMEM (1 g/L D-glucose, 1 mM sodium pruvate, 4.0 mM glutamine)	Thermo Fisher Scientific	#31885-023
DMEM (4.5 g/L D-glucose, 1 mM sodium pyruvate, 4.0 mM glutamine)	Thermo Fisher Scientific	#31966-021
DMEM/F-12Ham + GlutaMAX	Thermo Fisher Scientific	#31331-028
<i>Dimethylsulfoxide</i> (DMSO)	Sigma-Aldrich	#D8418
<i>Dulbecco's phosphate-buffered saline</i> (DPBS)	Thermo Fisher Scientific	#14190-094
<i>Foetal bovine serum</i> (FBS)	Thermo Fisher Scientific	#10270-106
<i>Foetal calf serum</i> (FCS)	ATCC	#62262399
Fibroblast basal medium	ATCC	#PCS-201-030
Gentamicin (10 mg/mL)	Thermo Fisher Scientific	#15710-049
Glucose solution (200 g/L)	Thermo Fisher Scientific	#A24940-01
GlutaMAX (100x)	Thermo Fisher Scientific	#35050-061
<i>3-Isobutyl-1-methylxanthine</i> (IBMX)	Sigma-Aldrich	#I5879
Indomethacin	Sigma-Aldrich	#I7378
Insulin solution human (10 mg/mL)	Sigma-Aldrich	#I9278
Isoproterenol hydrochloride	Sigma-Aldrich	#1351005
Matrigel membrane matrix	VWR	#734-0270
<i>Nonessential amino acids</i> (NEAA) (100x)	Thermo Fisher Scientific	#11140-050
Opti-MEM	Thermo Fisher Scientific	#31985-047
Penicillin/Streptomycin/Amphotericin (10000 U/mL/10 mg/mL/25 µg/mL) B solution	ATCC	#PCS-999-002

APPENDIX

REAGENT or RESOURCE	SOURCE	IDENTIFIER
<i>Penicillin/Streptomycin</i> (P/S) (10000 U/mL/10000 µg/mL)	Thermo Fisher Scientific	#15140-122
Polybrene	Sigma-Aldrich	#TR-1003
Puromycine (10mg/mL)	Thermo Fisher Scientific	#A11138-03
<i>Roswell Park Memorial Institute</i> (RPMI) 1640	US Biological Life Sciences	#R9010-01
Serotonin	Sigma-Aldrich	#14927
<i>Sodium pyruvate</i> (SP) (100 mM)	Thermo Fisher Scientific	#11360-039
<i>3,3',5-Triiodo-L-thyronine sodium salt</i> (T3)	Sigma-Aldrich	#T6397
Trypan blue stain	Thermo Fisher Scientific	#15250-061
0.05% Trypsin-EDTA	Thermo Fisher Scientific	#25300-054
Trypsin-EDTA for primary cells	ATCC	#PCS-999-003
Trypsin neutralizing solution	ATCC	#PCS-999-004
<b>Antibodies</b>		
Acetyl-CoA Carboxylase (C83B10) Rabbit mAb	Cell Signaling Technology	#3676
Alexa Fluor® 488 AffiniPure Donkey Anti-Chicken IgY	Jackson Immuno Research	#703-545-155
AMDEX™ Goat Anti Rabbit IgG Horseradish Peroxidase Conjugate	Sigma-Aldrich	#GERPN4301
AMDEX™ Sheep Anti Mouse IgG-HRP	Sigma-Aldrich	#GERPN4201
AMPKα (D5A2) Rabbit mAb	Cell Signaling Technology	#5831
Anti-β-3 Adrenergic Receptor antibody	Abcam	#ab59685
Anti-heavy chain Myosin antibody	Abcam	#124205
Anti-PRDM16 antibody	Abcam	#ab106410
Anti-UCP1 antibody	Abcam	#ab10983
ATGL (30A4) Rabbit mAb	Cell Signaling Technology	#2439

## APPENDIX

REAGENT or RESOURCE	SOURCE	IDENTIFIER
C/EBP $\alpha$ (D56F10) Rabbit mAb	Cell Signaling Technology	#8178
C/EBP $\beta$ (LAP) Ab	Cell Signaling Technology	#3087
C/EBP $\delta$ Rabbit Ab	Cell Signaling Technology	#2318
ERR $\alpha$ (E1G1J) Rabbit mAb	Cell Signaling Technology	#13826
GAPDH Rabbit Ab	Sigma-Aldrich	#G9545
HSL Rabbit Ab	Cell Signaling Technology	#4107
Myc-Tag (9B11) Mouse mAb	Cell Signaling Technology	#2276
Perilipin (D1D8) Rabbit mAb	Cell Signaling Technology	#9349
PGC-1 $\alpha$ (3G6) Rabbit mAb	Cell Signaling Technology	#2178
Phospho-Acetyl-CoA Carboxylase (Ser79) (D7D11) Rabbit mAb	Cell Signaling Technology	#11818
Phospho-Akt (Ser473) Rabbit Ab	Cell Signaling Technology	#4058
Phospho-Akt (T308) Rabbit Ab	Cell Signaling Technology	#2965
Phospho-AMPK $\alpha$ 1 (Ser485) /AMPK $\alpha$ 2 (Ser491) Rabbit Ab	Cell Signaling Technology	#4185
Phospho-AMPK $\alpha$ (Thr172) (40H9) Rabbit mAb	Cell Signaling Technology	#2535
Phospho-AMPK Substrate Motif [LXRXX(pS/pT) MultiMab™ Rabbit mAb	Cell Signaling Technology	#5759
Phospho-ATF-2 (Thr71) (11G2) Rabbit mAb	Cell Signaling Technology	#5112



## APPENDIX

REAGENT or RESOURCE	SOURCE	IDENTIFIER
Phospho-C/EBP $\beta$ (Thr235) Ab	Cell Signaling Technology	#3084
Phospho-CREB (Ser133) (87G3) Rabbit mAb	Cell Signaling Technology	#9198
Phospho-CtBP1/CtBP2 (Ser158, Ser164) Polyclonal Antibody	Thermo Fisher Scientific	#PA5-64665
Phospho-FoxO1 (Ser256) Ab	Cell Signaling Technology	#9461
Phospho-mTOR (Ser2448) Ab	Cell Signaling Technology	#2971
Phospho-p70 S6 Kinase (Thr389) Ab	Cell Signaling Technology	#9205
Phospho-PKD/PKC $\mu$ (Ser916) Rabbit Ab	Cell Signaling Technology	#2051
Phospho PKD/PKC $\mu$ (Ser744/748) Rabbit Ab	Cell Signaling Technology	#2054
Phospho-(Ser/Thr) PKD Substrate Ab	Cell Signaling Technology	#4381
Phospho-Rb (Ser807/811) (D20B12) Rabbit mAb	Cell Signaling Technology	#8516
PKD/PKC $\mu$ Rabbit Ab	Cell Signaling Technology	#2052
PKD2 (D1A7) Rabbit mAb	Cell Signaling Technology	#8188
PKD3/PKC $\nu$ (D57E6) Rabbit mAb	Cell Signaling Technology	#5655
PPAR $\gamma$ (81B8) Rabbit mAb	Cell Signaling Technology	#2443
Raptor (24C12) Rabbit mAb	Cell Signaling Technology	#2280
Rictor (53A2) Rabbit mAb	Cell Signaling Technology	#2114

## APPENDIX

REAGENT or RESOURCE	SOURCE	IDENTIFIER
SignalStain® Boost ICH Detection Reagent (HRP, Rabbit)	Cell Signaling Technology	#8114
$\alpha$ -Tubulin Rabbit Ab	Cell Signaling Technology	#2144
$\beta$ -Actin Mouse mAb	Sigma-Aldrich	#A5441
<b>Biological Samples</b>		
Human blood and subcutaneous adipose tissue	Department of Internal Medicine University Hospital of Salamanca	N/A
<b>Critical Commercial Assays</b>		
Adipocyte Differentiation ToolKit for AdiposeDerived MSCs and Preadipocytes	ATCC	#PCS-500 050
AMPK Kinase Assay Kit	CycLex	#CY-1182
Bio-Plex Pro Mouse Diabetes 8-plex Assay	Bio-Rad	#171-F7001M
Bio-Plex Pro Mouse Diabetes Adiponectin Assay	Bio-Rad	#171-F7002M
DNeasy Blood & Tissue Kit	Qiagen	#69504
Experion RNA StdSens Analysis Kit	Bio-Rad	#700-7103
Fast Start Tag DNA Polymerase	Roche	#12032929001
Fibroblast Growth Kit	ATCC	#PCS-201-041
First Strand cDNA Synthesis Kit	Thermo Fisher Scientific	#K1612
Library Prep Kit	NEB	#E7530S
NEFA Kit:	Wako	
NEFA-HR(2) R1 Set		#434-91795
NEFA-HR(2) R2 Set		#436-91995
NEBNext® Poly(A) mRNA Magnetic Isolation Module	NEB	#E7490S
NucleoBond® Xtra Midi	Macherey-Nagel	#740410.50
NucleoSpin® Gel and PCR Clean-up	Macherey-Nagel	#740609.250
NucleoSpin® Plasmid	Macherey-Nagel	#740588.250

## APPENDIX

REAGENT or RESOURCE	SOURCE	IDENTIFIER
PWO Master	Roche	#03789403001
RNeasy Plus Universal Tissue Mini Kit	Qiagen	#73404
Seahorse XF Cell Mito Stress Test	Agilent Technologies	#103015-100
SignalStain® DAB Substrate Kit	Cell Signaling Technology	#8059
TaqMan Gene Expression Assay	Thermo Fisher Scientific	#4331182
<b>Molecular cloning</b>		
Competent TOP10 E. coli	Thermo Fisher Scientific	
Restriction enzymes	NEB	
T4-DNA ligase	Thermo Fisher Scientific	
<b>Deposited Data</b>		
RNA sequencing data	This paper	GSE104797
<b>Experimental Models: Cell lines</b>		
3T3-L1	ATCC	
<i>Human embryonic kidney</i> (HEK) 293	Generous gift from Prof. Dr. Eilers	
Human subcutaneous preadipocytes <i>Platinum</i> (Plat)-E	ATCC	#PCS-210-010
	Generous gift from Prof. Dr. Eilers	
T37i	Generous gift from Dr. Lombes	
<b>Experimental Models: Organisms/Strains</b>		
B6;129S-Prkd1tm1Eno/J	The Jackson Laboratory	#014181
B6;FVB-Tg(Adipoq-cre)1Evdr/J (adiponectin Cre)	The Jackson Laboratory	#010803
Tg(Adipoq-cre/ERT2)1Soff	The Jackson Laboratory	#025124
<b>Oligonucleotides</b>		
Primers used for genotyping in this study	Custom primers, purchased from Eurofins	
<i>PRKD1</i> (TaqMan probe)	Thermo Fischer Scientific	Assay-ID: Hs00177037_m1

## APPENDIX

REAGENT or RESOURCE	SOURCE	IDENTIFIER
Real-time PCR primers used in this study siRNA (listed in 2.2.3.1)	Custom primers, purchased from Eurofins Thermo Fischer Scientific	
<b>Recombinant DNA</b>		
Packaging plasmid psPax	Adgene plasmid; gift from Didier Trono	# 12260
Packaging plasmid pMD2.G	Adgene plasmid; gift from Didier Trono	# 12259
pBabe-Puro	Cell Biolabs, Inc.	#RTV-001- PURO
pGIPZ shRNAmir	Thermo Fisher Scientific	N/A
<b>Software and Algorithms</b>		
DAVID functional annotation tool	NIH, Open source	<a href="https://david.ncifcrf.gov/">https://david.ncifcrf.gov/</a>
Illustrator CS6	Adobe	N/A
ImageJ	National Institutes of Health (NIH)	<a href="https://imagej.nih.gov/ij/">https://imagej.nih.gov/ij/</a>
MaxQuant version 1.6.2.2 [Trace finder software]	Thermo Fischer Scientific	
<b>Other</b>		
<i>High-Fat Diet</i> (HFD) with 58 kcal% fat w/sucrose	ResearchDiets	#D12331
Normal chow diet	sniff Spezialdiäten GmbH, Germany	#V1125-3

All unstated chemicals were purchased from AppliChem (Darmstadt, Germany), Sigma-Aldrich (Steinheim, Germany) or Roth (Karlsruhe, Germany).

**7.1.3 Media**3T3-L1 maintenance medium

DMEM (4.5 g/L D-Glucose)

FCS 10%

Gentamicin 40 µg/mL

3T3-L1 differentiation induction medium

DMEM (4.5 g/L D-Glucose)

FBS 10%

IBMX (100 mM stock) 0.5 mM

Dexamethasone (5 mM stock) 1 (µM)

Insulin 1.5 µg/mL

Gentamicin 40 µg/mL

3T3-L1 differentiation medium

DMEM (4.5 g/L D-Glucose)

FBS 10%

Insulin 1.5 µg/mL

Gentamicin 40 µg/mL

Freezing medium

DMEM (4.5 g/L D-Glucose)

FCS 20%

DMSO 10%

HEK/Plat-E medium

DMEM (4.5 g/L D-Glucose)

FBS 10%

P/S 1%

## APPENDIX

---

### Human subcutaneous preadipocyte maintenance medium

Fibroblast basal medium

<i>Recombinant human fibroblast growth factor</i> (rh FGF) $\beta$	5 ng/mL
L-glutamine	7.5 mM
Ascorbic acid	50 $\mu$ g/mL
Hydrocortisone hemisuccinate	1 $\mu$ g/mL
rh Insulin	5 $\mu$ g/mL
FBS	2%
Penicillin	10 Units/mL
Streptomycin	10 $\mu$ g/mL
Amphotericin B solution	25 ng/mL

### Human subcutaneous preadipocyte differentiation induction medium

Adipocyte basal medium

<i>Adipocyte differentiation</i> (AD) supplement	6.7%
Penicillin	10 Units/mL
Streptomycin	10 $\mu$ g/mL
Amphotericin B solution	25 ng/mL

### Human subcutaneous preadipocyte differentiation medium

Adipocyte basal medium

<i>Adipocyte differentiation maintenance</i> (ADM) supplement	17.6%
Penicillin	10 Units/mL
Streptomycin	10 $\mu$ g/mL
Amphotericin B solution	25 ng/mL

### *Lysogeny broth* (LB) medium, pH 7.0

Trypton/Pepton from casein	10 g/L
Yeast extract	5 g/L
NaCl	171 mM

### LB plates

LB medium	
Agar	15 g/L

## APPENDIX

---

### Serum starvation medium (cells)

DMEM (4.5 g/L D-Glucose)

BSA 0.5%

### Serum starvation medium (explants)

DMEM (1 g/L D-Glucose)

BSA 0.5%

### SVC maintenance medium (BAT)

DMEM/F-12

FBS 10%

NEAA 1%

SP 1%

P/S 1%

T3 (100 mM stock) 100 nM

Insulin 1.5 µg/mL

### SVC differentiation induction medium (BAT)

DMEM/F-12

FBS 10%

NEAA 1%

SP 1%

IBMX (100 mM stock) 0.5 mM

Indomethacin (1 mM stock) 0.2 µM

Dexamethasone (5 mM stock) 1 µM

Insulin 1.5 µg/mL

T3 (100 mM stock) 100 nM

P/S 1%

## APPENDIX

---

### SVC differentiation medium (BAT)

DMEM/F-12	
FBS	10%
NEAA	1%
SP	1%
Insulin	1.5 µg/mL
T3 (100 mM stock)	100 nM
P/S	1%

### SVC maintenance medium sWAT

DMEM/F-12	
FBS	10%
NEAA	1%
SP	1%
P/S	1%

### SVC differentiation induction medium (sWAT)

DMEM/F-12	
FBS	10%
NEAA	1%
SP	1%
IBMX (100 mM stock)	0.5 mM
Indomethacin (1 mM stock)	0.2 µM
Dexamethasone (5 mM stock)	1 µM
Insulin	1.5 µg/mL
P/S	1%

### SVC differentiation medium (sWAT)

DMEM/F-12	
FBS	10%
NEAA	1%
SP	1%
Insulin	1.5 µg/mL
P/S	1%



## APPENDIX

---

### T37i maintenance medium

DMEM/F-12	
FCS	10%
Gentamicin	40 µg/mL

### T37i differentiation medium

DMEM/F-12	
FCS	10%
Gentamicin	40 µg/mL
T3 (100 mM stock)	100 nM
Insulin	2 nM
Gentamicin	40 µg/mL

### **7.1.4 Buffers**

If not stated otherwise, all buffers were prepared in *distilled, deionized water* (ddH<sub>2</sub>O) obtained from a MilliQ Water Purification System. pH was adjusted with HCl or NaOH.

#### Blocking buffer (WB)

*Tris buffered saline with tween* (TBST)

BSA or fat-free dry milk	5%
--------------------------	----

#### Blocking buffer (IF)

PBS	
BSA	0.5%
Goat serum	20%

#### Coomassie staining solution

Acetic acid	10%
Methanol	40%
Coomassie Brilliant blue	0.01%

#### Coomassie destaining solution

Acetic acid	10%
Methanol	40%

## APPENDIX

---

### Crystal violet staining solution

Crystal violet (90% dye content)	2%
Ethanol	20%

### Digestion buffer (SVF isolation)

PBS	
Collagenase D	2 mg/mL
CaCl <sub>2</sub>	5 mM
BSA	1%

### Fixation solution

PFA	4%
-----	----

### IP-buffer

TRIS, pH 7.5 (1 M stock)	20 mM
NaCl (5 M stock)	150 mM
NP-40	0.5%
Glycerol	5%
DTT (1 M stock)	1 mM

→ 100x PPI was added fresh before usage

### IP-wash buffer

TRIS, pH 7.5 (1 M stock)	20 mM
NaCl (5 M stock)	150 mM
NP-40	0.5%

→ 100x PPI was added fresh before usage

### Laemmli buffer (SDS-PAGE)

TRIS, pH 6.8 (2 M stock)	300 mM
SDS	10%
Glycerol	50%
β-mercaptoethanol	25%
Bromophenolblue	spatual tip

## APPENDIX

---

### Lysis buffer (DNA Extraction)

TRIS, pH 8.5 (1.5 mM stock)	100 mM
EDTA (0.5 M stock)	5 mM
NaCl (5 M stock)	200 mM
SDS (20% stock)	0.2%

→ 0.1 mg/mL Proteinase K was added freshly before usage

### Lysis buffer (WB)

TRIS, pH 7.5 (1 M stock)	20 mM
NaCl (5 M stock)	150 mM
β-glycerophosphate	20 mM
MgCl	5 mM
Glycerol	5%
NP40	0.2%
Triton X-100	0.2%

→ 100x PPI was added fresh before usage

### 10x Running/Transfer buffer

TRIS	250 mM
Glycine	1.92 M

### 1x Running buffer

10x Running/Transfer buffer	10%
SDS (20% stock)	0.5%

### Sodium citrate buffer, pH 6

Sodium citrate (0.1 M stock)	8.2%
Citric acid (0.1 M stock)	1.8%

### 50x Tris-acetate-EDTA (TAE)

TRIS	2 mM
Acetic acid	5.7%
EDTA (0.5 M stock)	10%

### 1x TAE

50x TAE	2%
---------	----

## APPENDIX

---

### TRIS-EDTA (TE) buffer, pH 8

TRIS, pH 7.5 (1 M stock)	10 mM
EDTA (0.5 M stock)	1 mM

### 1x Transfer buffer

10x Running/Transfer buffer	10%
Methanol	20%

### 10x Tris-buffered saline (TBS), pH 7.6

TRIS	0.2 M
NaCl	1.4 M

### 1x TBS

10x TBS	10%
---------	-----

### 1x TBST

10x TBS	10%
Tween 20	0.1%

### 10% separating gel (WB – 20 mL)

ddH <sub>2</sub> O	9.8 mL
TRIS, pH 8.6 (1.5 mM stock)	5 mL
Acrylamide (40% stock)	5 mL
SDS (20% stock)	100 µL
APS (10% stock)	200 µL
TEMED	20 µL

### 12% separating gel (WB – 20 mL)

ddH <sub>2</sub> O	8.8 mL
TRIS, pH 8.6 (1.5 mM stock)	5 mL
Acrylamide (40% stock)	6 mL
SDS (20% stock)	100 µL
APS (10% stock)	200 µL
TEMED	20 µL

## APPENDIX

---

### 4% stacking gel (WB – 10 mL)

ddH <sub>2</sub> O	8.2 mL
TRIS, pH 8.6 (1.5 mM stock)	620 µL
Acrylamide (40% stock)	946 µL
SDS (20% stock)	50 µL
APS (10% stock)	100 µL
TEMED	10 µL

### **7.1.5 Real time PCR primers**

#### Acc:

Acc fwd: 5' – GACAGACTGATCGCAGAGAAAG – 3'

Acc rev: 5' – TGGAGAGCCCCACACACA – 3'

#### Adrb3:

Adrb3 fwd: 5' – GATCTGGTCATGGGATTGCT – 3'

Adrb3 rev: 5' – AAGTCCAGAGCTCGCAGAAG – 3'

#### Bmp7:

Bmp7 fwd: 5' – ACGGACAGGGCTTCTCCTAC – 3'

Bmp7 rev: 5' – ATGGTGGTATCGAGGGTGGAA – 3'

#### Cebpa:

Cebpa fwd: 5' – AAACAACGCAACGTGGAGA – 3'

Cebpa rev: 5' – GCGGTCATTGTCACTGGTC – 3'

#### Cebpδ:

Cebpδ fwd: 5' – TCAAATCCCTGCCCAAAGTG – 3'

Cebpδ rev: 5' – CTGCAGAGGGCAAAGATCAC – 3'

#### Chrebp:

Chrebp fwd: 5' – GTTCAGCATCCTCATCCGAC – 3'

Chrebp rev: 5' – GGAAGTGCTGAGTTGGCGAAG – 3'

## APPENDIX

---

### Cidea:

Cidea fwd: 5' – TGACATTCATGGGATTGCAGAC – 3'

Cidea rev: 5' – GGCCAGTTGTGATGACTAAGAC – 3'

### Cideb:

Cideb fwd: 5' – CAATGGCCTGCTAAGGTCAGT – 3'

Cideb rev: 5' – GATCACAGACACGGAAGGGTC – 3'

### Cidec:

Cidec fwd: 5' – ATGGACTACGCCATGAAGTCT – 3'

Cidec rev: 5' – CGGTGCTAACACGACAGGG – 3'

### Ckm:

Ckm fwd: 5' – CAGCACAGACAGACACTCAGG – 3'

Ckm rev: 5' – GAA CTT GTT GTG GGT GTT GC – 3'

### Ckmt2:

Ckmt2 fwd: 5' – GCATGGTGGCTGGTGATGAG – 3'

Ckmt2 rev: 5' – AAA CTG CCC GTG AGT AAT CTT – 3'

### Creb:

Creb fwd: 5' – TCGTGCCAGTGCGAGTGT – 3'

Creb rev: 5' – AGCCACGCGGGATGC – 3'

### Dgat:

Dgat fwd: 5' – GTGCCATCGTCTGCAAGATT – 3'

Dgat rev: 5' – CTGGATAGGATCCACCAGGA – 3'

### Fasn:

Fasn fwd: 5' – GGAGGTGGTGATAGCCGGTAT – 3'

Fasn rev: 5' – TGGGTAATCCATAGAGCCCAG – 3'

### Lpl:

Lpl fwd: 5' – GGGAGTTTGGCTCCAGAGTTT – 3'

Lpl rev: 5' – TGTGTCTTCAGGGGTCCTTAG – 3'

## APPENDIX

---

### Mck:

Mck fwd: 5' – GCAAGCACCCCAAGTTTGA – 3'

Mck rev: 5' – ACCTGTGCCGCGCTTCT – 3'

### Mt-CO1:

Mt-CO1 fwd: 5' – TGCGCCGCAGGCATTAC – 3'

Mt-CO1 rev: 5' – GGGTGCCCAAAGAATCAGAAC – 3'

### Myf5:

Myf5 fwd: 5' – CAGCCCCACCTCCAAGT – 3'

Myf5 rev: 5' – GGGACCAGACAGGGCTGTTA – 3'

### Myg:

Myg fwd: 5' – AGCGCAGGCTCAAGAAAGTGAATG – 3'

Myg rev: 5' – CTGTAGGCGCTCAATGTACTGGAT – 3'

### Myh1:

Myh1 fwd: 5' – TCTGCAGACGGAGTCAGGT – 3'

Myh1 rev: 5' – TTGAGTGAATGCCTGTTTGC – 3'

### Myh2:

Myh2 fwd: 5' – AAAGCTCCAAGGACCCTCTT – 3'

Myh2 rev: 5' – AGCTCATGACTGCTGAACTCAC – 3'

### Ndufv:

Ndufv fwd: 5' – CTTCCCCACTGGCCTCAAG – 3'

Ndufv rev: 5' – CCAAACCCAGTGATCCAGC – 3'

### Pgc-1α:

Pgc-1α fwd: 5' – AGCGCCGTGTGATTTACGTT – 3'

Pgc-1α rev: 5' – CCGCAGATTTACGGTGCATT – 3'

### Pkd1 Ex.1-2:

Pkd1 Ex.1-2 fwd: 5' – GGGGGCATCTCGTTCCATC – 3'

Pkd1 Ex.1-2 rev: 5' – GTGCCGAAAAAGCAGGATCTT – 3'

## APPENDIX

---

### Pkd1 Ex.16-17:

Pkd1 Ex.16-17 fwd: 5' – CCCTCAGGTGAAGCTCTGTG – 3'

Pkd1 Ex.16-17 rev: 5' – ACTTCAGGTGCCAGGTATGC – 3'

### Pkd1 seq3:

Pkd1 seq3 fwd: 5' – CCGTGAGAAGAGGTCAAATTCG – 3'

Pkd1 seq3 rev: 5' – GTGGCACCTTCACCTTAGACA – 3'

### Ppara:

Ppara fwd: 5' – AACATCGAGTGTCTGAATATGTGG – 3'

Ppara rev: 5' – CCGAATAGTTCGCCGAAAGAA – 3'

### Pparγ:

Pparγ fwd: 5' – GGAAGACCACTCGCATTCCCTT – 3'

Pparγ rev: 5' – GTAATCAGCAACCATTGGGTCA – 3'

### Prdm16:

Prdm16 fwd: 5' – CCACCAGCGAGGACTTCAC – 3'

Prdm16 rev: 5' – GGAGGACTCTCGTAGCTCGAA – 3'

### Rpl13a:

Rpl13a fwd: 5' – CCCTCCACCCTATGACAAGA – 3'

Rpl13a rev: 5' – GCCCCAGGTAAGCAAACCTT – 3'

### Scl6a8:

Scl6a8 fwd: 5' – TGCATATCTCCAAGGTGGCAG – 3'

Scl6a8 rev: 5' – CTACAAACTGGCTGTCCAGA – 3'

### Screbp1:

Screbp1 fwd: 5' – GGAGCCATGGATTGCACATT – 3'

Screbp1 rev: 5' – GGCCCGGGAAGTCACTGT – 3'

### Screbp2:

Screbp2 fwd: 5' – GCGTTCTGGAGACCATGGA – 3'

Screbp2 rev: 5' – ACAAAGTTGCTCTGAAAACAAATCA – 3'





## APPENDIX

gacctgaaatgacctgtgcttattgaactaaccaatcagttcgtctctgcttctgtcgcgcttctgctccccgagctcaataaaagagcccacaacccctcactcggggcgcc  
agtctccgattgactgagtcgcccgggtaccctgtatccaataaacctcttcagttgcatccgactgtggtctcgtctctgggaggtctctctgagtgattgactaccgctc  
agcgggggtcttccattccgactgtggtctcgtccttgggaggtctctctgagtgattgactaccgctcagcgggggtctcactgagcagatgatacaaaalttggttttttt  
taagtattacattaaatggccatagttgcattaatgaatcgccaacgcgaggggagaggggttgcgtattggcgtcttccgctctcgtcactgactcgtcgtcggctgctt  
ggctgcgggagcgggtatcagctcactcaaagcggtatcacagaatcaggggataacgcaggaaagaacatgtgagcaaaaggccagcaaaaggccagga  
accgtaaaaggccggtgctggcgttttccataggtcctcccccctgacgagcatcacaataacgacgctcaagtcagagggtggcgaacccgacagggactataagata  
ccaggcgtttccccctggaagctccctcgtcgtcctctctgtccgacctgcccgttaccggataacctgccccttctccctcgggaagcgtggcgttttctcatagctcacgctgag  
gtatctcagttcgtgtaggtcgtcctcaagctgggtgtgtgcacgaacccccgttaccgcccagcctcgtcgtcctatccgtaactatcgtctgagccaacccgtaagaca  
cgactatcggcactggcagcagccactgtaacaggattagcagagcgggtatgtaggcgtgctacagagttctgaagtggtggcctaactacggctactactagaaggacag  
tatttgatctcgtcgtcgtgaaagccagttacctcgaaaaagagttggtagctctgacggcaaaacacaccgctgtagcgggtgtttttttgttgcaagcagcagattacg  
cgcagaaaaaaaggatcacaagaagatccttctcttctacgggtgtgacgctcagtggaacgaaaaactcagtttaagggtttgtcatgagattataaaaggatctctac  
ctagatccttttaaaaaatgaagtttgcggccgcaaatcaatctaaagtatatagtaaaactgtgctgacagttaccaatgcttaacagtgaggcacctatctcagcagctgt  
ctatttcttcatcatagttgctgactccccgctgtagataactacgatacgggaggggttaccatctgccccagtgctgcaatgataccgagaccacgctcaccggctcca  
gattatcagcaataaacagccagccggaaggccgagcgcagaagtggtcctgcaacttaccgctccatccagcttataattgttccgggaagctagagtaagtagttcgc  
cagtaataagtttgcgaacgttggccattgctacaggcatcgtggtgtcagctcgtctgttggtagtgcctcattcagctcgggtcccaacgatcaaggcaggttacctatccccca  
tgttggtcagaaaaagcggtagctctcggctcccgactggtgcagaagtaagttggcgcagtggttactcactatggttagcagcactgataatctcttactgtcatgccatccgt  
aagatgcttttctgactggtgagtagtaaccaagtcattctgagaatagtgatgctgagcggcagcaggtgctctgcccggcgtcaacacgggataataccgcccacatagcaga  
acttaaaagtgctcatcattgaaaacgttctcggggcgaactcctaaggatcttaccgctgtgagatccagttcagtgatgtaaccactcgtgacccaactgatctcagcatcttt  
acttaccagcgtttcgggtgagcaaaaacaggaaggcaaaatgccgcaaaaaagggaataaggcgcacacgaaatgtgaatactcactcttcttctcaatattattgaa  
gcatattcaggggtattgtctatgagcgggatacatattgaaatgattgaaaaataaacaataaggggttccgcgacatttccccgaaaagtgccac

### multiple cloning site

#### Myc

#### pBabepuro PKD1 wt:

ctcagcctgaatattggccaacagggatctgtgtaagcagttcgtccccggctcagggccaagaacagatggaacagctgaatattggccaacagggatctgtgtaaa  
gcagttcgtccccggctcagggccaagaacagatgtccccagatgctgctccagcctcagcagttctagagaacacatcagatgttccaggggtcccccaaggactgaaatga  
ccctgctcctatttgaactaaccaatcagttcgtctcgtcttctgtcgcgcttctgctccccgagctcaataaaagagcccacaacccctcactcggggcgccagctccgattga  
ctgagtcgcccgggtaccctgtatccaataaacctcttcagttgcatccgactgtggtctcgtctccttgggaggggtcctctgagtgattgactaccgctcagcgggggtcttc  
atttgggggtcgtcgggatcgggagaccctgccagggaccaccgaccaccgggaggttaagctggccaactatctgtgctgctcggatgtctagtgctatgactg  
attttatgcctcgtcgtgactagtttagtaactagctctgtatctgcccggaccctgggtggaactgacgagttctgaacacccggccgaacccctgggagacgtcccagggacttt  
gggggcccgttttggcccagcctgaggaaggagtcgatgtggaatccgaccccgtcaggatattggttctggttaggagacgagaacctaacaacagttcccgcctcgtgtaa  
ttttgcttctggttgaaccgaagcgcgctctgtctcgtcagcatcgttctgttctgtcgtcactggttctgtatttctgtaaattagggccagactgttaccactcccttaagt  
ttgacctagatcaggaagatgctgagcggctcgtcacaaccagtcggtatgtaagaagagacgttgggttacctctgctcgcagaatggcaaccttaacgtcggatg  
gcccgcagcggcaccttaaccgagacctcatcaccaggttaagatcaaggtctttcacctggcccgtgacacccagaccaggtcccacatcgtgacctgggaagcctt  
ggctttgacccccctcctgggtcaagccctttgacaccctaagcctccgctcctctcttccatccgcccgtctctccccctgaaacctctcttgcaccccgcctcaatcctccctta  
tccagccctcactcctctctagcgcggcc**GGATCCATGAGCGCCCTCCGGTCTGCGGCCGCCAGTCCGCTGCTGCCCGTGGCG**  
**GCGGCAGCTGCCGACGCGGCCGCCGCACTGGTCCCAGGGTCCGGGCCCGGCCCGCCGCGCTTCTTGCTCCTGTCCGG**  
**GCCCCGGTCCGGGGCATCTCGTTCATCTGCAGATCGGCCCTGAGCCGTGAGCCGGTCTGCTGCTGCAGGACTCGTCCG**  
**GGGACTACAGCCTGGCGCAGTCCGCGAGATGGCTTCTCCATTGTCGACCAGAAGTTCCTGAATGTGGTTTCTACGGA**  
**ATGTATGATAAGATCCTGCTTTTTCGCCATGACCCTACCTCTGAAAACATCCTTCAGCTGGTGAAGCGGCCAGTGATATCC**  
**AGGAAGGCATCTTATTGAAGTGGTCTTGTGAGCTTCCGCCACCTTTGAAGACTTTCAGATTCTGTCGCCACGCTCTCTTTGT**  
**TCATTCATACAGAGCTCCAGCTTTCTGTGATCACTGTGGAGAAATGCTGTGGGGGCTGGTACGTCAAGTCTTAAATGTGA**  
**AGGGTGTGGTCTGAATTACCATAAGAGATGTGCATTTAAATACCCAACAATTGCAGCGGTGTGAGGCGGAGAAGGCTCTC**  
**AAACGTTTCCCTCACTGGGGTCCAGCACCATCCGCACATCATCTGCTGAACTCTCTACAAGTCCCCCTGATGAGCCCCCTCT**  
**GCAAAAATCACCATCAGAGTCGTTTATTGGTTCGAGAGAAGAGGTCAAATTCTCAATCATACATTGGACGACCAATTACCTT**  
**GACAAGATTTTGTGCTAAAGTAAAGTGCCGCACACATTTGTATCCACTCTACACCCGGCCACAGTGTGCCAGTACT**  
**GCAAGAAGCTTCTGAAGGGGCTTTTCAGGCAGGGCTTGCAGTGCAAAAGATTGCAGATTCAACTGCCATAAACGTTGTGCAC**  
**CGAAAGTACCAAACTGCCTTGCGAAGTGACCATTAATGGAGATTGCTTAGCCCTGGGGCAGAGTCTGATGTGGTCA**



## APPENDIX

agtcattctgagaatagtgatgctgcccggcgaccgagtgctctgcccggcgctcaacacgggataataccgcccacatagcagaacttaaaagtgctcatcattggaaaacgttctcg  
ggcgaaaaactcctcaaggatctaccgctgttgagatccagttcgtatgtaaccactcgtgcaccaactgatctcagcatctttactttaccagcgttctgggtgagcaaaaacag  
gaaggcaaaatgccgcaaaaagggaataaggcgacacggaaatgtgaatactcatactctctctttcaatattattgaagcattatcaggggtattgtctcatgagcggataca  
tattgaatgatttagaaaaataacaaataggggtcccgccacatttccccgaaaagtccac

multiple cloning site

PKD1wt

Myc

### pBabepuro PKD1ca:

ctgcagcctgaatatgggccaacaggatctgtggtaagcagttcctgccccggctcaggccaagaacagatggaacagctgaatatgggccaacaggatctgtggtaa  
gcagttcctgccccggctcaggccaagaacagatgtccccagatgctgctccagccctcagcagttctagagaaccatcagatgtttcagggtgccccaaaggacctgaaatga  
ccctgtgcttattgaaactaaccaatcagttcgtctcgtctgttcgctgctctgctccccgagctcaataaaagagcccacaacccctcactcggggcgccagctccgattga  
ctgagtcgccccgggtaccggtgatccaataaacctcttgacgttgcacccgactgtggtctcgtctccttgggaggggtcctctgagtgattgactaccgctcagcggggctttc  
attggggctcgtccgggatcgggagaccctgccaggaccaccgaccaccgggaggtgaagctggccagcaactatctgtctgtcctgattgtctatgctatgactg  
atthttatgcgctcgtcgtgactagttagtaactagctctgtatctggcggaccctgggtggaactgacgagttctgaacacccggccgaacccctgggagagctccaggactt  
ggggcgctttttgfgccgacactgaggaaggagtcgatgtggaatccgacccctcaggatattgttctgtaggagacgagaacctaaaacagttcccgcctcctgtaa  
ttttgcttcggttggaaccgaaccgctgctgtctgctgcagcatcgtctgtgtctgctgctgactgtttctgtattgtctgaaaattaaggccagactgtaccactccctaagt  
ttgacctagatcactgaaagatgctgagcggctcgtcacaaccagctggtatgtaagaagagacgttgggttacctctgctctgcagaatggcaaccttaacgtcggatg  
ggcgagacggcacccttaaccgagacctcaccaggttaagatcaaggcttttaccctggccgacatgacacccagaccaggtcccctacatcgtgacctgggaagcct  
ggctttgacccccctccctgggcaagccctttgacaccctaaagcctccgctcctctctccatccgcccgtctcctcccctgaaacctcctctttcgacccccgctcaatcctccctta  
tccagccctcactcctctctagcgcggcc**GGATCCATGAGCGCCCTCCGGTCTCGGCCGCCAGTCCGCTGCTGCCCGTGGCG**  
**GCGGCAGCTGCCGACGGCCGCCGCACTGGTCCCAGGGTCCGGGCCGGGCCGCGCGTTCCTGGCTCCTGTCGGC**  
**GCCCCGGTCCGGGGCATCTCGTTCATCTGCAGATCGGCCCTGAGCCGTGAGCCGGTCTGCTGCTGCAGGACTCGTCCG**  
**GGGACTACAGCCTGGCGCACGTCCGCGAGATGGCTTGCTCCATTGTCGACCAGAAGTTCCTGAATGTGGTTTCTACGGA**  
**ATGTATGATAAGATCCTGCTTTTCGCCATGACCCTACCTCTGAAAACATCCTTCAGCTGGTAAAAGCGCCAGTGATATCC**  
**AGGAAGGCGATCTTATTGAAGTGGTCTTGTCAGCTTCCGCCACCTTTGAAGACTTTCAGATTTCGTCGCCACGCTCTCTTTGT**  
**TCATTCATACAGAGCTCCAGCTTTCTGTGATCACTGTGGAGAAATGCTGTGGGGGCTGGTACGTCAAAGTCTTAAATGTGA**  
**AGGGTGTGGTCTGAATTACCATAAGAGATGTGCATTTAAAATACCCAACAATTGCAGCGGTGTGAGGCGGAGAAGGCTCTC**  
**AAACGTTTCCCTCACTGGGGTCAACACCATCCGCACATCATCTGCTGAACTCTCTACAAGTGGCCCTGATGAGCCCTTCT**  
**GCAAAAATCACCATCAGAGTCGTTTATTGGTCGAGAGAAGAGGTCAAATTCTCAATCATAATTGGACGACCAATTCACCTT**  
**GACAAGATTTTGTGCTAAAGTAAAGTGCCGCACACATTTGTCTACCTCCTACACCCGGCCACAGTGTGCCAGTACT**  
**GCAAGAAGCTTCTGAAGGGGCTTTTCAGGCAGGGCTTGCAGTGCAAGATTGCAGATTCAACTGCCATAAACGTTGTGCAC**  
**CGAAAGTACCAAACTGCCCTTGGCGAAGTGACCTAATGGAGATTGCTTAGCCCTGGGGCAGAGTCTGATGTGGTCA**  
**TGGAAGAAGGGAGTGATGACAATGATAGTGAAGGAACAGTGGGCTCATGGATGATATGGAAGAAGCAATGGTCCAAGAT**  
**GCAGAGATGGCAATGGCAGAGTGCCAGAACGACAGTGGCGAGATGCAAGATCCAGACCCAGACCACGAGGACGCCAAC**  
**GAACCATCAGTCCATCAACAAGCAACAATATCCCACTCATGAGGGTAGTGCAGTCTGTCAAACACACGAAGAGGAAAAGCA**  
**GCACAGTCAAGAAAGGATGGATGGTCCACTACACCAGCAAGGACACGCTGCGGAAACGGCACTATTGGAGATTGGAT**  
**AGCAAATGTATTACCCTTTTTCAGAATGACACAGGAAGCAGGTAACAAGGAAATTCCTTTATCTGAAATTTGTCTCTGGA**  
**ACCAGTAAAACTTCAGCTTTAATTCCTAATGGGGCCAATCCTCATTGTTTCGAAATCACTACGGCAAATGTAGTGTATTATG**  
**TGGGAGAAAATGTGGTCAATCCTTCCAGCCATCACCAAAATAACAGTGTCTCACCAGTGGCGTTGGTGCAGATGTGGCCA**  
**GGATGTGGGAGATAGCCATCCAGCATGCCCTTATGCCCGTCAATCCCAAGGGCTCCTCCGTGGGTACAGGAACCAACTTG**  
**CACAGAGATATCTCTGTGAGTATTTCAGTATCAAATGGCCAGATTCAAGAAAATGTGGACATCAGCACAGTATATCAGATTTT**  
**TCCTGATGAAGTACTGGGTTCTGGACAGTTTGGAAATGTTTTATGGAGGAAAACATCGTAAAACAGGAAGAGATGTAGCTATT**  
**AAAATCATTGACAAATTACGATTTCCAACAAAACAGAAAGCCAGCTTCGTAATGAGGTTGCAATTCTACAGAACCTTCATCA**  
**CCCTGGTGTGTAATTTGGAGTGTATGTTTGGACGCCTGAAAGAGTGTGTTGTTGTTATGGAAAACTCCATGGAGACATG**  
**CTGAAAATGATCTTGTCAAGTGAAGGGCAGGTTGCCAGACACATAACGAAGTTTTAATTACTCAGATACTCGTGGCTT**  
**TGCGGCACCTTCATTTAAAAATATCGTTCACCTGTGACCTCAAACAGAAAATGTGTTGCTAGCCCTCAGCTGATCCTTTTCT**

## APPENDIX

CAGGTGAAACTTTGTGATTTTGGTTTTGCCCGGATCATTGGAGAGAAGGAGTTCCGGAGGGAGGTGGTGGGTACCCCGC  
TTACCTGGCTCCTGAGGTCCTAAGGAACAAGGGCTACAATCGCTCTCTAGACATGTGGTCTGTTGGGGTCATCATCTATGT  
AAGCCTAAGCGGCACATTCCCATTAAATGAAGATGAAGACATACACGACCAAATTCAGAATGCAGCTTTCATGTATCCACCA  
AATCCCTGGAAGGAAATATCTCATGAAGCCATTGATCTTATCAACAATTTGCTGCAAGTAAAAATGAGAAAGCGCTACAGTG  
TGGATAAGACCTTGAGCCACCCTTGCTACAGGACTATCAGACCTGGTTAGATTTGCGAGAGCTGGAATGCAAAATCGGGG  
AGCGCTACATCACCCATGAAAGTGATGACCTGAGGTGGGAGAAGTATGCAGGCGAGCAGCGGCTGCAGTACCCACACAC  
CTGATCAATCCAAGTGCTAGCCACAGTGACACTCTGAGACTGAAGAAACAGAAATGAAAGCCCTCGGTGAGCGTGTCCAGC  
ATCCTCGAACAAAACTCATCTCAGAAGAGGATCTGTAA GAATTCgccagcacagtggctgaccctgtggaatgtgtgtagtagggtgtgaaagtc  
cccaggctccccagcaggcagaagatgcaagcatgcatctcaattagtcagcaaccagggtgtgaaagtccccaggctccccagcaggcagaagatgcaagcatgcatc  
caattagtcagcaaccatagctcccgccctaactccgccatccccgccctaactccgccagttccgccattccgcccatggctgactaattttttatgatgagaggccgag  
gccgctcggcctctgagctattccagaagtagtgaggaggctttttggaggcctaggcttttgcataaaagcttaccatgaccgagtaacagccacggctgacctgcccagc  
acgagctcccaggccgtacgcaccctgccgcccgttcgactccccgccacgcccacaccgtcagaccgaccacatcagcgggtcaccgagctgcaaga  
actctctcactacgcgctcgggtcgcacatcggcaaggtgtgggtcgggacgacgcccggcgggtggcggctggaccacgccggagagcgtcgaagcggggcgggttctg  
ccgagatcggcccgcgatgcccaggttgagcggttcccggctggccgcgacgaacagatggaagcctcctgcccgcaccggcccaaggagcccgggttctggtcc  
accgtcggcgtctcggccaccaccagggaagggctgtggcagcgcgctgctccccggagtgaggcggccgagcgcgcccgggtgcccgcctctgagacctccgc  
gccccgcaacctcccctctacgagcggctcggctcaccgtcaccgccagctcagctgcccgaaggaccgcccagcctggtcagaccgcaagcccggctgctgagccc  
gccccagaccgcagcggccaccgaaaggagcgcagcaccatgcatgataaataaaagattttatgtctccagaaaaaggggggaatgaaagacccccactgta  
ggttggcaagctagcttaagtaacgccattttgcaaggcatgaaaaatacataactgagaatagagaagttcagatcaaggtcaggaacagatggaacagctgaatggcc  
aaacaggatactgtgtaagcagttcctgccccggctcaggccaaagaacagatggaacagctgaatggccaaacaggatactgtgtaagcagttcctgccccggctca  
gggcaagaacagatggccccagatcggctccagccctcagcagttctagagaacatcagatgttccagggtgcccaaggacctgaaatgacctgtccttattgaaacta  
accaatcagttcgtctcgtctgttcgcccgttctgctccccgagctcaataaagagccacacaccctcactcggggcgcagctcctcagttgactgagtcgcccgggtacc  
cgtgatccaataaacctctgagttgcatccgacttggctcgtgcttctggagggtcctctgagtgattgactaccctcagcgggggtcttcttccgactgtggtctcgc  
tgcttggggaggtctcctctgagtgattgactaccctcagcgggggtctcactgagcatgatacaaaatattggttttttcttaagtattacataaaggccatagttgcaata  
tgaatcggcaacgcgcccgggagaggcgttgcgattggcgtctcctcctcgtcactgactcgtcgcgctcgttgcggtcggctgcccgcagcggatcagctcaaaag  
gcgtaatacggttatccacagaatcaggggataacgcaggaagaacatgtgagcaaaaggccagcaaaaggccaggaaccgtaaaaaggccggtgctggttttcca  
taggtccgccccctgacgagcatcaaaaaatcgacgctcaagtcagaggtggcgaaccggacaggactataagataaccagggcttccccctggaagctccctcgtgcg  
ctcctcttccgacctgccgttaccggatccctgccccttctccctcgggaagcgtggcgttctcagatcagctcagctgtaggtatctcagttcgggtgaggtcgtcctcaag  
ctgggctgtgtcacgaaacccccgtcagcccagccgctgcgcttaccggtaactatcgtctgagtcacaccgtaagacacgacttatcggcactggcagcagccactgga  
acaggttagcagagcggaggtatgtaggggtgctacagagttcttgaagtggtgacctactacggtactagaaggacagatattggtatctcgtcctgctgaagccagttac  
cttggaaaaagagttgtagctctgatcggcaaaacacaccgctggtagcgggtggtttttgttgcagcagcagattcgcgcaaaaaaggatctcaagaagatcct  
ttgatctttctcaggggtctgagctcagtggaacgaaaactcacgtaagggtatttggctagatgattcaaaaaggatctcactagatcctttaaataaaatgaagttgagg  
ccgcaaatcaatcaagatataatgagtaaaactggtctgacagttaccaatgcttaacagtgaggcacctatcagcagatctgctatttctgctcatcagttgctgactccccgtc  
gtgtagataactacgatacgggagggcttaccatctgccccagtgctcaatgataccgcgagaccacgctcaccggctccagattatcagcaataaacagccagccggaa  
gggcccagcgcagaagtgctcctgcaactttaccgctccatccagctattaattgttccgggaagctagagtaagtagtccagtaataagttgcccacagttgttccattgct  
acaggtcagctggtgtcacgctcgtctggttggatggctcattcagctcgggtcccaacagatcaaggcagattacatgacccccatgttggcaaaaagcgggttagctcctcggctc  
ctccgatcgtgtcagaagtaagttggccgaggttatcactcatggtatggcagcactgcataattcttactgctatgccatccgtaagatgctttctgtagctggtgagtagctcaac  
caagtcattctgagaatagtgatcggcgaccgagttgctcttcccggcgtcaacacgggataataaccgcccacatagcagaactttaaagtgctcatcattgaaaaagcttct  
cggggcgaaaaactcaaggatctaccgctgtgagatccagttcagatgtaaccactcgtgacccaactgatctcagcatctttactttaccagcgttctggtgagcaaaaac  
aggaaaggcaaaatgccgcaaaaagggaataaggcgcacaggaatgtgaatactacatactctcttttcaatattatgaagcattatcaggggtattgtctcatgagcggata  
catattgaaatgatttagaaaaataaacaatagggttccgcgacatttccccgaaaagtgccac

multiple cloning site

PKD1ca

S744E/S748E

Myc

## APPENDIX

### pGIPZ shNTC:

tggaagggtcaattcactcccaagaagacaagatatccttgatctgtgatctaccacacacaaggctactccctgattagcagaactacaccagggccagggtcagatata  
cactgaccttggatggtgctacaagctagfaccaggtgagccagataaggtagaagaggccaataaaggagagaacaccagctgttacacctgtgacccctgcatgggtggt  
gaccggagagagaagtgttagagtgagggtttgacagccgctagcattcatcagctggcccagagactgcatccggagtagcttcaagaactgctgatatcgagctgtcacaag  
ggactttccgctggggactttccaggagggctggcctggcgggactggggagtgccgagccctcagatcctgcatataagcagctgttttgcctgactgggtctctcgtgtaga  
ccagatctgagcctgggagctctctgcttaactaggaaccactgcttaagcccaataaagctgcttgagtgctcaagtagtgtgcccgtctgtgtgactctggaactag  
agatccctcagacccttttagctagtggaatctctagcagtgccgcccgaacaggactgaaagcgaagggaaccagaggactctctcagcagcaggactcggctg  
tgaagcgcgcacggcaagaggcaggggcggcactggtgagtagcggcaaaaattttagctagcggaggtagaaggagagagatgggtgagagcgtcagattaagcg  
ggggagaattagatcgcatgggaaaaattcggtaaggccaggggaaagaaaaataataaataatataatagtggaagcaggggagctagaacgattcgcagtta  
atcctggcctgttagaaatcagaaggctgtagcaaaatactgggacagctacaacctccctcagacaggatcagaagaacttagatcattataatacagtagcaacctct  
attgtgtcatcaaaagataagataaaagacaccaaggaagcttttagacaagatagaggaagagcaaaaaaagtaagaccaccgcacagcaagcggccggcctg  
ctcagacctggaggagatagtagggacaattggagaagtgaattataataataagtagtaaaattgaaccattaggtagtagcaccaccaaggcaagagaagagt  
ggtgcagagagaaaaagcagtggaatagggactttcctgggttctgggagcagcaggaagcactatggcgcagcgtcaatgacgctgacggtcagccagaca  
attattgtctgtatagtgacgagcagaacaattgctgaggctattgagcgaacagcatctgttgaactcacagctgggcatcaagcagctccaggaagaatcctggct  
gtgaaagatacctaaaggatcaacagctcctgggattgggttctctgaaaactcattgcaccactgctgtccttgaatgtagtggagtaataaatctggaacagatt  
ggaatcacacagcctggatggagtgggacagagaaattaacaattacaaagcttaatacactccttaattgaagaatcgaaaaccagcaagaaaagaatgaacaagaattat  
tggaattagataaattggcaagtttgggaattggttaacatacaaaattggctgtgtatataaaattattcataatgatagtaggagcttggtaggttaagaatagtttctgacttt  
ctatagtgatagattaggcaggatattcaccattatcgttcagaccacctcccaaccccgaggggacccgacagggccgaaggaatagaagaagaaggtggagagaga  
gacagagacagatccattcagtagaacggatcgccactgctgccaattctgcagacaaatggcagtagtcatccacaattttaaagaaaagggggattgggggtaca  
gtcaggggaaagaatagtagacataatagcaacagacatacaaaactaaagaattacaaaacaaattcaaaaattcaaaaatttccgggtttattacagggacagcagatcc  
agtttggtagtaccggccgctctagtcggaatcagtcctgctcctcgccacgaagtgcacgcagtgccggccgggtcgcgagggcgaactcccggccacggctgctc  
gccgatctcggatcgccggccgggagggctcccggaagttcgtgacacgacctccgaccactcggctacagctcgtccaggccgcgacccacaccaggccagggtgtt  
gtccggcaccacctgctcggaccgctgatgaacagggcagctgctccggaccacaccggcgaagtcctccacgaagtcgggagaaccggagccggctcgtcc  
agaactcagccctccggcagctcgcgcgggtgagcaccggcaacggcactggtcaactggcattggtgctcctatagtgagctgtattactatgccgataactatgcc  
gatgattaattgtcaacacgctgctcaggtccgaggtctagacgtattaccgcatcattagttataatagtaatacattacggggtcattagttcatagccatataatggagttccg  
ttacataactacgtaaatggcccctggtgaccgccaacgacccccgcccattgacgtcaataatagcagtagtcccatagtaacgcaatagggacttccattgacgtcaa  
tgggtggagtagtttacgtaaaactcccacttggcagtagcatcaagtgatcatatgccaagtagcggcccttagcgtcaatgacggtaaatggcccctggcattatgccagtag  
atgacctatgggacttctacttggcagtagatctactgtattagctcgtattaccatgggtgatgctggtttggcagtagcatcaatgggctggatagcgggttactcacgggatttc  
caagctccaccctgacgtcaatgggagtttggcaccaaaatcaacgggacttccaaaatgtcgtacaactccgcccattgacgcaaatggcggtgagcgtgtagc  
gtgggaggtctataaagcagagctgttttagtaaccgtcagatcgctggagacgcatccacgctgtttgacctcatagaagacaccgactactagaggatctgccacat  
ggagagcagcagagagcggcctgcccgatggatcagtgagtcgagtcgcatcaccggcaccctgaacggcgtgagttcagctggtggcggcggagagggcacccccagc  
agggccgatgaccaacaagatgaagagcaccaaaaggcctgacctcagcccctactcgtgtagccagctgagggtagcggcttaccacttggcacctacccccagc  
gtagcagaaccctctcagcagccatcaacaacggcgtacaccaacaccgcatcgagaagtagcagggcggcgtgctgacgtgagctcagctaccgctacgag  
gcccggcggctgacggcactcaaggtatgggacaccggcttccccaggacagcgtgattcaccgacaagatcatccgagcaacgccaccgtggagcactgaccccc  
atggcgataacgatctggatggcagcttaccggcactcagcctgacgacggcggctactacagctccgtggtagcaccatgactcaagagcgcacccccc  
gcatcctgcagaaccggggcccattgctcctccgctgggagggatcagcaaacaccgagctggcagctgtagtagcagcctcaagaccccggatgca  
gatccgggtgaagaataatgtacaagtagcggccgcaaatccgcccctcctccccccccctaacgttactggccgaagccgcttgaataaggccggtgctgttctat  
gtattttccaccatattgccgtctttgcaatgtgagggccggaaaacctgcccctgctctgacgagcattcctaggggtcttccccctcgcgcaaaaggaatgaaggctgtgta  
gtcgtgaaggaagcagttctctggaagcttctggaagacaacaacgctgtagcaccctttgacggcagcggaaacccccaccctggcagaggtcctctcggccaaaagc  
cacgtgtataagatacactgcaaaaggcggcacaaccccagtgccacgtgtgagttgtagattgtggaagagtaaatggctctcctcaagcgtattcaacaagggctgaag  
gatccccagaaggtaccctttagtgatctggtggcctcgtgacatgctttacatgttttagcaggttaaaaaacgcttagcggcccccgaaccacggggcagctgg  
tttcttggaaaaacacgataatacattggccaccgagtagcaagcccaggtgctcctgcccaccggcagcagctccccggcgtacgcacctcggcggctgctcgg  
actaccggccacgcccacaccgtcagcccggaccgccacatcgagcgggtcaccgagctgcaagaactctcctcacgcgctgggctcagatcggcaaggtgtgggtg  
cggacgacggcggcgggtggcgtgtagaccacggcggagagcgtgaaagcggggcgggttccggagatcggctcgcgcatggcaggtgagcgggttccggctggc  
cgcgacgaacagatggaagcctcctggcggcaccggcccaaggagcccggctggttctgcccaccctcggcgtctcggccgaccaccagggcaagggctctggcagc  
gcccgtgctccccggatggaggcggcggcagcgcgtgggtgcccgcctctggagacctccgccccgcaacctccccctctacgagcggctcggctcaccgtcaccgc  
cgacgtcaggggtcccgaaggaccgacacgtgctgacccgcaagcccgtgctgagttgttgaatgaggtcagtagctttacagaatcgttgcctgacatcttggaaa  
cacttgcgggattacttctcaggttaacccaacagaaggctcag **GTAACCGGATCCTGATCA** gaattcaaggggctactttaggagcaattatctgttactaaaactg  
aataccttctatctcttgatacattttacaagctgaattaaaatggtataaataaactcttttaattggaagactaatgcccggccattactcctcgtctgtctgtgcatatgt  
ctgctggttggtagtgggttggggcggccctatagtgagctattacataggacgctgctggaacaatacaaccttggattcaaaaattgtgaagattgactggtatttcaacta

# APPENDIX

tgttgctcctttacgctatgtggatacgcctgcttaatgcctttgatcatgctattgctcccctatggcttcattttcctcctgtataaatcctgggtgctctcttatgaggagtgtggccc  
gttgtagcgaacggtggctgtgtgctactgtgttgctgacgaacccccactggtggggcattgccaccacctgacgctctttccgggacttccgtttccccctcctattgccag  
gcggaactcatcgccgctgcttgcctgctggacaggggctggctgtgggactgacaatccgtgggtgtgctggggaagctgacgctcttccatggctgctcgcctgtgtg  
ccacctgattctgcgctgggacgctcttctgctacgctccctcggccctcaatccagcggacctcttcccggcctgctgctggcctctcggccttccgctcttcgcctcgcctc  
agacgagtcggatctcccttggggcgcctccccctggaattaatctgcagtcgagacctagaaaaacatggagcaatcacaagtagcaatacagcagctaccaatgctgattg  
tgcctggctagaagcacaagaggaggagggtgggtttccagtcacacctcaggtaccttaagaccaatgactacaaggcagctgtagacttagccattttaaagaaaa  
gaggggactggaaggctaactcctcaacgaagacaagatctgctttgctgtactgggtctctggttagaccagatctgagcctgggagctctctggtaactagggaaacc  
cactgctaaagctcaataagcttgccttgagtgctcaagtagtgctgcccgtgtgtgactctgtaactagagatccctcagacccttttagctagtgtaaactctctagca  
gtagtagttcatgtcatcttattatcagttataactgcaaaagaaatgaatcagagagtgagggccttgacattgttaaacccgctgacgctcagctgctcttagttgcc  
agccatctgtgtttgccctccccctgcttccctgacctggaagggtccactccactgcttcttaataaaatgaggaaatgcatcgattgtctgtaggtgtcattctattctg  
gggggtgggtgggagcagcaaggggaggtgggaaagacaatagcagcagctgctgggatgctgggtctatggctctgagcggaaagaaaccagctggggct  
ctaggggtatccccacgctgtagcggcgatgaagcggcggtgtgtgtgtacgcgagctgacctgacctgaccagcgccttagcgccttagcgccttctgcttctc  
cttctcttccgacgttccgcttccccctcaagctctaaatcggggctccttttaggttccgatttagctttacggcacctgcaccccaaaaactgattaggggtgatgggt  
cacgtagtgggccatgcctgatagacggttttcccttgcctggagtcacgttcttaatagtgactctgttccaaaactggaacaacactcaaccctatctcggtctattctt  
gattataagggttttccgattcggcctattggttaaaaaatgagctgatttaaaaaatcgaatcctgtggaatgtgtgctaggtgggtgtggaagctcccaggct  
ccccagcagcagaagtagcaaaagcagctcaatagtcagcaaccagggtgtgaaagctcccaggctcccagcaggcagaagtagcaaaagcagctcaatagtc  
agcaaccatagctcccctcaactcggccatcccggcctcaactcggccagttccgcccattctcggcccatggctgactaattttttattatgagagggcaggccgctct  
gcctctgagctattccagaagtagtgaggaggcttttggaggcctaggctttgcaaaaagctcccgggagctgtatctcatttccgatctgatcagcagctgataaaaagcctg  
aactcaccgcgagctgtcgcagaagtttctgatcgaaaagttcagacgcctcggacctgatgagctctcggaggggcagaagatctcgtgcttccagctcagctgtagggggcg  
tggatagctcgcgggtaaaagctgcggcaggttctcaaaagatcgttatgtttatcggcactttgatcggcgcctcccgattccggaagtgctgacattggggaattcagcg  
agagcctgacctattgcatctcccggctgacaggggtgacgttgcaagacctgctgaaaccgaactcccgcctgtctgacggcggcggagggccatggatgcatgctg  
cggcagatcttagccagacgagcgggttccggccattcggaccgaagaaatcgtgcaatacactacatggcgtgattcatatgcgcgattgctgatccccatgtgatcactggca  
aaactgtatggagcagaccgctagctgcctcgcgaggtctcagtagctgcttggggcggaggactcccgaagtcggcaccctgacagcgggatttccgctccaa  
caatgtcctgacggacaatggccgataaacagcggctcattgactggagcagggcagatgtcggggattcccaatacagaggctcccaactctctctgaggccgtgtggtgtg  
atggagcagcagcgcctactcagcggaggcatccggagctgagatcggcggctcgggcttatatgctcgcattggtctgaccaactctatcagagctgtgtgac  
ggcaatttcatgatgacgcttggcgagggctgatgcagcgaatcgtccgatccggagcgggactgctgggctacacaatcggccgcagaagcggcggcctctggacc  
gatggctgtgtagaagtagctcggatagtggaaccgacgccccagcactgctcggaggcgaaggaatagcagctgactagatttccattccaccgctctctatgaaag  
gtgggctcggatcgttccgggacgcccggctggatgatcctcagcggggatctcatgctggatttctcggccacccaactgtttattgagcttataatggtacaataaaa  
gcaatagatcacaaattcacaataaagcatttttctactgacttagttgtgttttccaaactcatcaatgtatcttcatgtctgtataccgtcagctctagctagagctggcgt  
aatcatggctagatgcttctgtgaaattgtatcgcctcacaattccacacaacatacagcgggaagcataaaagttaaaagctggggctcctaatgagtagactcaatca  
taattcgttgcgctcactgccccttccagctgggaaacctgctgctgaccagctgcaatgaatcggccaacgcggggagaggcggttgcgtattggcgctcttccgctcctc  
gctcactgactcgtcgcctcggctgctgctgctgctggcagcgggtatcagctcactcaaaagcggtaatacggttatccacagaatcaggggataacgcaggaagaacatgta  
gcaaaagggcagcaaaagggcaggaaccgtaaaagggcggctgctgctgctttccataggtccgccccctgacgagcatcaaaaatcagcgtcaagtcagaggtg  
gcgaaccggcagaggactataaagatacaggcgttccccctggaagctcctcgtgctctcctgttccgacctgcccgttaccggatacctgccccttctccttccgggag  
cgtggccttctcatagctcagcgttaggtatctcagttcgggtgaggtctgctcctaagctgggtgtgtgacgaacccccgttccagcccagcgtcgccttaccggtaact  
atcgtctgagtcaaccggtaagacacgactatcggcactggcagcagccactgtaaacaggattagcagagcagggtatgaggcgtctacagattctgaaagtgtggc  
ctaactcggctcactagaagaacagatttggtagtctgctgctgtagaccagttacctcggaaaaagagttgtagctcttgcggcaaaaaccaccctggtgagcgg  
tggtttttgttgaagcagcagattacgcgcaaaaaaagagctcaagaagatcctttgacttttctacggggctgacgctcagtggaacgaaaactcagtaagggtttgg  
tcatgagattcaaaaagatctcacctagatcctttaaataaaaaatgaagtttaaatcaatcaagtatatatgagtaaaactggctgacagttaccaatgctaatcagtgagg  
cacctatctcagcgtatgcttattcgttcatcatagttgcctgactccccgctgtagataactacgatacggggggcttaccatctgccccagtgctgcaatgataccgggaga  
cccacgctcaccggctcagattatcagcaataaaccagccagcgggaaggcggagcagaaagtgctcctgcaactttaccgctccatccagcttataattgttggcggga  
agctagagtaagtagttccagtaataatgttgcgaacggttggcattgtacagcagctgctgctcagcctcgtgttggtagcttaccagctccgggtccaacatcaag  
gcgagttacatgacccccatgtgtgcaaaaagcgggtagctccttccgctccgatgttgcagaagtaagttggccgaggttattactcatgttatgagcagcactgataatt  
cttactgtcatgcatcggtaagatgctttctgactggtgagtagtcaaccaagctcttctgagaatagtagtgcggcgaccgaggtgtcttccggcgctcaatacgggataat  
accgcccacatagcagaactttaaagtgctcatattggaacgcttctcggggcgaaaactctcaaggatctaccgctgttggatccagttcagatgaaccactcgtgcacc  
caactgatctcagcatctttacttaccagcgttctgggtgagcaaaaacaggaaggcaaaatcggcgaaaaagggaataagggcgacagcggaaatgttgaatactcatact  
cttcttttcaatattatgaagcattatcagggttattgtctatgagcggatacatattgaatgtattgaaaaataaacaaataggggtccgcaattccccgaaaagtcca  
cctgacgtcagcggatcgggagatcaactgtttattgacgttataatggttacaataaagcaatagcatcacaatttcaaaaataaagcatttttctactgacttagttgtgtttg  
ccaaactcaatgtatctatctgctgagcaactgataactcaagtaacaaaatcctcccaactccaccctattaccactgccaattacctgtgtttcatttac  
tctaaactgctgattctctgaatttttcaaaagaaattgtattgtaaatatgactacaacttagtagt

NTC sequence

pGIPZ shPKD1:

tggaaaggcttaattaccctcccaagaagacaagatatcctgatctgtgtagctaccacacacaaggctacttccctgattagcagaactacaccaggccaggggtcagatatac  
 cactgacctttggatggtgctacaagctagaccagttgagccagataaggtagaagaggccaataaaggagagaacaccagctgttacacctgtgagcctgcatggatggat  
 gaccggagagagaagtgtagtgagggttgacagccctagcattcatcagctggcccagagctgcatccggagtactcaagaactgctgatatcgagcttctgctacaag  
 ggactttccgctggggactttccaggggagcgtggcctggcgggactggggagtgccgagccctcagatccctgcatataagcagctgttttgcctgactgggtctctggttga  
 ccagatctgagcctgggagctcctgctaaactagggaaaccactgcttaagcctcaataaagctgcttgtagtctcaagtagtggtgcccctgtgtgactctgtaactag  
 agatccctcagacccttttagctagtggtgaaaatcctagcagtgccgccaagacagggactgaaagcgaaggaaaccagaggagctctctcgacgcaggactcggctgc  
 tgaagcgcgacggcaagaggcagggggcggcactgggtgagtacgcaaaaaattttagctagcggaggctagaaggagagagatgggtgagagcgtcagttataagcg  
 ggggagaattagatcgcatgggaaaaaattcggtaaggccaggggaaagaaaaatataaataaaacatatagtagggcaagcagggagctagaacgattcgcagtta  
 atcctggcctgtagaacatcagaaggctgtagacaaatactgggacagctacaacctccctcagacaggatcagaagaacttagatcattatataatacagtagcaacctct  
 attgtgctcatcaaggatagagataaaagacaccaaggaagcttttagacaagatagaggaagagcaaaaagtaagaccaccgcacgcaagcggccggcctgtag  
 cttcagaccctggaggagagatagagggacaattggagaagtgaattataaataaagtagtaaaaattgaaccattaggagtagcaccaccaaggcaagagaagagt  
 ggtgcagagagaaaaagacagtggaatagggactttgtcctgggttctgggacagcaggaagcactatggcgcagcgtcaatgacgctgacggtaacagccagaca  
 attattgtctgtatagtcgacgacgagaacaatttctgagggctattgagcgcacacatctgttgaactcacagctggggcatcaagcagctccaggcaagaatcctggct  
 tggaaagatacctaaaggatcaacagctcctgggatttggggtgctctggaaaactcattgcaccactgctgtccttggaaatgctagtggagtaataaactctggaacagatt  
 ggaatcacacgacctggatggagtgggacagagaaattaacaattacacaagcttaatacactccttaattgaagaatcgcaaacaccgaagaaaagaatgaacaagaattat  
 tggaaatagataaattggcaagtttgggaattggttaacatacaaaattggctgtggtatataaaatattcataatgatagtaggagcttggtaggttaagaatgttttctgactt  
 ctatagtgaaatagataggcaggatattaccattatcgtttcagacccacctcccaaccccgaggggacccgacagggcccgaaggaatagaagaagaaggtggagagaga  
 gacagagacagatccattcattgtagaacggatcgccactgctgcccacttctgcagacaaatggcagattcatcccaattttaaagaaaaggggggattgggggtgaca  
 gtgcaggggaaagaatagtagacataatagcaacagacatacaactaagaattacaaaacaaattcaaaaattcaaaatttccgggtttattacagggacagcagagatcc  
 agtttggtagtaccggccctctagctcgggaatcagctcctgctcctggccacgaagtgcacgcagctgcccggcgggtgcccaggggcaactccccccccacggctgctc  
 gccgatctcggctgagccggccggaggcgtccgggaagtctggacacgacctccgaccactcggctacagctcgtccaggccgcgaccacaccagccaggggtgtt  
 gtccggcaccacctgtcctggaccgctgtagaacagggtcacgtcctccggaccacaccggcgaagtcctccacgaagtcggggagaaaccgagccgctcgtcc  
 agaactcagaccctccggcagctcggcgggtgagcaccggaaacggcactggtcaacttggcattggcctcctatagtagctgattataactatgcccagataactatgcc  
 gatgattaattgtcaacacgtgctgacggctccgaggtctagacgtattaccgccatgattagttataatagtaatacaattacggggctcattagttcatagcccatataggagttccggc  
 ttacataactacgtaaatggcccgcctggtgaccgccaacgacccccgcccattgacgtcaataatgacgtatgttccatagtaacgccaatagggactttccattgacgtcaa  
 tgggtggagattttacggtaaaactgcccacttggcagtagcatcaagtgatcatatgcaagtagcggccttattgacgtcaatgacggtaaatggcccgcctggcattatgccagtagc  
 atgaccttatgggacttctacttggcagtagactctagctattagctatcgtattaccatggtgatcggttttggcagtagcatcaatggcggtgtagagcgtttagctacggggattt  
 caagctccaccctttagctcaatgggagttgttttggcaccaaaataacgggactttcaaaaatgctgtaacaactccgcccattgacgcaaatggcggtgagcgtgtacg  
 gtgggaggtctatataagcagagctcgttttagtgaaccgtcagatcgcctggagacggccatccacgctgtttgacctcatagaagacaccgactactagaggatctgccacat  
 ggagagcagcagagagcggcctgcccgcattgagatcagctgcccacatcaccggcaccctgaacggcgtggagttcagctggtggcgggagagggcaccggcggagc  
 agggccgatgaccaacaagatgaagagcaccaaaaggcgcctgacctcagcccctacctgtgagccacgtatgggctacggcttaccactcggcacctacccccagcg  
 gctacgagaacccttctgacgcatcaacaacggcggctacaccaacaccggcagcagagaagtagcagggcggcgtgctgacgtgagctttagctaccgctacgag  
 gccggcggcgtgacggcactcaaggtgatggcaccggcttccccgaggacagcgtgatcttaccgacaagatcctcagcagcaacggcaccgtggagcactgaccccc  
 atggggataacgatctggatggcagcttaccggcaccctcagcctgcccagcggcggctactacagctcctggtggagacccatgcaactcaagagcggccatccacccca  
 gcatcctgcagaacggggggcccatgttcgcttccgcccgtggaggatcagcaacaccgagctgggcatcgtggagtagcagcagcctcaagacccccgatgca  
 gatccggtgagaataatgtacaagtagcggccgcaaatccgcccctctccctccccccccctaacgttactggccgaagccgcttgaataaggccggtgtgctgttctatata  
 gttattttccaccatattgcccgttttggcaatgtgagggccggaaacctggccctgtcttctgacgagcattcctaggggtcttccccctctcgcaaaaggaatgaaggtctgtgaa  
 gtctgtaaggagagcttcttggaaagcttctgaagacaacaacgtctgtagcacccttgcagcagcggaaacccccaccctggcgacaggtgcctctcggccaaaagc  
 cacgtgtataagatacacctgcaaaaggcggcacaacccagtgccacgttgtgagttggatagttgtgaaagagcacaatggctctcctcaagcgtattcaacaaggggtgaag  
 gatgccagaaggtaccctattgtaggtatgctggtggcctcgtgacatgcttcatgctttagctagggtaaaaaaacgtctagggcccccgaccacggggagcgtgg  
 tttcttggaaaaacacgataatacattggccaccgagtagcaagcccaggtgcccctcggcaccggcagcagctccccggcggctacgaccctcggccggcgttgc  
 actaccggccacgcccacaccgtgaccggaccgcccacatcagcgggtcaccgagctgcaagaactctcctcacgcccgtcgggctcagatcggcaaggtgtgggtgc  
 cggacgacggcggcgggtcgtggaccacgggagagcgtcgaagcggggcgggttccgagatcggctcgcgatggcggagttgagcgggttccggctggc  
 cggcagcaacagatggaaggcctcctggcggcagcggcccaaggagcccggctggttctggccaccctcggcgtctcggccgaccaccagggcaagggctcgggagc  
 gccgtgctccccggagtgaggcggcggagcggcgtgggtgccctcctggagacctccggccccgcaacctccccctctacgagcggctcggcttaccgtcaccgc  
 cgagctcaggtgcccgaaggaccgacacctggtgcatgaccgcaagcccggctgctgagttgttgaatgaggctcagcttaccagaatcgttgcctgcacatcttgaaa





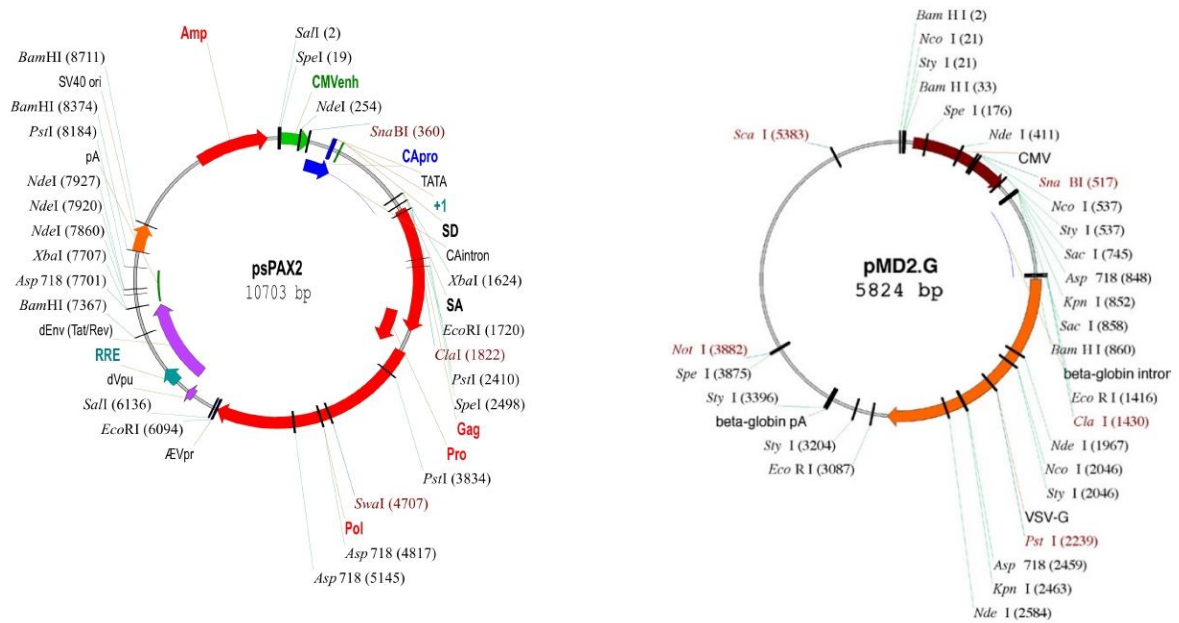
## APPENDIX

cacggaaatgttgaatactcactctccttttcaatattattgaagcattatcagggttattgtctcatgagcggatacatatttgaatgtatttagaaaaataaacaatagggttccg  
cgcacatccccgaaaagtgccactgacgtcgacggatcgggagatcaactgtttattgcagctataatggttacaaataaagcaatagcatcacaattcacaaataaagcat  
tttttactgcattctagttggtttgtccaaactcatcaatgtatcttcatgtctggatcaactggataactcaagctaaccacaaatcatccaaactcccaccataccctattacca  
ctgccaattacctggttcattactctaaacctgtgattcctctgaattttttcattttaagaatgtatttgtaaatatgtactacaaacttagtagt

### PKD1 sequence

Primer: BE933/BE934

### packaging vectors:



## 7.2 List of Figures

Figure 1. Different types of adipose tissue.....	3
Figure 2. Adipokines secreted from adipose tissue. ....	5
Figure 3. Energy balance.....	7
Figure 4. High caloric food consumption leading to adiposity. ....	8
Figure 5. Mitochondrial fission and fusion processes. ....	12
Figure 6. PKD isoforms.....	14
Figure 7. Signaling pathway of the PKD isoforms.....	15
Figure 8. Activation of AMPK.....	18
Figure 9. The role of AMPK in the regulation of energy homeostasis in adipocytes. ....	20
Figure 10. The potential impact of PKD1 in the development of adipocyte dysfunction and obesity. ....	22
Figure 11. Scheme of mutation in mice to generate conditional PKD1 deletion. ....	24
Figure 12. PKD1 is predominantly expressed in adipose tissues. ....	48
Figure 13. PKD1 is activated upon purinergic stimulation in white adipocytes. ....	49
Figure 14. DAG is directly activating PKD1 in white adipocytes. ....	50
Figure 15. PKD1 is activated upon stimulation with several endocrine factors in brown adipocytes. ....	51
Figure 16. Inhibition of PKD reduces TG accumulation in 3T3-L1 cells.....	52
Figure 17. Effective generation of stable cells lines.....	52
Figure 18. PKD1 promotes TG accumulation in differentiated 3T3-L1 cells. ....	53
Figure 19. Deletion of PKD1 reduces TG accumulation in differentiated SVF derived from mice.....	54
Figure 20. PKD1 does not regulate adipocyte differentiation.....	55
Figure 21. Deletion of PKD1 does not affect lipolysis rate in adipocytes. ....	56
Figure 22. PKD1 promotes lipogenesis rate in adipocytes. ....	57
Figure 23. PKD1 suppresses energy dissipation in adipocytes. ....	58
Figure 24. Deletion of PKD1 increases OCR and mitochondrial content in adipocytes. ....	59
Figure 25. Deletion of PKD1 in BAT decreases lipogenesis rate in adipocytes without affecting their OCR. ....	60
Figure 26. Deletion of PKD1 enhances expression of genes involved in the creatine metabolism. ....	61

---

Figure 27. PKD1 suppresses mitochondrial fragmentation.....	62
Figure 28. Pull-down of Myc in differentiated 3T3-L1 cells. ....	63
Figure 29. PKD1 interacts with Rictor in differentiated 3T3-L1 cells. ....	64
Figure 30. Inhibition of PKD1 results in an upregulation of Akt activity.....	65
Figure 31. PKD1 is impeding mTORC2 signaling, while it is upregulating the mTORC1 complex and its downstream targets. ....	66
Figure 32. PKD1 regulates adipocyte function in an AMPK-dependent manner.....	68
Figure 33. AMPK substrate recognition is PKD1-dependent. ....	69
Figure 34. PKD1 regulates AMPK activity in adipocytes.....	70
Figure 35. Successful silencing or activation of AMPK.....	71
Figure 36. PKD1 regulates TG accumulation in adipocytes in an AMPK-dependent manner. ....	72
Figure 37. PKD1 regulates lipogenesis rate in adipocytes through AMPK. ....	73
Figure 38. PKD1 regulates OCR in adipocytes through AMPK. ....	74
Figure 39. PKD1 regulates mitochondrial fragmentation in adipocytes in an AMPK- dependent manner. ....	75
Figure 40. DAG levels are not influenced by the diet.....	76
Figure 41. PKD1 expression and activity is induced upon feeding. ....	77
Figure 42. PKD1 is effectively and specifically deleted in adipocytes.....	78
Figure 43. Deletion of PKD1 reduces body weight gain in mice on HFD. ....	79
Figure 44. Deletion of PKD1 reduces overall fat mass in mice on ND.....	79
Figure 45. PKD1 regulates white adipose tissue in an AMPK-dependent manner also <i>in vivo</i> . ....	81
Figure 46. PKD1 does not affect AMPK phosphorylation in brown adipose tissue...	82
Figure 47. Deletion of PKD1 does not affect lipolysis or glucose levels in young mice upon fasting. ....	83
Figure 48. Deletion of PKD1 affects AMPK phosphorylation in the fasted-refed stage. .....	84
Figure 49. PKD1 deletion does not affect food intake, activity, or respiratory exchange ratio. ....	85
Figure 50. PKD1 promotes obesity by suppressing energy dissipation in adipocytes. .....	86
Figure 51. Deletion of PKD1 decreases overall adipocyte size in mice fed HFD.....	87

---

Figure 52. PKD1 deletion in adipocytes does not change adipocyte size in mice fed ND. ....	88
Figure 53. RNA sequencing of gWAT revealed an upregulation of browning genes in PKD1-deleted mice.....	89
Figure 54. Increased expression of browning genes in sWAT shown by RNA sequencing analysis. ....	90
Figure 55. PKD1 suppresses expression of genes characteristic for beigeing. ....	92
Figure 56. PKD1 does not affect lipid metabolism. ....	93
Figure 57. PKD1adipo.Δ/Δ mice show an increased mitochondrial content and increased UCP1 levels in their sWAT.....	94
Figure 58. Deletion of PKD1 does not alter gene expression in mice fed ND.....	95
Figure 59. Deletion of PKD1 does not show formation of ectopic myofibers. ....	96
Figure 60. Effects on energy expenditure are abolished under thermoneutral conditions. ....	96
Figure 61. UCP1 expression is regulated by the ADRB3 in PKD1-deficient adipocytes. ....	97
Figure 62. PKD1 suppresses ADRB3 expression in an AMPK-C/EBP-α/C/EBP-δ-dependent manner. ....	98
Figure 63. PKD1 suppresses C/EBP-α and C/EBP-δ abundance in an AMPK-dependent manner in order to regulate ADRB3 expression. ....	100
Figure 64. Deletion of PKD1 reduces leptin levels but does not affect any of the other adipokines. ....	101
Figure 65. FFA levels are reduced in mice lacking PKD1 in adipocytes.....	101
Figure 66. PKD1 deletion protects against insulin resistance and type 2 diabetes. ....	102
Figure 67. Impaired insulin sensitivity, but not insulin secretion, is the major cause for the reduced glucose tolerance.....	103
Figure 68. PKD1 deletion protects against diet-induced fatty liver disease. ....	103
Figure 69. PKD1 positively correlates with HOMA-IR.....	105
Figure 70. PKD1 inhibition reduces lipogenesis rate and increases OCR also in human adipocytes. ....	106
Figure 71. Inactivation of PKD1 in obese mice prevents further body weight gain. ....	107
Figure 72. PKD1 deletion in obese mice increases energy expenditure.....	107

Figure 73. Inactivation of PKD1 in obese mice protects against development of diabetes. .... 108

Figure 74. Loss of PKD1 promotes AMPK activity, mitochondrial function and beiging of white adipocytes. .... 109

### **7.3 List of Tables**

Table 1. PKD1 interaction partners identified through mass spec analysis. .... 64

Table 2. Characteristics of human subjects and blood analysis. .... 104

Table 3.Characteristics of human blood samples. .... 105

## 7.4 List of Abbreviations

AA	amino acids
ACC	acetyl-CoA carboxylase
ACTA1	actinin $\alpha$ 1
ACTN	actinin $\alpha$
AD	adipocyte differentiation
ADM	adipocyte differentiation maintenance
ADP	adenosine diphosphate
adipo.	adiponectin
ADRB3	$\beta$ 3 adrenergic receptor
AICAR	5-aminoimidazole-4-carboxamide 1- $\beta$ -d-ribofuranoside
AMP	adenosine monophosphate
AMPK	AMP-activated protein kinase
ANOVA	analysis of variance
APS	ammonium peroxodisulphate
ARID5B	AT-rich interaction domain 5b
ASP	acylation stimulating protein
ATF2	activating transcription factor 2
ATGL	adipose triglyceride lipase
ATP	adenosine triphosphate
AU	arbitrary units
BAT	brown adipose tissue
BCL2	B-cell lymphoma 2
BMI	body mass index
BMP7	bone morphogenic protein 7
Bnip3	BCL2 interacting protein 3
BSA	bovine serum albumin
bZip	basic leucine zipper
C	cysteine-rich domains
ca	constitutive active
CaCl <sub>2</sub>	calcium chloride
cDNA	complementary DNA
CH <sub>3</sub> COOK	potassium acetate

## APPENDIX

---

CAMK	Ca <sup>2+</sup> /calmodulin-dependent protein kinase
cAMP	cyclic adenosine monophosphate
CC	compound C
C/EBP	CCAAT/enhancer-binding protein
CHREBP	carbohydrate-responsive element-binding protein
CID 755673	<i>2,3,4,5-tetrahydro-7-hydroxy-1H-benzofuro[2,3-c] azepin-1-one</i>
CIDE	cell death-inducing DNA fragmentation factor, $\alpha$ subunit-like effector
CIDEC	cell death-inducing DFFA-like effector c
CKM	creatine kinase muscle
CKMT	creatine kinase mitochondrial
CoA	coenzyme A
cont.	control
COX	cytochrome c oxidase, subunit
cPKC	conventional PKC
CPM	counts per million
CPT1	carnitine palmitoyl-transferase 1
CRE	cAMP response element
CREB	cAMP-response element-binding protein
CRT 0066101	2 [4 [(2R) 2 aminobutyl]amino] 2 pyrimidinyl] 4 (1 methyl 1H pyrazol 4 yl) phenol dihydrochloride
CT	computed tomography
CtBP	C-terminal binding protein
CUL7	cullin 7
1,2-DAG	1,2-dioctanoyl-sn-glycerol
DAG	diacylglycerol
DAPI	4',6-diamidino-2-phenylindole
ddH <sub>2</sub> O	distilled, deionized water
DEPC	diethylpyrocarbonate
DGAT	diacylglycerol-O-acyltransferase
diff.	differentiated
DIO2	iodothyronine deiodinase 2
DMEM	dulbecco's modified eagle's medium



## APPENDIX

---

DMSO	dimethylsulfoxid
DNA	deoxyribonucleic acid
dNTP	2'-deoxynucleoside 5'-triphosphate
	dATP          2'-deoxyadenosine-5'-triphosphate
	dCTP          2'-deoxycytidin-5'-triphosphate
	dGTP          2'-deoxyguanosine-5'-triphosphate
	dTTP          2'-deoxythymidin-5'-triphosphate
DPBS	dulbecco's phosphate-buffered saline
dpm	disintegrations per minute
DRP1	synamin related protein 1
DTT	1,4-dithiothreitol
E	glutamic acid
ECL	enhanced chemiluminescence
EDTA	ethylenediaminetetraacetic acid
ELISA	enzyme-linked immunosorbent assay
ER	endoplasmic reticulum
ERK	extracellular regulated protein kinase
ERR $\alpha$	estrogen-related receptor $\alpha$
ETC	electron transport chain
FA	fatty acids
FAO	fatty acid oxidation
FAS	fatty acid synthase
FBS	fetal bovine serum
FC	fold change
FCCP	carbonyl cyanide-4-(trifluoromethoxy) phenylhydrazone
FCS	fetal calf serum
FDG PET	2-fluoro-D-2-deoxy-D-glucose positron emission tomography
FFA	free fatty acid
FGF21	fibroblast growth factor 21
FIS1	fission 1 homolog protein
flox/flox	f/f
FoxO1	forkhead box protein O1
fragm.	Fragmented

## APPENDIX

---

G	gauge
g	gravitation force
GAPDH	glyceraldehyd-3-phosphat-dehydrogenase
gDNA	genomic DNA
Glc	glucose
GLP-1	glucagon-like peptide-1
GPCR	G-protein coupled receptors
GSEA	gene set enrichment analysis
GTPase	guanosine triphosphate hydrolase
GTT	glucose tolerance test
gWAT	gonadal white adipose tissue
h	hours
HCl	hydrochloric acid
HDACs	class II histone deacetylases
H&E	hematoxylin and eosin
HEK	human embryonic kidney
HEPES	N-2-hydroxyethylpiperazine-N'-2-ethanesulfonic acid
HFD	high-fat diet
H <sub>2</sub> O <sub>2</sub>	hydrogen peroxide
HOMA-IR	H
HRP	horseradish peroxidase
HSL	hormone-sensitive lipase
HTR2B	5-hydroxytryptamine receptor 2b
Hypo.	hypothalamus
IB	immunoblot
IBMX	3-isobutyl-1-methylxanthine
IF	immunofluorescence
IgG	immunoglobulin G
IκBα	inhibitor of kappa B
IKK	inhibitor of kappa B-kinase-complexes
IL-6	interleukin-6
Ind.	inducible
interm.	intermediate

## APPENDIX

---

IP3	inositol-1,4,5-trisphosphate
IP6K1	inositol hexakisphosphate kinase 1
IP	immunoprecipitation
IR	insulin receptor
IRS	insulin receptor substrate
Iso	isoproterenol
ITT	insulin tolerance test
JNK	c-Jun NH2-terminal kinase
KCl	Potassium chloride
KHCO <sub>3</sub>	potassium bicarbonate
LB	lysogeny broth
LC3	light chain 3
LC	liquid chromatography
LDS	lithium dodecyl sulfate
LFQ	Label-free quantification
LKB1	liver kinase B 1
LPL	lipoprotein lipase
M	molar
MAPK	mitogen-activated protein kinase
MB	myoglobin
MCP1	monocyte chemoattractant protein 1
MEF-2	myocyte enhancer factor-2
MEF2D	myocyte enhancer factor 2D
MFF	mitochondrial fission factor
MFN1	mitofusin 1
MgCl <sub>2</sub>	magnesium chloride
MGL	monoglyceride lipase
min	minutes
MOPS	3-(N-Morpholino) propansulfonsäure
MRF2	modulator recognition factor 2
ms	milliseconds
MS	mass spectrometry
mtDNA	mitochondrial DNA

## APPENDIX

---

mTORC	mammalian target of rapamycin complex
MYBPC	myosin binding protein C
MYF5	myogenic factor 5
MYG	melanocyte proliferating gene
MYH	myosin heavy polypeptide
MYLK	myosin light chain kinase
MYO18B	myosin XVIIIb
MYOT	myotilin
MYLPF	myosin light chain, phosphorylatable, fast skeletal muscle
n	number
N <sub>2</sub>	nitrogen
NaCl	sodium chloride
Na <sub>3</sub> C <sub>6</sub> H <sub>5</sub> O <sub>7</sub>	sodium citrate
NaN <sub>3</sub>	sodium azide
NAFLD	non-alcoholic fatty liver disease
NaOH	sodium hydroxide
ND	normal diet
NEAA	non-essential amino acids
NE	norepinephrine
NEO	neomycin resistance cassette
NF-κB	nuclear factor 'kappa-light-chain-enhancer'
NH <sub>4</sub> Cl	ammonium chloride
NH <sub>4</sub> HCO <sub>3</sub>	ammonium bicarbonate
NMR	nuclear magnetic resonance
NP-40	Nonidet P-40
Ns	non-significant
NTC	non-targeting control
OBSCN	obscurin, cytoskeletal calmodulin and titin-interacting RhoGEF
OCR	oxygen consumption rate
OD	optical density
OPA1	optic atrophy-1
p	phospho
Panc.	pancreas

## APPENDIX

---

P-ase	protein phosphatase
PBS	phosphate-buffered saline
PCR	polymerase chain reaction
PDZ	postsynaptic density-95/discs large/zona occludens-1
PFA	paraformaldehyde
PGC1 $\alpha$	proliferator-activated receptor $\gamma$ coactivator 1 $\alpha$
PH	pleckstrin homology
PHOSPHO1	phosphoethanolamine/phosphocholine phosphatase 1
PI3K	phosphoinositid-3-kinasen
PI4KB	phosphatidylinositol 4-kinase III $\beta$
PI4P	phosphatidylinositol 4-phosphate
PIP2	phosphatidylinositol-4,5-bisphosphate
PKA	protein kinase A
PKB	protein kinase B
PKC	protein kinase C
PKD	protein kinase D
PKD1ca	PKD1 constitutive active
PKD1f/f	PKD1 flox/flox
PKD1wt	PKD1 wild-type
Plat	platinum
PLC	phospholipase C
PPAR	peroxisome proliferator-activated receptor
PPI	protease and phosphatase inhibitor
PRDM16	PR domain containing 16
P/S	Penicillin-Streptomycin
PTEN	phosphatase and tensin homolog
PVDF	polyvinilidene fluoride
Quad.	Quadriceps
QEMS	Q exactive mass spectrometer
Rb	retinoblastoma protein
RER	respiratory exchange ratio
rh FGF	recombinant human fibroblast growth factor
RNA	ribonucleic acid

## APPENDIX

---

ROS	reactive oxygen species
RPL13a	ribosomal protein L13a
RPMI	roswell park memorial institute
RT-qPCR	real time quantitative polymerase chain reaction
RYR1	ryanodine receptor 1
18s	18S ribosomal 5
S	serine
s	seconds
SD	standard deviation
S6K	ribosomal protein S6 kinase
SDS-PAGE	sodium dodecyl sulfate-polyacrylamide gel electrophoresis
SERCA	sarcoendoplasmic reticulum Ca <sup>2+</sup> -ATPase
SEM	standard error of the mean
sh	small hairpin
shNTC	small hairpin NTC
shPKD1	small hairpin PKD1
shRNA	small hairpin RNA
si	small interfering
siRNA	small interfering RNA
SLC	solute carrier family
SNP	single nucleotide polymorphisms
SNYPO	synaptopodin
SP	sodium pyruvate
SREBP	sterol regulatory element-binding protein
SVC	stromal vascular cells
sWAT	subcutaneous WAT
T	threonine
T3	3,3',5-Triiodo-L-thyronine sodium salt
TAE	Tris-acetate-EDTA
TBST	TRIS buffered saline with tween
T2D	type 2 diabetes
TE	TRIS-EDTA
TEMED	tetramethylethylenediamine

## APPENDIX

---

TG	triglyceride
TGN	trans-Golgi network
TNF $\alpha$	tumor necrosis factor $\alpha$
TPM	tropomyosin
TSC	tuberous sclerosis complex
Tyr	tyrosine
UCP	uncoupling protein
undiff.	undifferentiated
w/o	without
WAT	white adipose tissue
WB	Western blot
WHO	world health organisation
wt	wild type
ZMP	5-amino-4-imidazolecarboxamide riboside 5'-monophosphate

## 7.5 Acknowledgements

The work presented here was accomplished at the Rudolf Virchow Center for Experimental Biomedicine, University of Würzburg, in the group of Dr. Grzegorz Sumara between November 2013 and September 2018. Some of the results presented in this thesis have been published, as indicated in the respective result sections.

Many people supported me throughout my PhD studies whom I would like to thank for their help and support:

First of all, my supervisor, Dr. Grzegorz Sumara, for giving me the opportunity to pursue my PhD in his laboratory, for his constant encouragement, support, critical and valuable scientific inputs, financial support, and creating the base of my scientific network and career.

The members of my thesis committee: Prof. Dr. Antje Gohla, Prof. Dr. Carsten Hoffmann, and Dr. Nabil Djouder for fruitful discussions and reviewing my thesis.

Prof. Dr. Manfred Gessler who agreed to be the chairperson during my thesis defense.

Alexander, Jonathan, Till, Rabih, Angel and Manu for their scientific support and critical discussions but also many fun moments, making these last years an unforgettable experience.

Prof. Dr. Martin Eilers, Dr. Carsten Ade (Theodor Boveri Institute, Biocenter, University of Würzburg, Germany), Prof. Dr. Guadelupe Sabio (Centro Nacional de Investigaciones Cardiovasculares Carlos III, Madrid, Spain), Prof. Dr Almut Schulze, Dr. Werner Schmitz (Theodor Boveri Institute, Biocenter, University of Würzburg, Germany), Prof. Dr. Andreas Schlosser, and Dr. Jens Vanselow (Rudolf Virchow Center for Experimental Biomedicine, University of Würzburg) for their excellent collaborations on this project.

Dr. Dr. Katharina Remer and all animal care takers for their excellent supervision of the animal facility.

Florian, Isabel, Till, Jonathan, Christian, and Ketan for carefully proofreading my thesis.



## APPENDIX

---

All the current and former members of the Sumara lab who have not been mentioned by name, but spent their time with me, gave me helpful scientific inputs, for the cooperative and supportive working atmosphere as well as for the great social interaction and many fun moments at work and outside of work.

All collaborators that have not been mentioned here by name, for their support and valuable contributions to the project.

The team of the Graduate School of Life Sciences for organizing and offering the transferable skill courses and the coordination of the PhD study program.

My friends in and outside of Würzburg for their (non)-scientific discussions and all the fun times together.

Last and most important, my deepest gratitude goes to my family who always supported, encouraged and believed in me.

## 7.6 Publications

### 7.6.1 Original articles

Mayer, AE., **Löffler, MC.**, Schmitz, W., Erk, M., El-Merahbi, R., Zhang, T., Braun, U., Heikenwalder M., Leitges, M., Schulze, A., Sumara, G. Hepatic Protein Kinase D3 provides the negative feedback on cholesterol and TG synthesis by suppressing insulin signaling. *Science Signaling*. In peer review. 2019.

**Löffler, MC.**, Mayer, AE., Trujillo Viera, J., Loza Valdes, A., El-Merahbi, R., Ade, CP., Karwen, T., Schmitz, W., Slotta, A., Erk, M., Janaki-Raman, S., Matesanz, N., Torres, JL., Marcos, M., Sabio, G., Eilers, M., Schulze, A., Sumara, G. Protein kinase D1 deletion in adipocytes enhances energy dissipation and protects against adiposity. *EMBO J*. 2018 Nov 15; 37(22).

Cai, K., El-Merahbi, R., **Loeffler M.**, Mayer, AE., Sumara, G. NDRG1 promotes adipocyte differentiation and sustains their function. *Sci Rep*. 2017; 7: 7191

Sukarieh, R., Joseph, R., Leow, SC., Li, Y., **Löffler, M.**, Aris, IM., Tan, JH., The, AL., Chen, L., Holbrook, JD., Ng, KL., Lee, YS., Chong, YS., Summers, SA., Gluckman, PD., Stünkel, W. Molecular pathways reflecting poor intrauterine growth are found in Wharton's jelly-derived mesenchymal stem cells. *Hum Reprod*. 2014 Oct 10; 29(10):2287-301.

### 7.6.2 Reviews

El-Merahbi, R., **Löffler M.**, Mayer, A., Sumara, G. The roles of peripheral serotonin in metabolic homeostasis. *FEBS letters*. 2015; 589, 1728-1734

### 7.6.3 Oral presentations

Protein Kinase D1 (PKD1)-dependent signaling in regulation of adipose tissue function. Rudolf-Virchow-Center retreat. September 14<sup>th</sup>, 2014. Würzburg, Germany.

Protein Kinase D1 (PKD1)-dependent signaling in regulation of adipose tissue function. PKD mini symposium. September 22<sup>nd</sup>, 2014. Würzburg, Germany.

#### **7.6.4 Posters**

Protein kinase D1-dependent signalling in adipocytes suppresses lipolysis and promotes appetite. 9<sup>th</sup> International Symposium organized by the Students of the Graduate School of Life Sciences. October 14<sup>th</sup>-15<sup>th</sup>, 2014. Würzburg, Germany.

Protein kinase D1 suppresses browning of subcutaneous white adipocytes and promotes obesity and diabetes. 40<sup>th</sup> European Symposium on Hormones and Cell Regulation. October 8<sup>th</sup>-11<sup>th</sup>, 2015. Strasbourg, France.

Protein kinase D1 suppresses browning of subcutaneous white adipocytes and promotes obesity and diabetes. 10<sup>th</sup> International Symposium organized by the Students of the Graduate School of Life Sciences. October 14<sup>th</sup>-15<sup>th</sup>, 2015. Würzburg, Germany

Protein kinase D1 suppresses browning of subcutaneous white adipocytes and promotes obesity and diabetes. Rudolf-Virchow-Center retreat. October 27<sup>th</sup>-29<sup>th</sup>, 2015. Würzburg, Germany.

Protein kinase D1 promotes lipid accumulation, obesity, and type 2 diabetes. The PI3K-mTOR-PTEN Network in Health and Disease. August 30<sup>th</sup> to September 3<sup>rd</sup>, 2016. Cold Spring Harbor, USA.

PKD1 is a novel kinase promoting lipid accumulation, obesity, and type 2 diabetes. 11<sup>th</sup> International Symposium organized by the Students of the Graduate School of Life Sciences. October 12<sup>th</sup>-13<sup>th</sup>, 2016. Würzburg, Germany

Protein kinase D1 promotes lipid accumulation, obesity, and type 2 diabetes. Keystone Symposia on Molecular and Cellular Biology, Diabetes/Obesity and Adipose tissue. January 22<sup>nd</sup>-27<sup>th</sup>, 2017. Colorado, USA.

Protein kinase D1 promotes obesity by suppressing AMPK activity and energy dissipation by adipocytes. Rudolf-Virchow-Center retreat. October 9<sup>th</sup>-10<sup>th</sup>, 2017. Würzburg, Germany.

Protein kinase D1 promotes obesity by suppressing AMPK activity and energy dissipation by adipocytes. 12<sup>th</sup> International Symposium organized by the Students of the Graduate School of Life Sciences. October 11<sup>th</sup>-12<sup>th</sup>, 2017. Würzburg, Germany.

## **7.7 Curriculum vitae**



## **7.8 Affidavit**

I hereby declare that my thesis entitled, "Protein kinase D1 deletion in adipocytes enhances energy dissipation and protects against adiposity", is the result of my own work. I did not receive any help or support from commercial consultants. All sources and/or materials applied are listed and specified in the thesis.

Furthermore, I confirm that this thesis has not yet been submitted as part of another examination process neither in identical nor in similar form.

Würzburg, February 2019 \_\_\_\_\_

Mona Löffler

## **7.9 Eidesstattliche Erklärung**

Hiermit erkläre ich an Eides statt, die Dissertation „Deletion der Protein Kinase D1 in Adipocyten fördert den Energieumsatz und schützt dadurch vor Adipositas“ eigenständig, d.h. insbesondere selbstständig und ohne Hilfe eines kommerziellen Promotionsberaters, angefertigt und keine anderen als die von mir angegebenen Quellen und Hilfsmittel verwendet zu haben.

Ich erkläre außerdem, dass die Dissertation weder in gleicher noch in ähnlicher Form bereits in einem anderen Prüfungsverfahren vorgelegen hat.

Würzburg, Februar 2019 \_\_\_\_\_

Mona Löffler